LBNL-45780

Synthesis and Structure of Bivalent Ytterbocenes and Their Coordination Chemistry with π-Acceptor Ligands

Madeleine Schultz
Ph.D. Thesis

Department of Chemistry
University of California, Berkeley

and

Chemical Sciences Division
Ernest Orlando Lawrence Berkeley National Laboratory
University of California
Berkeley, CA 94720

May 2000

This work was supported by the Director, Office of Science, Office of Basic Energy Sciences, Chemical Sciences Division, of the U.S. Department of Energy under Contract No. DE-AC03-76SF00098.

DISCLAIMER

Synthesis and Structure of Bivalent Ytterbocenes and their Coordination Chemistry with π-Acceptor Ligands

by

Madeleine Schultz

BSHon (Australian National University) 1995

BLaws (Australian National University) 1996

A dissertation submitted in partial satisfaction of the requirements for the degree of

Doctor of Philosophy

in

Chemistry

in the

GRADUATE DIVISION

of the

UNIVERSITY OF CALIFORNIA, BERKELEY

Committee in charge:

Professor Richard A. Andersen, Chair

Professor T. Don Tilley

Professor Jeffrey A. Reimer

Spring 2000

Abstract

Synthesis and Structure of Bivalent Ytterbocenes

and their Coordination Chemistry with π-Acceptor Ligands

by

Madeleine Schultz

Doctor of Philosophy in Chemistry

University of California, Berkeley

Professor Richard A. Andersen, Chair

The bivalent lanthanide metallocenes $[1,3\text{-}(Me_3C)_2C_5H_3]_2Yb$ and $(Me_4C_5H)_2Yb$ have been synthesized and their structures have been determined by X-ray crystallography. Comparison with the known structures of $(Me_5C_5)_2Yb$ and $[1,3\text{-}(Me_3Si)_2C_5H_3]_2Yb$ leads to an understanding of the role of intermolecular contacts in stabilizing these coordinatively unsaturated molecules. The optical spectra of the base-free ytterbocenes and their Lewis-base adducts have been measured; the position of the HOMO - LUMO transition can be correlated with the degree of bending of the complexes in solution according to a molecular orbital model. Electron - electron repulsion, resulting from additional σ-donor ligands, also affects the HOMO - LUMO transition by increasing the energy of the filled *f*-orbitals.

The base-free metallocene $(Me_5C_5)_2Yb$ coordinates carbon monoxide, resulting in a decrease in ν_{CO} relative to that of free carbon monoxide. This behavior is reminiscent of *d*-transition metallocene chemistry. Other base-free ytterbocenes also coordinate carbon monoxide and the degree of back-donation is related to the substituents on the cyclopentadienide rings. Isocyanides are coordinated in a 1:2 ratio by the ytterbocenes, giving complexes having ν_{CN} higher than those of the free isocyanides. An electrostatic bonding model has been used to explain the changes in CN stretching frequencies. The optical spectra of the carbonyl and isocyanide complexes are consistent with the molecular orbital model of the variation in the HOMO - LUMO gap upon bending, and the increase in electron - electron repulsion due to the additional ligands.

The complex $(Me_5C_5)_2Yb(bipy)$ exhibits optical, infrared and NMR spectroscopy and an X-ray crystal structure consistent with the presence of bipyridyl radical anion. However, the shape of the magnetic susceptibility curve is unusual. 2,2'-Bipyridyl and 1,10-phenanthroline complexes of several ytterbocenes have been prepared for comparison with this molecule. The phenanthroline complexes display strong electron exchange coupling, with the degree of coupling dependent on the substituents on the cyclopentadienide rings. The magnetism of the bipyridyl complexes may also be ascribed to electron exchange coupling, or to an equilibrium between a diamagnetic bivalent ytterbium complex and a trivalent complex resulting from the transfer of one electron from the metal to the bipyridyl ligand.

Table of Contents

Table of Abbreviations

For the purposes of clarity and conciseness, the following abbrevations have been used throughout this work.

Me:	$-CH_3$
Et:	$-CH_2CH_3$
bipy:	2,2'-bipyridyl
dmb:	4,4'-dimethyl-2,2'-bipyridyl
phen:	1,10-phenanthroline
Ln:	unspecified lanthanide metal
Cp':	unspecified cyclopentadienide anion
R:	unspecified organic group
HOMO:	Highest occupied molecular orbital
LUMO:	Lowest unoccupied molecular orbital
THF:	Tetrahydrofuran; C_4H_8O
dme:	dimethoxyethane; $CH_3OCH_2CH_2OCH_3$
pc:	phthalocyanato; $C_{32}H_{16}N_8^{2-}$

Acknowledgements

I thank Dick Andersen for his continuous guidance, inspiration and enthusiasm. He manages to strike the perfect balance between providing direction and encouraging independence, and has contributed immeasurably to my education.

I am grateful to many people in the College of Chemistry who have assisted me in the course of this work. Among them, PJ Alaimo, Brendon O'Sullivan and Jenn Polse have been particularly helpful and generous with their time and expertise.

Few people in CHAOS will understand a word of this thesis, yet it would not exist without the club. In particular, Jenn Dieges, Dave Jones, Neva Phair, Eric and Candace Renger, Lukas Chrostowski, Keren Zaks, Matthew Church and Don Coleman have shared my love of the mountains. Other friends whose encouragement and support have remained constant in spite of the distance are Rob Oldham, Kate Murphy, Janet Hope, Judy Williams, Rosalie Schultz and Gabriel Mazzuferi.

My parents have always encouraged me and guided me to independence, never trying to limit my aspirations. I am grateful to them and amazed at their generosity. Most importantly I thank Alan Doak, who has shown untiring patience and provided inspiration, reminding me of my priorities and keeping things in perspective.

Introduction

The valence *f*-orbitals of the lanthanide and actinide elements are spatially compact and radially diffuse, resulting in little orbital interaction between these metals and their ligands.[1,2] This contrasts with the behavior of *d*-transition metals, which can interact covalently with ligands through their *d*-orbitals. The lack of orbital interaction between the electropositive *f*-elements and their ligands results in predominantly ionic bonding in lanthanide and actinide complexes.[3,4]

A purely electrostatic bonding model implies that there is no possibility of π-back-donation from a filled orbital of an *f*-block metal to a π-acidic ligand. However, the actinide metal uranium has been shown to be capable of participating in π-back-donation to phosphines and carbon monoxide.[5-8] This behavior is thought to result from population of the 6*d*-orbitals or hybrid orbitals resulting from *f*-*d* mixing, as the 6*d*-orbitals have the correct symmetry and sufficient radial extent to interact with the orbitals of π-acceptor ligands.

A similar interaction of a lanthanide metal with a π-acid is less likely, given the more compact nature of the 4*f*-orbitals compared with the 5*f*-orbitals and the greater energy required for $4f \rightarrow 5d$ promotion compared with $5f \rightarrow 6d$ promotion.[1] However, the electrons in divalent lanthanides are less tightly held than those of trivalent ones, so a suitable coordinatively-unsaturated divalent lanthanide complex may be capable of such an interaction.

The base-free organolanthanide complexes $(Me_5C_5)_2Ln$ (Ln = Sm, Eu, Yb) exist as bent sandwich complexes in the solid state and $(Me_5C_5)_2Yb$ is also known to be bent in the gas phase.[9-14] Two other base-free lanthanide metallocenes, $[1,3\text{-}(Me_3Si)_2C_5H_3]_2Ln$ (Ln = Eu, Yb), have been reported, both of which also have bent sandwich structures in the solid state.[15] The bent structures result in an open coordination wedge, which, in conjunction with the electropositive nature of the lanthanide metals, leads to facile coordination of a variety of non-classical ligands.[16-19]

The base-free lanthanide metallocenes are prepared from their diethyl ether complexes, which can be synthesized by reaction of an alkali metal salt of the cyclopentadienide anion with the lanthanide diiodide in diethyl ether (Equation 1).[9,13,15]

$$2Cp'M + LnI_2 \rightarrow Cp'_2Ln(OEt_2) \quad (1)$$

M = Na, K; Ln = Sm, Eu, Yb; Cp' = Me_5C_5, 1,3-$(Me_3Si)_2C_5H_3$

Removal of the ether ligand from the electropositive metal center can be achieved by the toluene reflux method for $(Me_5C_5)_2Ln$ and by sublimation in the case of $[1,3\text{-}(Me_3Si)_2C_5H_3]_2Ln$.[9,15,20] The resulting base-free molecules exist as coordination dimers or polymers in the solid state with intermolecular Me ··· Ln interactions (Figure 1).[9,13,14] These interactions are thought to relieve the steric unsaturation of the molecules, but are weak enough that the molecules are soluble in hydrocarbon solvents.

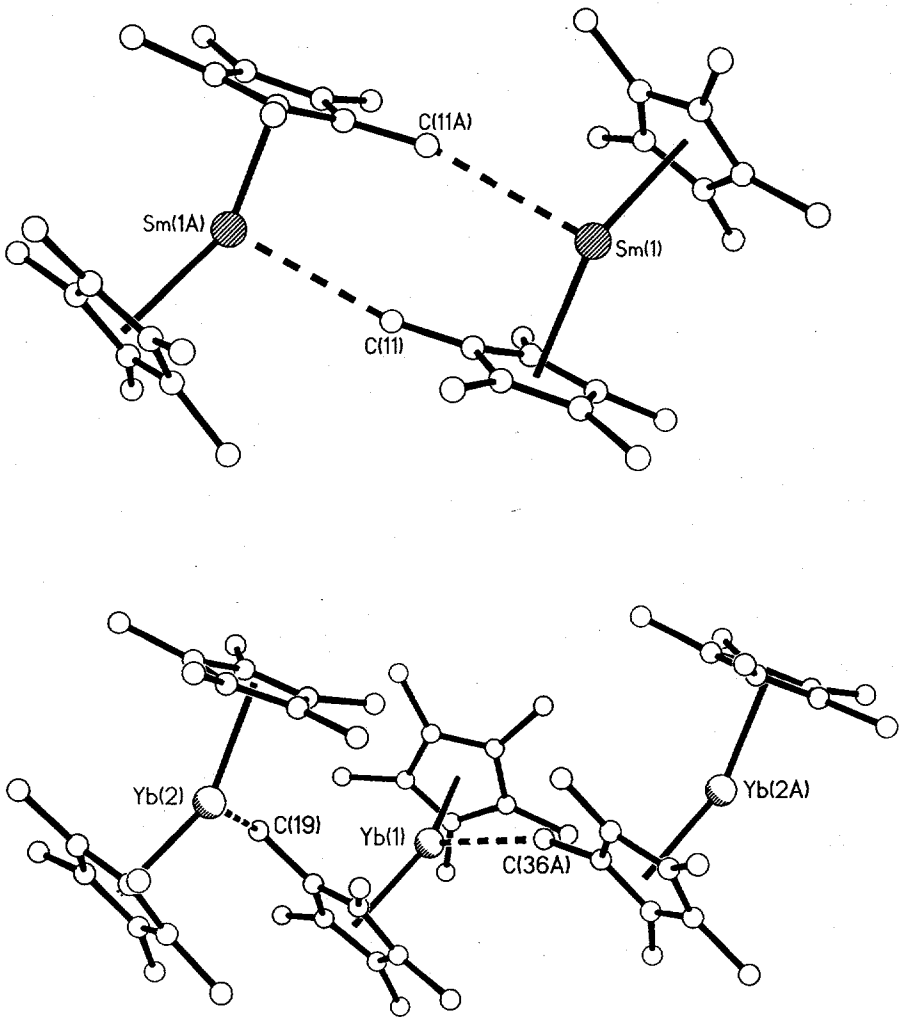

Figure 1. Ball and stick diagrams of the X-ray crystal structures of $(Me_5C_5)_2Sm$ and $(Me_5C_5)_2Yb$ (only one of the two crystalline forms shown) illustrating the intermolecular interactions (constructed from the published coordinates in ref. 13 and 14).

The complex $(Me_5C_5)_2Yb$ is known to interact with carbon monoxide since the polymerization of ethylene is inhibited by the presence of this gas.[9] Also, changes in the ^{13}C NMR spectrum of a methylcyclohexane-d_{14} solution of $(Me_5C_5)_2Yb$ under one

atmosphere of ^{13}CO as the temperature is lowered from 25 to -107°C are consistent with the formation of two carbonyl complexes, neither of which can be isolated.[21] In analogous uranium chemistry, the complex $(Me_3SiC_5H_4)_3U$ forms an unisolable carbonyl complex.[5] Changing the cyclopentadienide ligand to Me_4C_5H led to the isolation of the complex $(Me_4C_5H)_3U(CO)$, which has been characterized by X-ray crystallography.[7,8] It is therefore of interest to prepare a base-free ytterbocene with differently substituted cyclopentadienide ligands in an attempt to isolate an ytterbium carbonyl complex. In the absence of solid-state evidence, substituent effects on ν_{CO} provide a convenient gauge of the electron density at the ytterbium center.

The centroid - metal - centroid angle of a bent metallocene plays an important role in the ability of the metal to bind Lewis bases and other ligands. The smaller the centroid - metal - centroid angle, the greater the permanent dipole of the complex (Figure 2). In addition, little reorganization is required to coordinate a ligand in the open wedge, so the enthalpy of coordination does not have to compensate a large reorganization enthalpy. One method that has been used to enforce a very open coordination sphere in metallocene chemistry is to tie the two cyclopentadienide ligands together in an *ansa*-metallocene complex (Figure 2). *Ansa*-metallocenes of several main group metals,[22,23] transition metals,[24-26] trivalent lanthanides[27] and actinides[28] have been prepared having a variety of bridges between the cyclopentadienide rings.

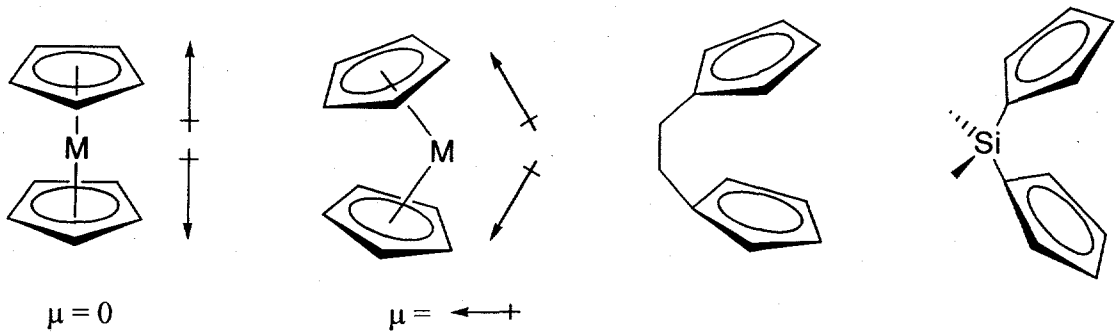

Figure 2. Illustration of the effect of an *ansa*-bridge on the dipole moment and centroid - metal - centroid angle of a metallocene.

A dimethylsilyl bridge has been used successfully to make *ansa*-metallocenes with small centroid - metal - centroid angles as it enforces an angle of close to 104° at the sp^3-hybridized silicon center. This has been shown to promote reactivity.[24,25] It is of interest to prepare base-free *ansa*-bridged ytterbocenes as such complexes would be expected to bind any available ligand strongly in order to reduce their coordinative unsaturation.

In addition to increasing the net dipole moment of the complex, lowering the centroid - metal - centroid angle of a metallocene changes its color and therefore its optical transitions. The optical transitions of $(C_5H_5)_2Yb$ in D_{5d} symmetry have been calculated and three transitions in the visible range are predicted.[29] The lowest energy transition is the HOMO $\rightarrow$ LUMO ($e_{1u} \rightarrow a_{1g}$ orbitals in D_{5d} symmetry) (Figure 3) and is predicted to occur at about 750 nm. The next lower wavelength transitions are predicted to occur at about 460 nm and 390 nm, due to the Cp(π) $\rightarrow$ LUMO ($e_{1u} \rightarrow a_{1g}$, LMCT) and the $f \rightarrow d$ ($e_{2u} \rightarrow e_{2g}$) transitions, respectively.[29] All of these transitions, in D_{5d} symmetry, are electric dipole and Laporte allowed, so they are expected to have large absorptivities.

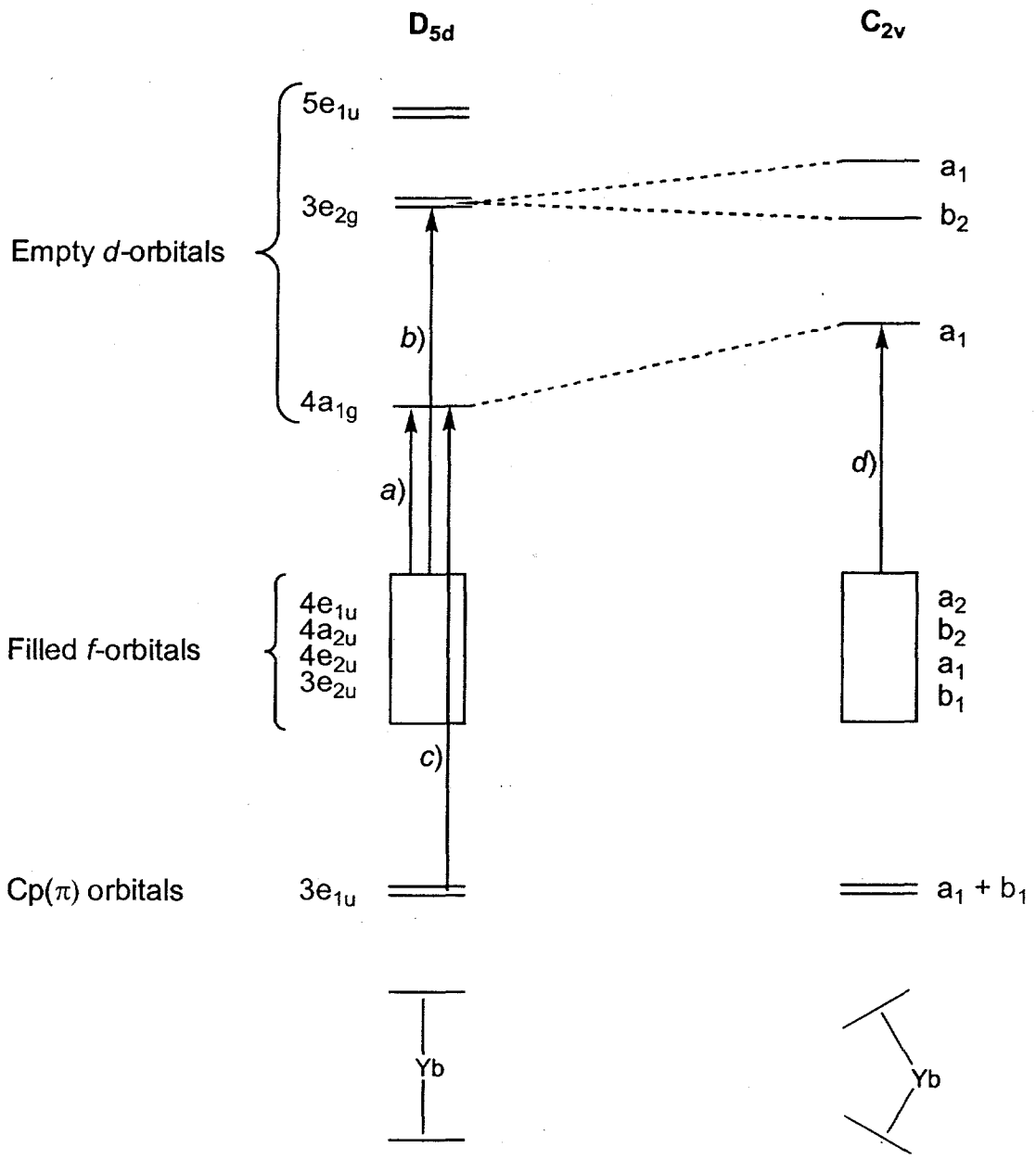

Figure 3. Schematic energy diagram showing the effect of bending on the energies of the molecular orbitals and the optical transitions of an ytterbocene. The diagram is constructed from the data in ref. 29 but is not to scale. The transitions depicted are: *a*) HOMO $\rightarrow$ LUMO, $4e_{1u} \rightarrow 4a_{1g}$; *b*) $f \rightarrow d$, $4e_{2u} \rightarrow 3e_{2g}$; *c*) LMCT, $3e_{1u} \rightarrow 4a_{1g}$; *d*) HOMO $\rightarrow$ LUMO, $f \rightarrow a_1$.

The principal change that is predicted to occur on bending $(C_5H_5)_2Yb$ from D_{5d} to C_{2v} symmetry is an increase in the HOMO - LUMO gap.[29] Thus, bending is predicted to result in a blue-shift of the HOMO $\rightarrow$ LUMO transition. The increased HOMO - LUMO gap that results from bending is largely due to destabilization of the lowest energy, empty a_1 symmetry orbital (in C_{2v} symmetry; a_{1g} in D_{5d}) while the next two higher energy orbitals (a_1 and b_2 in C_{2v}, e_{2g} in D_{5d}) change little on bending (Figure 3).

Coordination of any ligand is expected to cause a metallocene to bend more than the base-free molecule. Thus, optical spectroscopy provides a sensitive probe into the solution structure of base-free metallocenes. For example, toluene is known to interact with $(Me_5C_5)_2Yb$ in solution as it slows the rate of ethylene polymerization compared with aliphatic solvents.[9] However, no interaction is observed in the solid state, and the ^1H NMR spectrum of the ytterbocene in toluene is unchanged from the superposition of the spectra of the base-free ytterbocene and toluene in aliphatic solvent.[21] Any interaction is expected to alter the bend angle of the ytterbocene and it is therefore of interest to study solvent effects on the optical spectra of this complex and other base-free lanthanide metallocenes.

The primary goal of this research is to observe back-donation from ytterbium. Carbon monoxide is the ideal ligand for this purpose as the CO stretching frequency in the infrared spectrum is a very sensitive measure of the interaction between the ligand and the metal. A reduction in ν_{CO} is evidence for π-acceptance by CO, as the force constant

of the C - O bond can only be reduced by addition of electron density to the antibonding LUMO.[30] Isocyanides are expected to provide models for carbon monoxide, because the symmetries of the HOMO and degenerate LUMOs of isocyanides are identical to those of CO (Figure 4).

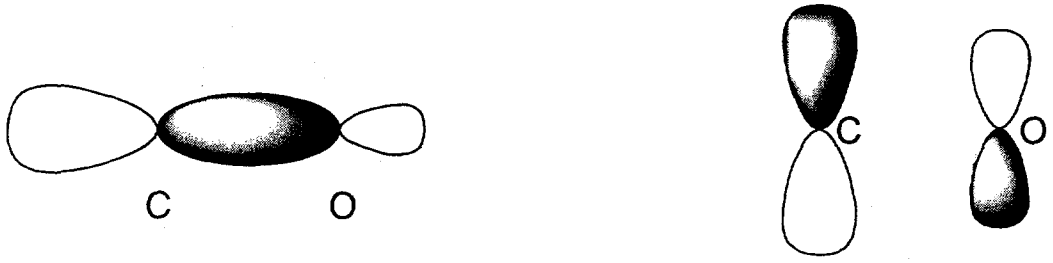

Figure 4. HOMO and one of the two degenerate LUMOs of carbon monoxide; the orbitals of isocyanides have the same symmetry but different coefficients (from ref. 31).

The oxidation potentials of the lanthanide decamethylmetallocenes, measured in acetonitrile vs. $(C_5H_5)_2Fe/[(C_5H_5)_2Fe]^+$, are $(Me_5C_5)_2Sm$, +2.4 V; $(Me_5C_5)_2Eu$, +1.22 V; $(Me_5C_5)_2Yb$, +1.78 V,[32] making the samarium and ytterbium complexes better reducing agents than the europium analogue. These complexes have been used to reduce a variety of nitrogenous bases and organic dichalcogenides.[20,33,34] In particular, 2,2'-bipyridyl is reduced by $(Me_5C_5)_2Sm$,[34] but not by $(Me_5C_5)_2Eu$.[35] In addition, ligands such as 2,2'-bipyridyl can act as π-acceptors.

The frontier orbitals of 2,2'-bipyridyl that are involved in binding to a metal are qualitatively similar to those of two carbon monoxide ligands, with σ-donor and π-acceptor components. It is therefore natural to extend this study to include 2,2'-bipyridyl and related ligands. The molecule $(Me_5C_5)_2Yb(bipy)$ was first reported in 1982 but its

magnetic behavior was not understood, in spite of efforts by a number of researchers, and despite the synthesis of a large number of related compounds having bidentate nitrogen donor ligands.[35-37] It was of interest to prepare bipyridyl complexes of ytterbocenes having differently-substituted cyclopentadienide ligands to assist the understanding of the original system.

References

1) Cotton, F. A.; Wilkinson, G.; Murillo, C. A.; Bochmann, M. *Advanced Inorganic Chemistry*; 6th ed.; John Wiley & Sons, Inc.: New York, 1999.

2) Gerloch, M.; Constable, E. C. *Transition Metal Chemistry*; VCH: Weinheim, 1995.

3) Raymond, K. N. *The Structure and Bonding of 4f and 5f Series Organometallic Compounds*; Marks, T. J. and Fischer, R. D., Ed.; D Reidel Publishing Company: Dordrecht, Netherlands, 1978; Vol. 44, pp 249-280.

4) Bochkarev, M. N.; Zakharov, L. N.; Kalinina, G. S. *Organoderivatives of Rare Earth Elements*; Kluwer Academic Publishers: Dordrecht, Netherlands, 1995; Vol. 3.

5) Brennan, J. G.; Andersen, R. A.; Robbins, J. L. *J. Am. Chem. Soc.* **1986**, *108*, 335.

6) Brennan, J. G.; Stults, S. D.; Andersen, R. A.; Zalkin, A. *Organometallics* **1988**, *7*, 1329.

7) Parry, J.; Carmona, E.; Coles, S.; Hursthouse, M. *J. Am. Chem. Soc.* **1995**, *117*, 2649.

8) del Mar Conejo, M.; Parry, J. S.; Carmona, E.; Schultz, M.; Brennan, J. B.; Beshouri, S. M.; Andersen, R. A.; Rogers, R. D.; Coles, S.; Hursthouse, M. *Chem: Eur. J.* **1999**, *5*, 3000.

9) Burns, C. J. *PhD Thesis*; University of California: Berkeley, 1987.

10) Andersen, R. A.; Boncella, J. M.; Burns, C. J.; Blom, R.; Haaland, A.; Volden, H. V. *J. Organomet. Chem.* **1986**, *312*, C49.

11) Andersen, R. A.; Boncella, J. M.; Burns, C. J.; Green, J. C.; Hohl, D.; Rösch, N. *J. Chem. Soc., Chem. Commun.* **1986**, 405.

12) Andersen, R. A.; Blom, R.; Boncella, J. M.; Burns, C. J.; Volden, H. V. *Acta Chem. Scand. A* **1987**, *A41*, 24.

13) Evans, W. J.; Hughes, L. A.; Hanusa, T. P. *Organometallics* **1986**, *5*, 1285.

14) Schultz, M.; Burns, C. J.; Schwartz, D. J.; Andersen, R. A. *Organometallics* **2000**, *19*, 781.

15) Hitchcock, P. B.; Howard, J. A. K.; Lappert, M. F.; Prashar, S. *J. Organomet. Chem.* **1992**, *437*, 177.

16) Burns, C. J.; Andersen, R. A. *J. Am. Chem. Soc.* **1987**, *109*, 5853.

17) Burns, C. J.; Andersen, R. A. *J. Am. Chem. Soc.* **1987**, *109*, 915.

18) Burns, C. J.; Andersen, R. A. *J. Am. Chem. Soc.* **1987**, *109*, 941.

19) Evans, W. J.; Ulibarri, T. A.; Ziller, J. W. *J. Am. Chem. Soc.* **1988**, *110*, 6877.

20) Berg, D. J.; Burns, C. J.; Andersen, R. A.; Zalkin, A. *Organometallics* **1989**, *8*, 1865.

21) Schwartz, D. J. *PhD Thesis*; University of California: Berkeley, 1995.

22) Harder, S.; Lutz, M.; Straub, A. W. G. *Organometallics* **1997**, *16*, 107.

23) Harder, S.; Lutz, M.; Obert, S. J. *Organometallics* **1999**, *18*, 1808.

24) Churchill, D.; Shin, J. H.; Hascall, T.; Hahn, J. M.; Bridgewater, B. M.; Parkin, G. *Organometallics* **1999**, *18*, 2403.

25) Shin, J. H.; Parkin, G. *J. Chem. Soc., Chem. Commun.* **1999**, 887.

26) Green, J. C. *Chem. Soc. Rev.* **1998**, 263.

27) Khvostov, A. V.; Belsky, V. K.; Bulychev, B. M.; Sizov, A. I.; Ustinov, B. B. *J. Organomet. Chem.* **1998**, *571*, 243.

28) Schnabel, R. C.; Scott, B. L.; Smith, W. H.; Burns, C. J. *J. Organomet. Chem.* **1999**, *591*, 14.

29) Green, J. C.; Hohl, D.; Rösch, N. *Organometallics* **1987**, *6*, 712.

30) Hush, N. S.; Williams, M. L. *J. Mol. Spect.* **1974**, *50*, 349.

31) Jorgensen, W. L.; Salem, L. *The Organic Chemists Book of Orbitals*; Academic Press: New York, 1973.

32) Finke, R. G.; Keenan, S. R.; Schiraldi, D. A.; Watson, P. L. *Organometallics* **1986**, *5*, 598.

33) Berg, D. J.; Andersen, R. A.; Zalkin, A. *Organometallics* **1988**, *7*, 1858.

34) Evans, W. J.; Drummond, D. K. *J. Am. Chem. Soc.* **1989**, *111*, 3329.

35) Tilley, T. D. *PhD Thesis*; University of California: Berkeley, 1982.

36) Boncella, J. M. *PhD Thesis*; University of California: Berkeley, 1984.

37) Berg, D. J. *PhD Thesis*; University of California: Berkeley, 1987.

Chapter One : The Synthesis and Structure of Substituted Ytterbocenes

Reaction of Magnesocenes with Ytterbium Iodide

Alkali metal salts have typically been used as cyclopentadienide transfer agents to bivalent lanthanide metals.[1-3] However, these salts are insoluble in hydrocarbon solvents and difficult to purify. Magnesocenes, on the other hand, are highly soluble in aliphatic and a romatic solvents and are readily purified by crystallization. Magnesocenes with substituted cyclopentadienide rings are synthesized from dibutylmagnesium and the substituted cyclopentadiene in refluxing heptane (Equation 1).[4,5]

$$2Cp'H + Bu_2Mg \rightarrow Cp'_2Mg + 2BuH \quad (1)$$

$Cp' = Me_5C_5$, 1,3-$(Me_3C)_2C_5H_3$, 1,3-$(Me_3Si)_2C_5H_3$;

Cp'_2 = *ansa*-[1,3-$(Me_3C)_2C_5H_2]_2SiMe_2$, *ansa*-[1,3-$(Me_3Si)_2C_5H_2]_2SiMe_2$

The *ansa*-magnesocenes cannot be crystallized and are obtained as white powders after removing the solvent from the reaction mixture under reduced pressure.[5]

Several a ttempts w ere m ade t o ut ilize m agnesocenes in t he s ynthesis o f die thyl e ther adducts or base-free ytterbocenes; however, no good synthetic routes were found. No reaction occurs between $(Me_5C_5)Mg$ and YbI_2 in diethyl ether; the solvent is not colored after stirring for 2 days at room temperature. Addition of THF to the diethyl ether slurry of $(Me_5C_5)_2Mg$ and YbI_2 results in an immediate color change to deep red-purple, and the

THF adduct $(Me_5C_5)_2Yb(THF)$[6] can be crystallized from the mother liquor after filtration. This technique is not useful for the preparation of the base-free ytterbocene, however, as THF cannot subsequently be removed.[7] No reaction occurs between $(Me_5C_5)_2Mg$ and YbI_2 at 140°C in refluxing dibutyl ether, or at 55°C in refluxing methyl-*tert*-butyl ether. The Yb(III) salt $Yb(OTf)_3$ reacts with $(Me_5C_5)_2Mg$ to transfer one ring to the metal, as determined by elemental analysis, which is the same result as is obtained from the reaction of $Yb(OTf)_3$ with $Na(Me_5C_5)$.

The magnesocene of *ansa*-$[1,3\text{-}(Me_3C)_2C_5H_2]_2SiMe_2$ reacts with YbI_2 in diethyl ether, and the solution becomes dark orange. Filtration and cooling gives an orange powder which is thought to be a one-ring complex, similar to that formed in the cases of 1,3-$(Me_3C)_2C_5H_3$ and 1,3-$(Me_3Si)_2C_5H_3$, based on the insolubility and color. In THF, the same reagents form an olive-brown solution after stirring overnight at room temperature. No clean product can be isolated from this reaction.

The compound, *ansa*-$[1,3\text{-}(Me_3Si)_2C_5H_2]_2SiMe_2Mg$, reacts with YbI_2 in THF to give a deep red solution. Upon filtration and cooling, red crystals form which appear, based on ^1H NMR spectroscopy, to be a THF adduct of *ansa*-$[1,3\text{-}(Me_3Si)_2C_5H_2]_2SiMe_2Yb$. However, a pure product cannot be obtained by recrystallization, and heating of the red product under dynamic vacuum leads to the sublimation of the cleaved ligand.

The initial yellow-green slurry of $[1,3\text{-}(Me_3C)_2C_5H_3]_2Mg$ or $[1,3\text{-}(Me_3Si)_2C_5H_3]_2Mg$ with YbI_2 in diethyl ether forms a deep green solution after stirring for two hours at room

temperature. The green color has previously been associated with formation of an ytterbocene. However, upon filtration a thermochroic solution results that is bright green below -30°C but becomes orange-brown upon warming to room temperature. The bright orange crystals that form at low temperature do not redissolve in diethyl ether and are insoluble in hydrocarbon solvents. The crystals dissolve in THF but cannot be recrystallized from that solvent. The ether adduct of magnesium iodide can be obtained as a first crop of colorless crystals from the mother liquor before crystallization of the orange product, and unreacted Cp'_2Mg can be crystallized from the mother liquor after all of the product has crystallized from the solution. Elemental analysis indicates an empirical formula with only one cyclopentadienide ring per ytterbium center, as well as one iodide ligand (Equation 2).

$$Cp'_2Mg + YbI_2 \rightarrow \{Cp'YbI(OEt_2)\}_2 + MgI_2(OEt_2) + Cp'_2Mg \qquad (2)$$

$Cp' = 1,3\text{-}(Me_3C)_2C_5H_3$, $1,3\text{-}(Me_3Si)_2C_5H_3$

The green color of the reaction mixture may indicate that there is an equilibrium with a small amount of ytterbocene present. However, only the one-ring compound can be crystallized from the reaction mixture. The reaction can also be performed using half an equivalent of magnesocene. Use of THF as solvent for this reaction, of $[1,3\text{-}(Me_3C)_2C_5H_3]_2Mg$ with YbI_2, leads to transfer of two cyclopentadienide rings to the metal and formation of the THF adduct $[1,3\text{-}(Me_3C)_2C_5H_3]_2Yb(THF)$, as was observed for Me_5C_5. In refluxing dibutyl ether, no reaction occurs.

The crystal structure of $\{[1,3\text{-}(Me_3C)_2C_5H_3]YbI(OEt_2)\}_2$ was determined to ascertain whether it is a monomer or dimer in the solid state. The structure indicates that it crystallizes as an iodide-bridged dimer, with the monomer forming the asymmetric unit. The Yb_2I_2 core is square and each ytterbium atom exhibits three-legged piano stool geometry. Important distances and angles are shown in Table 1.1 and an ORTEP diagram is shown in Figure 1.1.

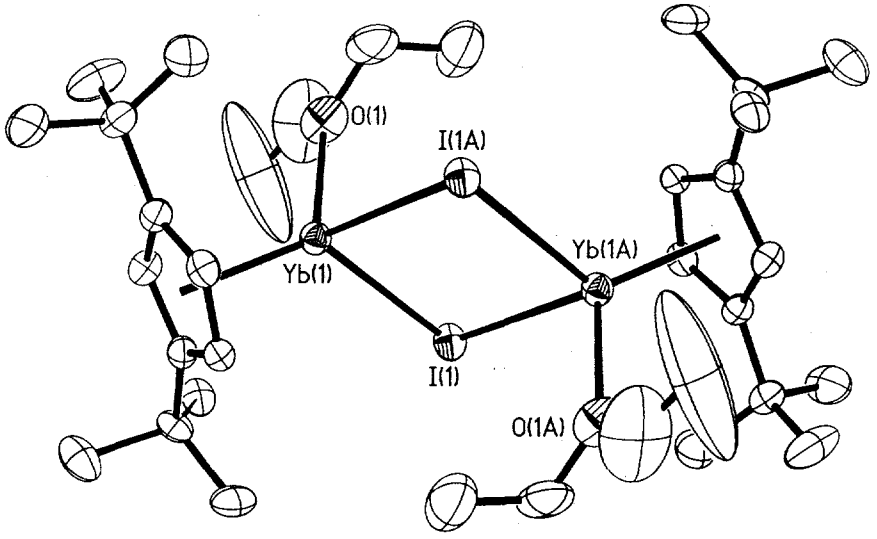

Figure 1.1. ORTEP diagram of $\{[1,3\text{-}(Me_3C)_2C_5H_3]YbI(OEt_2)\}_2$ (50% probability ellipsoids).

There is gross thermal motion in one ethyl group of the diethyl ether ligand, affecting the thermal parameters of that carbon atom, but this does not adversely impact the details of the core of the structure.

Because the bonding in lanthanide complexes is largely ionic, the distances from the ligands to the metal are relatively insensitive to the ligand environment and depend only on the oxidation state and coordination number of the metal.[8-11] The ytterbium center in this complex is in the bivalent oxidation state, in 6-coordination, which corresponds to an ionic radius of 1.02 Å.[12] The only reported structures involving 6-coordinate Yb(II) bound to a cyclopentadienyl ring are those of the base-free ytterbocenes $(Me_5C_5)_2Yb$, $[1,3\text{-}(Me_3C)_2C_5H_3]_2Yb$ and $[1,3\text{-}(Me_3C)_2C_5H_3]_2Yb$,[3,7,13] and the one-ring complex $(Me_5C_5)Yb(Si(SiMe_3)_3)THF_2$.[14] The Yb - ring C distances in the structures of those molecules range from 2.6 - 2.7 Å, so the distances observed in the dimer lie in the expected range.

The structure is similar to those of the published dimers $\{(Me_5C_5)YbI(THF)_2\}_2$, $\{(Me_5C_5)YbI(dme)\}_2$,[15] $\{[(Me_3Si)_3C]YbI(OEt_2)\}_2$,[16] $\{[(Me_3Si)_2(CH_2CHMe_2Si)C]YbI(OEt_2)\}_2$ and $\{[(Me_3Si)_2(MeOMe_2Si)C]YbI(OEt_2)\}_2$.[17] In those structures, the angles in the Yb_2I_2 core range from 85 - 92° and the oxygen atom of the ether in the dimers is located 2.35 - 2.37 Å from the metal. The oxygen atom is slightly further from the metal in the present structure, which is consistent with the lower coordination number and therefore greater ionic radius of the metal in this case.[12]

Table 1.1. Selected bond distances (Å) and bond angles (°) of $\{[1,3\text{-}(Me_3C)_2C_5H_3]YbI(OEt_2)\}_2$

Yb - C (mean)	2.66
Yb - C (range)	2.624(5) - 2.691(5)
Yb - centroid	2.37
Yb - O	2.390(5)
Yb - I	3.0851(4), 3.0955(5)
centroid - Yb - O	124.1
centroid - Yb - I	114.6, 126.7
O - Yb - I	96.3(1), 98.0(1)
I - Yb - I	88.78(1)
Yb - I - Yb	91.22(1)

Stirring a slurry of $\{[1,3\text{-}(Me_3C)_2C_5H_3]YbI(OEt_2)\}_2$ with two equivalents of Me_5C_5Na in diethyl ether leads to the formation of a dark green solution, which indicates that a metallocene may be formed. However, crystals cannot be obtained from the mother liquor after filtration. Methyl lithium reacts with the dimer to form a red product that appears to contain Yb(III), based on the ^1H NMR spectrum, but an alkyl complex cannot be isolated. The reaction of $NaN(SiMe_3)_2$ with the dimer likewise does not lead to tractable products. The dimer does not sublime, and attempted sublimation leads to decomposition and the isolation of the symmetric isomer of $1,3\text{-}(Me_3C)_2C_5H_4$ in low yield.

Synthesis and Structure of Diethyl Ether Complexes of Substituted Ytterbocenes

Magnesocenes are not effective cyclopentadienide transfer agents for ytterbocenes. Hence, the sodium salts were prepared from sodium amide and the cyclopentadiene in THF (Equation 3).[18]

$$NaNH_2 + Cp'H \rightarrow Cp'Na + NH_3 \qquad (3)$$

Cp' = 1,3-$(Me_3C)_2C_5H_3$, Me_4C_5H; Cp'$_2$ = *ansa*-[1,3-$(Me_3C)_2C_5H_2]_2SiMe_2$

This method cannot be used with 1,3-$(Me_3Si)_2C_5H_4$ or *ansa*-[1,3-$(Me_3Si)_2C_5H_3]_2SiMe_2$, however, as the reaction of those cyclopentadienes with sodium amide results in cleavage of silicon - carbon bonds. In the case of 1,3-$(Me_3Si)_2C_5H_4$, the potassium salt is prepared by stirring an excess of potassium metal with the cyclopentadiene in refluxing diethyl ether for a week (Equation 4).

$$K + 1,3\text{-}(Me_3Si)_2C_5H_4 \rightarrow [1,3\text{-}(Me_3Si)_2C_5H_3]K + \tfrac{1}{2}H_2 \qquad (4)$$

No alkali metal salt of *ansa*-[1,3-$(Me_3Si)_2C_5H_2]_2SiMe_2$ was successfully prepared; the reaction with potassium metal in refluxing diethyl ether leads to cleavage of the *ansa*-bridge. Similarly, the reaction of *ansa*-[1,3-$(Me_3C)_2C_5H_3]_2SiMe_2$ with potassium metal in refluxing diethyl ether leads to cleavage of the some of the *ansa*-bridges.

The diethyl ether complexes $(Me_4C_5H)_2Yb(OEt_2)$, $[1,3\text{-}(Me_3C)_2C_5H_3]_2Yb(OEt_2)$ and *ansa*-$[1,3\text{-}(Me_3C)_2C_5H_2]_2SiMe_2Yb(OEt_2)$ can be synthesized by the reaction of two equivalents of the sodium salt of the substituted cyclopentadienide with ytterbous iodide in diethyl ether, followed by filtration and crystallization from the deep green mother liquor (Equation 5).[19] A slight excess of ytterbous iodide is required, presumably as this reagent contains some insoluble impurities, and an excess is required to adjust the stoichiometry. A similar conclusion was deduced in the reported synthesis of $(Me_5C_5)_2Yb(OEt_2)$.[2,20]

$$2NaCp' + YbI_2 \rightarrow Cp'_2Yb(OEt_2) + 2NaI \qquad (5)$$

Cp' = Me_4C_5H, $1,3\text{-}(Me_3C)_2C_5H_3$; Cp'$_2$ = *ansa*-$[1,3\text{-}(Me_3C)_2C_5H_2]_2SiMe_2$

In some cases, a mixture of the diethyl ether complex and the THF complex is obtained. The latter is due to residual THF bound to the sodium salt of the cyclopentadienide. This can be removed by prolonged exposure of the powdered sodium salt to dynamic vacuum.

The structures of the diethyl ether complexes $[1,3\text{-}(Me_3C)_2C_5H_3]_2Yb(OEt_2)$, $(Me_4C_5H)_2Yb(OEt_2)$ and *ansa*-$[1,3\text{-}(Me_3C)_2C_5H_2]_2SiMe_2Yb(OEt_2)$ were determined for comparison with the known structure of $(Me_5C_5)_2Yb(OEt_2)$.[20] Table 1.2 contains important bond distances and angles while Figures 1.2, 1.3 and 1.4 show ORTEP diagrams of these complexes.

The structures of the three diethyl ether complexes involve typical Yb(II) bond distances to the cyclopentadienyl ligands in 7-coordination.[11] The geometries about the metal center are not surprising. One of the interesting features of these structures is the disposition of the diethyl ether ligand. In the structure of $(Me_5C_5)_2Yb(OEt_2)$, one of the γ-Me groups of the ether ligand is bent back towards the metal center, presumably to relieve steric unsaturation.[20] The Yb ··· C distance of this interaction is 3.23(1) Å, which is significantly shorter than the sum of the van der Waals radii of a methyl group (2.00 Å) and the metallic radius of Yb(II) (1.70 Å).[21] This type of interaction is typical of lanthanide complexes, which generally display the highest possible coordination number that does not involve steric congestion.[22]

In the structure of $[1,3\text{-}(Me_3C)_2C_5H_3]_2Yb(OEt_2)$, the ether ligand is twisted so that both γ-Me groups of the ligand point away from the metal (Figure 1.2). The centroid - metal - centroid angle in this structure is 8° lower than in $(Me_5C_5)_2Yb(OEt_2)$ at 132°, which would suggest that the metal is less coordinatively saturated than in the pentamethylcyclopentadienide analogue. However, the bulky Me_3C groups at the front of the wedge presumably prevent the close approach of the γ-Me groups of the ether ligand. While no non-bonded metal - carbon distance of less than 3.5 Å is observed in this structure, two of the methyl carbon atoms of the Me_3C groups approach the metal within the sum of the van der Waals radii; the Yb ··· C(13) distance is 3.67 Å and the Yb ··· C(24) distance is 3.59 Å. These two carbon atoms are located at the same side of the wedge, one on each cyclopentadienide ring.

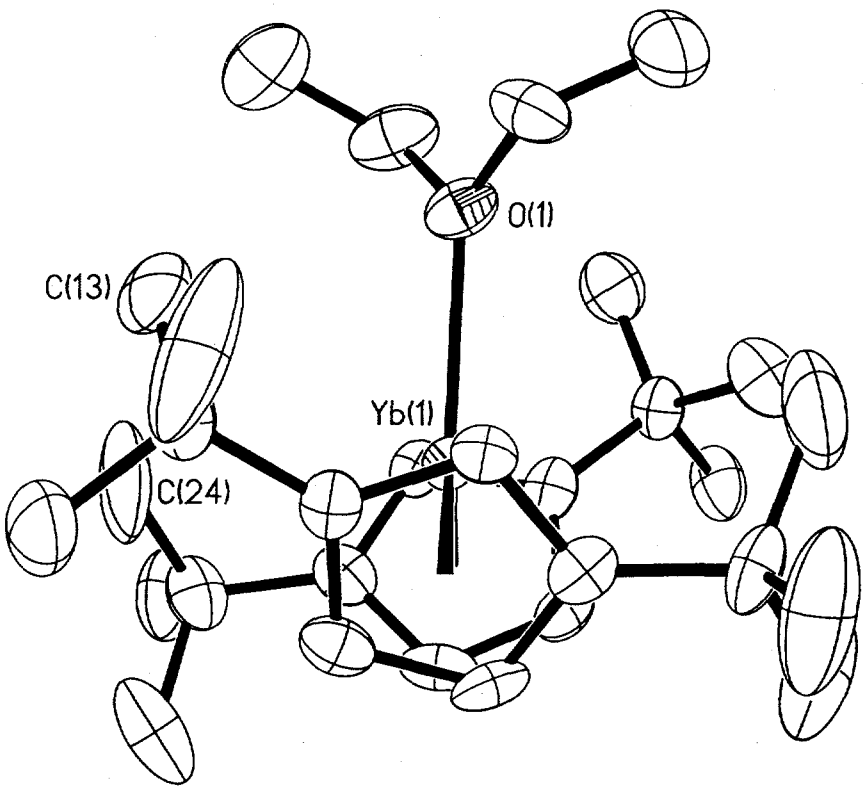

Figure 1.2. ORTEP diagram of $[1,3\text{-}(Me_3C)_2C_5H_3]_2Yb(OEt_2)$ (50% probability ellipsoids).

The structure of $[1,3\text{-}(Me_3C)_2C_5H_3]_2Yb(OEt_2)$ was published during the course of this work.[19] The published structure, determined at room temperature, is slightly different from that determined in this work, but the space group is the same and the important bond distances and angles are within 1 % of those determined here.

The molecule $(Me_4C_5H)_2Yb(OEt_2)$ crystallizes with two unique molecules in the unit cell (Figure 1.3). In both of these, one arm of the ether ligand is pointed back towards the metal as was observed for $(Me_5C_5)_2Yb(OEt_2)$. Molecule 1 has a Yb(1) ··· C(22) distance

of 3.21 Å, while molecule 2 has a slightly shorter Yb(2) ··· C(41) distance of 3.15 Å. The centroid - metal - centroid angle is also lower than in the pentamethylcyclopentadienide analogue, at 133°. This is directly attributable to the lack of the fifth methyl group, as can be seen from the orientation of the rings in the molecule. The ring carbon atoms C(1) and C(10) of molecule 1 and C(23) and C(32) of molecule 2 do not bear a methyl group, and these are located at the back side of the wedge in the two molecules.

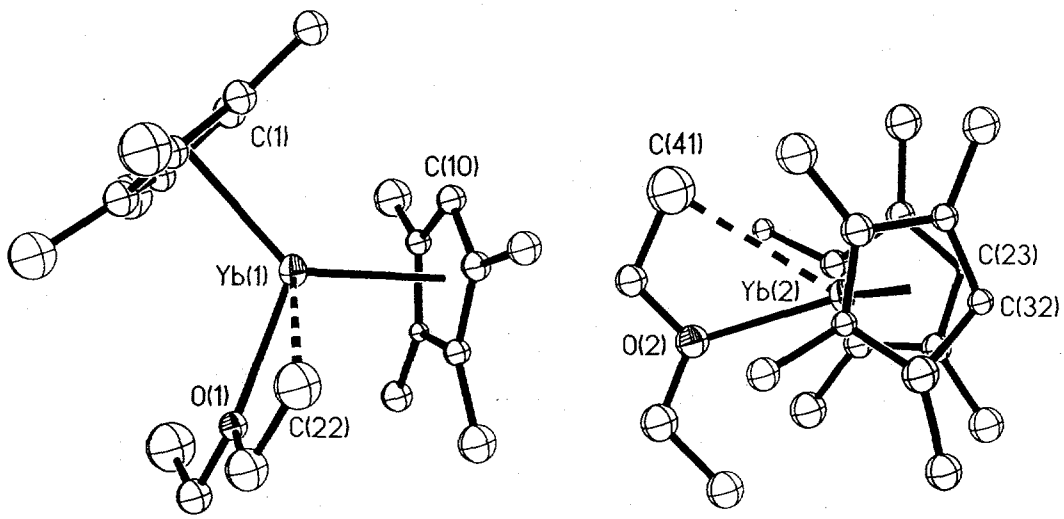

Figure 1.3. ORTEP diagram of $(Me_4C_5H)_2Yb(OEt_2)$ (50% probability ellipsoids) (2 unique molecules).

The molecule *ansa*-[1,3-$(Me_3C)_2C_5H_2]_2SiMe_2Yb(OEt_2)$ crystallizes with three unique molecules in the asymmetric unit (Figure 1.4). Each of these molecules has one very short Yb ··· γ-Me distance; in molecule 1, Yb(1) ··· C(29) is 3.14 Å; in molecule 2, Yb(2) ··· C(61) is 3.15 Å, and in molecule 3, the shortest distance yet seen is observed between Yb(3) and C(93), of 3.00 Å. This distance is not much greater than the longest ring

carbon - ytterbium distances observed in typical Yb(II) metallocenes.[3,6,23-26] The ytterbium atom is exposed to this interaction because of the *ansa*-bridge, which holds the metallocene wedge open with a centroid - metal - centroid angle of 124°. This allows the close approach of the γ-Me groups of the ether ligand without steric congestion between the ligands.

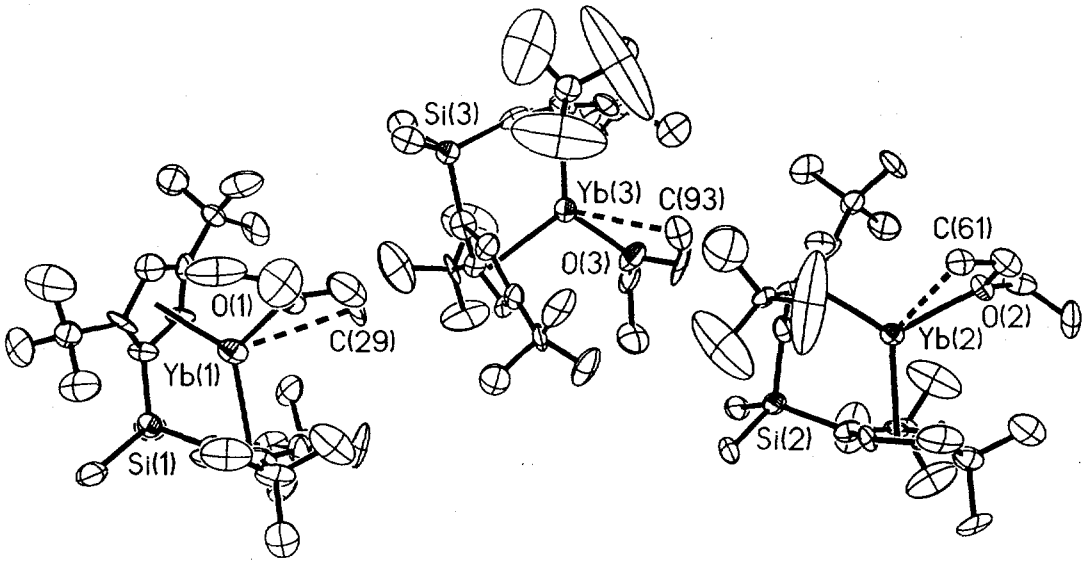

Figure 1.4. ORTEP diagram of *ansa*-[1,3-$(Me_3C)_2C_5H_2]_2SiMe_2Yb(OEt_2)$ (50 % probability ellipsoids) (3 unique molecules).

Table 1.2. Selected bond distances (Å) and bond angles (°) of diethyl ether adducts $Cp'_2Yb(OEt_2)$

Cp'	**1,3-$(Me_3C)_2C_5H_3$**	**Me_4C_5H**	***ansa*-[1,3-$(Me_3C)_2C_5H_2]_2SiMe_2$**	**Me_5C_5**[a]
Yb - C (mean)	2.71	2.68	2.71	2.69
Yb - C (range)	2.651(6) - 2.765(6)	2.53(2) - 2.79(2)	2.61(1) - 2.80(1)	2.66(1) - 2.729(7)
Yb - centroid	2.44	2.40	2.43	2.41
Yb - O	2.442(4)	2.52(1); 2.38(1)	2.44(1); 2.411(9); 2.36(1)	2.467(7)
centroid - Yb - centroid	131.8	132.7	123.8	140.6
intramolecular contact	none	3.21(2); 3.15(2)	3.14(1); 3.15(1); 3.00(1)	3.23(1)

a From ref. 20.

Data for unique molecules in the asymmetric unit presented as Yb(1); Yb(2); Yb(3).

The diethyl ether structures provide evidence that any available interaction will occur to reduce coordinative unsaturation in a bivalent ytterbocene. There is not enough room within the coordination sphere for a second diethyl ether ligand, so the Yb ··· γ-Me interaction occurs. In contrast, the ytterbocenes with the less-substituted cyclopentadienyl ligands $Me_3SiC_5H_4$ and $Me_3CC_5H_4$ coordinate two THF ligands.[27,28] Presumably this is due to the smaller size of both the cyclopentadienide ligand and the THF ligand in those complexes, as the disubstituted ytterbocene $[1,3\text{-}(Me_3Si)_2C_5H_3]_2Yb$ coordinates a single THF ligand,[11] along with the fully substituted $(C_5Me_5)_2Yb$.[6]

Synthesis and Structure of Base-free Ytterbocenes

The adduct $[1,3\text{-}(Me_3C)_2C_5H_3]_2Yb(OEt_2)$ can be desolvated by the toluene reflux method in a manner similar to that used to prepare $(Me_5C_5)_2Yb$ (Equation 6).[7] The resulting base-free ytterbocene is soluble in pentane and can be crystallized from that solvent at low temperature.

$$[1,3\text{-}(Me_3C)_2C_5H_3]_2Yb(OEt_2) \rightarrow [1,3\text{-}(Me_3C)_2C_5H_3]_2Yb + Et_2O \quad (6)$$

Bis(tetramethylcyclopentadienyl)ytterbium is fundamentally different from the other substituted ytterbocenes. The dark green etherate, $(Me_4C_5H)_2Yb(OEt_2)$, is relatively insoluble in pentane, while the etherates of the other ytterbocenes are soluble in that solvent. Dissolution of $(Me_4C_5H)_2Yb(OEt_2)$ in toluene and slow crystallization at -40°C

gives the base-free molecule. This is in stark contrast to the other ytterbocenes, which cannot be freed of coordinated diethyl ether by crystallization. The base-free $(Me_4C_5H)_2Yb$ can also be prepared by sublimation of the etherate. This also contrasts with $(Me_5C_5)_2Yb(OEt_2)$ and $[1,3\text{-}(Me_3Si)_2C_5H_3]_2Yb(OEt_2)$, which retain diethyl ether upon sublimation, although the ytterbocene $[1,3\text{-}(Me_3Si)_2C_5H_3]_2Yb$ can be desolvated by sublimation of the diethyl ether complex or by the toluene reflux method.[3] The THF adduct, $(Me_4C_5H)_2Yb(THF)_2$, is only sparingly soluble in toluene and diethyl ether, and does not sublime.[29] Base-free $(Me_4C_5H)_2Yb$ is completely insoluble in non-coordinating solvents including boiling toluene, while the other substituted base-free ytterbocenes are very soluble in solvents such as pentane. Table 1.3 summarizes some physical properties of the base-free ytterbocenes.

Table 1.3. Physical properties of base-free ytterbocenes

compound	**mp (°C)**	**color**	**density (calc)**	**ref.**
$(C_5H_5)_2Yb$	>400	red	2.38 g/cm^3	30
$(Me_5C_5)_2Yb$	189-191	brown-black	1.56 g/cm^3	7
$[1,3\text{-}(Me_3Si)_2C_5H_3]_2Yb$	119-121	purple	1.34 g/cm^3	3
$[1,3\text{-}(Me_3C)_2C_5H_3]_2Yb$	85-86	green-brown	1.40 g/cm^3	this work
$[1,2,4\text{-}(Me_3C)_3C_5H_2]_2Yb$	165 (dec.)	green-brown	1.31 g/cm^3	31, this work
$(Me_4C_5H)_2Yb$	324-326	pale green	1.71 g/cm^3	this work

The etherate *ansa*-[1,3-$(Me_3C)_2C_5H_2]_2SiMe_2Yb(OEt_2)$ cannot be desolvated by any of the reported methods. Attempted sublimation leads to the isolation of an insoluble brown solid, as does the toluene reflux method. The silicon - carbon bond can be broken relatively easily, as evidenced by its cleavage in the reaction of 1,3-$(Me_3Si)_2C_5H_4$ or *ansa*-[1,3-$(Me_3Si)_2C_5H_3]_2SiMe_2$ with sodium amide, and in the reaction of both of the *ansa*-tetraenes with potassium metal. The thermal decomposition of the *ansa*-bridge is thought to be occurring under the conditions used to remove the diethyl ether ligand.

Another technique that has been used to generate base-free ytterbocenes is the reaction of the cyclopentadiene with $Yb(N(SiMe_3)_2)_2$ in toluene solvent, which results in deprotonation of the cyclopentadiene to give the base-free metallocene (Equation 7).[32]

$$2Cp'H + Yb(N(SiMe_3)_2)_2 \rightarrow Cp'_2Yb + 2N(SiMe_3)_2H \quad (7)$$

However, in the case of *ansa*-[1,3-$(Me_3C)_2C_5H_3]_2SiMe_2$ no reaction occurs upon stirring overnight at room temperature. The *ansa*-bridged tetraene crystallizes from a pentane extract of the reaction mixture. This may imply that the protons on the *ansa*-tetraene are insufficiently acidic to be removed by the amide, or the rate may be slow.

The crystal structures of the base-free ytterbocenes $(C_5H_5)_2Yb$,[30] $(Me_5C_5)_2Yb$[7,13] and [1,3-$(Me_3Si)_2C_5H_3]_2Yb$[3] have previously been determined. The metallocenes all form polymeric chain structures but with different structural details. In $(C_5H_5)_2Yb$, the metallocene unit is a bent sandwich with a centroid - Yb - centroid angle of 118°. A

cyclopentadienide ring from an adjacent $(C_5H_5)_2Yb$ unit approaches the open side of the wedge, forming a one-dimensional chain structure. The chains are linked together by interchain Yb ··· H - C interactions with the terminal cyclopentadienide ligands. The structure is similar to that of $(C_5H_5)_2Ca$.[33]

The structure of $(Me_5C_5)_2Yb$ has been studied by gas-phase electron diffraction as well as X-ray crystallography.[7,34-36] In the gas phase, all intermolecular interactions are minimized and $(Me_5C_5)_2Yb$ is monomeric. The thermal average structure is a bent sandwich in which the centroid - Yb - centroid angle is 158°. Bis(pentamethylcyclopentadienyl)calcium is structurally similar in the gas phase, with a centroid - Ca - centroid angle of 154°.[36] In the solid state, $(Me_5C_5)_2Yb$ exists in two crystalline forms, one of which (the brown form) is a dimer isostructural to $(Me_5C_5)_2Sm$ and $(Me_5C_5)_2Eu$[37] and the other of which (the brown-black form) is a coordination polymer.[7] In each form, the metal center is stabilized by intermolecular interactions. The centroid - Yb - centroid angle of the brown-black form of $(Me_5C_5)_2Yb$ is somewhat lower in the solid state than in the gas phase at 145°,[7] and is similar to the centroid - metal - centroid angle of $(Me_5C_5)_2Ca$ (147°).[38]

In the solid state structure of $[1,3\text{-}(Me_3Si)_2C_5H_3]_2Yb$, the metallocene unit is also bent with a centroid - Yb - centroid angle of 138°.[3] A chain structure of Yb ··· Me - Si interactions results in a linear coordination polymer. The structure of $[1,3\text{-}(Me_3Si)_2C_5H_3]_2Eu$ is similar.[3]

The strength of the intermolecular interactions in both forms of $(Me_5C_5)_2Yb$ and $[1,3\text{-}(Me_3Si)_2C_5H_3]_2Yb$ as well as the calcium, samarium and europium analogues is obviously weak; it must be on the order of solvation energies, since the compounds are hydrocarbon soluble. In contrast, the intermolecular interactions of $(C_5H_5)_2Yb$ are much stronger and result in the high melting point and insolubility of this coordination polymer.

The twist angle of a metallocene is defined as the mean value of the five angles between a ring carbon atom on the upper ring and the closest one on the lower ring. The angles are measured between the planes defined by the two centroids and each ring carbon atom. Thus, it can vary from zero (perfectly eclipsed), in which the rings lie directly above one another, to 36° (completely staggered), in which the plane containing the lower carbon atom bisects the 72° angle between two carbon atoms of the upper ring. In the decamethylmetallocenes of ytterbium, samarium and europium, the twist angle is found to be between staggered and eclipsed. It has been suggested that deviations from a staggered twist angle of 36° indicate that the observed carbon - carbon distances that are smaller than the sum of the van der Waals radii at the back side of the metallocene wedge cannot be repulsive, because if they were the rings would be expected to rotate to minimize the repulsion.[37] One hypothesis that has been advanced to explain the bending in these molecules, which is observed in the gas phase as well as the solid state, is that there are favorable van der Waals attractions at the back side of the metallocene wedge.[34-36] Close back side interactions are also observed in the structures of the molecules determined in this work, all of which have bent sandwich structures.

From a structural perspective, $[1,3\text{-}(Me_3C)_2C_5H_3]_2Yb$ is simpler than the previously reported ytterbocenes. An ORTEP diagram is shown in Figure 1.5. As indicated in Table 1.4, it is a bent metallocene with a centroid - metal - centroid angle of 147°, an average Yb - C (ring) distance of 2.66 Å and an average Yb - centroid distance of 2.37 Å. There is no intermolecular Yb ··· C contact distance less than 4.0 Å and this ytterbocene is monomeric in the solid state. There are, however, two short intramolecular Yb ··· C contact distances of 3.09(1) Å and 3.20(2) Å, to C(24) and C(20) respectively. These are methyl carbon atoms located on two different Me_3C groups on one ring. As these groups are separated by a methine carbon on the ring, they approach the Yb atom from opposite sides of the wedge.

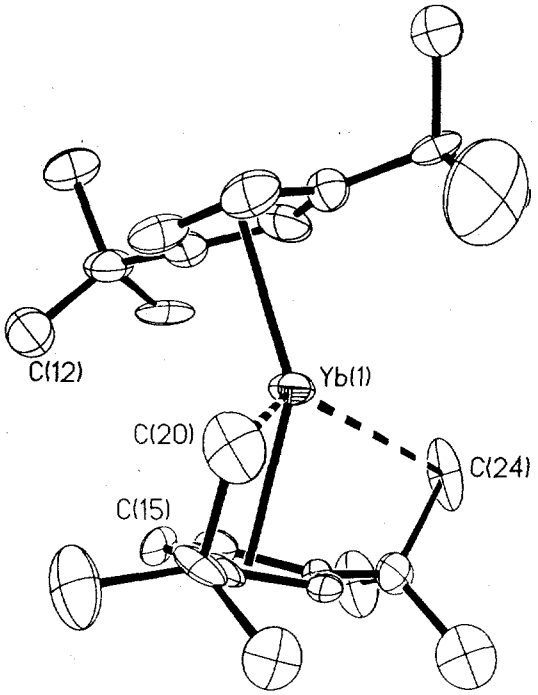

Figure 1.5. ORTEP diagram of $[1,3\text{-}(Me_3C)_2C_5H_3]_2Yb$ (50% probability ellipsoids).

In this structure, the twist angle of the rings is 19°, which allows the Me_3C groups on one ring to avoid those on the other ring. On the back side of the wedge, the methine carbon atom C(15) approaches a methyl carbon atom C(12) from a Me_3C group on the other ring at a distance of 3.87 Å.

It is informative to compare the solid state crystal structure of $[1,3\text{-}(Me_3C)_2C_5H_3]_2Yb$ with that of $[1,3\text{-}(Me_3Si)_2C_5H_3]_2Yb$.[3] In the Me_3Si analogue, the centroid - metal - centroid angle is 138°, 9° more bent than in the Me_3C analogue. The Yb - C (ring) and Yb - centroid distances are the same for the two molecules. In $[1,3\text{-}(Me_3Si)_2C_5H_3]_2Yb$, the small centroid - metal - centroid angle allows a close intermolecular contact between a Me_3Si carbon atom on one metallocene unit and the Yb atom of a neighboring unit of 2.872(7) Å, which results in a coordination polymer. An intermolecular interaction is presumably prevented in the Me_3C derivative since the centroid - metal - centroid angle cannot be smaller than its value of 147° without unfavorable back side steric interactions between the Me_3C groups, so the metal is effectively shielded from adjacent molecules.

The structure of $[1,2,4\text{-}(Me_3C)_3C_5H_2]_2Yb$ has also been determined and is shown in Figure 1.6, while important bond distances and angles are included in Table 1.4.[31] The compound crystallizes with two unique molecules in the unit cell. The two molecules are very similar, having centroid - metal - centroid angles of 165° and 168°, respectively, and eclipsed cyclopentadienide rings. The slightly open metallocene sandwich accommodates the two Me_3C groups that are forced to lie above one another in the eclipsed conformation. The eclipsed conformation is predicted for the trisubstituted

cyclopentadienide rings, as it allows four of the substituents to be arranged opposite gaps in substituents on the other ring. There are no intermolecular contacts of less than 4.0 Å between either ytterbium atom and carbon atoms of adjacent molecules. However, similar to the structure of $[1,3\text{-}(Me_3C)_2C_5H_3]_2Yb$, there are intramolecular contacts of less than 3.5 Å between the ytterbium and methyl carbon atoms in each molecule. In molecule 1, Yb(1) ··· C(16) is 3.47 Å and Yb(1) ··· C(30) is 3.40 Å; in molecule 2, Yb(2) ··· C(64) is 3.47 Å. These distances are somewhat greater than the corresponding distances o f 3. 09(1) a nd 3. 20(2) found in the disubstituted metallocene. This can be attributed to the extreme steric bulk of the ligands in this molecule, which cause the large centroid - metal - centroid angle; further bending would result in unfavorable steric interactions at the back side of the wedge. In typical bent metallocenes, the metal center is exposed in the open part of the wedge, while in this molecule the metal lies between the two cyclopentadienide rings. Molecule 1 has no back side interactions less than 4.0 Å, while the distance C(42) - C(53) in molecule 2 is 3.91 Å.

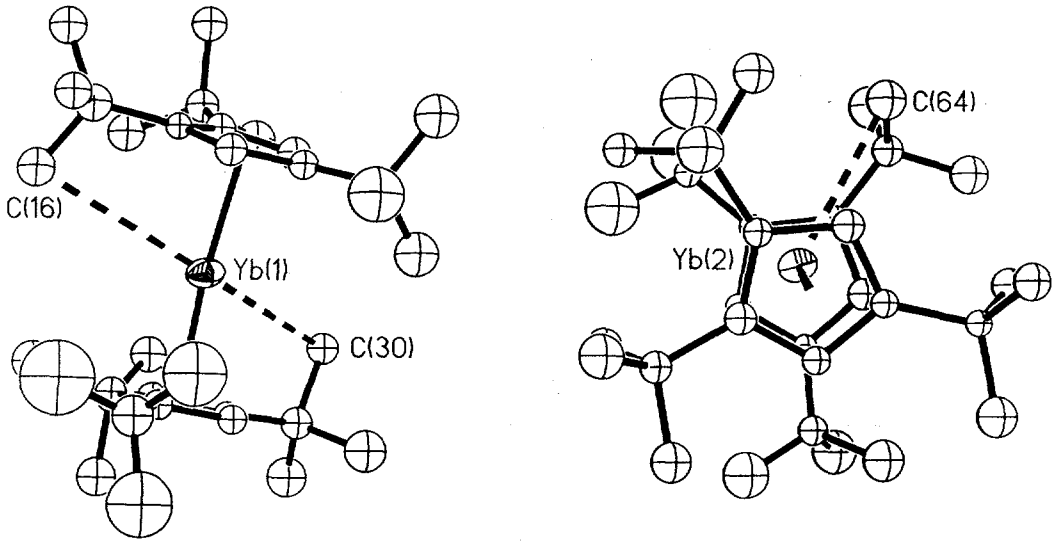

Figure 1.6. ORTEP diagram of $[1,2,4\text{-}(Me_3C)_3C_5H_2]_2Yb$ (50% probability ellipsoids) (2 unique molecules).

The solid state crystal and molecular structure of $(Me_4C_5H)_2Yb$, shown in Figure 1.7, indicates that the metallocene is a bent sandwich polymer. The individual $(Me_4C_5H)_2Yb$ units are bent with a centroid - metal - centroid angle of 132°, which is 13° more bent than the corresponding angle in $(Me_5C_5)_2Yb$. The average Yb - C (ring) distance of 2.69 Å and the Yb - centroid distance of 2.41 Å in $(Me_4C_5H)_2Yb$ are about 0.03 Å longer than the equivalent values found in $(Me_5C_5)_2Yb$. The range in Yb - C (ring) distances is much greater in $(Me_4C_5H)_2Yb$, 2.60(1) - 2.733(9) Å compared with 2.636(3) - 2.690(3) Å in $(Me_5C_5)_2Yb$. These differences result from the fact that the compound is polymeric with one ring forming a $\mu\text{-}\eta^5, \eta^1\text{-}Me_4C_5H$ bridge.

The bridging ring (C(1) - C(5)) connects the Yb atoms in the polymer chain. All Yb - C distances are equal (2.72(2) Å) in this ring. The shortest intermolecular ytterbium - carbon distance in the molecule (2.81(1) Å) involves the methine atom C(1) of this ring. The hydrogen atom H(1) bound to C(1) was located as the largest peak in the difference map but was not refined. This atom is bent out of the ring plane by 0.21 Å towards the Yb(1) atom of the molecule, away from the Yb(1B) atom involved in the close intermolecular contact. The Yb(1B) ··· H(1) distance is 3.04 Å and the Yb(1B) ··· C(1) - H(1) angle is 91°. This distortion seems to be the result of the Yb(1B) atom seeking the negative electron density at the methine site while pushing the H(1) atom out of the plane of the growing chain in a form of incipient rehybridization. The Yb(1B) ··· C(1) distance of 2.81(1) Å is 0.13 Å smaller than any intermolecular contact distance in the case of $(Me_5C_5)_2Yb$(black), and is only 0.08 Å longer than the longest intramolecular Yb - C (ring) distance in the structure of $(Me_4C_5H)_2Yb$. Hence, the ytterbium atom can be thought of as bis-η^5,η^1-coordinated, and this is presumably the reason for the low solubility of this ytterbocene.

The terminal ring (C(10) - C(14)) is nearly planar but is not symmetrically bound to the ytterbium atom, having two short Yb - C distances (Yb - C(10), 2.60(1) Å and Yb - C(14), 2.62(1) Å) and three longer ones (Yb - C(11), 2.67(1) Å, Yb - C(13), 2.70(1) Å and Yb - C(12), 2.71(1) Å). Atom C(10) is the methine carbon atom of that ring and participates in a n int ermolecular c ontact o f 3. 36(1) Å w ith C (3), a qua ternary c arbon atom on the bridging ring of an adjacent molecule.

The rings of $(Me_4C_5H)_2Yb$ are almost completely staggered (twist angle 31°) in a bent analogy to octamethylferrocene.[39,40] The closest back side distance is C(1) ··· C(17) 3.68 Å, which again is shorter than the sum of the van der Waals radii.

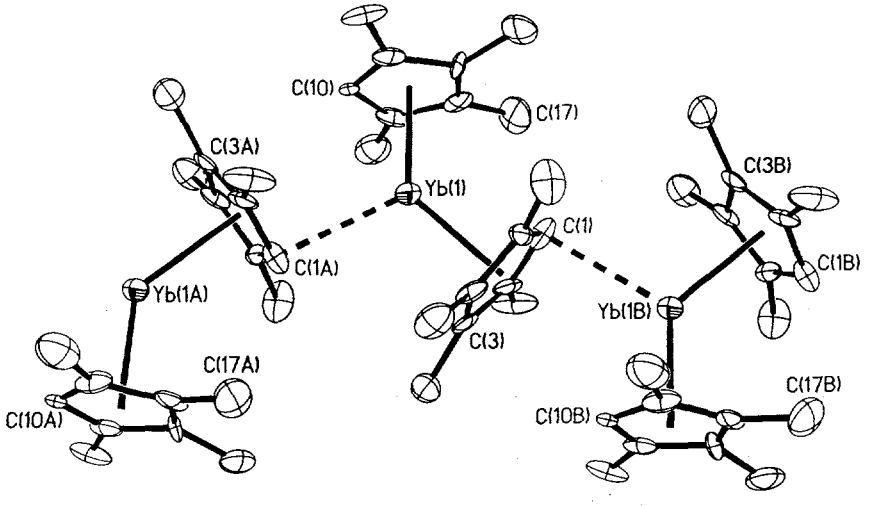

Figure 1.7. ORTEP diagram of $(Me_4C_5H)_2Yb$ (50% probability ellipsoids).

In the condensed phase, the intermolecular interactions observed for all of the ytterbocenes have the effect of compressing the centroid - metal - centroid angle relative to the gas phase value found for $(Me_5C_5)_2Yb$ of 158°.[36] The angle in these coordination oligomers is similar to that found in ytterbocene - Lewis base adducts.[6,24,25] This suggests that the base-free metallocenes associate to higher aggregates in order to maximize their bonding interactions. In every case except molecule 1 of [1,2,4-

$(Me_3C)_3C_5H_2]_2Yb$, there are intramolecular carbon - carbon distances on the back side of the wedge that are less than the sum of the van der Waals radii (4.0 Å) (Table 1.4).

The overall packing geometry is dependent on the substituents on the rings and how the molecules arrange to maximize the bonding interactions and minimize the steric repulsions between various groups.[41] The calculated densities of the molecules give some indication of how efficiently the structures are packed; $(Me_4C_5H)_2Yb$ has a density of 1.71 g/cm^3, which is greater than the densities of the other substituted ytterbocenes (Table 1.3). The higher calculated density is consistent with the insolubility and very close Yb ··· C interaction found in $(Me_4C_5H)_2Yb$. The trend in melting points of the ytterbocenes is also consistent with the observed intermolecular interactions; $(Me_4C_5H)_2Yb$ melts above 300°C while $[1,3\text{-}(Me_3C)_2C_5H_3]_2Yb$ melts below 100°C (Table 1.3).

Table 1.4. Selected bond lengths (Å) and bond angles (°) for brown-black form of $(Me_5C_5)_2Yb$, $[1,3\text{-}(Me_3C)_2C_5H_3]_2Yb$, $[1,2,4\text{-}(Me_3C)_3C_5H_2]_2Yb$ and $(Me_4C_5H)_2Yb$

compound	**$(Me_5C_5)_2Yb$[a]**	**$[1,3\text{-}(Me_3C)_2C_5H_3]_2Yb$**	**$[1,2,4\text{-}(Me_3C)_3C_5H_2]_2Yb$**	**$(Me_4C_5H)_2Yb$**
Yb - C (ring) (mean)	2.66; 2.67	2.66	2.67	2.69
Yb - C (ring) (range)	2.636(3) - 2.690(3)	2.628(9) - 2.70(1)	2.64 - 2.72	2.60(1) - 2.733(9)
Yb - centroid	2.38; 2.38	2.37	2.38; 2.38	2.41
centroid - Yb – centroid	146; 145	147	168; 165	132
twist angle	21; 25	19	2; 1	31
back side distance	3.49; 3.68	3.87	none; 3.91	3.68
non-bonded distances	2.944(4); 3.078(4)	3.09(1), 3.20(2)	3.40; 3.47	2.81(1)

a From ref. 7.

Data for two unique molecules in the asymmetric unit presented as Yb(1); Yb(2).

The net effect of the approach of a carbon atom to the ytterbium atom is to increase the coordination number of the metal and therefore its effective radius. This correlation can be seen in the data for each structure. An increase in the ytterbium to ring carbon distance, as well as the ytterbium - centroid distance, is correlated with a larger number of shorter metal to non-ring carbon interactions, which involve an increase in coordination number (Table 1.4). A larger effective metal radius means that to achieve the optimum van der Waals distance on the back side of the wedge of approximately 4.0 Å, the centroid - metal - centroid angle can be smaller than for a smaller effective metal radius. In other words, the incoming atoms involved in the close contacts push the rings out of the way and open the wedge.

Variation of the ring substituents while maintaining the back side C ··· C distance affects the centroid - metal - centroid angle. The most dramatic example of this is $(Me_4C_5H)_2Yb$, in which the angle is bent back to 132°. The reason for this is that the back side close contact in that molecule is between a methyl carbon atom and a methine carbon atom. In $[1,3\text{-}(Me_3Si)_2C_5H_3]_2Yb$, the small centroid - metal - centroid angle of 138° is possible due to a back side contact between the two methine carbon atoms. In the other molecules, the back side contact does not involve a methine carbon atom, so the angle is greater.

Optical Spectroscopy

The absorptions observed in the optical spectra of the base-free metallocenes from 1000 - 350 nm are listed in Table 1.5. The transitions of the ytterbocenes have been assigned on the basis of the calculated transition energies of $(C_5H_5)_2Yb$ in D_{5d} symmetry, as discussed in the Introduction. These energies are valid in the bent sandwich since the ground state energy does not change much on bending to C_{2v} symmetry.[42,43] The highest wavelength transition is the HOMO → LUMO ($e_{1u} \rightarrow a_{1g}$ orbitals in D_{5d} symmetry) and is predicted to occur at about 750 nm. This transition is responsible for the orange color of $(Me_5C_5)_2Yb$ and is observed at 751 nm in methylcyclohexane, indicating that the prediction is accurate for the closed-shell ytterbium system. The next lower wavelength transitions are predicted to occur at about 460 nm and 390 nm, due to the Cp(π) → LUMO ($e_{1u} \rightarrow a_{1g}$, LMCT) and the $f \rightarrow d$ ($e_{2u} \rightarrow e_{2g}$) transitions, respectively.[42] These transitions are observed at 515 nm, 474 nm and 429 nm. Three rather than two absorptions are observed, possibly due to the reduction in symmetry from D_{5d} to C_{2v}, which removes the orbital degeneracies. The average observed energy of these three bands is 473 nm, which is close to the average calculated value of 425 nm for $(C_5H_5)_2Yb$, so the predicted transition energies are in good agreement with the observed values.

The HOMO - LUMO and $f \rightarrow d$ absorptions involve transitions between *f*- and *d*-orbitals, which do not mix in D_{5d} symmetry. As the metallocenes bend and the symmetry is lowered to C_{2v}, mixing of the *f*- and *d*-orbitals occurs; however, the transitions are still electric dipole allowed, and the energy changes along with the color of the compound.

As described in the Introduction, the principal change that is predicted to occur on bending an ytterbocene is an increase in the HOMO - LUMO gap,[42] which corresponds to a blue-shift of the HOMO → LUMO transition. This prediction provides a possible explanation for the blue shift of 15 nm in the HOMO → LUMO transition of $(Me_5C_5)_2Yb$ from 751 nm to 736 nm on changing the solvent from methylcyclohexane to toluene, if the average geometry of the ytterbocene is more bent in aromatic solvents than in aliphatic ones (Figure 1.8; Table 1.5). This seems reasonable as toluene is a better electron donor than its saturated analogue, and toluene is known to inhibit ethylene polymerization by $(Me_5C_5)_2Yb$.[7]

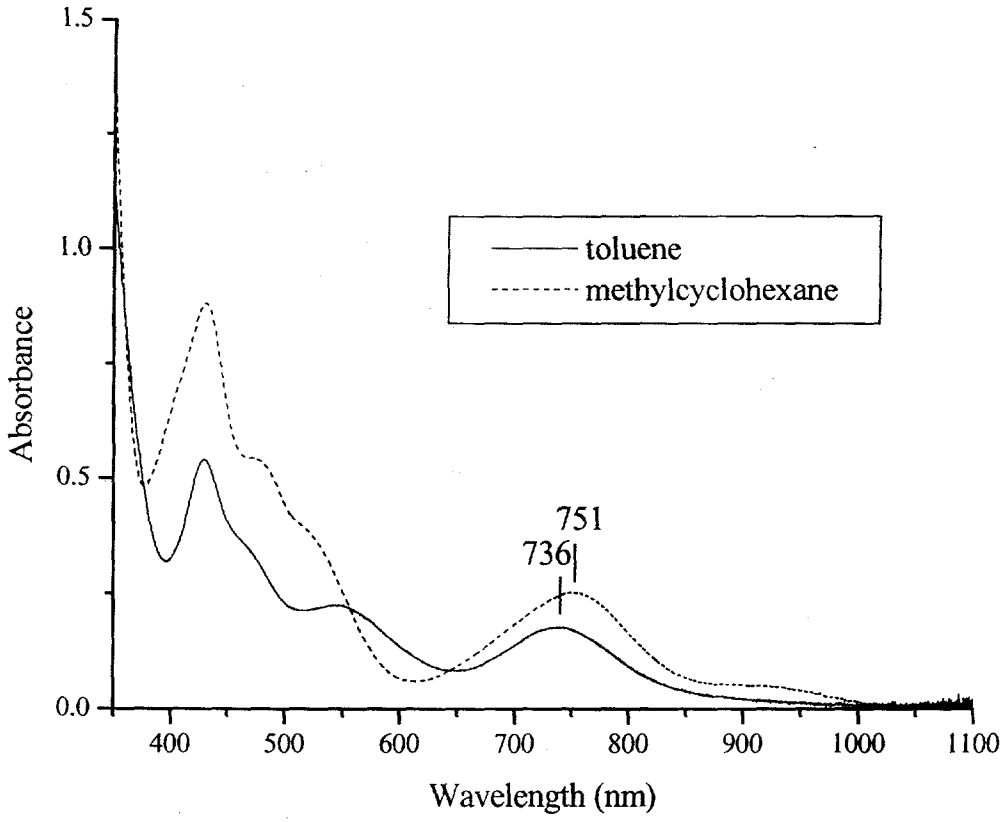

Figure 1.8. Optical spectra of $(Me_5C_5)_2Yb$ in methylcyclohexane and toluene.

Bis(pentamethylcyclopentadienyl)samarium and -europium were also studied by optical spectroscopy (Figure 1.9). The transitions for $(Me_5C_5)_2Sm$ in methylcyclohexane occur as a broad unresolved band from 820 - 560 nm. In toluene, these transitions are shifted and better resolved, with the lowest-energy band being shifted to still lower energy (903 nm), and the higher energy bands being shifted to higher energy. According to the model proposed for $(Me_5C_5)_2Yb$, a band that shifts to higher energy on changing the solvent from aliphatic methylcyclohexane to aromatic toluene is the HOMO $\rightarrow$ LUMO

transition, as bending the metallocene in aromatic solvent increases the HOMO - LUMO gap.

Green and Rösch predict a transition for $(C_5H_5)_2Eu$ at 850 nm although they acknowledge that the large spin-polarization effects of the open shell ($4f^7$) electronic configuration make the calculated transition energy less accurate than for the closed shell case.[42] No low-energy transition is observed in the optical spectrum of $(Me_5C_5)_2Eu$; the longest wavelength absorption occurs at 580 nm and there is a broad unresolved band from 510 - 350 nm. The spectrum of this molecule does not change significantly upon varying the solvent from methylcyclohexane to toluene. This suggests that either the observed transitions are not affected by bending the molecule, or that the molecule does not change geometry significantly upon changing the solvent. This is somewhat surprising, given that the transitions of $(Me_5C_5)_2Sm$ are affected by varying the solvent.

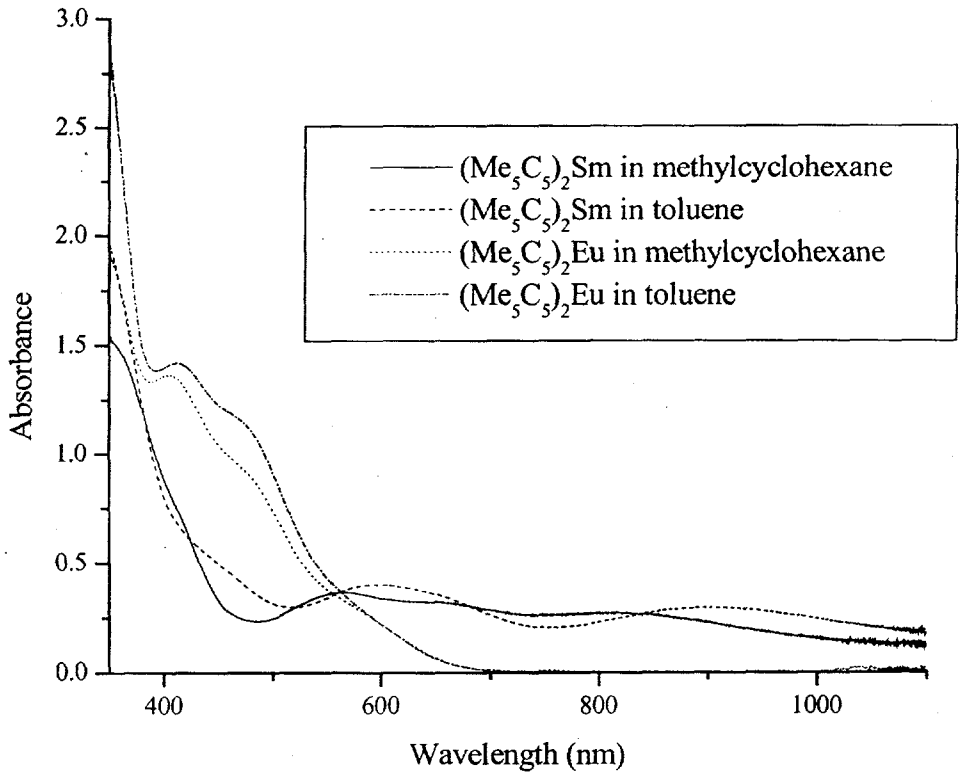

Figure 1.9. Optical spectra of $(Me_5C_5)_2Sm$ and $(Me_5C_5)_2Eu$ in methylcyclohexane and toluene.

The highest wavelength transitions of $[1,3\text{-}(Me_3C)_2C_5H_3]_2Yb$, $[1,2,4\text{-}(Me_3C)_3C_5H_2]_2Yb$ and $[1,3\text{-}(Me_3Si)_2C_5H_3]_2Yb$ in methylcyclohexane, at 655 nm, 675 nm and 648 nm, respectively, can be assigned as their HOMO $\rightarrow$ LUMO transitions using the Rösch-Green model (Figure 1.10).[42] The transitions in these metallocenes are blue shifted by about 100 nm (2 000 cm^{-1}) relative to $(Me_5C_5)_2Yb$. Their lower bands are observed at exactly the energies predicted for $(C_5H_5)_2Yb$, 460 and 390 nm. The similarity of the transitions in the two disubstituted ytterbocenes is surprising since the steric and

electronic effects of Me_3C and Me_3Si are quite different; Me_3C has a larger cone angle and is a better donor than Me_3Si. One explanation for the similar spectra is that the molecules have similar sandwich structures in methylcyclohexane, which are more bent than the structure of $(Me_5C_5)_2Yb$. This accounts for the nearly identical energies of their HOMO $\rightarrow$ LUMO transitions in solution. It also accounts for the purple solid [1,3-$(Me_3Si)_2C_5H_3]_2Yb$ (centroid - metal - centroid angle 138°[3]) becoming olive-brown when it is dissolved in methylcyclohexane. The red shift results when the bend angle becomes larger in solution, as the molecule is no longer constrained by the intermolecular interactions of the solid state. According to this argument, the trisubstituted complex [1,2,4-$(Me_3C)_3C_5H_2]_2Yb$ must have a more parallel ring structure in solution than the disubstituted complexes, as its HOMO $\rightarrow$ LUMO transition occurs at lower energy. This is consistent with the large centroid - metal - centroid angle observed in the solid state structure of this complex (165°). The bulky ligands make it impossible for the molecule to bend even in the absence of solid state interactions.

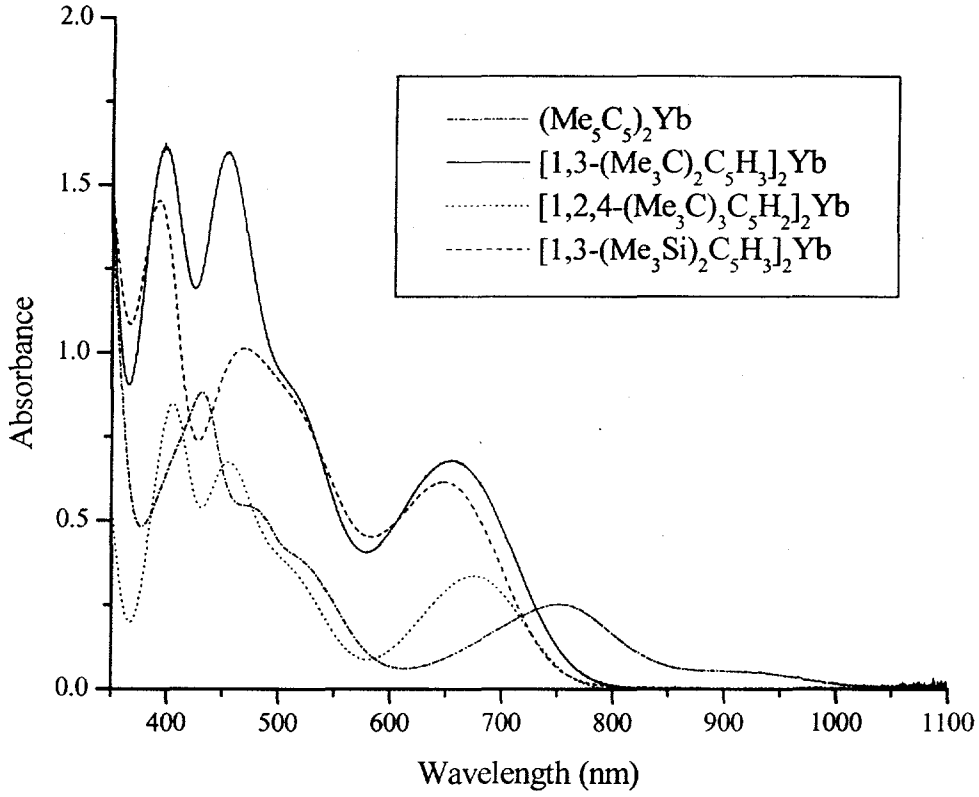

Figure 1.10. Optical spectra of $(Me_5C_5)_2Yb$, $[1,3\text{-}(Me_3C)_2C_5H_3]_2Yb$, $[1,2,4\text{-}(Me_3C)_3C_5H_2]_2Yb$ and $[1,3\text{-}(Me_3Si)_2C_5H_3]_2Yb$ in methylcyclohexane.

Table 1.5. Optical spectra of base-free lanthanide metallocenes (in methylcyclohexane unless specified)

compound	**λ_{max} in nm (ε in $Lmol^{-1}cm^{-1}$)**
$(Me_5C_5)_2Yb$	751 (173), 515 (277), 474 (374), 429 (610)
$(Me_5C_5)_2Yb$ in toluene	736 (221), 547 (277), 429 (665)
$(Me_5C_5)_2Sm$	819 (167), 657 (198), 568 (223)
$(Me_5C_5)_2Sm$ in toluene	903 (194), 650 (220), 595 (259)
$(Me_5C_5)_2Eu$	581 (144), 470 (441), 402 (636)
$(Me_5C_5)_2Eu$ in toluene	565 (162), 470 (521), 410 (638)
$[1,3\text{-}(Me_3C)_2C_5H_3]_2Yb$	655 (228), 453 (537), 396 (540)
$[1,2,4\text{-}(Me_3C)_3C_5H_2]_2Yb$	675 (286), 455 (564), 405 (716)
$[1,3\text{-}(Me_3Si)_2C_5H_3]_2Yb$	648 (244), 468 (404), 392 (584)

The optical spectra of the diethyl ether and THF complexes have also been measured and the data are presented in Table 1.6. The only complex measured for which the HOMO → LUMO transition of the ether complex is significantly different from that of the base-free molecule is $(Me_5C_5)_2Yb$, whose HOMO → LUMO transition changes from 751 nm to 690 nm with diethyl ether ligand. The colors and HOMO → LUMO transitions of the THF complexes vary more widely; some are bright green while others are red. These observations can be rationalized according to the Rösch-Green model as follows.[42]

When a 1:1 or 1:2 adduct of a metallocene forms, the resulting angle of the bent sandwich is smaller than in the base-free complex. Electronically, the donor ligands interact with the empty a_1 (a_1 and b_2 in a 1:2 adduct) (C_{2v} symmetry) orbitals, stabilizing the filled bonding orbitals and destabilizing the empty antibonding ones. The net result of adduct formation is therefore to raise the LUMO orbital in energy as described in the Introduction. However, the filled orbitals, including the HOMO, are also increased somewhat in energy since adding electron density raises their energy (Figure 1.11). This destabilization can be thought of as arising from the electron - electron repulsion within the *f*-orbitals in the closed shell, $4f^{14}$ Yb(II). This effect is not expected to be large, however, as the nephelauxetic effects for the lanthanides are of similar magnitude as for the *d*-transition metals, and cause a decrease in electron - electron repulsion due to the expanded *f*-orbitals.[44] Thus, the net effect on the HOMO $\rightarrow$ LUMO transition of adduct formation could be either a blue or a red shift depending on the extent of bending and the extent of electron - electron repulsion due to net electron donation from the added ligands.

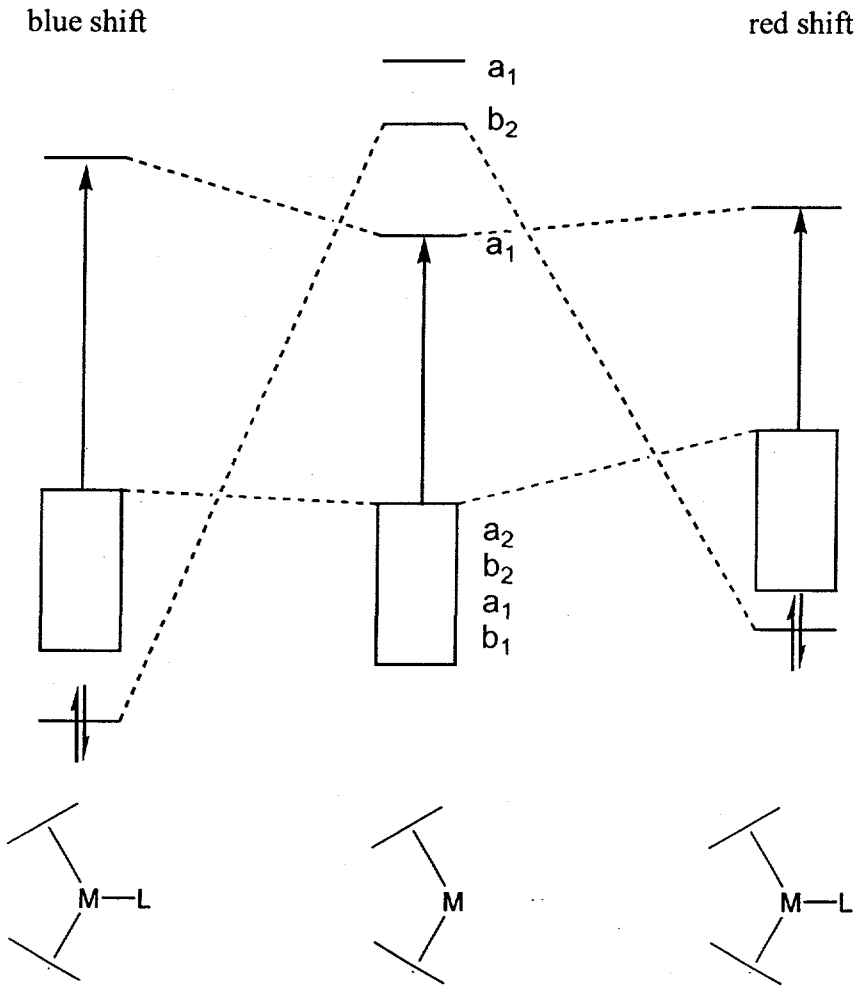

Figure 1.11. Schematic energy diagram showing the possible effects of an additional ligand on the energies of the molecular orbitals and the HOMO → LUMO transition of a bent metallocene.

Table 1.6. Optical spectra of ytterbocene, samarium and europium etherates (in methylcyclohexane unless specified)

compound	λ_{max} **in nm (ε in Lmol^{-1}cm^{-1})**
$(Me_5C_5)_2Yb(OEt_2)$	690 (216), 472 (356), 407 (435)
$(Me_5C_5)_2Yb(OEt_2)$ in toluene	686 (251), 449 (429), 393 (537)
$(Me_5C_5)_2Yb(THF)_2$	800 (266), 513 (437), 448 (533)
$(Me_5C_5)_2Yb(THF)$	801 (217), 513 (355), 447 (450)
$[1,3\text{-}(Me_3C)_2C_5H_3]_2Yb(OEt_2)$	655 (211), 455 (480), 397 (486)
$[1,3\text{-}(Me_3C)_2C_5H_3]_2Yb(THF)$	654 (188), 477 (395), 387 (366)
$[1,3\text{-}(Me_3C)_2C_5H_3]_2Yb(THF)$ in THF	641 (190), 467 (400), 386 (400)
$(Me_4C_5H)_2Yb(OEt_2)$	683 (186), 468 (294), 401 (382)
$(Me_4C_5H)_2Yb(THF)_2$	785 (107), 514 (230), 439 (280)
$(Me_4C_5H)_2Yb(THF)$	780 (146), 511 (286), 440 (353)
ansa-$[1,3\text{-}(Me_3C)_2C_5H_2]_2SiMe_2Yb(OEt_2)$	664 (199), 460 (410), 399 (552)
ansa-$[1,3\text{-}(Me_3C)_2C_5H_2]_2SiMe_2Yb(THF)_2$	676 (152), 490 (376), 378 (497)
ansa-$[1,3\text{-}(Me_3C)_2C_5H_2]_2SiMe_2Yb(THF)_2$ in toluene	670 (142), 484 (351), 375 (453)
$[1,3\text{-}(Me_3Si)_2C_5H_3]_2Yb(OEt_2)$	653 (216), 477 (333), 392 (466)
$[1,3\text{-}(Me_3Si)_2C_5H_3]_2Yb(THF)$	678 (161), 494 (252), 399 (292)
$(Me_5C_5)_2Sm(OEt_2)$	762 (229), 706 (232), 506 (262)
$(Me_5C_5)_2Sm(OEt_2)$ in toluene	764 (148), 684 (163), 497 (183)
$(Me_5C_5)_2Eu(OEt_2)$	565 (143), 465 (385), 400 (428)

The blue-shift of the HOMO → LUMO transition of $(Me_5C_5)_2Yb(OEt_2)$ in methylcyclohexane relative to the base-free molecule of 61 nm implies that the effect of bending is more important in this complex than electron - electron repulsion. In toluene, the HOMO → LUMO transition of $(Me_5C_5)_2Yb(OEt_2)$ (686 nm) is similarly blue shifted by 50 nm relative to base-free $(Me_5C_5)_2Yb$ in toluene (736 nm). A slightly different value, 670 nm, has been reported as the lowest energy absorption band for $(Me_5C_5)_2Yb(OEt_2)$ in toluene;[45,46] only the values found in this study will be used for comparison as the conditions and instrumentation are identical. For the other two molecules for which both the ether complex and the base-free complex were studied, $[1,3\text{-}(Me_3C)_2C_5H_3]_2Yb$ and $[1,3\text{-}(Me_3Si)_2C_5H_3]_2Yb$, the HOMO → LUMO transition occurs at the same energy with or without the diethyl ether ligand. This illustrates the balance between the effects of bending and electron - electron repulsion.

The ytterbocene diethyl ether complexes all have very similar spectra, with the HOMO → LUMO transition varying only slightly from 690 nm for $(Me_5C_5)_2Yb(OEt_2)$ to 653 nm for $[1,3\text{-}(Me_3Si)_2C_5H_3]_2Yb(OEt_2)$ (Figure 1.12). Again, this trend can be attributed to the higher bend angle maintained by the disubstituted complexes in solution. Although the solid state structure of $[1,3\text{-}(Me_3Si)_2C_5H_3]_2Yb(OEt_2)$ is not known, it is presumably similar to that of $[1,3\text{-}(Me_3C)_2C_5H_3]_2Yb(OEt_2)$ as their solution optical spectra are the same. It is interesting that the complex $(Me_4C_5H)_2Yb(OEt_2)$ exhibits a HOMO → LUMO transition at 683 nm, close to that for the penta-substituted analogue, given that in the solid state it has a low bend angle of 133° which is more like that of the disubstituted

[1,3-$(Me_3C)_2C_5H_3]_2Yb(OEt_2)$ (132°) than $(Me_5C_5)_2Yb(OEt_2)$ (141°). An explanation for this behavior is that, in solution, the rings of the complex $(Me_4C_5H)_2Yb(OEt_2)$ are not constrained as they are in the solid state so that the averaged solution structure is similar to that of $(Me_5C_5)_2Yb(OEt_2)$. The *ansa*-bridged complex has a much lower centroid - metal - centroid angle in the solid state and presumably in solution also, yet it has a HOMO $\rightarrow$ LUMO transition that is similar to those of the other ytterbocene - ether adducts. Presumably, the sterically accessible metal center leads to greater electron - electron repulsion, so the transition is red-shifted relative to the unbridged disubstituted ytterbocenes. The two high energy transitions are the same for all of the ytterbocene ether complexes, at 465 and 400 nm, which indicates that the $f \rightarrow d$ and LMCT transitions are insensitive to the ligand environment.

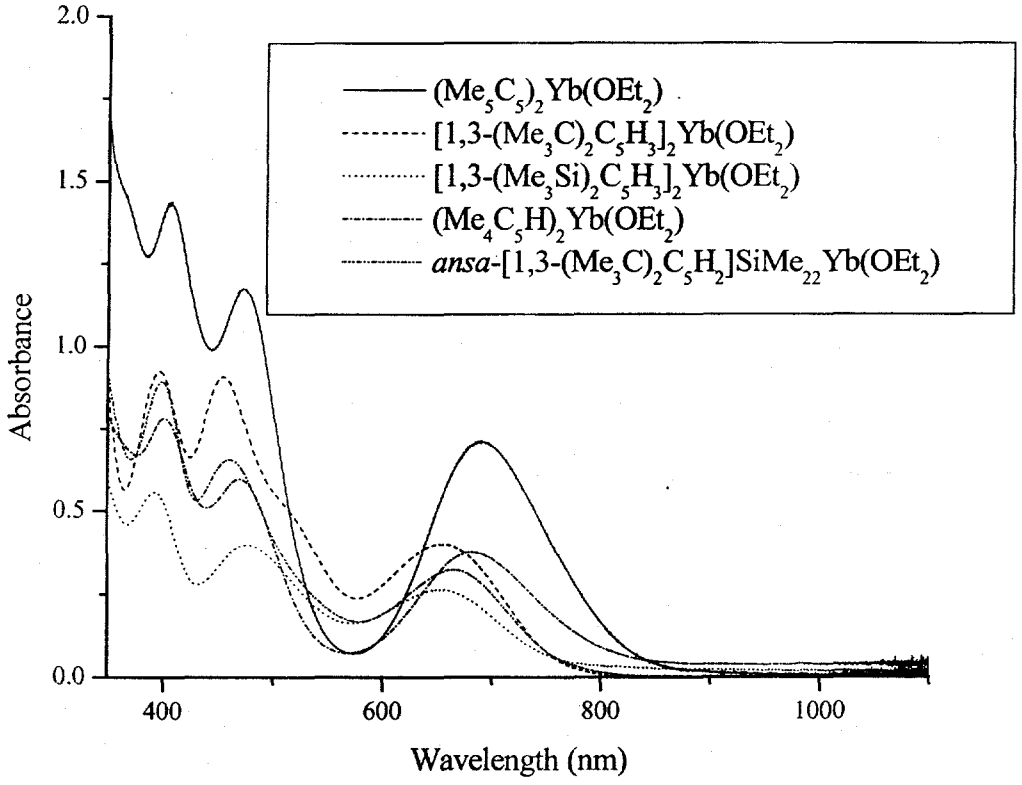

Figure 1.12. Optical spectra of diethyl ether adducts of ytterbocenes in methylcyclohexane.

The colors and transitions of the THF complexes are less readily explained. The complex $(Me_5C_5)_2Yb(THF)$ crystallizes from toluene as bright red crystals with half an equivalent of toluene of crystallization.[6] However, in THF solvent the molecule is thought to have two equivalents of THF per metal center, $(Me_5C_5)_2Yb(THF)_2$, and a red molecule containing two equivalents of THF, by integration of the ^1H NMR spectrum, can be crystallized from pentane solvent. The slightly less substituted analogue $(Me_4C_5H)_2Yb(THF)_2$ crystallizes with two equivalents of THF from diethyl ether, and is

also red. This molecule has been reported in low yield crystallized from THF.[29] Crystallization from toluene yields a molecule that, by integration of the ^{1}H NMR spectrum, contains a single THF molecule per ytterbium atom and is also bright red. In contrast, the molecule $[1,3\text{-}(Me_3C)_2C_5H_3]_2Yb(THF)$ contains a single THF ligand whether crystallized from diethyl ether or toluene and is green, with an optical spectrum that is not dissimilar from the diethyl ether adduct (Table 1.6, Figure 1.13). The brown Me_3Si analogue also has a single THF ligand, $[1,3\text{-}(Me_3Si)_2C_5H_3]_2Yb(THF)$.[11] When dissolved in THF, this complex changes color to bright purple, but an adduct containing more than one equivalent of THF cannot be obtained by crystallization. Presumably, the steric bulk of the disubstituted cyclopentadienide rings leads to the 7- rather than 8-coordinate complexes in the solid state. The sterically less-encumbered, and electronically more exposed *ansa*-$[1,3\text{-}(Me_3C)_2C_5H_2]_2SiMe_2Yb(THF)_2$ crystallizes with two equivalents of THF as red needles. Dissolution of this compound in aromatic solvent gives green solutions, which can be recrystallized to give the same red product.

Thus, the ytterbocenes with two equivalents of THF are all red, while those with a single THF ligand vary from green to brown to red, depending on the substituents on the cyclopentadienide rings. In the solid state, the bend angle of an ytterbocene complex with two ethereal ligands is no different from that of a complex with only one.[11] It is therefore tempting to suggest that the red color of the ytterbocenes with two equivalents of THF results from a red-shift in the HOMO $\rightarrow$ LUMO transition due to increased electron - electron repulsion from the second ligand, which raises the energy of the HOMO, while the LUMO is not strongly affected as the bend angle is not changed.

However, the optical spectra of the complexes which can be crystallized with either one or two equivalents of THF are identical, regardless of the stoichiometry deduced from the ^{1}H NMR spectra (Table 1.6). This suggests that the second THF is not bound to the metal in solution, and exchanges rapidly on the NMR timescale. No crystal structures have been obtained for these complexes, and the reported structures of ytterbocenes bound to two THF ligands involve less-substituted cyclopentadienide rings.[27,28] Thus, the differences in color must result from the balance of electron - electron repulsion with the bend angle of the ytterbocene.

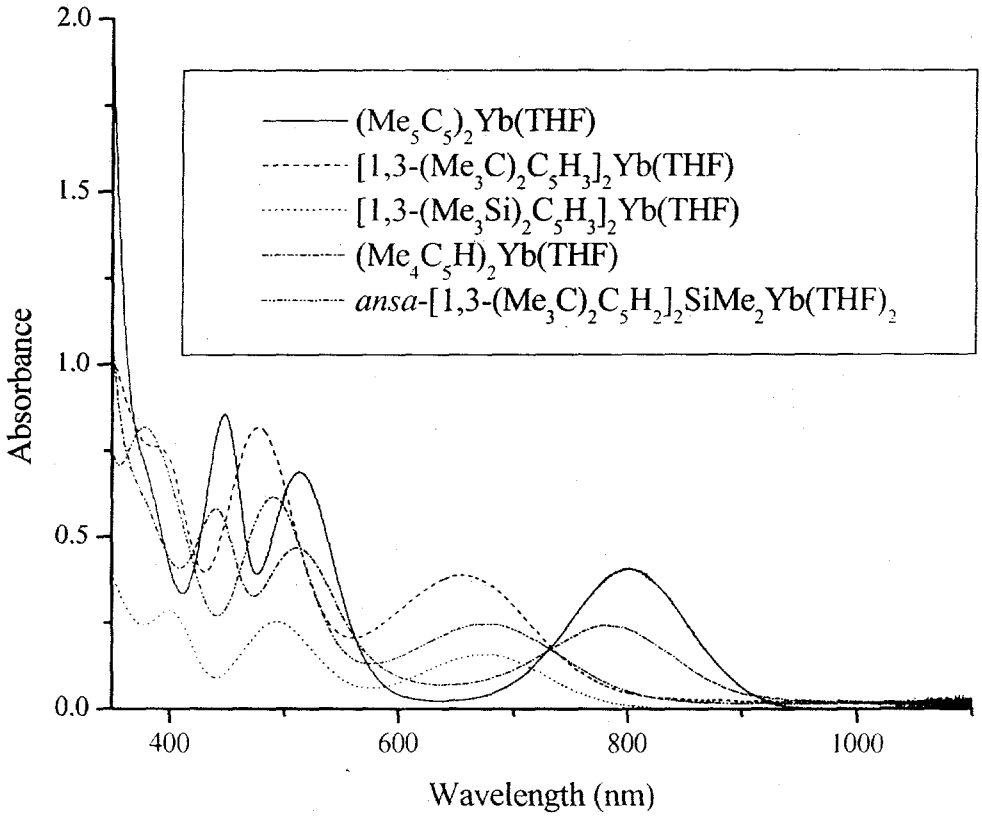

Figure 1.13. Optical spectra of THF adducts of ytterbocenes in methylcyclohexane.

Changing the solvent from aliphatic methylcyclohexane to aromatic toluene results in a noticeable color change from orange-red to green of *ansa*-[1,3-$(Me_3C)_2C_5H_2]_2SiMe_2Yb(THF)_2$. However, the position of the HOMO → LUMO transition changes only slightly, 6 nm (Table 1.6), and is blue-shifted. The bend angle of this compound is fixed by the *ansa*-bridge, so the cause of the blue shift may be a reduction in electron - electron repulsion, as toluene displaces THF in the coordination sphere of the metal.

Addition of a small amount of THF to a cuvette containing $(Me_5C_5)_2Yb(THF)$ or [1,3-$(Me_3Si)_2C_5H_3]_2Yb(THF)$ in methylcyclohexane, or measuring the optical spectrum in THF solvent, results in a large change to the optical spectrum of these compounds, which appear red under these conditions. The HOMO → LUMO transition is not observed, presumably as it is red-shifted into the infrared region of the spectrum. The only absorptions observed are the higher energy transitions below 520 nm, which appear at the same wavelengths as observed in methylcyclohexane. Apparently with an excess of THF ligand, there is increased electron - electron repulsion in these complexes, resulting in a large red-shift of the HOMO → LUMO transition. In contrast, the position of the HOMO → LUMO transition of $[1,3\text{-}(Me_3C)_2C_5H_3]_2Yb(THF)$ in THF solvent is slightly blue-shifted from the value in methylcyclohexane, which indicates that the sterically bulky Me_3C-substituted ligand does not allow the close approach of further ligands.

The optical spectrum of the diethyl ether complex of samarium, $(Me_5C_5)_2Sm(OEt_2)$, changes somewhat on varying the solvent from methylcyclohexane to toluene. No structural conclusions can be drawn, however, as the transitions are not assigned. The optical spectrum of the europium etherate is similar to the spectra of the base-free molecule in methylcyclohexane and toluene. This implies that the solution structure of the molecule is insensitive to minor changes in the ligand environment. It is possible that the HOMO $\rightarrow$ LUMO transition of this complex is not being observed in the wavelength range covered by the spectrum, or that the transitions of the europium complex are insensitive to the ligand environment.

References

1) Berg, D. J.; Burns, C. J.; Andersen, R. A.; Zalkin, A. *Organometallics* **1989**, *8*, 1865.

2) Tilley, T. D.; Boncella, J. M.; Berg, D. J.; Burns, C. J.; Andersen, R. A. *Inorg. Synth.* **1990**, *27*, 146.

3) Hitchcock, P. B.; Howard, J. A. K.; Lappert, M. F.; Prashar, S. *J. Organomet. Chem.* **1992**, *437*, 177.

4) Sofield, C. D.; Andersen, R. A. *J. Organomet. Chem.* **1995**, *501*, 271.

5) Sofield, C. D. *PhD Thesis*; University of California: Berkeley, 2000.

6) Tilley, T. D.; Andersen, R. A.; Spencer, B.; Ruben, H.; Zalkin, A.; Templeton, D. H. *Inorg. Chem.* **1980**, *19*, 2999.

7) Burns, C. J. *PhD Thesis*; University of California: Berkeley, 1987.

8) Baker, E. C.; Halstead, G. W.; Raymond, K. N. *Structure and Bonding* **1976**, *25*, 23.

9) Raymond, K. N. *The Structure and Bonding of 4f and 5f Series Organometallic Compounds*; Marks, T. J. and Fischer, R. D., Ed.; D Reidel Publishing Company: Dordrecht, Netherlands, 1978; Vol. 44, pp 249-280.

10) Raymond, K. N.; Eigenbrot, C. W. *Acc. Chem. Res.* **1980**, *13*, 276.

11) Rogers, R. D. *J. Organomet. Chem.* **1996**, *512*, 97.

12) Shannon, R. D. *Acta Crystallogr., Sect. A* **1976**, *A32*, 751.

13) Schultz, M.; Burns, C. J.; Schwartz, D. J.; Andersen, R. A. *Organometallics* **2000**, *19*, 781.

14) Corradi, M. M.; Frankland, A. D.; Hitchcock, P.; Lappert, M. F.; Lawless, G. A. *Chem. Commun.* **1996**, *20*, 2323.

15) Constantine, S. P.; De Lima, G. M.; Hitchcock, P. B.; Keates, J. M.; Lawless, G. A. *Chem. Commun.* **1996**, 2421.

16) Eaborn, C.; Hitchcock, P. B.; Izod, K.; Smith, J. D. *J. Am. Chem. Soc.* **1994**, *116*, 2071.

17) Eaborn, C.; Hitchcock, P. B.; Izod, K.; Lu, Z.-R.; Smith, D. J. *Organometallics* **1996**, *15*, 4783.

18) Bercaw, J. E.; Marvich, R. H.; Bell, L. G.; Brintzinger, H. H. *J. Am. Chem. Soc.* **1972**, *94*, 1219.

19) Khvostov, A. V.; Sizov, A. I.; Bulychev, B. M.; Knjazhanski, S. Y.; Belsky, V. K. *J. Organomet. Chem.* **1998**, *559*, 97.

20) Watson, P. L., Structure of $(Me_5C_5)_2Yb(OEt_2)$, personal communication, 1983.

21) Pauling, L. *The Nature of the Chemical Bond*; Cornell University Press: Ithaca, NY, 1960.

22) Cotton, F. A.; Wilkinson, G.; Murillo, C. A.; Bochmann, M. *Advanced Inorganic Chemistry*; 6th ed.; John Wiley & Sons, Inc.: New York, 1999.

23) Tilley, T. D.; Andersen, R. A.; Spencer, B.; Zalkin, A. *Inorg. Chem.* **1982**, *21*, 2647.

24) Burns, C. J.; Andersen, R. A. *J. Am. Chem. Soc.* **1987**, *109*, 915.

25) Burns, C. J.; Andersen, R. A. *J. Am. Chem. Soc.* **1987**, *109*, 941.

26) Burns, C. J.; Andersen, R. A. *J. Am. Chem. Soc.* **1987**, *109*, 5853.

27) Shen, Q.; Zheng, D.; Lin, L.; Lin, Y. *J. Organomet. Chem.* **1990**, *391*, 321.

28) Lappert, M. F.; Yarrow, P. I. W.; Atwood, J. L.; Shakir, R.; Holton, J. *J. Chem. Soc., Chem. Commun.* **1980**, 987.

29) Schumann, H.; Glanz, M.; Hemling, H.; Hahn, F. E. *Z. Anorg. Allg. Chem.* **1995**, *621*, 341.

30) Apostolidis, C.; Deacon, G. B.; Dornberger, E.; Edelmann, F. T.; Kanellakopulos, B.; MacKinnon, P.; Stalke, D. *J. Chem. Soc., Chem. Commun.* **1997**, 1047.

31) Sitzmann, H.; Weber, F., sample of $[1,2,4\text{-}(Me_3C)_3C_5H_2]_2Yb$, personal communication, 1999.

32) Boncella, J. M. *PhD Thesis*; University of California: Berkeley, 1984.

33) Zerger, R.; Stucky, G. *J. Organomet. Chem.* **1974**, *80*, 7.

34) Andersen, R. A.; Boncella, J. M.; Burns, C. J.; Blom, R.; Haaland, A.; Volden, H. V. *J. Organomet. Chem.* **1986**, *312*, C49.

35) Andersen, R. A.; Boncella, J. M.; Burns, C. J.; Green, J. C.; Hohl, D.; Rösch, N. *J. Chem. Soc., Chem. Commun.* **1986**, 405.

36) Andersen, R. A.; Blom, R.; Boncella, J. M.; Burns, C. J.; Volden, H. V. *Acta Chem. Scand. A* **1987**, *A41*, 24.

37) Evans, W. J.; Hughes, L. A.; Hanusa, T. P. *Organometallics* **1986**, *5*, 1285.

38) Williams, R. A.; Hanusa, T. P.; Huffman, J. C. *Organometallics* **1990**, *9*, 1128.

39) Struchkov, Y. T.; Andrianov, V. G.; Sal'Nikova, T. N.; Lyatifov, I. R.; Materikova, R. B. *J. Organomet. Chem.* **1978**, *145*, 213.

40) Schmitz, D.; Fleischhauer, J.; Meier, U.; Schleker, W.; Schmitt, G. *J. Organomet. Chem.* **1981**, *205*, 381.

41) Hays, M. L.; Hanusa, T. P. *Adv. Organomet. Chem.* **1997**, *40*, 117.

42) Green, J. C.; Hohl, D.; Rösch, N. *Organometallics* **1987**, *6*, 712.

43) DeKock, R. L.; Peterson, M. A.; Timmer, L. K.; B aerends, E. J.; Ve rnooijs, P. *Polyhedron* **1990**, *9*, 1919.

44) Gerloch, M.; Constable, E. C. *Transition Metal Chemistry*; VCH: Weinheim, 1995.

45) Thomas, A. C.; Ellis, A. B. *Organometallics* **1985**, *4*, 2223.

46) Thomas, A. C. *PhD Thesis*; University of Wisconsin-Madison: Madison, WI, 1985.

Chapter Two : Coordination of Carbon Monoxide and Isocyanides: Back-donation from Ytterbium(II)

Carbonyl Complexes

A dark brown methylcyclohexane solution of base-free $(Me_5C_5)_2Yb$ turns deep brown-green on exposure to one atmosphere of carbon monoxide with stirring at 25°C. The infrared spectrum of the solution under a CO atmosphere contains two absorption peaks at 2114 cm^{-1} ($\nu_{1/2}$ = 10 cm^{-1}) and 2072 cm^{-1} ($\nu_{1/2}$ = 35 cm^{-1}) (Figure 2.1). Exposure of the solution to vacuum followed by nitrogen results in the disappearance of both peaks; they reappear when the solution is again exposed to carbon monoxide. This cycle can be repeated at least four times before decomposition of the air-sensitive starting material occurs. The $(Me_5C_5)_2Yb$ starting material can be recrystallized unchanged after an exposure to CO, showing that the reaction is reversible. The two peaks in the infrared spectrum appear to correspond to two discrete carbonyl complexes that are in equilibrium with each other (Equation 1). The same absorptions are also observed for a toluene solution of $(Me_5C_5)_2Yb$ under CO at 2117 cm^{-1} ($\nu_{1/2}$ = 55 cm^{-1}) and 2072 cm^{-1} ($\nu_{1/2}$ = 50 cm^{-1}), although the intensity is lower and the peaks are broadened.

$$(Me_5C_5)_2Yb + 2CO \rightleftharpoons (Me_5C_5)_2Yb(CO) + CO \rightleftharpoons (Me_5C_5)_2Yb(CO)_2 \quad (1)$$

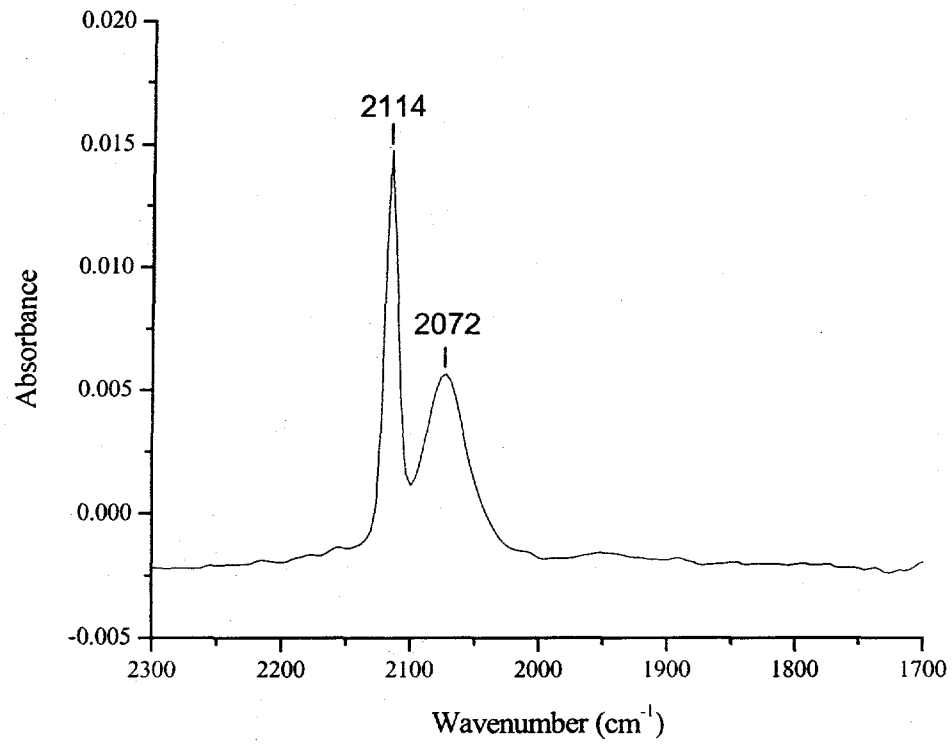

Figure 2.1. Infrared spectrum of $(Me_5C_5)_2Yb$ in methylcyclohexane under one atmosphere of CO. This spectrum is background corrected for solvent and CO.

Both ν_{CO} values are lower than that of free CO, consistent with population of the C - O π-antibonding orbital by metal $\rightarrow$ ligand donation. In a detailed study of the pressure and temperature dependence of these two absorptions, the 2114 cm^{-1} band is attributed to a monocarbonyl and the 2072 cm^{-1} band to a dicarbonyl species.[1] The explanation that two carbonyl species are in equilibrium is supported by the variable temperature ^{13}C NMR spectra of a $(Me_5C_5)_2Yb$ solution under one atmosphere of ^{13}CO.[2] At room temperature, only a single ^{13}CO resonance is observed at δ 203 ppm ($\nu_{1/2}$ = 425 Hz), which is deshielded by 18 ppm relative to free ^{13}CO at the same temperature and pressure. The

single averaged resonance decoalesces into two at -107°C at δ 243 ppm ($\nu_{1/2}$ = 2800 Hz) and δ 199 ppm ($\nu_{1/2}$ = 100 Hz), both of which are deshielded relative to free ^{13}CO. The ^{13}C chemical shift of a carbonyl complex is correlated with the CO stretching frequency in the infrared spectrum; π-backbonding increases the electron density in the metal - carbon bond, shortening it and deshielding the ^{13}C resonance, while simultaneously lengthening the C - O bond and reducing the CO stretching frequency. This correlation is graphically illustrated for d^0-metallocene carbonyl complexes by Parkin.[3]

The $^{13}C\{^1H\}$ NMR spectrum of a saturated methylcyclohexane-d_{14} solution of $(Me_5C_5)_2Yb$ under natural isotopic abundance CO varies with CO pressure. The changes in chemical shifts of both the ring and methyl carbon atoms are non-linear with pressure, although saturation is not reached up to 220 psi. The chemical shift changes are reversible; exposure of the NMR tube to vacuum followed by nitrogen results in return of the chemical shifts to their original values.

It is of interest to compare the $(Me_5C_5)_2Yb$ result with the corresponding experiment on $(Me_5C_5)_2Ca$.[4] Exposure of a solution of $(Me_5C_5)_2Ca$ in toluene to CO pressures of 2.5 - 70 bar gives rise to a single ν_{CO} of 2158 cm^{-1}, which is 22 cm^{-1} higher than the value for free CO. This process is reversible and the adduct has a 1:1 stoichiometry. The averaged chemical shift of the carbonyl carbon atom in the ^{13}C NMR spectrum is shielded (δ_{CO} 180.4 ppm) with respect to free CO,[4] in accord with the correlation of ν_{CO} and δ_{CO} described above. The radii of Ca(II) and Yb(II) are similar,[5] and the structures of their decamethylmetallocenes in the solid state and the gas phase are also similar.[6-9] However,

changing from the $3d^0$ metal calcium to the $4f^{14}\ 5d^0$ metal ytterbium alters the behavior of these two decamethylmetallocenes towards carbon monoxide.

The samarium and europium analogues were studied by infrared spectroscopy under the same conditions. In the case of $(Me_5C_5)_2Sm$, no peak was observed in the infrared spectrum and it is likely, based on the optical data discussed below, that the molecule decomposes under these conditions. Bubbling carbon monoxide into a blood-red methylcyclohexane solution of $(Me_5C_5)_2Eu$ results in the appearance of a peak at 2150 cm^{-1} ($\nu_{1/2}$ = 10 cm^{-1}) in the infrared spectrum. This is the same frequency as has been observed in high-pressure experiments.[10] It corresponds to an increase in stretching frequency of 14 cm^{-1} above that of free CO, but is lower than the value of ν_{CO} (2158 cm^{-1}) observed for $(Me_5C_5)_2Ca(CO)$.[4]

A green-brown methylcyclohexane solution of $[1,3\text{-}(Me_3C)_2C_5H_3]_2Yb$, when exposed to one atmosphere of carbon monoxide, produces a single peak at 2128 cm^{-1} ($\nu_{1/2}$ = 10 cm^{-1}) in the infrared spectrum. The peak disappears upon exposure of the solution to vacuum followed by nitrogen. Similarly, when a solution of $[1,3\text{-}(Me_3Si)_2C_5H_3]_2Yb$ in methylcyclohexane is stirred under carbon monoxide, a peak is observed in the infrared spectrum at 2138 cm^{-1}($\nu_{1/2}$ = 8 cm^{-1}). Again, the reaction is reversible and only a single absorption band is observed for the carbonyl adducts of both of these ytterbocenes. The more heavily substituted $[1,3\text{-}(Me_3C)_3C_5H_2]_2Yb$ does not appear to bind carbon monoxide as no peak is observed in the infrared spectrum after stirring a solution of the ytterbocene under CO. This is presumably due to the steric bulk of the trisubstituted

cyclopentadienide rings, which prevents the approach of a ligand. The effect of this bulky ligand was also observed in the solid state structure of $[1,3\text{-}(Me_3C)_3C_5H_2]_2Yb$ which has a larger centroid - metal - centroid angle than the other ytterbocenes described in Chapter 1.

The infrared data for the CO adducts of the base-free ytterbocenes and europium are collected in Table 2.1. It can be seen that the CO stretch is reduced from that of free CO in the cases of $(Me_5C_5)_2Yb$ and $[1,3\text{-}(Me_3C)_2C_5H_3]_2Yb$, while in the case of $[1,3\text{-}(Me_3Si)_2C_5H_3]_2Yb$, the CO adduct has a stretching frequency only 2 cm^{-1} higher than the free ligand. The only difference between these molecules is the substitution of the cyclopentadienide rings.[11] The small size of a CO ligand implies that the differences in the three carbonyl compounds result from electronic rather than steric effects.

Table 2.1. Infrared spectra of bivalent lanthanide metallocenes under CO in methylcyclohexane

compound	ν_{CO} **(cm^{-1})**	ν_{CO}**(complex) -** $\nu_{free\ CO}$ **(cm^{-1})**
$(Me_5C_5)_2Yb$	2114, 2072	-22, -64
$(Me_5C_5)_2Eu$	2150	+14
$[1,3\text{-}(Me_3C)_2C_5H_3]_2Yb$	2126	-10
$[1,3\text{-}(Me_3C)_3C_5H_2]_2Yb$	none	
$[1,3\text{-}(Me_3Si)_2C_5H_3]_2Yb$	2138	+2

An electrostatic bonding model has been advanced to explain the increase in CO stretching frequency above that of free CO in some metal carbonyl compounds.[12-15] In this model, when the carbon atom of CO is located near an electropositive metal atom, the polarization in the CO ligand changes as shown in the valence diagram **A**. Upon adduct formation the carbon atom carries a less negative charge, and its orbital energy becomes closer to that of the oxygen atom, making the bond more covalent. Hence, the force constant of the C - O bond increases, ν_{CO} increases and δ_{CO} is shielded. In cases where ν_{CO} is reduced, π-backbonding from the metal fragment competes with or dominates the electrostatic interaction and δ_{CO} is deshielded. The resulting charge distribution is illustrated by the valence bond picture **B**. Thus, the variation of ν_{CO} observed in the three ytterbocene molecules examined here, from slightly higher than that of free CO to somewhat lower, is an indication of the balance between the resonance forms **A** and **B**.

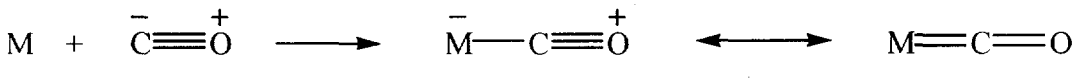

A **B**

Europium has a lower oxidation potential than ytterbium and is more stable in the bivalent state, indicating that this metal is more likely to favor resonance form **A**. In addition, the orbitals of europium are less available for π-back bonding as they are more diffuse than those of ytterbium are. The increase in CO stretching frequency above that of free CO for the compound $(Me_5C_5)_2Eu(CO)$ supports this model.

Since the color of a solution of $(Me_5C_5)_2Yb$ in methylcyclohexane changes upon exposure to CO, the optical spectrum of the $(Me_5C_5)_2Yb$ solution was measured in a separate experiment. Base-free $(Me_5C_5)_2Yb$ has four absorbances at 751 nm, 515 nm, 474 nm and 429 nm, all of which have similar extinction coefficients, as described in Chapter 1. The highest wavelength absorption is thought to correspond to the HOMO → LUMO transition, and the three lower wavelength features are due to higher-energy ligand field transitions.[16] Upon brief exposure of the cuvette to vacuum followed by backfilling with carbon monoxide, the HOMO → LUMO transition is blue-shifted to 699 nm (Figure 2.2). This procedure is also reversible, although the peaks become broad and some resolution is lost, probably due to decomposition of the sample since the solute concentration is small.

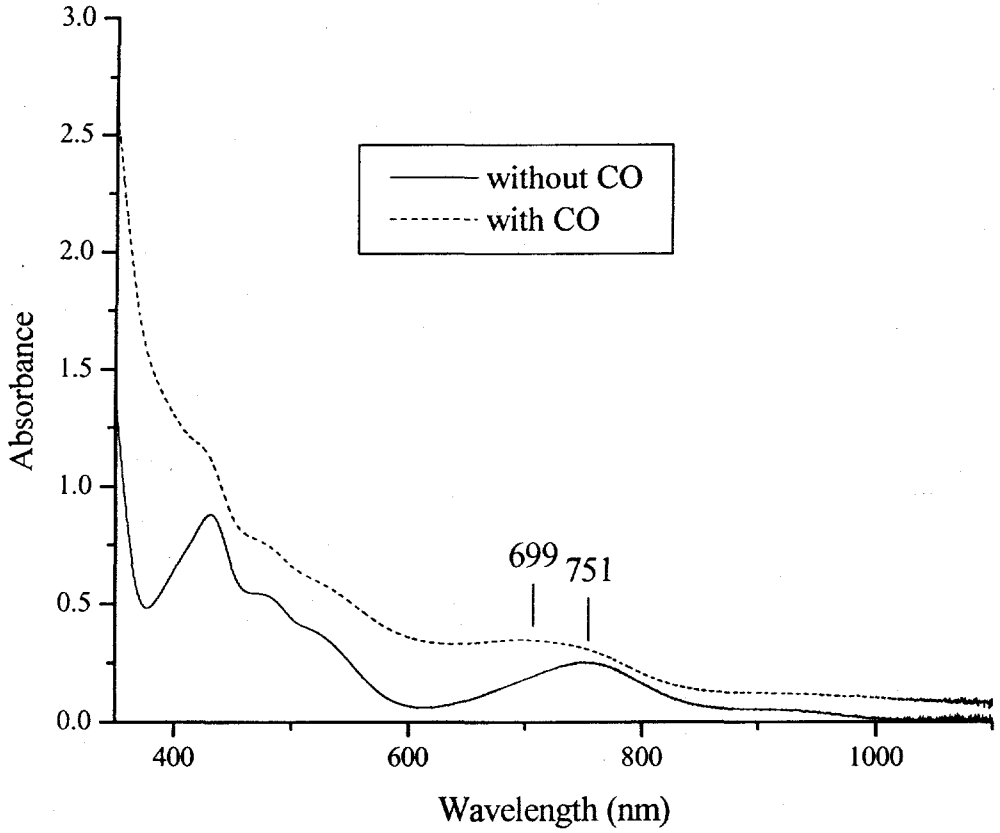

Figure 2.2. Optical spectra of $(Me_5C_5)_2Yb$ in methylcyclohexane with and without CO.

The shift to 699 nm of the HOMO → LUMO transition of $(Me_5C_5)_2Yb$ in methylcyclohexane when it is exposed to CO corresponds to a blue shift of 52 nm. The lower wavelength transitions shift less than 5 nm. According to the model outlined in Chapter 1, the addition of a ligand to the coordination sphere of an ytterbocene has two opposing effects on the HOMO → LUMO transition. One is to increase the bend angle, which increases the energy of the HOMO → LUMO transition according to the Rösch-Green model,[16] while the other is to increase electron-electron repulsion, which raises the

energy of the *f*-orbitals and decreases the HOMO - LUMO gap. In the $(Me_5C_5)_2Yb$ and CO system, the blue shift of 52 nm (1 000 cm^{-1}) is presumably due mainly to bending, which raises the LUMO more than the HOMO, as the interaction with the ligand is expected to be small.

In toluene solution, the HOMO → LUMO transition of $(Me_5C_5)_2Yb$ is observed at 736 nm, as described in Chapter 1, and the spectrum does not change significantly when carbon monoxide is added. This indicates that toluene may be competing with, or inhibiting, carbon monoxide binding. Exposure of a cuvette containing a solution of $[1,3\text{-}(Me_3C)_2C_5H_3]_2Yb$ or $[1,3\text{-}(Me_3Si)_2C_5H_3]_2Yb$ to carbon monoxide does not alter the optical spectra of either of these ytterbocenes (Table 2.2).

Table 2. 2. Optical spectra of ytterbocenes under CO (in methylcyclohexane unless specified)

compound	**λ_{max} in nm (ε in $Lmol^{-1}cm^{-1}$)**
$(Me_5C_5)_2Yb$	699 (256), 520 (436), 472 (540), 425 (831)
$(Me_5C_5)_2Yb$ in toluene	733 (249), 425 (754)
$[1,3\text{-}(Me_3C)_2C_5H_3]_2Yb$	653 (171), 451 (440), 396 (483)
$[1,3\text{-}(Me_3Si)_2C_5H_3]_2Yb$	645 (168), 463 (320), 391 (500)

The optical spectra of the metallocenes $(Me_5C_5)_2Sm$ and $(Me_5C_5)_2Eu$ were also examined in the presence of CO. Bubbling carbon monoxide into a pale blue-gray solution of

$(Me_5C_5)_2Sm$ in methylcyclohexane results in an immediate color change to bright blue-green, followed by a slower change to red-brown. The blue-green color is transient so the optical spectrum cannot be obtained at room temperature. The red-brown color is thought to correspond to a decomposition product, because the optical spectrum then consists of a single transition from 615 - 350 nm. Exposure of the cuvette to vacuum followed by back-filling with nitrogen results in a very slight change in the position of the absorption, but the extremely intense band remains. This provides a possible explanation for the reported reductive homologation of CO by $(Me_5C_5)_2Sm(THF)$;[17] it may result from decomposition due to impurities in the CO. Under these conditions, no carbonyl band is observed in the infrared spectrum. Also, the reported reaction of $(Me_5C_5)_2Sm$ with N_2 to yield a bridging dimer[18] seems quite unlikely given that all of the chemistry described here was carried out under nitrogen, and a red-brown solution was only observed in the case of decomposition. Bubbling nitrogen gas into a solution of $(Me_5C_5)_2Sm$ in methylcyclohexane does not change the color or optical spectrum of the solution, and the base-free molecule can be recrystallized unchanged. The optical spectrum of the europium complex in methylcyclohexane does not change upon exposure to CO.

Interaction of $(Me_5C_5)_2Yb$ with Small Molecules

Ethylene is polymerized by $(Me_5C_5)_2Yb$,[6] so the experiment with $[1,3\text{-}(Me_3C)_2C_5H_3]_2Yb$ and $[1,3\text{-}(Me_3Si)_2C_5H_3]_2Yb$ as well as a slurry of $(Me_4C_5H)_2Yb$ was attempted. No polymerization was observed.

The optical spectrum of $(Me_5C_5)_2Yb$ in methylcyclohexane changes upon bubbling ethylene into the cuvette. The HOMO → LUMO transition shifts to 742 nm, a blue shift of 9 nm. This is presumably because the metallocene is bent by the approach of the ethylene before the polymerization is initiated. The interaction is weak enough that the *f*-orbitals do not increase in energy, so the net effect is a slight expansion of the HOMO - LUMO gap. After 10 minutes, polyethylene is observed in the cuvette. Propylene is not polymerized by $(Me_5C_5)_2Yb$ and there is no change in the optical spectrum upon bubbling that gas into the sample.

The polymerization of ethylene by $(Me_5C_5)_2Yb$ is slowed by the use of toluene as solvent, and is inhibited by the presence of Xe.[6] As the optical spectrum of $(Me_5C_5)_2Yb$ was found to change by 14 nm on varying the solvent from methylcyclohexane to toluene, the spectrum in the presence of xenon and other small molecules was examined in methylcyclohexane solvent. Bubbling Xe, H_2 or propylene into the cuvette does not change the optical spectrum (Table 2.3). As described above and in Chapter 1, CO changes the position of the HOMO → LUMO transition by 52 nm and diethyl ether changes it by 61 nm in methylcyclohexane. The lack of change in the presence of other gases indicates that there is no appreciable change in bend angle, or that the blue-shift due to bending is counteracted by a red-shift due to electron - electron repulsion upon adduct formation.

The adducts $(Me_5C_5)_2Yb(MeC{\equiv}CMe)$, $(Me_5C_5)_2Yb(MeC{\equiv}CCMe_3)$ and $(Me_5C_5)_2Yb(\mu\text{-}Me)Be(Me_5C_5)$ have been reported.[6,19,20] The optical spectra of the two acetylene complexes as methylcyclohexane solutions are unchanged from that of base-free $(Me_5C_5)_2Yb$. This is somewhat surprising, as both the averaged ^1H and ^{13}C resonances of the bound acetylene ligand are changed from the free acetylene in the NMR spectra, even though the ligand exchanges rapidly on the NMR timescale. The timescale for optical spectroscopy is shorter than for NMR spectroscopy, so it was expected that the interaction would be observed. However, addition of an excess of dimethyl acetylene to a cuvette containing $(Me_5C_5)_2Yb$ in methylcyclohexane does result in a small red-shift of the HOMO $\rightarrow$ LUMO transition to 759 nm. This result shows that an excess of ligand, such as a dissolved gas or a solvent, is required to affect the optical transitions of the ytterbocene. The NMR spectrum reflects the average charge on the ligand caused by the metal, while the optical spectrum addresses the HOMO - LUMO gap. Bending the molecule allows more ligands to approach the metal center, as was observed in the solid state structures of the bivalent ytterbocenes. In the case of the $(Me_5C_5)_2Yb\text{-}\mu\text{-}MeBe(Me_5C_5)$ adduct, the lowest energy absorbance is also slightly red shifted by 10 nm (Table 2.3) from that of free $(Me_5C_5)_2Yb$. This indicates that the HOMO $\rightarrow$ LUMO transition is reduced in energy, presumably due to an increase in energy of the *f*-orbitals due to electron - electron repulsion.

Table 2.3. Optical spectra of $(Me_5C_5)_2Yb$ with small molecules in methylcyclohexane (λ_{max} is the position of the lowest energy band)

small molecule	λ_{max}	$\Delta(\lambda_{max} - \lambda_{max}$**(base-free))** **(nm)**
methylcyclohexane	751	0
toluene (solvent)	736	-15
OEt_2	690	-61
CO	699	-52
H_2	751	0
C_2H_4	742	-9
Xe	751	0
C_3H_6	751	0
MeC≡CMe (1:1 isolated)	751	0
MeC≡CMe (excess)	759	+8
MeC≡$CCMe_3$ (1:1 isolated)	751	0
MeBe(Me_5C_5) (1:1 isolated)	760	+10

The blue shift of ethylene is presumably related to its π-acceptor character, which makes it similar to CO. The red shifts of excess dimethylacetylene and MeBe(Me_5C_5) are somewhat surprising, but these molecules are net donors and are expected to cause greater electron - electron repulsion than ethylene, without any significant change in the bend angle of the ytterbocene.

Isocyanide Complexes

Isocyanide complexes of $(Me_5C_5)_2Yb$, $[1,3\text{-}(Me_3C)_2C_5H_3]_2Yb$, $[1,3\text{-}(Me_3Si)_2C_5H_3]_2Yb$, $(Me_4C_5H)_2Yb$ and *ansa*-$[1,3\text{-}(Me_3C)_2C_5H_2]_2SiMe_2Yb$ are prepared from the corresponding etherates, $Cp'_2Yb(OEt_2)$, in toluene (Equation 2). The 1:2 adducts are relatively insoluble in aromatic and aliphatic solvents and can be crystallized from toluene as dark red (Cp' = Me_5C_5, $1,3\text{-}(Me_3C)_2C_5H_3$, $1,3\text{-}(Me_3Si)_2C_5H_3$, Me_4C_5H; R = C_6H_{11}, Me_3C and Cp'_2 = *ansa*-$[1,3\text{-}(Me_3C)_2C_5H_2]_2SiMe_2$; R = $2,6\text{-}Me_2C_6H_3$), blue (Cp' = $1,3\text{-}(Me_3C)_2C_5H_3$, $1,3\text{-}(Me_3Si)_2C_5H_3$; R = $2,6\text{-}Me_2C_6H_3$) or green (Cp' = Me_5C_5, Me_4C_5H; R = $2,6\text{-}Me_2C_6H_3$) blocks.

$$Cp'_2Yb(OEt_2) + 2CNR \rightarrow Cp'_2Yb(CNR)_2 + OEt_2 \qquad (2)$$

Cp' = Me_5C_5, $1,3\text{-}(Me_3C)_2C_5H_3$, $1,3\text{-}(Me_3Si)_2C_5H_3$, Me_4C_5H

Cp'_2 = *ansa*-$[1,3\text{-}(Me_3C)_2C_5H_2]_2SiMe_2$

R = $2,6\text{-}Me_2C_6H_3$, Me_3C, C_6H_{11}

Infrared data for the isocyanide complexes are presented in Table 2.4. The infrared spectra contain a single, sharp CN stretch in both the solid state and toluene solution for each adduct. This contrasts with the expected result for a metal center bound to two isocyanide ligands, as both a symmetric stretch and an asymmetric stretch are infrared active in idealized C_{2v} symmetry. One explanation for this observation is that the two isocyanide ligands are not electronically or mechanically coupled. The observed values

of ν_{CN} for the isocyanide adducts are higher in frequency than those of the free isocyanides, but the changes are much less than for the previously reported isocyanide complexes $(C_5H_5)_3LnC_6H_{11}NC$ (Ln = La - Lu) of trivalent lanthanide metals, for which ν_{CN} increases around between 60 and 74 cm^{-1} on coordination.[21,22] For a given ytterbocene fragment, the complex with 2,6-$Me_2C_6H_3NC$ as the isocyanide ligand has its CN stretching frequency increased from that of the free ligand to a lesser extent than the complexes derived from aliphatic isocyanide ligands. This is most reasonably associated with the electron-withdrawing nature of the aryl group, making 2,6-$Me_2C_6H_3NC$ a weaker electron donor. Isocyanide complexes with a 1:1 stoichiometry cannot be isolated; mixing an ytterbocene with one equivalent of an isocyanide ligand results in the isolation of the 1:2 isocyanide complex and the ytterbocene starting complex.

Table 2.4. Infrared spectra of isocyanide complexes of ytterbocenes (Nujol mulls)

compound	ν_{CN} (cm^{-1})	ν_{CN}(complex) - $\nu_{free\ CNR}$ (cm^{-1})
$(Me_5C_5)_2Yb(2,6\text{-}Me_2C_6H_3NC)_2$	2131	+13
$(Me_5C_5)_2Yb(Me_3CNC)_2$	2160	+26
$(Me_5C_5)_2Yb(C_6H_{11}NC)_2$	2164	+26
$[1,3\text{-}(Me_3C)_2C_5H_3]_2Yb(2,6\text{-}Me_2C_6H_3NC)_2$	2129	+11
$[1,3\text{-}(Me_3C)_2C_5H_3]_2Yb(Me_3CNC)_2$	2161	+27
$[1,3\text{-}(Me_3C)_2C_5H_3]_2Yb(C_6H_{11}NC)_2$	2166	+28
$[1,3\text{-}(Me_3Si)_2C_5H_3]_2Yb(2,6\text{-}Me_2C_6H_3NC)_2$	2142	+24
$[1,3\text{-}(Me_3Si)_2C_5H_3]_2Yb(C_6H_{11}NC)_2$	2168	+30
$(Me_4C_5H)_2Yb(2,6\text{-}Me_2C_6H_3NC)_2$	2132	+14
$(Me_4C_5H)_2Yb(Me_3CNC)_2$	2162	+28
$(Me_4C_5H)_2Yb(C_6H_{11}NC)_2$	2173	+35
ansa-$[1,3\text{-}(Me_3C)_2C_5H_2]_2SiMe_2Yb(2,6\text{-}Me_2C_6H_3NC)_2$	2127	+9

It is interesting to compare $(Me_5C_5)_2Yb(2,6\text{-}Me_2C_6H_3NC)_2$ with the analogous calcium complex, $(Me_5C_5)_2Ca(2,6\text{-}Me_2C_6H_3NC)_2$.[23] In the calcium adduct, the CN stretching frequency of the complex is increased by 30 cm^{-1} relative to the free ligand, while the CN stretching frequency increases by only 13 cm^{-1} in the ytterbium adduct. This parallels the result observed in the CO experiment, in which ν_{CO} of $(Me_5C_5)_2Ca(CO)$ is 2158 cm^{-1}, 42

cm^{-1} higher than that of the monocarbonyl complex of $(Me_5C_5)_2Yb$ and reflects the tendency of the ytterbocene fragment to participate in π-back bonding.

Even though 1:2 isocyanide adducts are isolated in the solid state, only a single, sharp CN stretching frequency is observed in the solid state (Nujol) or solution infrared spectra. In addition, the values of ν_{CN} for all of the adducts are greater than those found in the free isocyanides by 9 - 35 cm^{-1}. The electrostatic model, persuasively argued by Berke for borane adducts of isocyanides,[24,25] can be applied to these isocyanide complexes in an analogous manner to the carbonyl complexes just described. When an isocyanide is placed near a positive charge, the negative charge on the carbon atom is reduced. This lowers the atomic orbital energy of the carbon atom, bringing it closer in energy to the NR fragment. The net effect is to shorten and strengthen the C - N bond, resulting in an increase in ν_{CNR}. This is illustrated by the valence bond structure **C** in which the charge distribution is similar to that in the CO complexes described above.

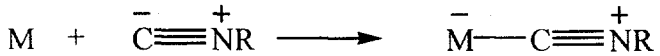

C

This model should be particularly applicable to the isocyanide adducts described here since the bonding in lanthanide compounds is largely electrostatic in nature. The interaction of an isocyanide ligand with a bivalent metal is expected to be weaker than with a trivalent metal in the electrostatic bonding model because of the smaller charge in the former. Consistent with this argument, the increase in ν_{CN} in the trivalent complexes

$(C_5H_5)_3Ln(C_6H_{11}NC)$ of 60 - 74 cm^{-1} is greater than that observed for the bivalent complexes described here of 11 - 35 cm^{-1}.[21,22] In addition, the electrostatic model implies that when two isocyanide ligands are present in the same molecule they will behave as independent dipoles giving rise to a single ν_{CN} stretch, in accord with the observed data (Table 2.4).

The optical spectra of the isocyanide complexes have been measured to investigate the dramatically different colors observed. Data are presented in Table 2.5. The position of the band assigned as the HOMO $\rightarrow$ LUMO transition depends on the substituents on the cyclopentadienide rings and on the isocyanide ligand. The bands for the isocyanide complexes are all very broad with $\nu_{1/2}$ = 200 nm or more (Figure 2.3).

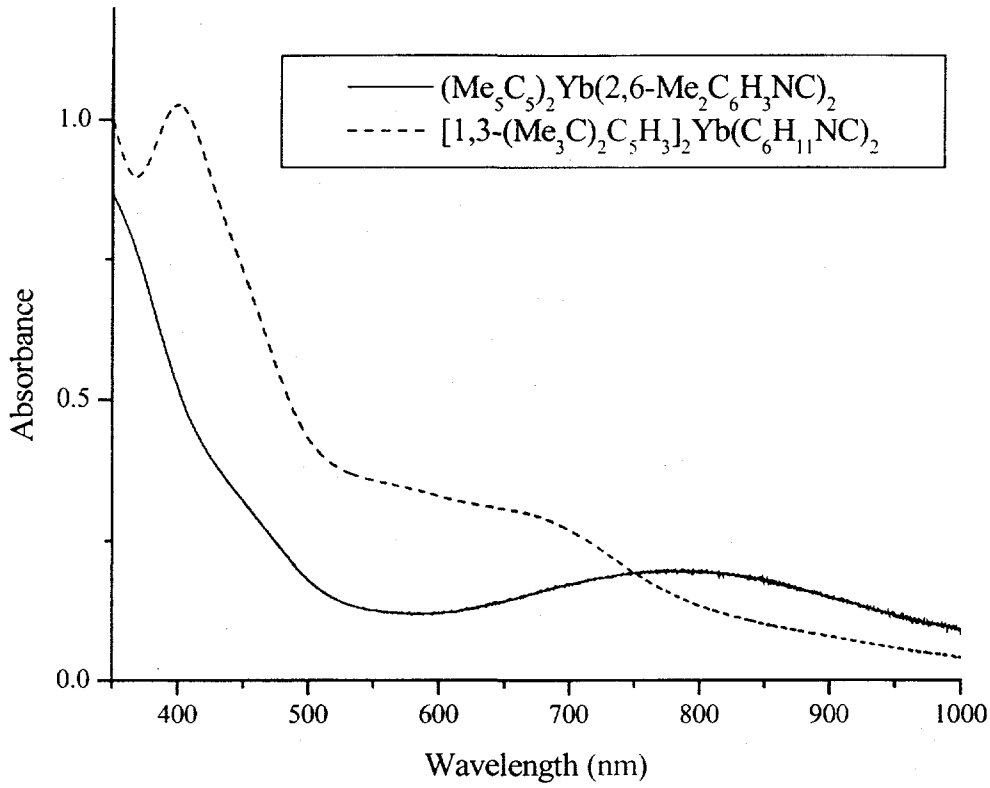

Figure 2.3. Optical spectra of $(Me_5C_5)_2Yb(2,6\text{-}Me_2C_6H_3NC)_2$ and $[1,3\text{-}(Me_3C)_2C_5H_3]_2Yb(C_6H_{11}NC)_2$ in toluene.

Table 2.5. Optical spectra of isocyanide complexes of ytterbocenes in toluene

compound	λ_{max} **in nm (ε in Lmol^{-1}cm^{-1})**
$(Me_5C_5)_2Yb(2,6\text{-}Me_2C_6H_3NC)_2$	776 (610), 434 (1114)
$(Me_5C_5)_2Yb(Me_3CNC)_2$	955 (137), 450 (676)
$(Me_5C_5)_2Yb(C_6H_{11}NC)_2$	942 (234), 453 (963)
$[1,3\text{-}(Me_3C)_2C_5H_3]_2Yb(2,6\text{-}Me_2C_6H_3NC)_2$	586 (755), 390 (1086)
$[1,3\text{-}(Me_3C)_2C_5H_3]_2Yb(Me_3CNC)_2$	648 (197), 397 (692)
$[1,3\text{-}(Me_3C)_2C_5H_3]_2Yb(C_6H_{11}NC)_2$	606 (260), 399 (916)
$[1,3\text{-}(Me_3Si)_2C_5H_3]_2Yb(2,6\text{-}Me_2C_6H_3NC)_2$	617 (533), 389 (1111)
$[1,3\text{-}(Me_3Si)_2C_5H_3]_2Yb(C_6H_{11}NC)_2$	830 (234), 431 (1059)
$(Me_4C_5H)_2Yb(2,6\text{-}Me_2C_6H_3NC)_2$	776 (952), 448 (1251)
$(Me_4C_5H)_2Yb(C_6H_{11}NC)_2$	950 (252), 458 (968)
ansa-$[1,3\text{-}(Me_3C)_2C_5H_2]_2SiMe_2Yb(2,6\text{-}Me_2C_6H_3NC)_2$	686 (500), 500 (613)

The model developed in Chapter 1 and above for the position of the HOMO → LUMO transition can be extended to the isocyanide adducts. In these complexes, the low-energy band that is a measure of the HOMO - LUMO gap changes significantly depending on the substituents on the cyclopentadienide ring and on the isocyanide ligand. In crystalline $(Me_5C_5)_2Yb(2,6\text{-}Me_2C_6H_3NC)_2$, the bend angle of 145° is similar to that found in the 1:1 THF adduct,[26] and the HOMO → LUMO transition in solution (776 nm) is also similar to that of the THF adduct (800 nm). Replacing the xylyl group with the more strongly

donating alkyl groups on the isocyanides results in a red shift of the HOMO → LUMO transition (Table 2.5), which indicates that the HOMO - LUMO gap is decreasing. This effect is presumably the result of the higher electron density on the carbon atom of the alkyl isocyanide ligands, which increases the energy of the HOMO by electron - electron repulsion. Changing the substituents on the cyclopentadienide ring to $(Me_3C)_2$ and $(Me_3Si)_2$ decreases the centroid - metal - centroid angles of the isocyanide complexes in the solid state relative to $(Me_5C_5)_2Yb(2,6\text{-}Me_2C_6H_3NC)_2$, and the HOMO → LUMO transitions for the xylyl isocyanide adducts in toluene solution are blue-shifted to 586 and 617 nm, respectively, consistent with a greater degree of bending in solution. For those ytterbocenes, the alkyl isocyanide complexes are also red-shifted from the xylyl isocyanide complexes. The ytterbocene $(Me_4C_5H)_2Yb$ appears to be very similar to $(Me_5C_5)_2Yb$, based on the optical spectra of its isocyanide complexes. The position of the HOMO → LUMO transitions follows the trend observed in Chapter 1 for the diethyl ether and base free ytterbocenes; the disubstituted complexes have a larger HOMO - LUMO gap than the more fully substituted analogues, presumably due to their more bent structures in solution.

The complex *ansa*-$[1,3\text{-}(Me_3C)_2C_5H_2]_2SiMe_2Yb(2,6\text{-}Me_2C_6H_3NC)_2$ has a much smaller centroid - metal - centroid angle than the complexes with unbridged cyclopentadienide ligands (see below). However, the HOMO → LUMO transition in the optical spectrum is observed at an energy between those of $(Me_5C_5)_2Yb(2,6\text{-}Me_2C_6H_3NC)_2$ and the disubstituted ytterbocene analogues. This is presumably related to increased electron-electron repulsion in this complex, which raises the energy of the *f*-orbitals, so that the

effect of the increased bend angle on the HOMO → LUMO transition is offset. This may reflect the fact that the sterically exposed metal center receives more electron density from the incoming xylyl isocyanide ligands, resulting in electron - electron repulsion that increases the energy of the filled orbitals of the metal. This is expected within the electrostatic bonding model, because the decrease in centroid - metal - centroid angle increases the dipole of the metallocene fragment. Therefore, the electrostatic attraction between the metal and the Lewis base increases, which increases the electron - electron repulsion in the filled shell molecule.

The ^{1}H NMR spectrum in C_6D_6 of the adduct $(Me_5C_5)_2Yb(2,6\text{-}Me_2C_6H_3NC)_2$ has broad peaks at room temperature (Me_5C_5 $\nu_{1/2}$ = 5 Hz; Me_2C_6 $\nu_{1/2}$ = 3 Hz). Solid state magnetic susceptibility measurements on this molecule show that it is diamagnetic, indicating that the broadened signals are probably due to chemical exchange.[6] Variable temperature ^{1}H NMR experiments have been carried out on this adduct both with and without added isocyanide ligand. Adding an excess of isocyanide causes the room temperature resonances to broaden further; warming this sample to +70°C causes the resonances to sharpen, indicating that the rate of exchange is increasing. When the sample is cooled, the resonances remain unchanged to -50°C; below that temperature the signals begin to sharpen as the exchange between free and bound ligand is slowed. The stopped exchange region cannot be reached. The ^{1}H NMR spectra of all the other isocyanide complexes of the ytterbocenes also have broad peaks at room temperature, indicating that intermolecular exchange is occurring; in no case can the exchange be stopped by lowering the temperature. Mixing adducts of different isocyanides on different

ytterbocenes results in a statistical mixture, by ^{1}H NMR spectroscopy, of the four possible products, all of which have broad peaks and exchange rapidly at room temperature on the NMR timescale.

The structures of four of the 2,6-$Me_2C_6H_3NC$ complexes have been determined by X-ray crystallography. Important structural data are presented in Table 2.6. Each molecule crystallizes as a monomer and the overall structures are unsurprising, yet there are important differences in how the isocyanide ligands are arranged relative to the two cyclopentadienide rings. ORTEP diagrams of the four molecules are shown in Figures 2.4, 2.5, 2.6 and 2.7.

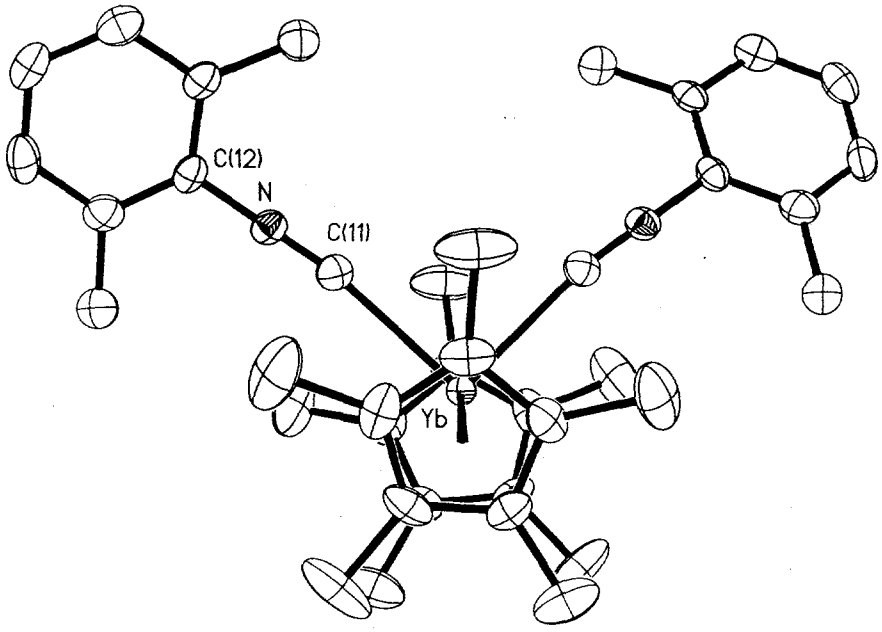

Figure 2.4. ORTEP diagram of $(Me_5C_5)_2Yb(2,6\text{-}Me_2C_6H_3NC)_2$ (50% probability ellipsoids).

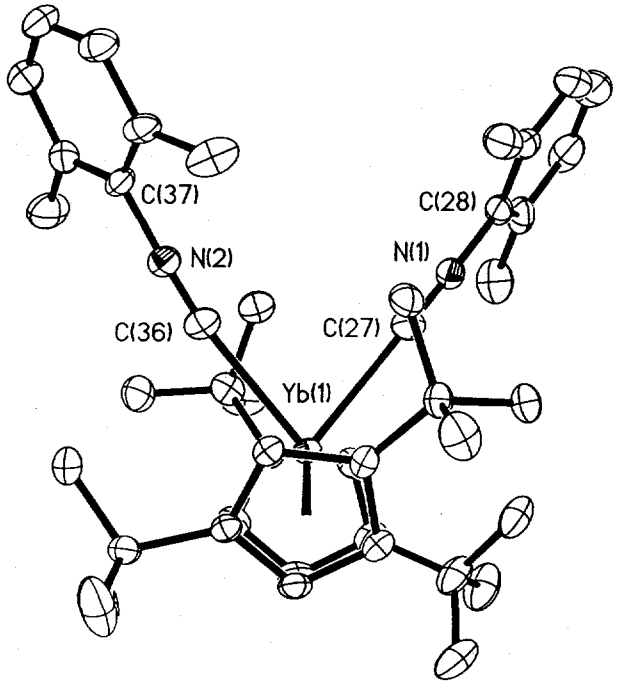

Figure 2.5. ORTEP diagram of $[1,3\text{-}(Me_3C)_2C_5H_3]_2Yb(2,6\text{-}Me_2C_6H_3NC)_2$ (50% probability ellipsoids).

For the two molecules with disubstituted cyclopentadienide rings, the centroid - metal - centroid angles are similar, yet the twist angle of the two cyclopentadienide rings changes from eclipsed in the Me_3C example to staggered in the Me_3Si case. In addition, the xylyl rings of the isocyanide ligands lie in different orientations for these two molecules; in the Me_3C case, they are perpendicular to the plane bisecting the metallocene wedge, while in the Me_3Si case they lie in that plane. This is presumably due to the steric demands of the Me_3C groups on the cyclopentadienide rings, which avoid each other to the greatest possible degree when the rings are eclipsed. The two xylyl rings tilt to minimize steric repulsions with the Me_3C groups, and the resulting isocyanide C_{CNR} - Yb - C_{CNR} angle is 80°. In the Me_3Si derivative, the isocyanide C_{CNR} - Yb - C_{CNR} angle is 10° larger than in

the Me_3C derivative and the xylyl rings lie in the same plane. All of the C_{CNR} - N distances are very close to that of the free ligand 2,6-$Me_2C_6H_3NC$ (1.16 Å). The centroid - metal - centroid angles of the three complexes are smaller than in the base-free complexes.[8,27] This is an expected consequence of the addition of two ligands to the coordination sphere of the metal; the distances and angles are similar to those found for other complexes of the type Cp'_2YbL_2.[26,28]

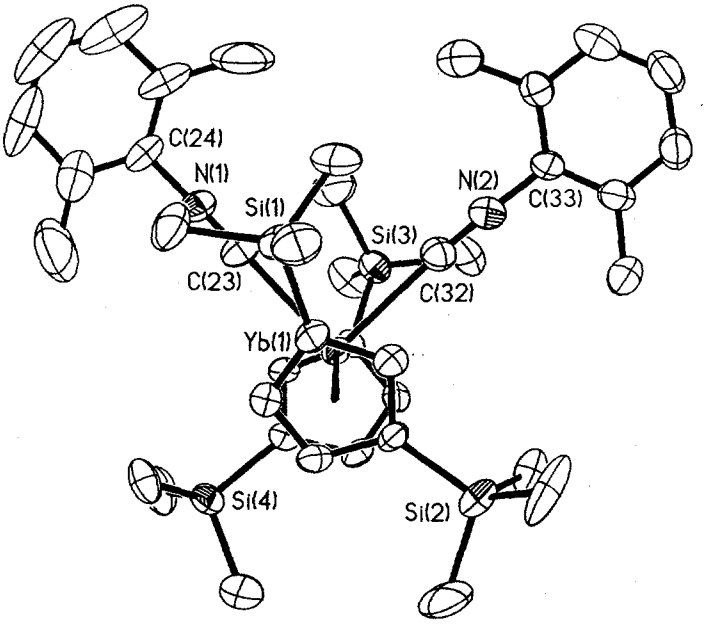

Figure 2.6. ORTEP diagram of [1,3-$(Me_3Si)_2C_5H_3]_2$Yb(2,6-$Me_2C_6H_3NC)_2$ (50% probability ellipsoids).

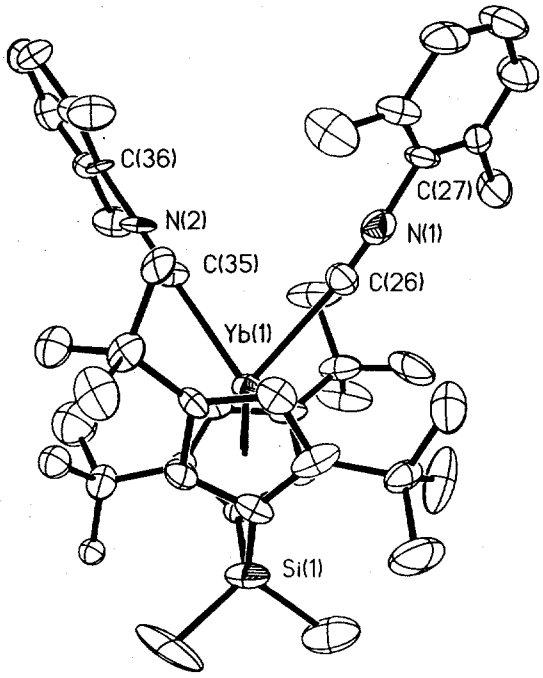

Figure 2.7. ORTEP diagram of *ansa*-[1,3-$(Me_3C)_2C_5H_2]_2SiMe_2Yb(2,6\text{-}Me_2C_6H_3NC)_2$ (only one of disordered Me_3C groups shown) (50% probability ellipsoids).

Table 2.6. Selected bond lengths (Å) and bond angles (°) for $Cp'_2Yb(2,6\text{-}Me_2C_6H_3NC)_2$

Cp'	Me_5C_5	$1,3\text{-}(Me_3C)_2C_5H_3$	$1,3\text{-}(Me_3Si)_2C_5H_3$	*ansa*-$[1,3\text{-}(Me_3C)_2C_5H_2]_2SiMe_2$
Yb - C_{ring} (mean)	2.69	2.72	2.70	2.71
Yb - C_{ring} (range)	2.668(4) - 2.724(4)	2.661(4) - 2.776(4)	2.579(6) - 2.750(6)	2.63(1) - 2.81(1)
Yb - centroid	2.41	2.44	2.42	2.43
centroid - Yb - centroid	144.5	133.4	137.1	123.1
twist angle	8.7	1.0	34.0	13.5
Yb - C_{CNR}	2.538(4)	2.61	2.56	2.57
C_{CNR} - N	1.165(5)	1.15	1.16	1.15
N - C_R	1.403(4)	1.40	1.42	1.44
C_{CNR} - Yb - C_{CNR}	91.7(2)	79.9(1)	90.5(2)	78.5(4)
Yb - C_{CNR} - N	167.3(3)	171.7	176.4	172.5
C_{CNR} - N - C_R	174.0(4)	177.1	177.8	178.0

The compound *ansa*-[1,3-$(Me_3C)_2C_5H_2]_2SiMe_2Yb(2,6\text{-}Me_2C_6H_3NC)_2$ shows the expected reduction in centroid - ytterbium - centroid angle due to the *ansa*-bridge. The arrangement of the xylyl isocyanide ligands is not affected, however.

The isocyanide complexes of the ytterbocenes are isolable 1:2 adducts which are therefore structural models for the postulated dicarbonyl adduct of $(Me_5C_5)_2Yb$. Structurally, the only notable difference between the three ytterbocene xylyl isocyanide complexes is the orientation of the disubstituted rings and the isocyanide ligands of those complexes as described above. The solid state structure is not maintained in solution since the adducts undergo fast intermolecular exchange on the NMR timescale, as expected for ytterbocene adducts.[19,29]

Addition of two equivalents of an impure (although distilled) sample of Me_3CNC to a solution of $(Me_5C_5)_2Yb(OEt_2)$ in toluene led to the isolation of an insoluble red crystalline solid. The infrared spectrum contains three bands at 2094, 2159 and 2197 cm^{-1}. These values suggest that the molecule is a mixed-valence dimer, as the lowest value of ν_{CN} is close to those reported for the bridging cyanide groups in the cyclic samarium(III) trimers $[(Me_5C_5)_2Sm(CNR)(\mu\text{-}CN)]_3$ (R = C_6H_{11}, Me_3C) of 2105 and 2110 cm^{-1}, respectively.[30] The other two values correspond to the CN stretching frequencies of isocyanide ligands bound to bivalent and trivalent ytterbocenes; 2159 cm^{-1} is similar to the values found for the bivalent isocyanide complexes discussed in this work, and 2197 cm^{-1} is close to the values reported for the complexes $(C_5H_5)_3Ln(CNC_6H_{11})$,[21] suggesting

a higher oxidation state metal. The elemental analysis of the red compound is consistent with the formulation $\{(Me_5C_5)_2Yb(Me_3CNC)\}_2$-μ-CN, with one molecule of toluene per dimer. The crystal structure of this complex was determined and it is found to be a mixed-valence dimer with a bridging cyanide ligand (Figure 2.8).

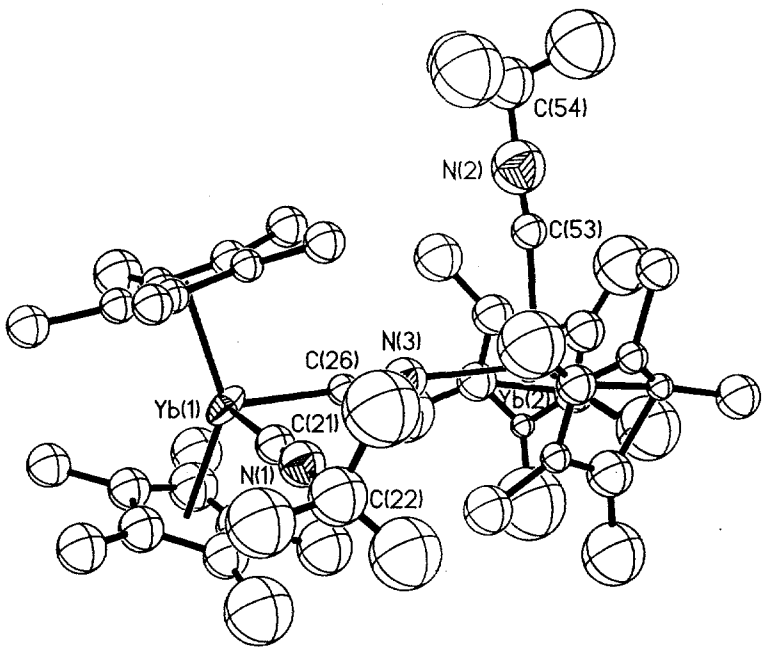

Figure 2.8. ORTEP diagram of $\{(Me_5C_5)_2Yb(Me_3CNC)\}_2$-μ-CN (50% probability ellipsoids). The toluene molecule and the disordered cyclopentadienyl atoms have been removed for clarity.

There is extensive disorder in the cyclopentadienide ligands on one metal center (Yb(2)) but the connectivity of the complex is established by the structure. Based on the metal - ring carbon distances and the metal - C_{CNR} distances, the two ytterbium centers appear to be localized as one Yb(III) (Yb1) and one Yb(II) (Yb2) (Table 2.7). These data are also

consistent with the orientation of the cyanide bridge, as the carbon end is bound to Yb(III) while the nitrogen end forms a dative bond to Yb(II).

Table 2.7. Selected bond distances (Å) and bond angles (°) of $\{(Me_5C_5)_2Yb(Me_3CNC)\}_2$-μ-CN

Yb(1) - C_{ring} (mean)	2.60	Yb(2) - C_{ring} (mean)	2.71
Yb(1) - C_{ring} (range)	2.53(3) - 2.66(3)	Yb(2) - C_{ring} (range)	2.62(4) - 2.77(3)
Yb(1) - centroid	2.30	Yb(2) - centroid	2.42
Yb(1) - C(21)	2.42(3)	Yb(2) - C(53)	2.52(3)
Yb(1) - C(26)	2.26(3)	Yb(2) - N(3)	2.53(2)
centroid - Yb(1) - centroid	142.3	centroid - Yb(2) - centroid	140.0
Yb(1) - C(21) - N(1)	178(2)	Yb(2) - C(53) - N(2)	170(2)
C(21) - N(1)	1.20(3)	C(53) - N(2)	1.17(3)
N(1) - C(22)	1.49(3)	N(2) - C(54)	1.51(3)
C(21) - N(1) - C(22)	176(2)	C(53) - N(2) - C(54)	176(3)
C(21) - Yb(1) - C(26)	92.1(8)	N(3) - Yb(2) - C(53)	87.5(7)
N(3) - C(26)	1.19(2)		

The magnetism of this complex was measured to determine whether it acts as a single Yb(III) center, diluted by the diamagnetic part of the molecule. Plots of $1/\chi$ vs T and μ vs T are shown in Figure 2.9.

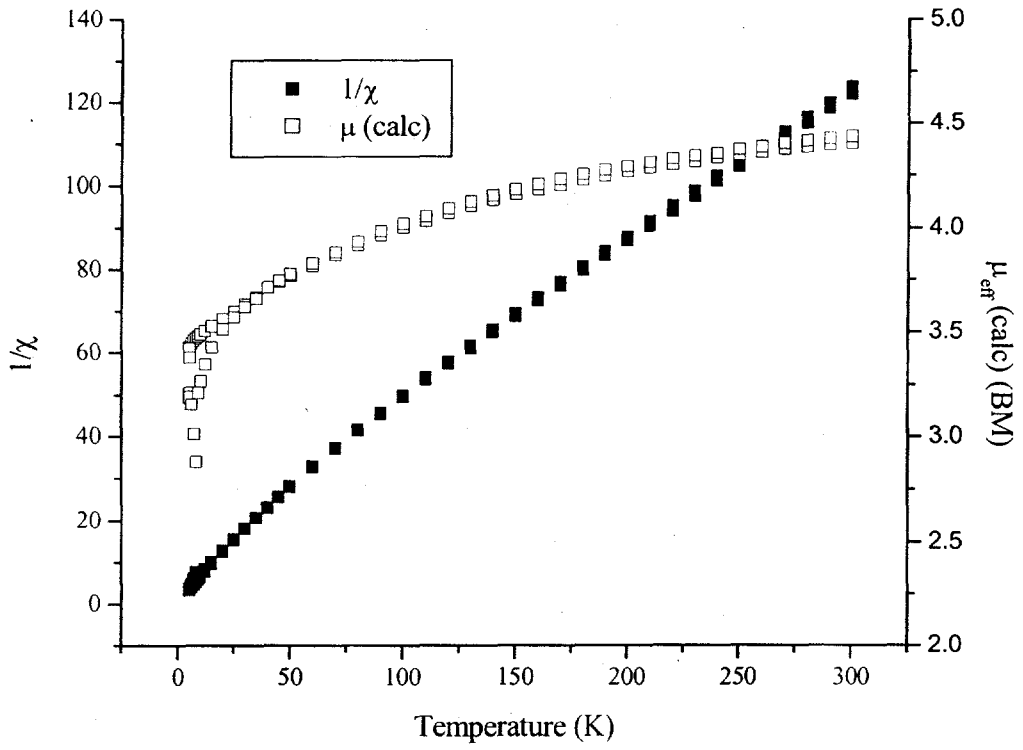

Figure 2.9. $1/\chi$ vs T and μ_{eff} vs T plots for $\{(Me_5C_5)_2Yb(Me_3CNC)\}_2$-$\mu$-CN.

Trivalent ytterbium is a paramagnetic $4f^{13}$ ion. In a low-symmetry ligand field the $^2F_{7/2}$ free ion ground state is split into four Kramer's doublets with a total separation that is less than kT at room temperature.[31] At low temperatures, only the two lowest levels are populated and contribute to the magnetic moment. As a result, at temperatures from 5 - 30 K, an Yb(III) complex is predicted to follow the Curie law ($C = \chi T$), with $\mu = 3.8$ BM as determined empirically. At temperatures above 30 K, thermal population of the third and fourth doublet levels becomes increasingly significant and the contribution of these levels to the magnetic moment results in a deviation from Curie law behavior. By 90 K,

both upper levels are easily accessible while the next manifold of states, arising from the $^2F_{5/2}$ term, is 10 300 cm^{-1} higher in energy and is not thermally accessible. The value of the magnetic moment can then be predicted using the formula $\mu = g\sqrt{J(J+1)}$ where $g = 1 + [J(J+1) - L(L+1) + S(S+1)]/[2J(J+1)]$ for the ground state $^2F_{7/2}$.[32] For J = 7/2, L = 3 and S = 1/2 this gives a predicted moment of $1.14\sqrt{(63/4)} = 4.52$ BM. A value of 4.5 BM has also been obtained empirically. Thus from 90 - 300K, the temperature dependence of the magnetic susceptibility follows the Curie-Weiss law ($C = \chi(T - \theta)$) with $\mu = 4.5$ BM. A plot of the inverse molar susceptibility ($1/\chi$) as a function of temperature for a typical Yb(III) compound therefore has two linear regions. The slope (1/C) of each region is directly related to the magnetic moment as $\mu = 2.828\ C^{1/2}$.

It can be seen that the plot of $1/\chi$ vs T for $\{(Me_5C_5)_2Yb(Me_3CNC)\}_2$-μ-CN does have two linear regions. The calculated moment is 3.6 BM at low temperature and 4.4 BM at high temperature, which are close to the predicted values for a single Yb(III) center. Thus, the molecule behaves as a localized trivalent ytterbium center bound to a bivalent center, as suggested by the X-ray crystal structure and infrared spectrum.

Conclusions

The interaction of a base-free ytterbocene with a π-acceptor ligand is a combination of σ-donation in the electrostatic model, and π-acceptance typical of *d*-transition metals. The former of these tends to reduce the electron density on the ligand, while the latter

increases the electron density on the ligand. In the case of carbon monoxide interacting with the electron-rich ytterbocenes $(Me_5C_5)_2Yb$ and $[1,3\text{-}(Me_3C)_2C_5H_3]_2Yb$, the σ-donation component is weak and the π-acceptance by CO is strong, resulting in an increase in the electron density of the ligand. This reduces the CO bond order and stretching frequency, because the LUMO of CO is a C - O antibonding orbital. The Me_3Si groups of $[1,3\text{-}(Me_3Si)_2C_5H_3]_2Yb$ are electron-withdrawing, so that the ytterbium center is relatively electropositive, and the σ-component of bonding outweighs the π-acceptance. This results in a slight increase in CO bond order and ν_{CO} as the electron density on CO is reduced.

Isocyanides are better σ-donors and poorer π-acceptors than carbon monoxide, so the CN stretching frequency is always increased when an isocyanide binds to any ytterbocene. However, this does not rule out the possibility of any π-acceptance, and the CN stretching frequency indicates the balance of σ-donation and π-acceptance by the ligand. Comparison of the CN stretching frequencies of $(Me_5C_5)_2Ca(2,6\text{-}Me_3C_6H_3NC)_2$ and $(Me_5C_5)_2Yb(2,6\text{-}Me_3C_6H_3NC)_2$ indicates that ytterbium is acting as a π-donor to a small extent in that molecule, consistent with the values of ν_{CO} in the analogous carbonyl compounds.

References

1) Selg, P.; Brintzinger, H. H.; Andersen, R. A., in preparation.

2) Schwartz, D. J. *PhD Thesis*; University of California: Berkeley, 1995.

3) Howard, W. A.; Parkin, G. F. R.; Rheingold, A. L. *Polyhedron* **1995**, *14*, 25.

4) Selg, P.; Brintzinger, H. H.; Andersen, R. A.; Horvath, I. T. *Angew. Chem., Int. Ed. Engl.* **1995**, *34*, 791.

5) Shannon, R. D. *Acta Crystallogr., Sect. A* **1976**, *A32*, 751.

6) Burns, C. J. *PhD Thesis*; University of California: Berkeley, 1987.

7) Andersen, R. A.; Blom, R.; Boncella, J. M.; Burns, C. J.; Volden, H. V. *Acta Chem. Scand. A* **1987**, *A41*, 24.

8) Schultz, M.; Burns, C. J.; Schwartz, D. J.; Andersen, R. A. *Organometallics* **2000**, *19*, 781.

9) Williams, R. A.; Hanusa, T. P.; Huffman, J. C. *Organometallics* **1990**, *9*, 1128.

10) Selg, P. *PhD Thesis*; University of Konstanz: Konstanz, Germany, 1996.

11) Hays, M. L.; Hanusa, T. P. *Adv. Organomet. Chem.* **1997**, *40*, 117.

12) Goldman, A. S.; Krogh-Jesperson, K. *J. Am. Chem. Soc.* **1996**, *118*, 12159.

13) Hush, N. S.; Williams, M. L. *J. Mol. Spect.* **1974**, *50*, 349.

14) Willner, H.; Aubke, F. *Angew. Chem., Int. Ed. Engl.* **1997**, *36*, 2402.

15) Strauss, S. H. *Chemtracts - Inorg. Chem.* **1997**, *10*, 77.

16) Green, J. C.; Hohl, D.; Rösch, N. *Organometallics* **1987**, *6*, 712.

17) Evans, W. J.; Grate, J. W.; Hughes, L. A.; Zhang, H.; Atwood, J. L. *J. Am. Chem. Soc.* **1985**, *107*, 3728.

18) Evans, W. J.; Ulibarri, T. A.; Ziller, J. W. *J. Am. Chem. Soc.* **1988**, *110*, 6877.

19) Burns, C. J.; Andersen, R. A. *J. Am. Chem. Soc.* **1987**, *109*, 941.

20) Burns, C. J.; Andersen, R. A. *J. Am. Chem. Soc.* **1987**, *109*, 5853.

21) Fischer, E. O.; Fischer, H. *J. Organomet. Chem.* **1966**, *6*, 141.

22) von Ammon, R.; Kanellakopulos, B. *Ber. Buns. Phy. Chem.* **1972**, *76*, 995.

23) Burns, C. J.; Andersen, R. A. *J. Organomet. Chem.* **1987**, *325*, 31.

24) Jacobsen, H.; Berke, H.; Doring, S.; Kehr, G.; Erker, G.; Frohlich, R.; Meyer, O. *Organometallics* **1999**, *18*, 1724.

25) Stauch, H. C.; Wibbeling, B.; Frohlich, R.; Erker, G.; Jacobsen, H.; Berke, H. *Organometallics* **1999**, *18*, 3802.

26) Tilley, T. D.; Andersen, R. A.; Spencer, B.; Ruben, H.; Zalkin, A.; Templeton, D. H. *Inorg. Chem.* **1980**, *19*, 2999.

27) Hitchcock, P. B.; Howard, J. A. K.; Lappert, M. F.; Prashar, S. *J. Organomet. Chem.* **1992**, *437*, 177.

28) Tilley, T. D.; Andersen, R. A.; Spencer, B.; Zalkin, A. *Inorg. Chem.* **1982**, *21*, 2647.

29) Burns, C. J.; Andersen, R. A. *J. Am. Chem. Soc.* **1987**, *109*, 915.

30) Evans, W. J.; Drummond, D. K. *Organometallics* **1988**, *7*, 797.

31) Boudreaux, E. A.; Mulay, L. N. *Theory and Applications of Molecular Paramagnetism*; Wiley-Interscience: New York, 1976.

32) Gerloch, M.; Constable, E. C. *Transition Metal Chemistry*; VCH: Weinheim, 1995.

Chapter Three : The Electronic Structure of Polypyridyl Complexes of Ytterbocenes

2,2'-Bipyridyl Complexes

The dark red-brown complex $(Me_5C_5)_2Yb(bipy)$ (bipy = 2,2'-bipyridyl) has been synthesized previously.[1,2] The 2,2'-bipyridyl complexes of the other substituted ytterbocenes are synthesized in a similar manner, in toluene (Equation 1). The solubility of these complexes is relatively low, which makes recrystallization and low-temperature solution measurements difficult. Some physical characteristics of the complexes are collected in Table 3.1.

$$Cp'_2Yb(OEt_2) + bipy \rightarrow Cp'_2Yb(bipy) + OEt_2 \qquad (1)$$

$Cp' = Me_5C_5$, 1,3-$(Me_3C)_2C_5H_3$, 1,3-$(Me_3Si)_2C_5H_3$, Me_4C_5H

Cp'_2 = *ansa*-[1,3-$(Me_3C)_2C_5H_2]_2SiMe_2$

The parent complex $(C_5H_5)_2Yb(bipy)$ is prepared by reaction of KC_5H_5 with YbI_2 in THF followed by addition of the filtrate into a stoichiometric amount of 2,2'-bipyridyl. This compound is only sparingly soluble in aliphatic and aromatic solvents, and cannot be recrystallized. It is purified by repeated washing with hot toluene and diethyl ether.

Previous studies concluded that the bipyridyl ligands in $(Me_5C_5)_2Yb(bipy)$ and $(Me_5C_5)_2Yb(dmb)$ (dmb = 4,4'-dimethyl-2,2'-bipyridyl) are reduced, based on crystallographic, infrared and optical spectroscopic data.[1-3] However, the magnetism of these molecules does not follow the expected curve and the observations warranted re-examination and extension to the new ytterbocenes prepared in this work.

Table 3.1. Solid state characteristics of ytterbocene bipyridyl complexes

compound	**color**	**mp (°C)**	**IR (cm^{-1})**	**μ_{eff} (300K)**	**ref.**
$(Me_5C_5)_2Yb(bipy)$	red-brown	322-323	942, 1553	2.4 BM	1,2
$[1,3\text{-}(Me_3C)_2C_5H_3]_2Yb(bipy)$	blue-green	278-280	1593	diamagnetic	this work
$[1,3\text{-}(Me_3Si)_2C_5H_3]_2Yb(bipy)$	green	208-212	1594	diamagnetic	this work
$(Me_4C_5H)_2Yb(bipy)$	red-brown	285-288	948, 1549	2.9 BM	this work
ansa-$[1,3\text{-}(Me_3C)_2\text{-}C_5H_2]_2SiMe_2Yb(bipy)$	blue	337-338	1594	diamagnetic	this work
$(C_5H_5)_2Yb(bipy)$	dark blue	218-220	1587	diamagnetic	this work
$[(Me_5C_5)_2Yb(bipy)]^+[I]^-$	red-brown	125-130	1595	4.2 BM	2,3
$[(Me_5C_5)_2Yb(bipy)]^+$ $[(Me_5C_5)_2YbCl_2]^-$	red	264-266	1598	6.4 BM	2
$(Me_5C_5)_2Eu(bipy)$	red-brown	328-332	1591	7.4 BM	1, this work
$(Me_5C_5)_2Ca(bipy)$	orange	>300	1598	diamagnetic	4, this work

The reduction potentials of the bipyridyl ligands used here are as follows (V vs SCE in anhydrous DMF)[5]: 2,2'-bipyridyl, 2.10; 4,4'-dimethyl-2,2'-bipyridyl, 2.12. These values can be compared with the measured oxidation potential of $(Me_5C_5)_2Yb$ in acetonitrile of 1.78 V vs $Cp_2Fe/[Cp_2Fe]^+$ [6] which is equivalent to 1.3 V vs SCE. Based on these values, the ytterbium center is not capable of reducing the organic ligand by an outer sphere process. However, when a ligand is coordinated to a metal the reduction potential of the ligand is reduced, which promotes electron transfer. This is expected because reduction increases the basicity of the reduced ligand, which increases its affinity for the electropositive ytterbium center.

The complex $(Me_5C_5)_2Yb(bipy)$ is oxidized by silver iodide to give the brown complex $[(Me_5C_5)_2Yb(bipy)]^+[I]^-$, which can be converted back to $(Me_5C_5)_2Yb(bipy)$ by reaction with sodium amalgam in THF.[2] Addition of bipyridyl to the trivalent complex $(Me_5C_5)_2YbCl(THF)$ results in isolation of the red-brown salt $[(Me_5C_5)_2Yb(bipy)]^+[(Me_5C_5)_2YbCl_2]^-$.[2] These two salts of the $[(Me_5C_5)_2Yb(bipy)]^+$ cation as well as the complexes $(Me_5C_5)_2Eu(bipy)$[1] and $(Me_5C_5)_2Ca(bipy)$[4] contain the metal and ligand in known oxidation states, making these molecules useful for comparison with $(Me_5C_5)_2Yb(bipy)$ and other ytterbocene-bipyridyl complexes.

The infrared spectrum of bipyridyl as a neutral and reduced ligand has been studied extensively, enabling the oxidation state of this ligand to be determined by infrared spectroscopy.[7] A strong absorbance is expected for bipyridyl radical anion in the region 1000 - 900 cm^{-1} due to ring deformation modes of the ligand. In the 1625 - 1475 cm^{-1}

region, where the C=C and C=N stretching bands of the bipyridyl ligand are expected, both bands are shifted to lower frequencies as the oxidation state of the ligand is lowered. Thus, Saito *et al.* classify bipyridyl ligands as neutral if no strong absorption is present in the range 1000 to 900 cm^{-1} and a strong band is present around 1610 - 1600 cm^{-1}, and reduced if a strong absorption is present in the 1000 - 900 cm^{-1} region and several strong to medium intensity bands in the 1575 - 1490 cm^{-1} region are observed. Table 3.1 includes only the bands in those regions for the molecules described here. The infrared spectrum of free 2,2'-bipyridyl as a Nujol mull contains peaks at 1620 and 1580 cm^{-1}, so peaks at those frequencies observed for the molecules described here may also be due to the presence of free ligand.

The infrared spectrum of $(Me_5C_5)_2Yb(bipy)$ contains a peak at 942 cm^{-1}, as does the infrared spectrum of $(Me_5C_5)_2Yb(dmb)$, which identifies the ligand as the reduced radical anion.[1,3] The complexes $[1,3\text{-}(Me_3C)_2C_5H_3]_2Yb(bipy)$, $[1,3\text{-}(Me_3Si)_2C_5H_3]_2Yb(bipy)$ and *ansa*-$[1,3\text{-}(Me_3C)_2C_5H_2]_2SiMe_2Yb(bipy)$ do not have such a peak in their infrared spectra; instead they have a peak at 1594 cm^{-1}, identifying the bipyridyl ligand as neutral. Similarly, the cationic complexes $[(Me_5C_5)_2Yb(bipy)]^+[I]^-$ and $[(Me_5C_5)_2Yb(bipy)]^+[(Me_5C_5)_2YbCl_2]^-$ have peaks at 1595 and 1598 cm^{-1},[2] while the europium and calcium complexes $(Me_5C_5)_2Eu(bipy)$[1] and $(Me_5C_5)_2Ca(bipy)$[4] also have peaks in their infrared spectra at 1591 and 1592 cm^{-1}, respectively, consistent with the bipyridyl ligand being neutral in the cationic, europium and calcium complexes. The infrared spectrum of $(Me_4C_5H)_2Yb(bipy)$ contains similar bands to those of $(Me_5C_5)_2Yb(bipy)$, which are diagnostic of the presence of the radical anion of bipyridyl.

The infrared spectrum of $(C_5H_5)_2Yb(bipy)$ is different from those of substituted ytterbocene - bipyridyl complexes, but the strong band at 1587 cm^{-1} is interpreted as diagnostic of neutral bipyridyl. The infrared criterion is necessarily qualitative since the interpretation is based on the presence of features rather than their intensity.

The X-ray crystal structures of bipyridyl complexes have been used as evidence for the oxidation state of bipyridyl, because donation of electron density into the LUMO of bipyridyl causes known changes to the bond lengths in that ligand.[8] The LUMO of bipyridyl is represented in Figure 3.1.[9]

Figure 3.1. Schematic diagram of the LUMO of 2,2'-bipyridyl and diagram showing bond labelling scheme.

It can be seen that upon acceptance of an electron into the LUMO, the bonds A, C and E are expected to shorten, while the bonds B, D, F and G are expected to lengthen. The structures of $(Me_5C_5)_2Yb(bipy)$, and $[(Me_5C_5)_2Yb(bipy)]^+[(Me_5C_5)_2YbCl_2]^-$ have previously been determined.[2] The structure of $[1,3\text{-}(Me_3C)_2C_5H_3]_2Yb(bipy)$ was determined for comparison, and an ORTEP diagram is shown in Figure 3.2. Table 3.2 compares the metrical parameters of the bipyridyl ligand in these complexes with that of free bipyridyl. Based on these values, the bipyridyl ligand appears to be reduced in $(Me_5C_5)_2Yb(bipy)$, but neutral in the other two structurally characterized complexes.

This is consistent with the oxidation state of the bipyridyl ligand as determined from the infrared data for these compounds.

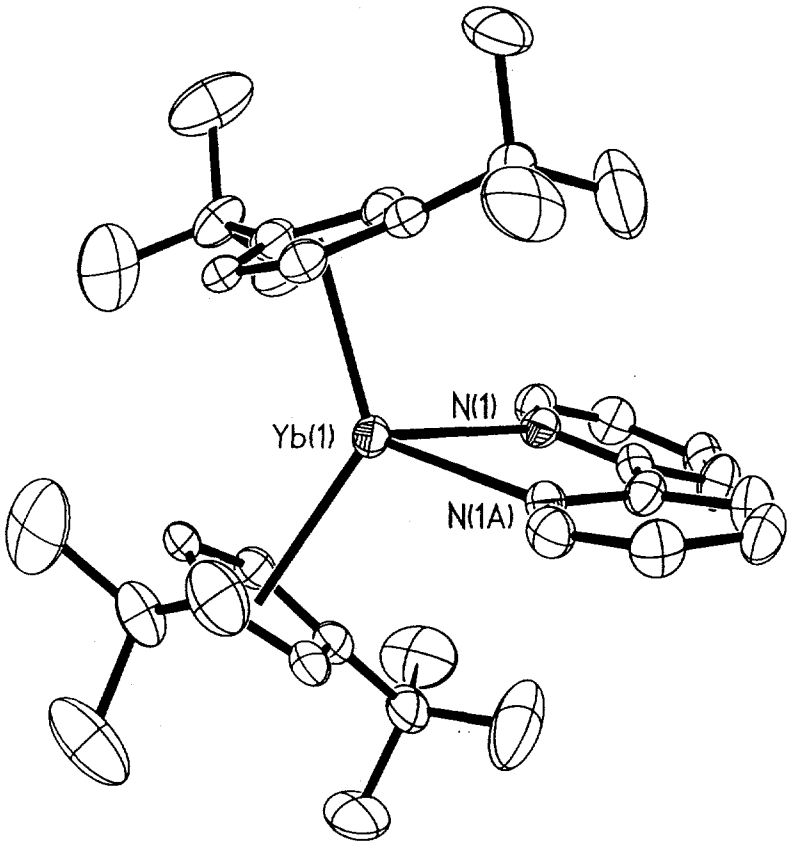

Figure 3.2. ORTEP diagram of $[1,3\text{-}(Me_3C)_2C_5H_3]_2Yb(bipy)$ (50% probability ellipsoids) showing torsion of 2,2'-bipyridyl ligand.

Table 3.2. Bond distances (Å) of 2,2'-bipyridyl from X-ray crystallography

bond	free bipyridyl[a]	$(Me_5C_5)_2Yb(bipy)$[b]	$[(Me_5C_5)_2Yb(bipy)]^+$ $[(Me_5C_5)_2YbCl_2]^-$[b]	$[1,3\text{-}(Me_3C)_2\text{-}C_5H_3]_2Yb(bipy)$
A	1.490(3)	1.434	1.492(4)	1.48(1)
B	1.394(2)	1.419	1.385	1.392(8)
C	1.385(2)	1.387	1.380	1.386(9)
D	1.383(3)	1.420	1.370	1.376(8)
E	1.384(2)	1.398	1.370	1.369(8)
F	1.341(2)	1.358	1.339	1.338(8)
G	1.346(2)	1.383	1.343	1.351(7)

a From ref. 8; *b* from ref. 2.

Acceptance of an electron into the LUMO shown in Figure 3.1 is also expected to flatten the bipyridyl ligand as it gives double bond character to the bond A. Conversely, if a bipyridyl ligand has a high torsion angle between the two pyridyl rings, this is an indication that the ligand is neutral in that complex. From Figure 3.2 and Table 3.3 it can be seen that the bipyridyl ligand is planar in the molecule $(Me_5C_5)_2Yb(bipy)$ but not planar in the other two bipyridyl complexes. This is further evidence for the oxidation state of the ligand in these three molecules. The bipyridyl ligand of $[1,3\text{-}(Me_3C)_2C_5H_3]_2Yb(bipy)$ is twisted towards the nearest Me_3C groups on the cyclopentadienide rings, indicating that the twist is not the result of steric hindrance to planarity. However, were the ligand reduced, the ionic radius of the metal would also

decrease, reducing the metal - cyclopentadienide distance, which may cause unfavourable interactions of the Me_3C groups at the back side of the metallocene wedge.

Table 3.3 contains other important bond distances and angles for these molecules. The distance from a ligand to a metal is correlated with the oxidation state of the metal, as the ionic radius is smaller in a higher oxidation state.[10] Examination of the mean metal - ring carbon distance, the metal - centroid distance and the metal - nitrogen distance indicates that in the first two structures, the ytterbium atom is Yb(III) while in $[1,3\text{-}(Me_3C)_2C_5H_3]_2Yb(bipy)$ it is Yb(II). This is consistent with the oxidation state as determined from the metrical parameters of the bipyridyl ligand. These values can also be compared with the corresponding values for $(Me_5C_5)_2Yb(py)_2$, in which the metal is divalent.[11] In that molecule, the mean metal - ring carbon distance is 2.74 Å and the mean metal - nitrogen distance is 2.56 Å.

Table 3.3. Selected bond distances (Å) and bond angles (°) of $(Me_5C_5)_2Yb(bipy)$, $[(Me_5C_5)_2Yb(bipy)]^+[(Me_5C_5)_2YbCl_2]^-$ and $[1,3\text{-}(Me_3C)_2C_5H_3]_2Yb(bipy)$

	$(Me_5C_5)_2Yb(bipy)$[a]	**$[(Me_5C_5)_2Yb(bipy)]^+$ $[(Me_5C_5)_2YbCl_2]^-$[a]**	**$[1,3\text{-}(Me_3C)_2C_5H_3]_2$ Yb(bipy)**
Yb - C_{ring} (mean)	2.62	2.59	2.75
Yb - C_{ring} (range)	2.592(9) - 2.647(7)	2.582(3) - 2.614(3)	2.674(6) - 2.803(6)
Yb - centroid	2.34; 2.34	2.30	2.47
centroid - Yb - centroid	138.8; 139.9	141.5	131.6
twist angle	31; 27	33	22
Yb - N	2.32	2.37	2.503(4)
torsion angle N-C-C-N	3	7	15
torsion angle C-C-C-C	3	8	19

a From ref. 2.

Data for two unique molecules in the unit cell presented as Yb(1); Yb(2).

Magnetic susceptibility measurements provide direct information on the electronic structure of the molecule, and the interaction of unpaired ligand spins with paramagnetic Yb(III). For a complex containing Yb(III) and a reduced bipyridyl ligand, if the ytterbium and radical anion spins are non-interacting, the contribution of the spins to

molar magnetic susceptibility are additive. The expected moment per molecule can then be calculated as follows:

$$\chi_T = \chi_1 + \chi_2$$

$$\chi_T T = \chi_1 T + \chi_2 T$$

$$\mu^2 = (2.828)^2(\chi T)^2$$

$$\mu_T^2 = \mu_1^2 + \mu_2^2$$

$$\mu_T = (\mu_1^2 + \mu_2^2)^{1/2}$$

Using the low and high temperature values of μ for the ytterbium center, as described in Chapter 2, the predicted magnetic moment can then be calculated.

Low temperature: $\mu = \sqrt{(3.8)^2 + (1.73)^2} = 4.2$ BM.

High temperature: $\mu = \sqrt{(4.5)^2 + (1.73)^2} = 4.8$ BM.

This calculation is not valid for a molecule in which the unpaired spins are coupled. Hatfield has studied lanthanide - phthalocyaninato complexes in which exchange coupling is observed.[12] Figure 3.3 represents the energy level splitting for a Yb(III) ion that is strongly coupled to an organic radical. For a system involving strong electron exchange coupling, the new term symbol can be calculated based on a linear combination of the $^2F_{7/2}$ term of ytterbium and the $^2S_{1/2}$ term of the radical. For an antiferromagnetic interaction, this new term is $^{2S}L_{J\,-\,1/2} = {}^1F_3$, while for a ferromagnetic interaction the new term is $^{2S\,+\,2}L_{J\,+\,1/2} = {}^3F_4$.

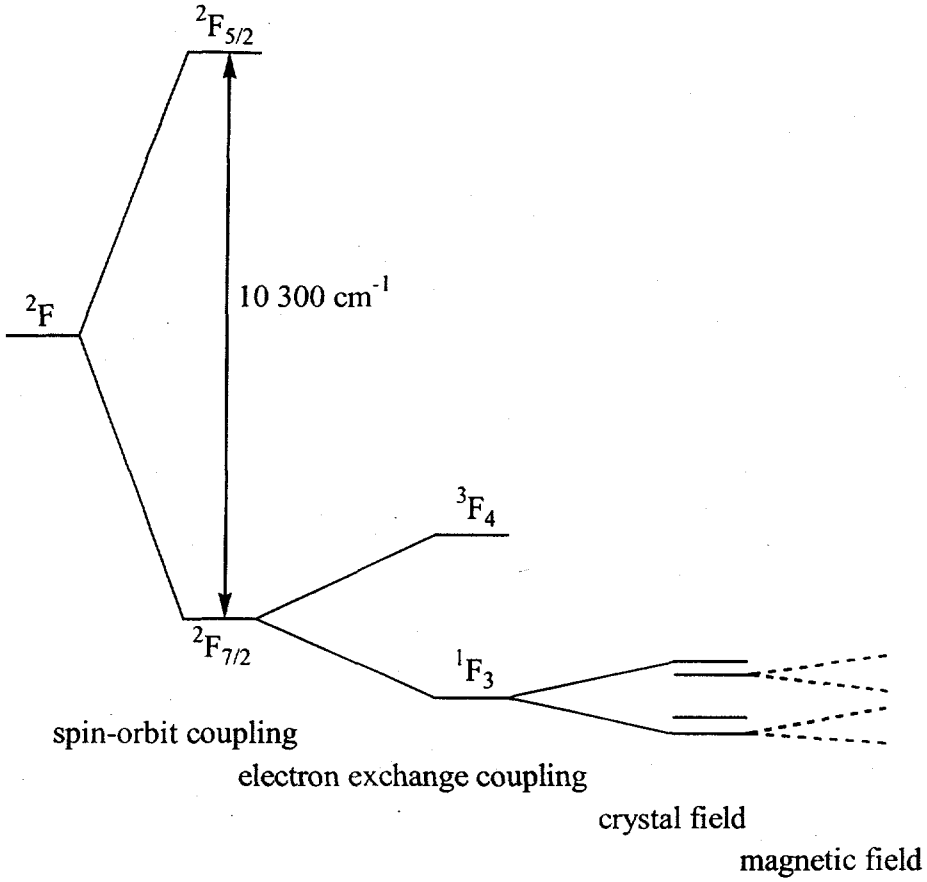

Figure 3.3. Schematic diagram of the energy level splitting for a Yb(III) ion including a strong interaction with an organic radical anion (from ref. 12).

The low and high limiting values for the room temperature moment of Yb(III), antiferro- or ferromagnetically coupled with an organic radical, can then be calculated from the new term symbols as was done for the ground state $^2F_{7/2}$ of non-interacting Yb(III) in Chapter 2. For the antiferromagnetically coupled system, the term symbol $^1F_3$ implies S = 0, L = 3, J = 3. Then g = 1 + [3(4) - 3(4) + 0]/2(3)(4) = 1, and $\mu = 1\sqrt{3(4)} = 3.46$ B M. Similarly, for ferromagnetic coupling, the term symbol $^3F_4$ implies S = 1, L = 3, J = 4. Then g = 1 + [4(5) - 3(4) + 1(2)]/2(4)(5) = 5/4, and $\mu = (5/4)\sqrt{4(5)} = 5.59$ BM. Strong

antiferromagnetic coupling in this system corresponds to a molecule with no formally unpaired spins, and the magnetism is attributed solely to orbital angular momentum.

The experimental value of the room temperature effective moment found for $Yb(pc)_2$ (pc = phthalocyanine) is 4.3 BM, and the authors conclude that this molecule exhibits both the antiferro- and ferromagnetically coupled states of the lanthanide and the phthalocyanine radical electrons.[12] As shown in Figure 3.3, depending on the magnitude of the splitting between the antiferro- and ferromagnetically coupled states, the ferromagnetically coupled state may become populated at high temperatures.

Although the value of the magnetic moment can vary between 3.46 BM and 5.59 BM according to this model, the shapes of the plots of $1/\chi$ vs T and μ vs T are expected to be the same for all molecules involving a single Yb(III) center. Those shapes were seen in Chapter 2 for $\{(Me_5C_5)_2Yb(Me_3CNC)\}_2$-$\mu$-CN; the $1/\chi$ vs T plot has two linear regions with similar gradients, and the calculated μ vs T plot increases slightly from low temperature to an asymptotic value at high temperature, corresponding to the limiting value of the magnetic moment just described. This behavior is also observed for the cationic complexes $[(Me_5C_5)_2Yb(bipy)]^+[(Me_5C_5)_2YbCl_2]^-$ and $[(Me_5C_5)_2Yb(bipy)]^+[I]^-$. For the former, the room temperature effective moment is 6.6 BM, close to the predicted $\mu = \sqrt{(4.5)^2 + (4.5)^2} = 6.4$ BM, corresponding to the two uncoupled Yb(III) centers. The latter cationic salt has an effective moment of 4.2 BM, close to the predicted 4.5 BM due to the single Yb(III) center.[2,3]

Magnetic measurements have been made on the complexes described here from 5 - 300K at high and low magnetic fields (5, 40 kG). Plots of $1/\chi$ vs T and μ vs T for $(Me_4C_5H)_2Yb(bipy)$ are shown in Figure 3.4. These data are very similar to those previously measured for $(Me_5C_5)_2Yb(bipy)$,[2] and do not follow the predicted shape described above. The plot of $1/\chi$ vs T increases sharply and has a maximum at approximately 150 K, while the calculated μ vs T plot increases linearly from a low value of 0.8 BM to a maximum of 2.9 BM. The value of μ is calculated as described in Chapter 2 as $2.828\sqrt{(\chi T)}$.

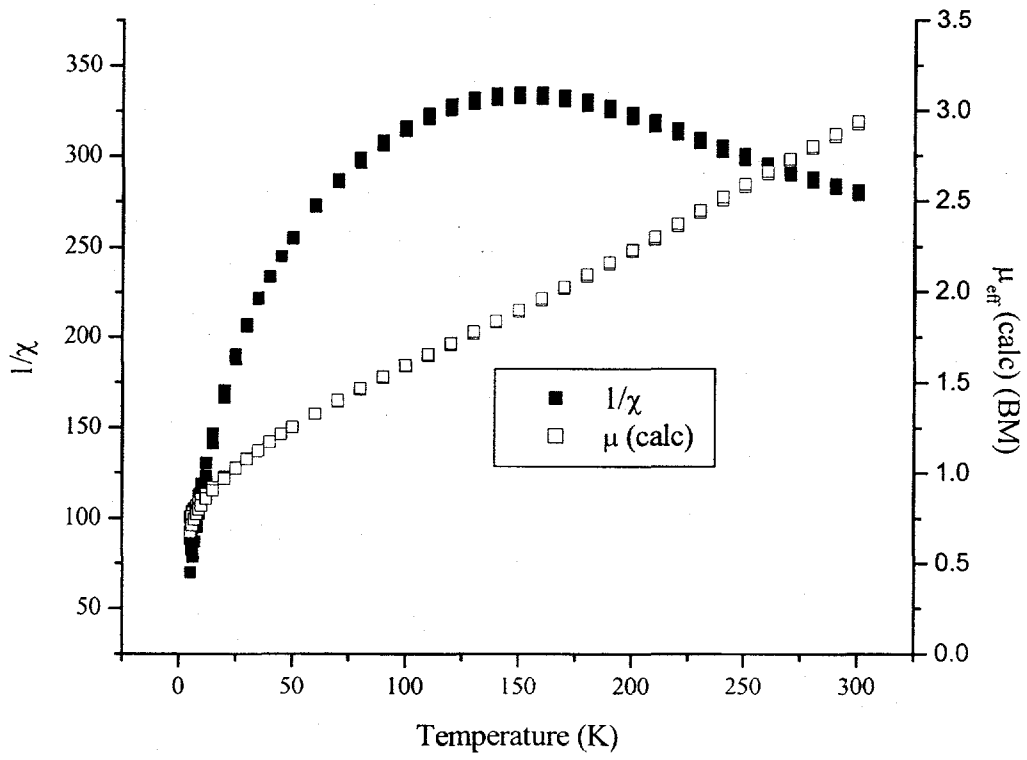

Figure 3.4. $1/\chi$ vs T and μ_{eff} vs T plots for $(Me_4C_5H)_2Yb(bipy)$.

These data may be explained by electron exchange coupling if the lowest spin J state is occupied at low temperatures, and the relative energies of the four J states change over the temperature range examined. This is precedented in calculations on U(IV) ($5f^2$), for which the relative energies of the J states are expected to change dramatically over the temperature range 5 - 300 K.[13,14]

Kahn *et al.* have studied lanthanide - radical anion complexes for Ln = Ce - Dy.[15] They address the issue of thermal population of crystal field levels of lanthanide metals, which leads to a temperature-dependent magnetic moment. The degree of spin-orbit coupling to an organic radical also varies with temperature, so that phenomenon also gives rise to a temperature-dependent magnetic moment. The two effects cannot be disentangled as there is no general theoretical model to describe the magnetic behavior of a lanthanide ion in its ligand field. Thus, the data shown above cannot be modelled.

It can be seen from the divergence of the data at the two fields used in Figure 3.4 that the magnetic moment is field dependent at low temperatures. The magnetization of $(Me_5C_5)_2Yb(bipy)$ was examined as a function of the applied field at temperatures of 5, 10 and 20K (Figure 3.5).

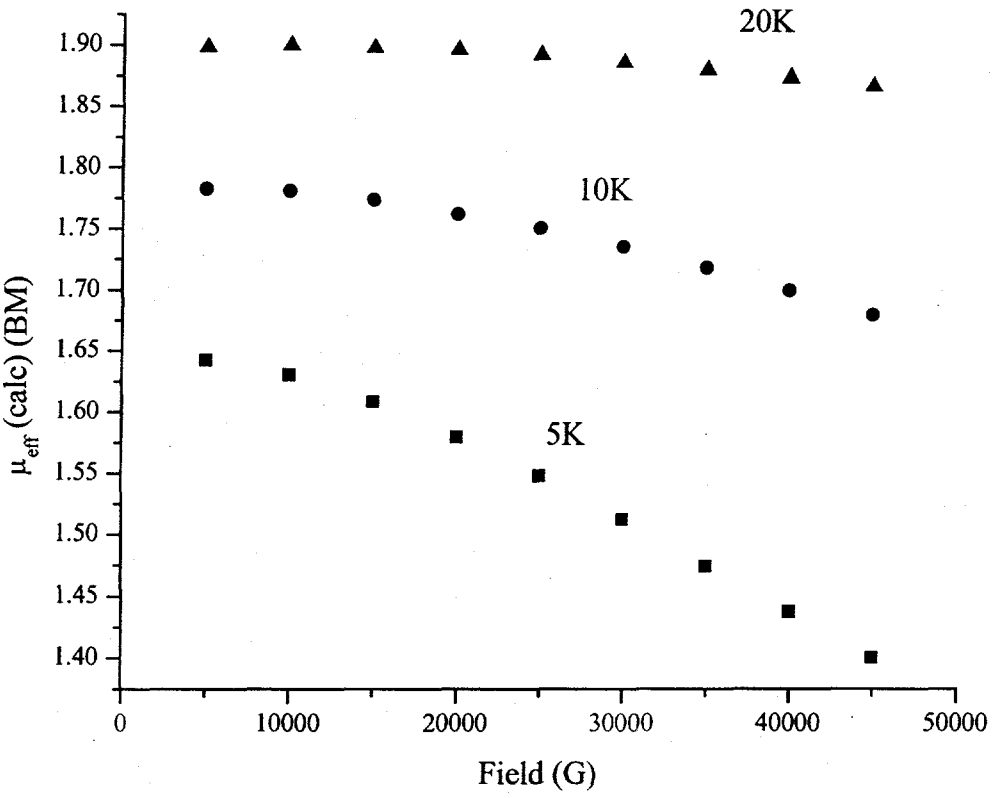

Figure 3.5. Field dependence of magnetic moment of $(Me_5C_5)_2Yb(bipy)$ at 5, 10 and 20K.

At 5K, the effective moment becomes smaller as the field is increased, while above 20K the moment is field-independent. This indicates that at low temperatures, the internal field of the sample is reduced by antiferromagnetic interactions. The overall moment becomes higher as the temperature increases, due to population of higher spin states as described above, and the effect of varying the field is no longer observed. The observed field dependence of the magnetic moment therefore supports the proposition that there is

antiferromagnetic coupling between the radical anion and the Yb(III) center which reduces the magnetic moment at low temperatures.

A model involving a reversible electron exchange equilibrium can also be proposed to rationalize the magnetic susceptibility data of the ytterbocene - bipyridyl complexes. According to this model, the ytterbocene - bipyridyl compounds consist, in the solid state, of a mixture of the two molecules $Cp'_2Yb(II)(bipy^0)$ and $Cp'_2Yb(III)(bipy^-)$ which interconvert by transferring an electron between the metal and the ligand (Scheme 1). This results in a magnetic moment that is lower than expected for a compound consisting only of Yb(III) centers, as $Cp'_2Yb(II)(bipy^0)$ is diamagnetic and acts as a dilutant to the magnetism of the bulk compound. The proportion of the dilutant varies with temperature, which leads to an unusual shape of $1/\chi$ vs T and a linearly increasing μ vs T plot. The translational and rotational entropy of the two molecules is similar, and although the diamagnetic compound has more vibrational entropy, the paramagnetic complex should be entropically favored, as it has many more possible electronic states.

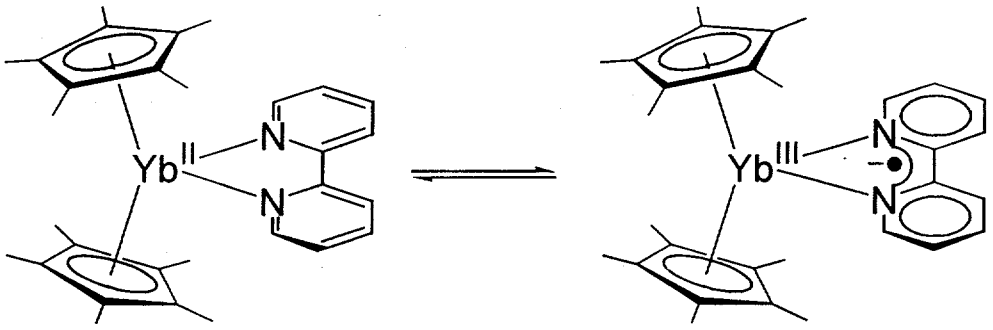

diamagnetic paramagnetic

Scheme 1. Proposed electron exchange equilibrium for ytterbocene - bipyridyl complexes.

Attempts were made to calculate the proportion of the paramagnetic complex by dividing the measured moment by the expected moment at each temperature. This leads to values for the equilibrium constant K_{eq} for the reaction shown in Scheme 1. However, the resulting plot of ΔG_0 vs T is non-linear, so no useful thermodynamic information could be obtained. This implies that the system is not a simple equilibrium, presumably due to variable mixtures of both the antiferro- and ferromagnetically coupled states.[12] Previous research has concluded that the system cannot be modelled.[2,3] However, other experiments described below support the proposal of an electron transfer equilibrium.

For either an electron exchange coupling or an equilibrium model, varying the substituents should perturb the system and lead to different magnetic behavior. This is in fact observed; the disubstituted ytterbocenes $[1,3\text{-}(Me_3C)_2C_5H_3]_2Yb(bipy)$ and $[1,3\text{-}(Me_3Si)_2C_5H_3]_2Yb(bipy)$, as well as *ansa*-$[1,3\text{-}(Me_3C)_2C_5H_2]_2SiMe_2Yb(bipy)$ and

$(C_5H_5)_2Yb(bipy)$ are found to be diamagnetic in the solid state. The measured magnetic susceptibility is expected to be negative and the measured values were negative for extremely pure samples. Thus, both models provide qualitative explanations for the observed magnetic data; however, the physical process of electron exchange coupling or reversible electron transfer are very different.

Berg has examined the effects of varying the substituents on the bipyridyl ligand. Use of 4,4'-dimethyl-2,2'-bipyridyl and 4,4'-dicarboxylate-2,2'-bipyridine diethyl ester as ligands leads $(Me_5C_5)_2Yb$ complexes with $1/\chi$ vs T and μ vs T plots that are similar in shape to those of 2,2'-bipyridyl.[3] The value of μ is found to be higher for the carboxylate complex, varying from 1.3 BM at low temperature to 3.4 BM at high temperature, presumably due to the electron-withdrawing effect of the substituents on the bipyridyl, which perturb the equilibrium towards the paramagnetic side. Also, the $(Me_5C_5)_2Yb$ complex of N,N'-(p-tolyl)$_2$-1,4-diazadiene has similar curves for $1/\chi$ vs T and μ vs T although the maximum value of $1/\chi$ occurs at 80 K rather than 150 K, and the values of μ for that compound range from 0.7 - 3.9 BM. The unsubstituted diazadiene complex $(C_5H_5)_2Yb$(N,N-$(Me_3C)_2$-1,4-diazadiene) also has the unusual curves of $1/\chi$ vs T and μ vs T, with the maximum value of $1/\chi$ at 130 K, and μ ranging from 0.8 - 3.3 BM.[16] The fact that curves of this type have been observed for a variety of ligand sets on ytterbium suggests that the $(Me_5C_5)_2Yb(bipy)$ is not an anomalous sample. The model proposed above to rationalize the data on the basis of an electron transfer equilibrium is supported by the variation in the equilibrium position upon changing the substituents on the cyclopentadienide rings and bipyridyl ligand. In all complexes with this type of magnetic

data, the calculated effective moment approaches zero as the temperature is lowered. This implies that the electron exchange coupling model can only be valid if the lowest spin-orbit coupled J state, J = 1/2, is the only state populated at low temperatures.

The complexes are strongly colored and their solution optical spectra were examined to determine whether the bipyridyl ligand has been reduced in solutions of these complexes. It has been shown that the bipyridyl radical anion has a diagnostic optical spectrum, as would be expected for a species in which the odd electron is located in a π^* molecular orbital.[17] These characteristic strong absorbances, exemplified by Na(bipy), can be compared with the absorbances of the molecules described here. The UV data for the bipyridyl complexes as toluene solutions are included in Table 3.4, along with the data for Na(bipy) as well as the pyridine adducts $(Me_5C_5)_2Yb(py)_2$ and $[1,3\text{-}(Me_3Si)_2C_5H_3]_2Yb(py)_2$. It can be seen that the spectra of $(Me_5C_5)_2Yb(bipy)$, $[1,3\text{-}(Me_3C)_2C_5H_3]_2Yb(bipy)$, $(Me_4C_5H)_2Yb(bipy)$, *ansa*-$[1,3\text{-}(Me_3C)_2C_5H_2]_2SiMe_2Yb(bipy)$ and $(C_5H_5)_2Yb(bipy)$ contain the absorbances of bipyridyl radical anion, while those of $[1,3\text{-}(Me_3Si)_2C_5H_3]_2Yb(bipy)$, $(Me_5C_5)_2Eu(bipy)$, $(Me_5C_5)_2Ca(bipy)$ and the bis(pyridine) compounds do not. This is consistent with the oxidation state of the bipyridyl ligand in each of these complexes as deduced from infrared spectroscopy and crystallography, except for the three molecules $[1,3\text{-}(Me_3C)_2C_5H_3]_2Yb(bipy)$, *ansa*-$[1,3\text{-}(Me_3C)_2C_5H_2]_2SiMe_2Yb(bipy)$ and $(C_5H_5)_2Yb(bipy)$. Those compounds are diamagnetic in the solid state but show transitions of bipyridyl radical anion in their optical spectra. Further data described below support the proposition that these molecules are paramagnetic in solution, presumably as the geometric constraints of the solid state,

shown in the crystal structure of $[1,3\text{-}(Me_3C)_2C_5H_3]_2Yb(bipy)$, are removed in solution and allow population of the LUMO of bipyridyl.

Table 3.4. Optical spectra of ytterbocene and other bipyridyl complexes (in toluene unless otherwise specified)

compound	**λ_{max} in nm ($\varepsilon \times 10^{-3}$ in $Lmol^{-1}cm^{-1}$)**
$(Me_5C_5)_2Yb(bipy)$[a]	1020 (0.88), 890 (2.96), 855 (2.63), 800 (2.37), 505 (5.71), 475 (4.79), 385 (8.98)
$(Me_5C_5)_2Yb(py)_2$	800 (0.47), 441 (0.85)
$[1,3\text{-}(Me_3C)_2C_5H_3]_2Yb(bipy)$	880 (1.00), 845 (1.06), 767 (1.01), 678 (0.76), 488 (1.91), 465 (1.77), 380 (4.19)
$[1,3\text{-}(Me_3Si)_2C_5H_3]_2Yb(bipy)$	668 (0.41), 392 (1.29)
$[1,3\text{-}(Me_3Si)_2C_5H_3]_2Yb(py)_2$	670 (0.17), 401 (0.24)
$(Me_4C_5H)_2Yb(bipy)$	1035 (0.73), 891 (2.58), 866 (2.36), 801 (2.02), 502 (4.99), 475 (3.94), 383 (9.85)
ansa-$[1,3\text{-}(Me_3C)_2C_5H_2]_2SiMe_2Yb(bipy)$	890 (0.70), 835 (0.73), 779 (0.73), 697 (0.66), 485 (1.10), 461 (1.01), 382 (2.42)
$(C_5H_5)_2Yb(bipy)$	881 (0.42), 850 (0.44), 778 (0.39), 697 (0.30), 493 (0.55), 467 (0.49), 379 (1.57)
$(Me_5C_5)_2Eu(bipy)$	790 (0.42), 494 (1.62)
$(Me_5C_5)_2Ca(bipy)$	509 (0.97), 365 (0.77)
Na(bipy) in THF[b]	952 (1.3), 833 (1.5), 752 (1.1), 562 (6.5), 532 (6.2), 386 (29.5)

a From ref. 2; *b* from ref. 17.

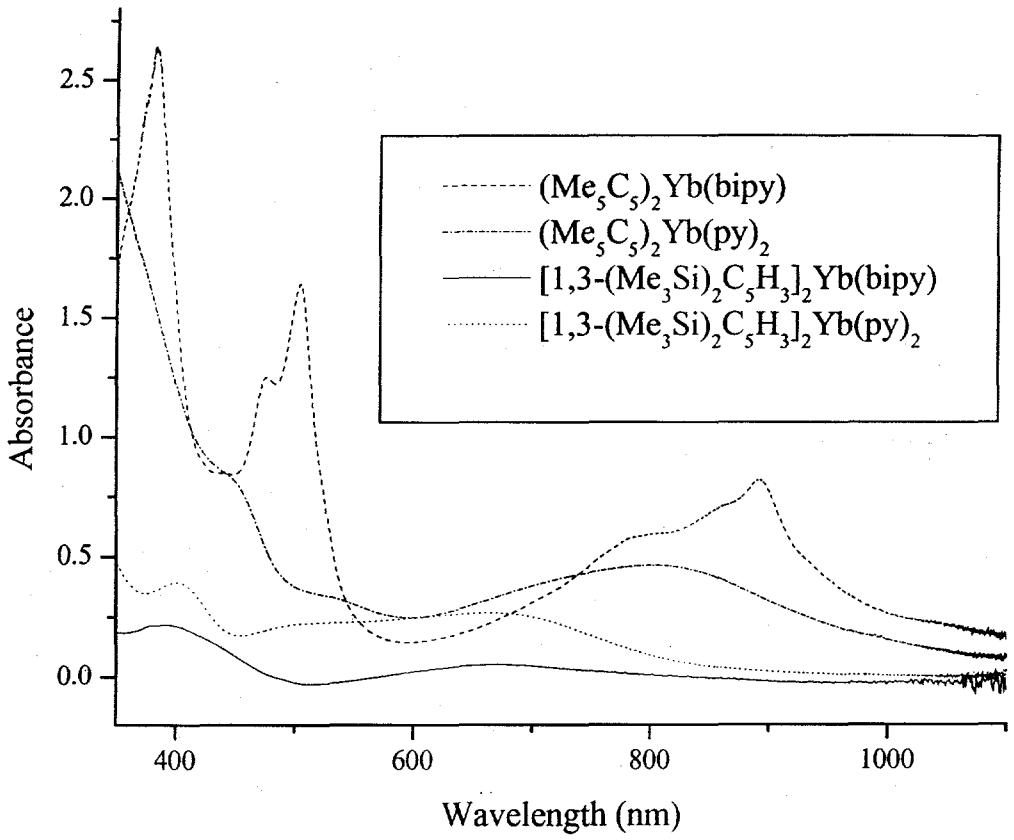

Figure 3.6. Optical spectra of $(Me_5C_5)_2Yb(bipy)$, $(Me_5C_5)_2Yb(py)_2$, $[1,3\text{-}(Me_3Si)_2C_5H_3]_2Yb(bipy)$, $(Me_5C_5)_2Yb(py)_2$ and $[1,3\text{-}(Me_3Si)_2C_5H_3]_2Yb(py)_2$ in toluene.

Figure 3.6 shows the optical spectra of $(Me_5C_5)_2Yb(bipy)$, $(Me_5C_5)_2Yb(py)_2$, $[1,3\text{-}(Me_3Si)_2C_5H_3]_2Yb(bipy)$ and $[1,3\text{-}(Me_3Si)_2C_5H_3]_2Yb(py)_2$ in toluene. The spectrum of $[1,3\text{-}(Me_3Si)_2C_5H_3]_2Yb(bipy)$ is virtually identical to that of $[1,3\text{-}(Me_3Si)_2C_5H_3]_2Yb(py)_2$, confirming that the bipyridyl ligand is neutral and behaves as two independent pyridyl ligands in that complex. The ytterbocene $[1,3\text{-}(Me_3Si)_2C_5H_3]_2Yb$ was shown in Chapter 2 to be less electron rich than the other substituted ytterbocenes used in this work, as the

CO stretch of the carbonyl complex $[1,3\text{-}(Me_3Si)_2C_5H_3]_2Yb(CO)$ is increased from that of free CO. This is consistent with the inability of this ytterbocene to reduce bipyridyl.

The proton NMR spectra of these molecules were collected as this technique gives an indication of whether a molecule is dia- or paramagnetic. The complex $[1,3\text{-}(Me_3Si)_2C_5H_3]_2Yb(bipy)$ has sharp peaks with resolved coupling patterns, while the other bipyridyl complexes have broadened and shifted peaks in their ^1H NMR spectra, consistent with their formulation as paramagnetic Yb(III) complexes.

^1H NMR spectra were collected at temperatures from -70 to +90°C for each bipyridyl complex. The chemical shifts change with temperature, as expected for paramagnetic molecules. A plot of δ vs 1/T is shown in Figure 3.7 for $(Me_5C_5)_2Yb(bipy)$ and in Figure 3.8 for *ansa*-$[1,3\text{-}(Me_3C)_2C_5H_2]_2SiMe_2Yb(bipy)$, while a stacked plot of ^1H NMR spectra is shown in Figure 3.9 for *ansa*-$[1,3\text{-}(Me_3C)_2C_5H_2]_2SiMe_2Yb(bipy)$. It can be seen that the variation of chemical shift with 1/T is not linear. A linear relation is expected for Curie-Weiss behavior. Also, in the case of *ansa*-$[1,3\text{-}(Me_3C)_2C_5H_2]_2SiMe_2Yb(bipy)$, the variation of chemical shift with temperature is not monotonic; some resonances move to higher chemical shifts and then back. This supports the contention that the compounds are not simple paramagnetic molecules in solution, as was deduced in the solid state from the magnetic susceptibility data. The curved lines in the δ vs 1/T plots are presumably the superposition of curves due to the individual species. Since the population of each species changes with temperature, the net curve is non-linear.

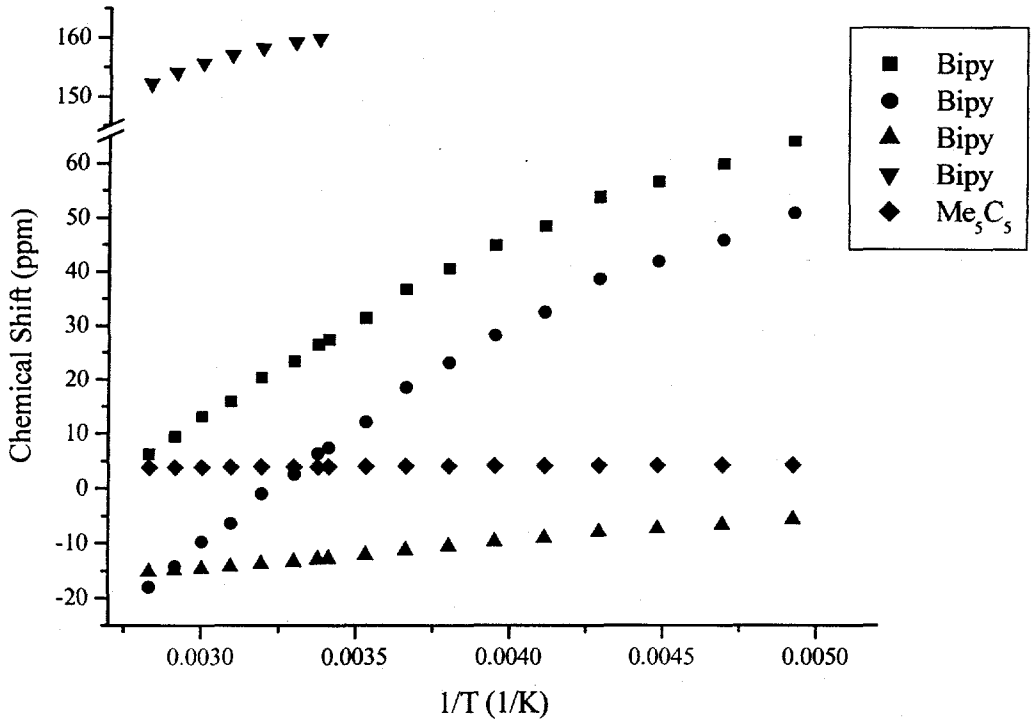

Figure 3.7. Variable temperature ^{1}H NMR data for $(Me_5C_5)_2Yb(bipy)$ in toluene-d_8.

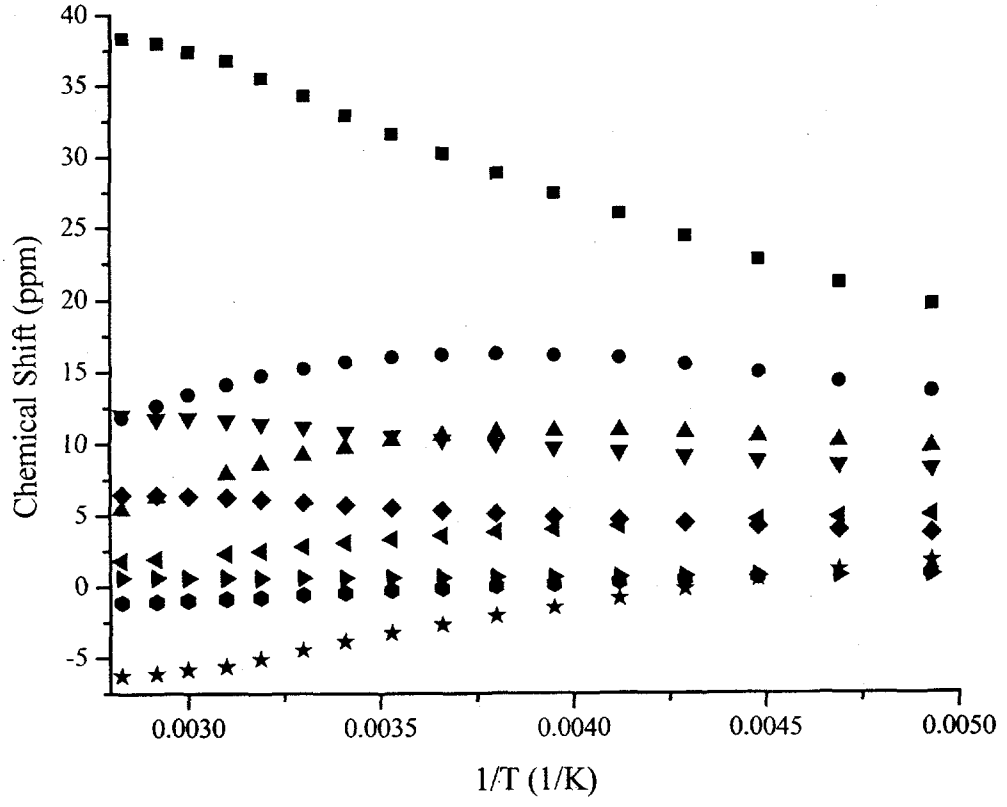

Figure 3.8. Variable temperature ^{1}H NMR data for *ansa*-[1,3-$(Me_3C)_2C_5H_2]_2SiMe_2]_2$ Yb(bipy) in toluene-d_8.

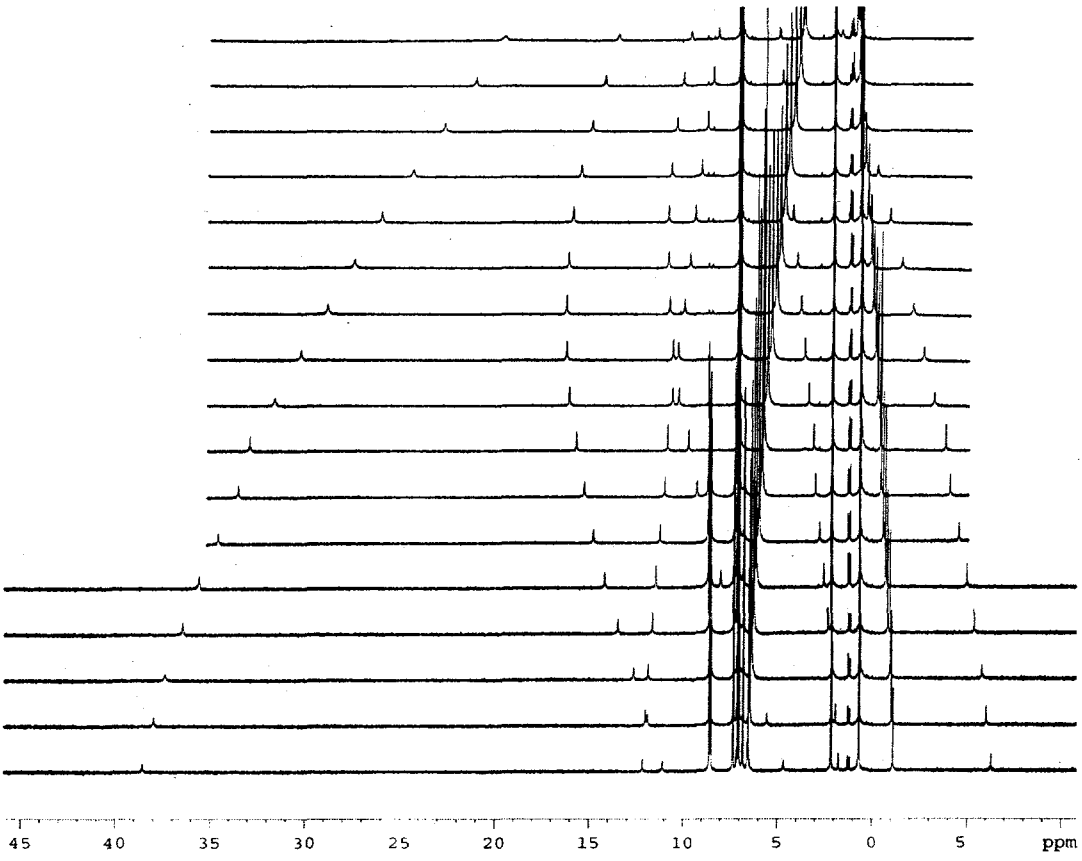

Figure 3.9. Stacked plot of ^{1}H NMR spectra of *ansa*-[1,3-$(Me_3C)_2C_5H_2]_2SiMe_2]_2Yb(bipy)$ in toluene-d_8 at temperatures from -70 to +90°C. Spectra were collected every 10°C, and the plot is from low temperature (top) to high temperature (bottom).

Addition of free bipyridyl to solutions of the ytterbocene bipyridyl complexes did not affect the positions or breadth of the resonances of the protons in the NMR spectra. This is consistent with the hypothesis that on the NMR timescale, the complexes do not exchange with added bipyridyl. Similarly, upon addition of one equivalent of 4,4'-dimethyl-2,2'-bipyridyl (dmb) to an NMR solution of $(Me_5C_5)_2Yb(bipy)$, the ^{1}H NMR

spectrum consists of resonances corresponding to the two molecules in the solution. However, after several hours resonances corresponding to $(Me_5C_5)_2Yb(dmb)$ and free bipyridyl are observed. After approximately 7 days, equilibrium is reached and the solution contains equal amounts of the four molecules. Heating the solution does not change the spectrum after this point. Figure 3.10 shows the ^1H NMR spectrum of a solution of $(Me_5C_5)_2Yb(bipy)$ with half an equivalent of 4,4'-dimethyl-2,2'-bipyridyl after 2 weeks.

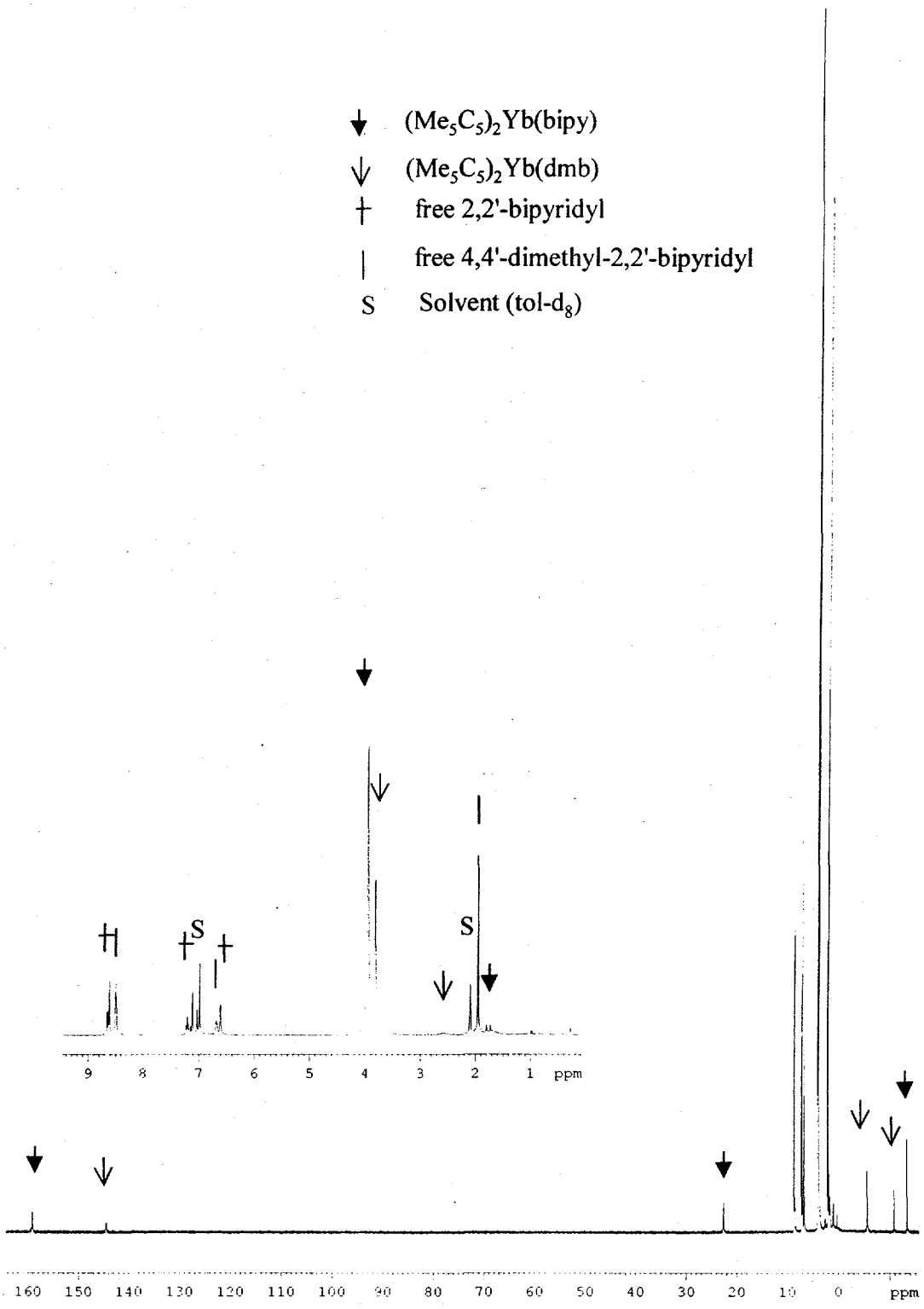

Figure 3.10. ^{1}H NMR spectrum of $(Me_5C_5)_2Yb(bipy)$ with half an equivalent of 4,4'-dimethyl-2,2'-bipyridyl at equilibrium (tol-d_8, 20°C).

Similar experiments conducted with the other ytterbocene bipyridyl complexes give widely varying rates of exchange. In the cases of $[1,3\text{-}(Me_3C)_2C_5H_3]_2Yb(bipy)$ and $[1,3\text{-}(Me_3Si)_2C_5H_3]_2Yb(bipy)$, the equilibrium is reached by the time the spectrum is measured, while the rate for $(Me_4C_5H)_2Yb(bipy)$ is very similar to that for $(Me_5C_5)_2Yb(bipy)$, which is slow. The equilibrium can also be approached from the reverse direction. Addition of free bipyridyl to a solution of $(Me_5C_5)_2Yb(dmb)$ results in exchange at a very similar rate to reach the same equilibrium position, and the complex $[1,3\text{-}(Me_3Si)_2C_5H_3]_2Yb(dmb)$ exchanges with bipyridyl as rapidly as the complex $[1,3\text{-}(Me_3Si)_2C_5H_3]_2Yb(bipy)$. None of these molecules exchanges with added bipyridyl ligand on the NMR timescale, so sharp resonances corresponding to free and bound ligand are observed.

The exchange behavior of $(C_5H_5)_2Yb(bipy)$ with 4,4'-dimethyl-2,2'-bipyridyl differs from that of the other ytterbocene - bipyridyl complexes. Addition of one equivalent of free 4,4'-dimethyl-2,2'-bipyridyl to an NMR tube containing a solution of $(C_5H_5)_2Yb(bipy)$ in C_6D_6 or toluene-d_8 leads to an immediate change in the ^1H NMR spectrum. Resonances corresponding to the free ligands are not observed, indicating that this complex exchanges with the ligand rapidly on the NMR timescale. Only very broadened peaks due to exchanging ligands are observed. Thus, the unsubstituted ytterbocene appears to be more labile than the other ytterbocenes studied here. The reason for this is most likely the steric encumbrance of the substituted cyclopentadienide ligands on the other ytterbocenes.

These results can be compared with the same experiment conducted on $(Me_5C_5)_2Ca(bipy)$; in that case, although the complex has extremely low solubility, it can be seen that exchange with added 4,4'-dimethyl-2,2'-bipyridyl is complete by the time the spectrum is acquired.

The exchange of the bipyridyl ligand for added 4,4'-dimethyl-2,2'-bipyridyl is rapid for the diamagnetic molecules, and slow for the molecules that have a reduced bipyridyl ligand. This is consistent with the stronger binding that a negatively charged ligand has to an electropositive metal. Scheme 2 illustrates a proposed mechanism for ligand exchange, which is rapid for the diamagnetic species as there is a small barrier to ligand dissociation (the base-free complexes are known). For the paramagnetic complexes, ligand exchange is slow as the electron must first transfer back to the metal before exchange can occur. Electron exchange from one bipyridyl ligand to another is disfavored so the exchange is unlikely to proceed by the right-hand mechanism.

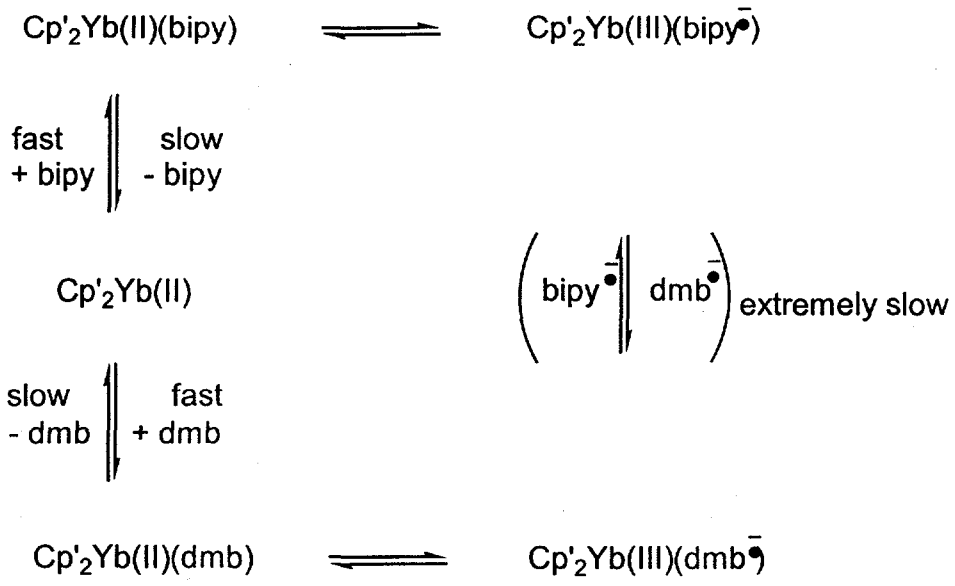

Scheme 2. Proposed mechanism of ligand exchange for ytterbocene - bipyridyl complexes.

Support for this mechanism is derived from the analogous experiment on [1,2,4-$(Me_3C)_3C_5H_2]_2$Ce(bipy).[18] That molecule does not exchange with free 4,4'-dimethyl-2,2'-bipyridyl in solution after 2 weeks at room temperature. Heating to 50°C results in very slow exchange, and equilibrium is not reached after 2 weeks at 50°C. Cerium does not have an accessible bivalent oxidation state, so the only possible mechanism is the right-hand one which is expected to be slow.

The ytterbocene complex [1,3-$(Me_3C)_2C_5H_3]_2$Yb(bipy) is diamagnetic in the solid state, deduced from the infrared spectrum, X-ray crystal structure and SQUID data, but has

some paramagnetic character in solution, deduced from the UV spectrum and ^{1}H NMR spectrum. Nonetheless it undergoes exchange with added 4,4'-dimethyl-2,2'-bipyridyl as rapidly as the compounds that are diamagnetic in solution ([1,3-$(Me_3Si)_2C_5H_3]_2$Yb(bipy) and $(Me_5C_5)_2$Ca(bipy)), consistent with the small energy required to transfer the electron back to the ytterbium atom in this compound. The unsubstituted $(C_5H_5)_2$Yb(bipy) is also diamagnetic in the solid state and paramagnetic in solution, and exchanges with added bipyridyl or 4,4'-dimethyl-2,2'-bipyridyl rapidly on the NMR timescale, which is faster than any of the other metallocenes studied.

The exchange experiments support the electron exchange equilibrium model for the magnetic susceptibility data, because they indicate that even in the paramagnetic compounds, the diamagnetic state is populated and this is the one in which ligand exchange originates.

1,10-Phenanthroline Complexes

1,10-Phenanthroline is similar to 2,2'-bipyridyl, and so the phenanthroline adducts of the ytterbocenes were prepared in order to examine their magnetic behavior (Equation 2).

$$Cp'_2Yb(OEt_2) + phen \rightarrow Cp'_2Yb(phen) + OEt_2 \qquad (2)$$

Cp' = Me_5C_5, 1,3-$(Me_3C)_2C_5H_3$, 1,3-$(Me_3Si)_2C_5H_3$, Me_4C_5H

The phenanthroline complexes are less soluble than the bipyridyl complexes, and they precipitate from the reaction mixture as fine dark powders. They can be recrystallized from a large volume of toluene. Some physical characteristics are presented in Table 3.5.

Table 3.5. Physical characteristics of phenanthroline compounds

compound	**color**	**mp (°C)**	**IR (cm^{-1})**	**μ_{eff} (300K)**
$(Me_5C_5)_2Yb(phen)$	dark blue	297-300	1610	4.0 BM
$[1,3\text{-}(Me_3C)_2C_5H_3]_2Yb(phen)$	dark blue	224-228	1615	3.4 BM
$[1,3\text{-}(Me_3Si)_2C_5H_3]_2Yb(phen)$	red	216-218	830	diamagnetic
$(Me_4C_5H)_2Yb(phen)$	purple	230-233	1612	3.8 BM
$[(Me_5C_5)_2Yb(phen)]^+[I]^-$	red-brown	173-177	855	4.5 BM

The cationic complex $[(Me_5C_5)_2Yb(phen)]^+[I]^-$ was synthesized by stirring the trivalent iodide $(Me_5C_5)_2YbI$ with phenanthroline in toluene. This compound can be recrystallized from methylene chloride as red-brown blocks.

Although the reduction potential of 1,10-phenanthroline does not differ greatly from that of bipyridyl, 2.19 V vs SCE,[5] the magnetism of the phenanthroline complexes is quite different from that of the bipyridyl complexes. The phenanthroline adduct of $[1,3\text{-}(Me_3Si)_2C_5H_3]_2Yb$ is diamagnetic, as is $[1,3\text{-}(Me_3Si)_2C_5H_3]_2Yb(bipy)$, again demonstrating the electron-withdrawing characteristics of the Me_3Si groups. However,

the other ytterbocene complexes do not display the unusual magnetic behavior observed for their bipyridyl adducts.

The infrared spectrum of phenanthroline as a reduced and neutral ligand has not been studied in the same detail as that of bipyridyl, so the infrared spectra of the compounds cannot be used to characterize the valence of the ligand. It was noticed, however, that the only diamagnetic complex $[1,3\text{-}(Me_3Si)_2C_5H_3]_2Yb(phen)$ has a very strong absorbance at 830 cm^{-1} that is not observed for the other complexes, which have absorbances at 1615 cm^{-1}. The cationic complex has a strong absorbance at 855 cm^{-1}, so this may be characteristic of the neutral ligand.

The LUMO of 1,10-phenanthroline is depicted in Figure 3.11. It should be noted that although the symmetry is identical to the symmetry of the 2,2'-bipyridyl LUMO, the coefficients on each atom are different.

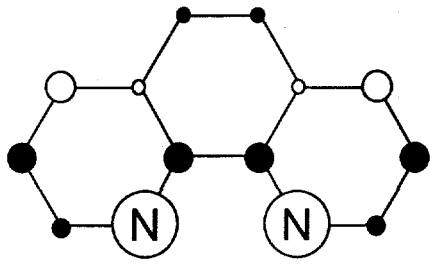

Figure 3.11. Schematic diagram of the LUMO of 1,10-phenanthroline (from ref. 19).

The structure of $[1,3\text{-}(Me_3Si)_2C_5H_3]_2Yb(phen)$ was determined by X-ray crystallography. In this molecule, the distances around the metal indicate that the metal is in the bivalent oxidation state (Table 3.6). The structure of the molecule is unusual, however, in that the

phenanthroline ligand does not lie on the plane bisecting the metallocene wedge. Instead, it forms an angle of 15° to that plane (Figure 3.12). This feature is most reasonably associated with the steric hindrance caused by the Me_3Si groups on the cyclopentadienide rings; the phenanthroline ligand has tilted to avoid the closest Me_3Si group from above and below. Unlike bipyridyl, the phenanthroline ligand cannot twist so it tilts.

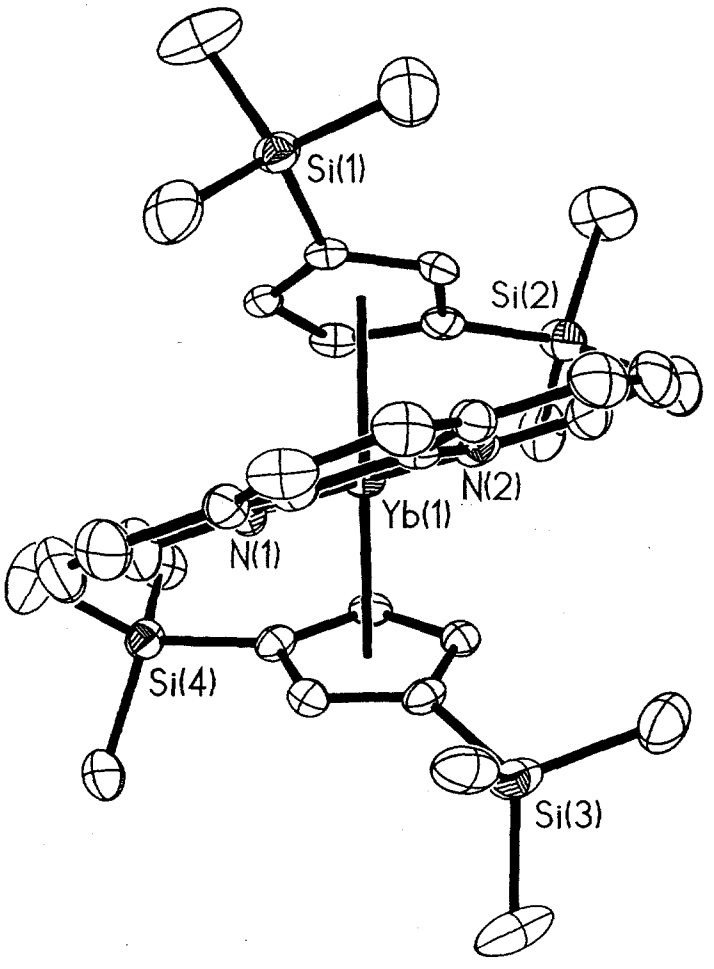

Figure 3.12. ORTEP diagram of $[1,3\text{-}(Me_3Si)_2C_5H_3]_2Yb(phen)$ (50% probability ellipsoids) showing twist of 1,10-phenanthroline ligand.

The structure of the cationic complex $[(Me_5C_5)_2Yb(phen)]^+[I]^-$ was also determined by X-ray crystallography for comparison with the neutral compound and also with the cationic bipyridyl complex (Figure 3.13). The iodide counterion is located more than 3.9Å from the nearest carbon atom and the molecule consists of discrete metallocene cations and iodide anions. In this compound, the phenanthroline ligand lies on the plane bisecting the metallocene wedge. The distances and angles about the ytterbium center (Table 3.6) confirm that the metal is in the trivalent oxidation state.

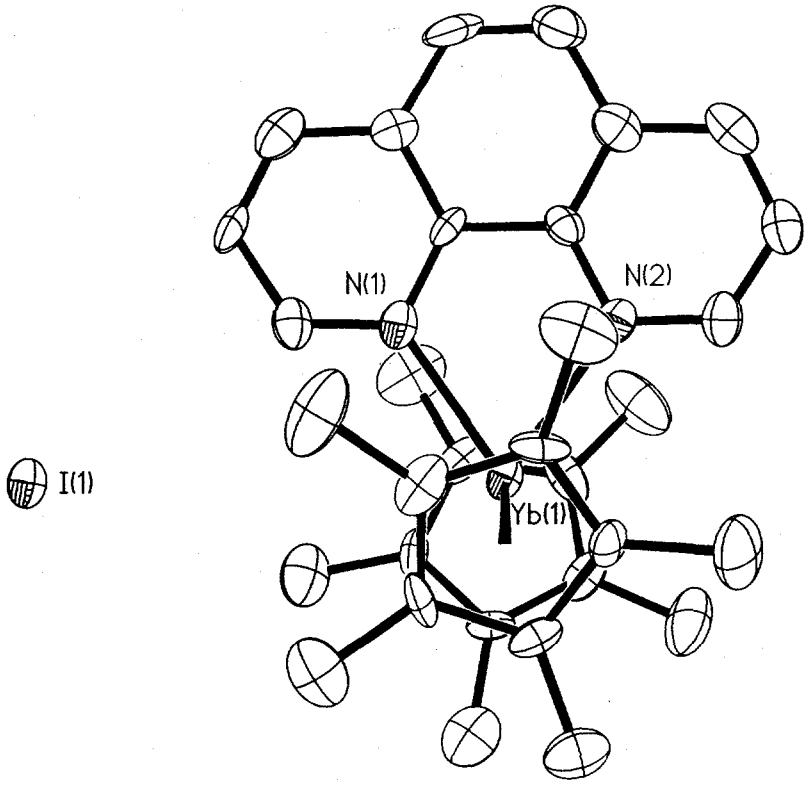

Figure 3.13. ORTEP diagram of $[(Me_5C_5)_2Yb(phen)]^+[I]^-$ (50% probability ellipsoids).

Table 3.6. Selected bond distances (Å) and bond angles (°) for [1,3-$(Me_3Si)_2C_5H_3]_2Yb(phen)$ and $[(Me_5C_5)_2Yb(phen)]^+[I]^-$

	$[1,3\text{-}(Me_3Si)_2C_5H_3]_2Yb(phen)$	**$[(Me_5C_5)_2Yb(phen)]^+[I]^-$**
Yb - C_{ring} (mean)	2.72	2.605
Yb - C_{ring} (range)	2.672(5) - 2.752(5)	2.591(5) - 2.622(9)
Yb - centroid	2.43	2.31
centroid - Yb - centroid	130.9	141.1
twist angle	20	26
Yb - N	2.50	2.36

Magnetic susceptibility measurements of the 1,10-phenanthroline adducts of $(Me_5C_5)_2Yb$, $[1,3\text{-}(Me_3C)_2C_5H_3]_2Yb$ and $(Me_4C_5H)_2Yb$ indicate that these molecules involve Yb(III) and the phenanthroline radical anion. The calculated moments at room temperature are lower than the predicted 4.8 BM for two non-interacting spins, but the shapes of the $1/\chi$ vs T and μ vs T plots are normal for Yb(III) species (Figures 3.14, 3.15).

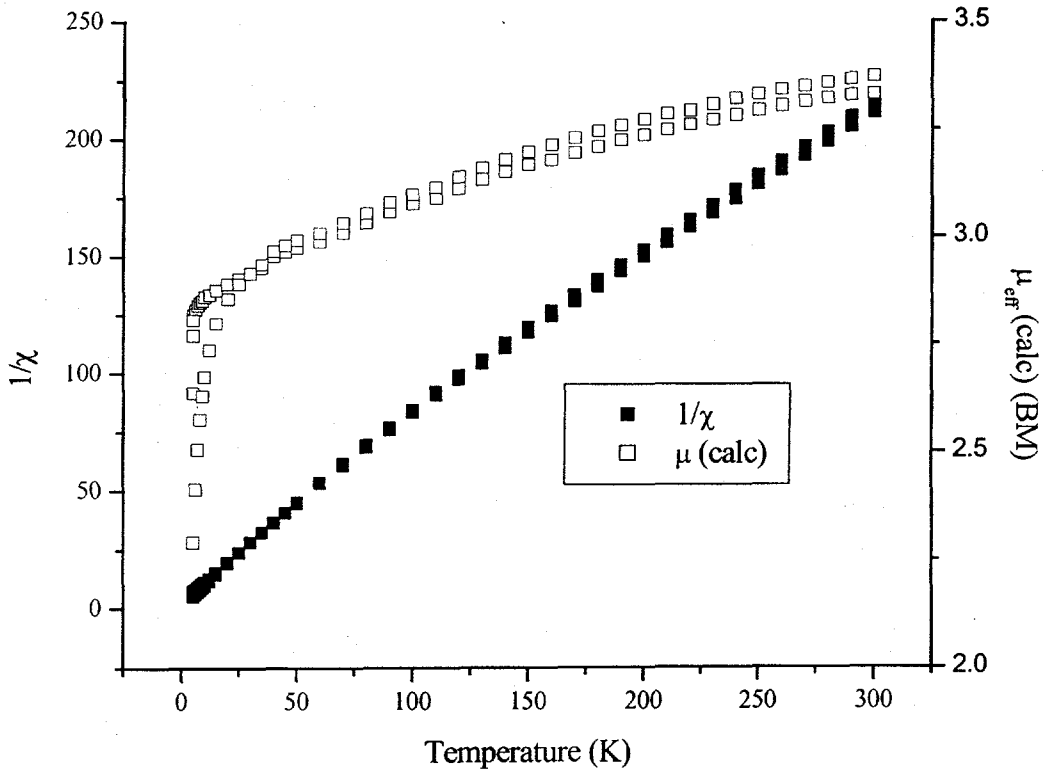

Figure 3.14. $1/\chi$ vs T and μ_{eff} vs T plots for $[1,3\text{-}(Me_3C)_2C_5H_3]_2Yb(phen)$.

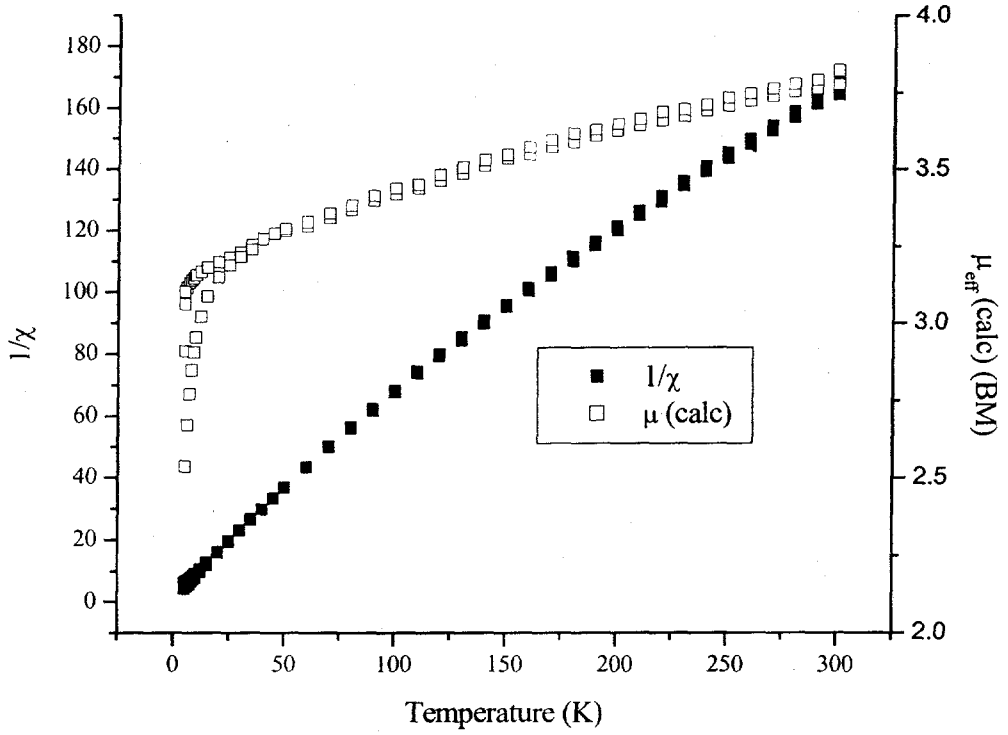

Figure 3.15. $1/\chi$ vs T and μ_{eff} vs T plots for $(Me_4C_5H)_2Yb(phen)$.

The low calculated effective moments indicate electron exchange coupling is occuring between the metal center and the radical anion, as described above. The shape of the μ_{eff} vs T plot is very similar to that of $Yb(pc)_2$.[12] The degree of antiferromagnetic coupling differs for the three molecules, with the molecule $[1,3\text{-}(Me_3C)_2C_5H_3]_2Yb(phen)$ having the lowest moment. The room temperature effective moment of 3.4 BM is close to that predicted for strong antiferromagnetic coupling of an organic radical with Yb(III) of 3.46 BM.[12] The higher values observed for $(Me_5C_5)_2Yb(phen)$ and $(Me_4C_5H)_2Yb(phen)$ are very close to that observed by Hatfield for $Yb(pc)_2$ of 4.3 BM, which is attributed to the

presence of both ferro- and antiferromagnetically coupled states of the ytterbium and radical electrons.

It can be seen from the plots in Figures 3.14 and 3.15 that there is a field dependence to the magnetic susceptibility of these molecules at low temperatures, similar to that observed for the bipyridyl complexes as described above. The field dependence of the effective moment of $(Me_5C_5)_2Yb(phen)$ at 5, 10 and 20K measured and is shown in Figure 3.16. It confirms that antiferromagnetic coupling is occurring at low temperatures, because when a stronger field is applied, more spins are aligned and the effective moment is lower. At high temperatures, the moment is greater due to the thermal population of higher spin states, and the effect of increasing the field is less important, so the magnetic susceptibility is field independent.

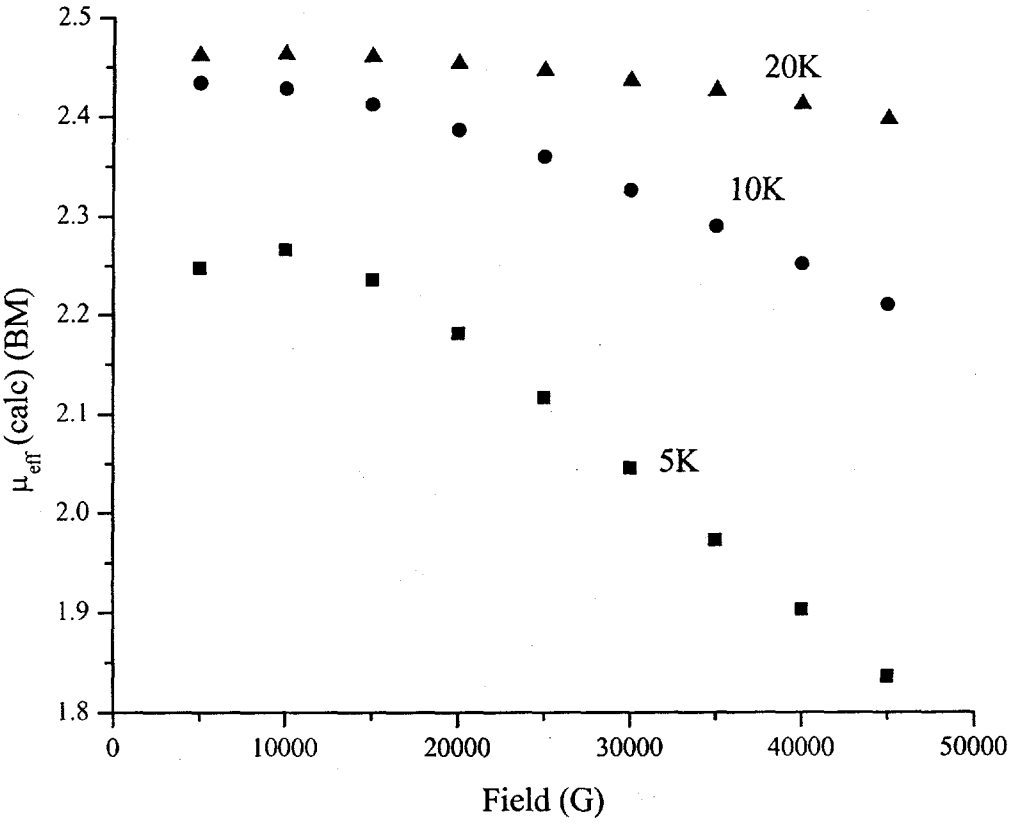

Figure 3.16. Field dependence of magnetic moment of $(Me_5C_5)_2Yb(phen)$ at 5, 10 and 20K.

The magnetic susceptibility of the cationic $[(Me_5C_5)_2Yb(phen)]^+[I]^-$ was also measured, and plots of $1/\chi$ vs T and μ vs T are shown in Figure 3.17. The compound displays the magnetic behavior expected for a single Yb(III) center, with a moment of 4.5 BM at room temperature.

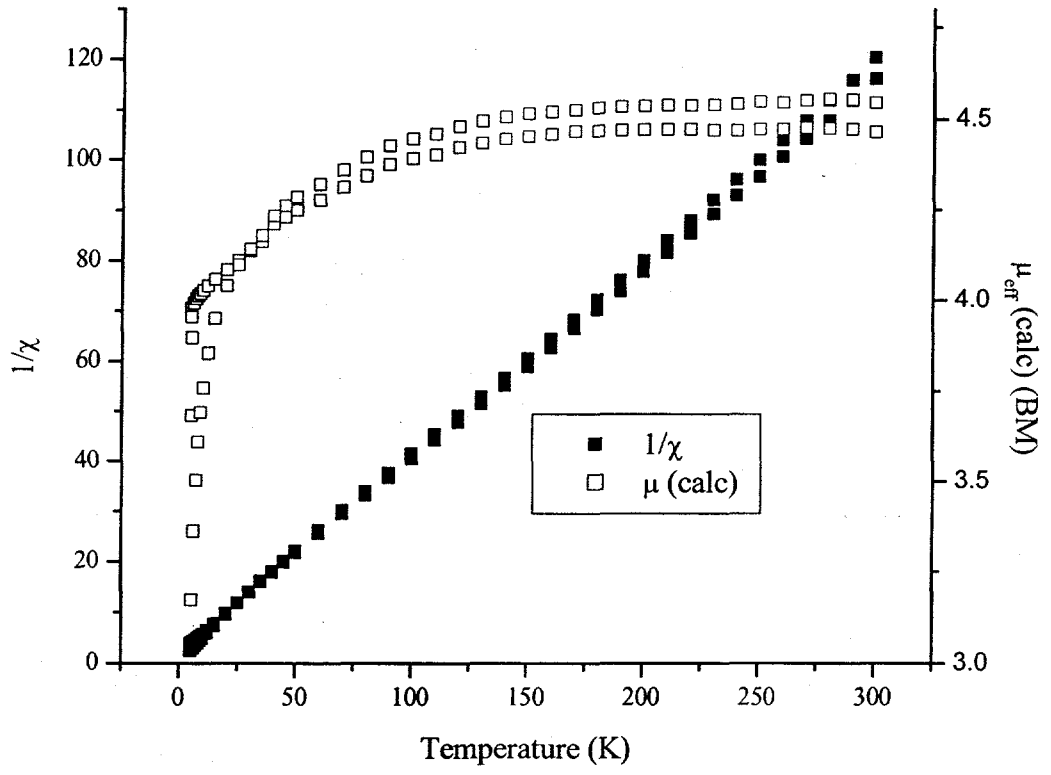

Figure 3.17. $1/\chi$ vs T and μ_{eff} vs T plots for $[(Me_5C_5)_2Yb(phen)]^+[I]^-$.

Thus, changing the ligand from bipyridyl to phenanthroline results in a large change in the magnetic behavior of ytterbocene complexes. The electron exchange equilibrium that is postulated for $(Me_5C_5)_2Yb(bipy)$ and $(Me_4C_5H)_2Yb(bipy)$, as well as other similar compounds, is not observed for phenanthroline complexes. Instead, systems with variable degrees of electron exchange coupling are formed.

Complexes of Yb(III) have *f-f* transitions in their optical spectra, which are observed as sharp absorbances from 900 - 1100 nm.[20] These can be observed in the UV spectra of the cationic $[(Me_5C_5)_2Yb(bipy)]^+[(Me_5C_5)_2YbCl_2]^{-2}$ and $[(Me_5C_5)_2Yb(phen)]^+[I]^-$, as well as

the phenanthroline adducts of all of the ytterbocenes other than $[1,3\text{-}(Me_3Si)_2C_5H_3]_2Yb$. The optical data of the phenanthroline compounds are presented in Table 3.7 while Figure 3.18 shows the solution optical spectra of $(Me_5C_5)_2Yb(phen)$, $[1,3\text{-}(Me_3Si)_2C_5H_3]_2Yb(phen)$ and $[(Me_5C_5)_2Yb(phen)]^+[I]^-$. A characteristic strong narrow absorbance at 890 nm is observed for the compounds involving phenathroline radical anion. The optical spectrum of the phenanthroline radical anion has not been studied in detail, so it is not possible to assign this band, but it is suggested that the presence of this feature can be used as a diagnostic absorbance for that anion. The sodium salt Na(phen) was prepared for comparison but its solubility is so low in THF that the optical spectrum cannot be measured. Several weak bands are observed in the range 800 - 600 nm for each of the phenanthroline complexes.

Table 3.7. Optical spectra of 1,10-phenanthroline complexes in toluene

compound	**λ_{max} in nm ($\varepsilon \times 10^{-3}$ in $Lmol^{-1}cm^{-1}$)**
$(Me_5C_5)_2Yb(phen)$	1007 (0.21), 891 (1.44), 569 (1.29)
$[1,3\text{-}(Me_3C)_2C_5H_3]_2Yb(phen)$	1002 (0.13), 886 (0.53), 539 (1.26), 383 (1.89)
$[1,3\text{-}(Me_3Si)_2C_5H_3]_2Yb(phen)$	513 (1.93), 392 (2.04)
$(Me_4C_5H)_2Yb(phen)$	1001 (0.28), 891 (1.42), 569 (2.50)
$[(Me_5C_5)_2Yb(phen)]^+[I]^-$	1006 (0.20), 978 (0.04), 957 (0.04), 570 (0.16)

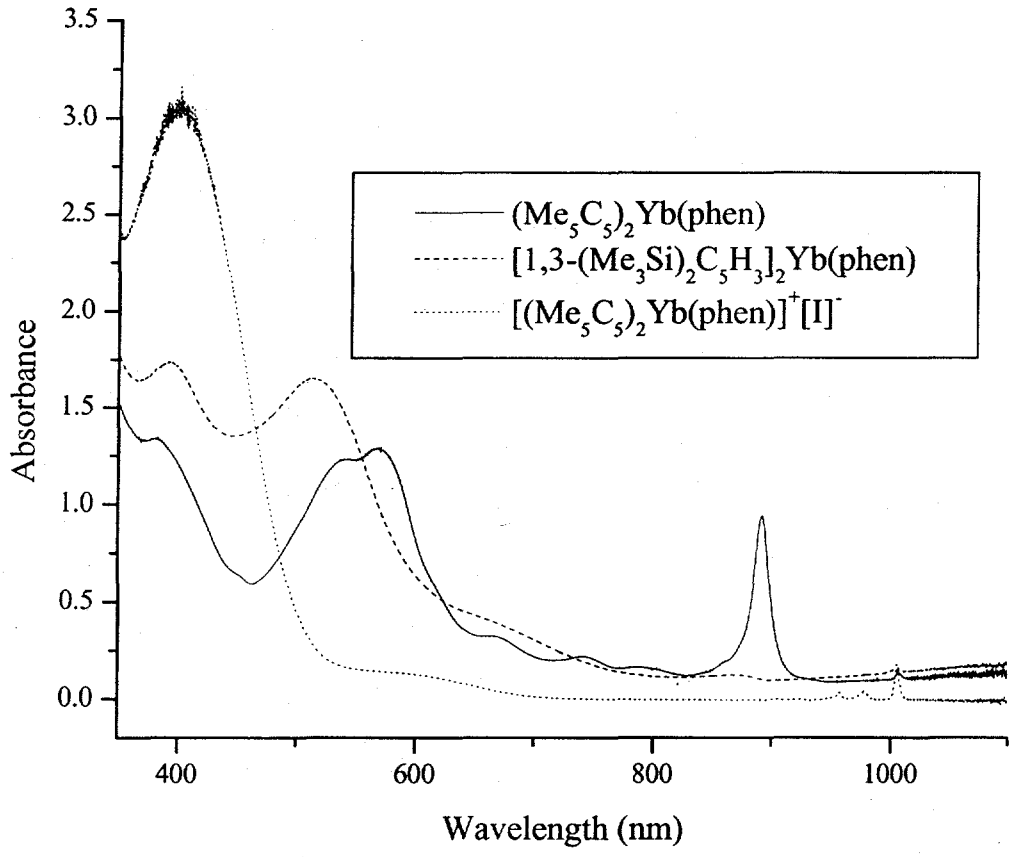

Figure 3.18. Optical spectra of $(Me_5C_5)_2Yb(phen)$ and $[1,3\text{-}(Me_3Si)_2C_5H_3]_2Yb(phen)$ in toluene, and $[(Me_5C_5)_2Yb(phen)]^+[I]^-$ in methylene chloride.

The ^1H NMR spectrum of $[1,3\text{-}(Me_3Si)_2C_5H_3]_2Yb(phen)$ indicates that this molecule is diamagnetic in solution, as the coupling patterns of the protons are resolved and the chemical shifts are in the range 15.0 - 0.17 ppm. The ^1H NMR spectra of the other phenanthroline compounds show the broadened and shifted resonances characteristic of paramagnetic Yb(III). The complexes are insufficiently soluble for the variable temperature NMR experiment to be useful.

The exchange experiments with added ligand were also performed on the phenanthroline complexes. The rates are much slower for these complexes than for the bipyridyl complexes. Addition of free bipyridyl to a solution of $(Me_5C_5)_2Yb(phen)$, $[1,3\text{-}(Me_3C)_2C_5H_3]_2Yb(phen)$ or $(Me_4C_5H)_2Yb(phen)$ does not result in perceptible exchange even after heating to 60° for several weeks. The only phenanthroline complex for which solution exchange with free bipyridyl is observed is $[1,3\text{-}(Me_3Si)_2C_5H_3]_2Yb(phen)$, and in that case the exchange is only 20% complete after 2 weeks at room temperature. Thus, the rate of substitution of phenanthroline is slower than that of bipyridyl. The rigid frame of phenanthroline may contribute to the low lability of this ligand even on a diamagnetic complex. This is consistent with a bidentate → monodentate rate-limiting step in the exchange reactions, which is supported by the rapid rates found for unsubstituted $(C_5H_5)_2Yb(bipy)$.

Conclusions

The magnetism of the bipyridyl complexes of ytterbocenes is complex and cannot be modelled. However, comparison with the phenanthroline complexes, which have similar magnetic behavior to the reported ytterbium phthalocyanato complex,[12] indicates that there is an additional process at work in the bipyridyl complexes that is not observed for the phenanthroline complexes. This may be a reversible electron transfer equilibrium, as suggested by the rates of the exchange reactions with added bipyridyl ligand, or it may be that the energy of the LUMO of bipyridyl is close to that of Yb(III), resulting in a high

degree of electron exchange coupling. The observed increase in magnetic moment with temperature is expected for lanthanide complexes in which thermally accessible excited states are populated.[15] The interaction between Yb(III) and the ligand radical anion is antiferromagnetic at low temperatures, as shown by the decrease in magnetic susceptibility as the field is increased. The overall temperature dependence of the magnetic susceptibility is due to both variation of the populated states of the metal, and coupling between the metal and the ligand radical.[15]

The different ytterbocene fragments studied here interact differently with their ligands, depending on the substituents on the cyclopentadienide rings. As described in Chapter 2, the Me_3Si substituents are electron-withdrawing, which makes the metal more electropositive, so it does not reduce bipyridyl or phenanthroline. The penta- and tetramethylcyclopentadienide rings display identical behavior, which is to create an electronegative ytterbium center which reduces bipyridyl and phenanthroline. The Me_3C substituents are slightly less electron-donating, and the ytterbium center of $[1,3\text{-}(Me_3C)_2C_5H_3]_2Yb$ has electronegativity intermediate between those of $(Me_5C_5)_2Yb$ and $[1,3\text{-}(Me_3Si)_2C_5H_3]_2Yb$. These conclusions, based on the magnetism of the bipyridyl and phenanthroline complexes, are consistent with the characters of the Cp'_2Yb fragments as deduced from the CO stretching frequencies of the carbonyl complexes described in Chapter 2.

References

1) Tilley, T. D. *PhD Thesis*; University of California: Berkeley, 1982.

2) Boncella, J. M. *PhD Thesis*; University of California: Berkeley, 1984.

3) Berg, D. J. *PhD Thesis*; University of California: Berkeley, 1987.

4) Burns, C. J.; Andersen, R. A. *J. Organomet. Chem.* 1987, *325*, 31.

5) Saji, T.; Aoyagui, S. *Electroanal. Chem. Interfac. Electrochem.* 1975, *58*, 401.

6) Finke, R. G.; Keenan, S. R.; Schiraldi, D. A.; Watson, P. L. *Organometallics* 1986, *5*, 598.

7) Saito, Y.; Takemoto, J.; Hutchinson, B.; Nakamoto, K. *Inorg. Chem.* 1972, *11*, 2003.

8) Chisholm, M. H.; Huffman, J. C.; Rothwell, I. P.; Bradley, P. G.; Kress, N.; Woodruff, W. H. *J. Am. Chem. Soc.* 1981, *103*, 4945.

9) McPherson, A. M.; Fieselmann, B. F.; Lichtenberger, D. L.; McPherson, G. L.; Stucky, G. D. *J. Am. Chem. Soc.* 1979, *101*, 3425.

10) Shannon, R. D. *Acta Crystallogr., Sect. A* 1976, *A32*, 751.

11) Tilley, T. D.; Andersen, R. A.; Spencer, B.; Zalkin, A. *Inorg. Chem.* 1982, *21*, 2647.

12) Trojan, K. L.; Kendall, J. L.; Kepler, K. D.; Hatfield, W. E. *Inorg. Chim. Acta* 1992, *198-200*, 795.

13) Edelstein, N. *Electronic Structure of f-Block Compounds*; Marks, T. J. and Fischer, R. D., Ed.; D Reidel Publishing Company: Dordrecht, Netherlands, 1978, pp 37-79.

14) Edelstein, N. *Electronic Structure and Optical Spectroscopy of f^n Ions and Compounds*; Marks, T. J. and Fragala, I. L., Ed.; D Reidel Publishing Company: Dordrecht, Netherlands, 1984, pp 229-276.

15) Kahn, M. L.; Sutter, J.-P.; Golhen, S.; Guionneau, P.; Ouahab, L.; Kahn, O.; Chasseau, D. *J. Am. Chem. Soc.* 2000, *122*, 3413.

16) Bochkarev, M. N., sample of $Cp_2Yb(Me_3CN(CH)_2NCMe_3)$.

17) König, E.; Kremer, S. *Chem. Phys. Lett.* 1970, *5*, 87.

18) Werkema, E. L., Sample of $[1,2,4\text{-}(Me_3C)_3C_5H_2]_2Ce(bipy)$.

19) Ernst, S.; Vogler, C.; Klein, A.; Kaim, W. *Inorg. Chem.* 1996, *35*, 1295.

20) Thomas, A. C. *PhD Thesis*; University of Wisconsin-Madison: Madison, WI, 1985.

Chapter Four : Infrared Studies of Metallocenes under Carbon Monoxide

Infrared Instrumentation and Technique

The ReactIR instrument used for the solution infrared studies is manufactured by ASI Applied Systems and uses total attenuated reflectance from a laser to determine the infrared absorption of the sample.[1] The probe is a 12" × 1" stainless steel cylinder with a 5 mm silicon wafer at the sensor tip. The glassware set-up is shown schematically in Figure 4.1, and allows the use of standard Schlenk techniques with the probe. Two Cajon adapters were welded together to form the 1" - 1.5" adapter between the glassware and the infrared probe.

The probe is cleaned with acetone and spectra are collected repeatedly until the spectrum no longer changes with cleaning. The flask is then assembled hot from the oven and placed under vacuum. A background spectrum of nitrogen (or argon) is collected after flushing three times with nitrogen. The solvent (methylcyclohexane in the experiments described here) is introduced to the flask *via* cannula, and a sample spectrum of solvent is collected, spectrum A. The solvent is then removed *via* cannula and the compound under investigation is dissolved in that solvent, which is then returned to the flask. A sample spectrum of the molecule dissolved in the solvent is then collected, spectrum B.

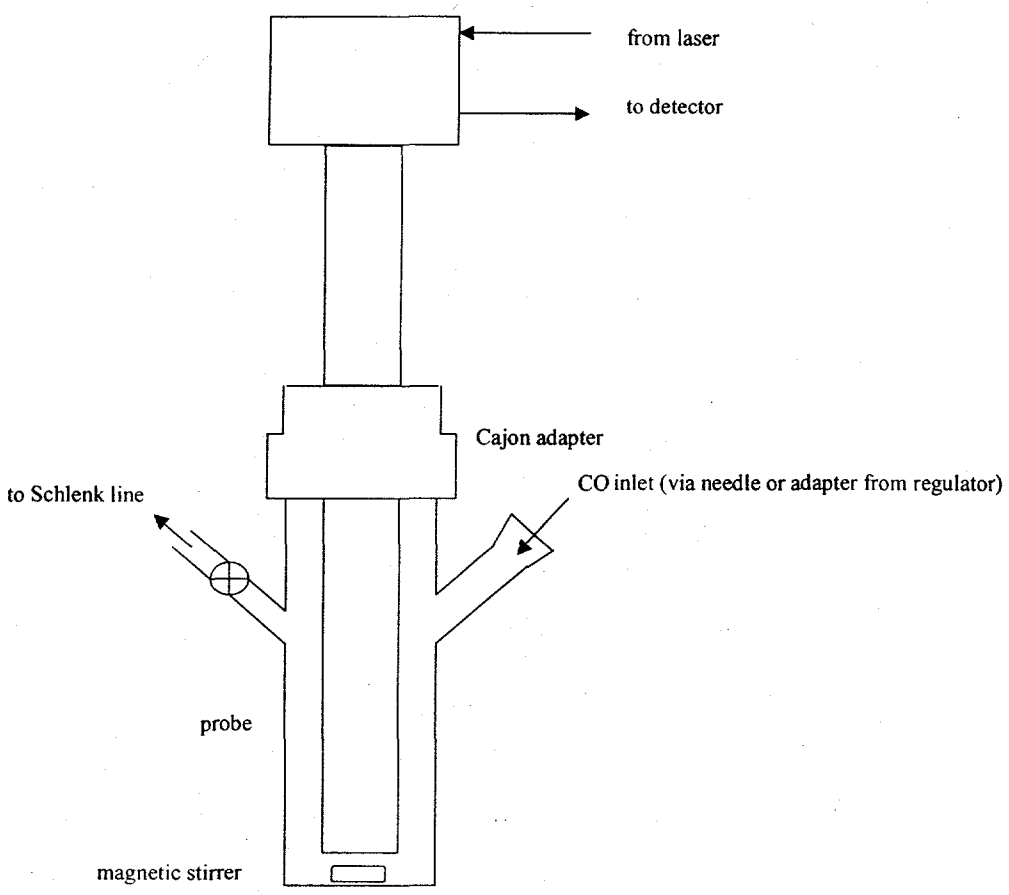

Figure 4.1. Schematic diagram of glassware and ReactIR infrared probe.

Carbon monoxide gas can be introduced into the system in one of three ways: by passing the gas over the dissolved sample with stirring, by bubbling the gas into the sample with a needle, or by exposing the flask briefly to vacuum and backfilling with carbon monoxide with stirring. A spectrum is then collected of the sample under carbon monoxide, spectrum C. Under these conditions, the CO stretch of free CO is not observed in the presence or absence of a metallocene sample. At high pressures, this absorption has been observed at 2136 cm^{-1}.[2]

Spectrum B is subtracted from spectrum C using an interactive subtraction program that allows the relative proportions of the spectra to be varied between 0.9 - 1.1, to achieve the flattest possible baseline.

Carbonyl Complexes of Metallocenes

The ReactIR system was used to collect data on carbonyl complexes of several metallocenes (Table 4.1). In each case for which a carbonyl stretch was observed, the absorbance due to the carbonyl ligand becomes smaller or vanishes when the flask is exposed to vacuum and backfilled with nitrogen, which indicates that the reaction is reversible.

Table 4.1. Infrared data for carbonyl complexes of metallocenes measured in solution under one atmosphere of CO

compound	ν_{CO} **(cm^{-1})**
$(C_5H_5)_2Cr$	1912
$(Me_5C_5)_2Cr$	1876
$[1,3\text{-}(Me_3C)_2C_5H_3]_2Cr$	nr
$[1,3\text{-}(Me_3Si)_2C_5H_3]_2Cr$	1900
$(C_5H_5)_2V$	1895
$[1,3\text{-}(Me_3Si)_2C_5H_3]_2V$	1883
$[1,3\text{-}(Me_3C)_2C_5H_3]_2Mn$	nr
$[1,3\text{-}(Me_3Si)_2C_5H_3]_3U$	nr
$[1,3\text{-}(Me_3C)_2C_5H_3]_3Ce$	nr
$Yb(N(SiMe_3)_2)_2$	nr

The two chromocene carbonyl complexes $(C_5H_5)_2Cr(CO)$ and $(Me_5C_5)_2Cr(CO)$ have been isolated and their CO stretches are reported as 1900 and 1857 cm^{-1}, respectively, in toluene solution.[3,4] Changing the solvent to methylcyclohexane is the probable cause of the higher values of ν_{CO} observed in this work of 1912 and 1876 cm^{-1}, respectively (Figure 4.2). At high pressures, these metallocenes are known to bind a second CO ligand to form ring-slipped 18-electron compounds.[3,4] Under the conditions used here, no evidence for coordination of a second CO is observed, and the compounds appear to decompose after relatively short periods (approx. 1 hr), based on the appearance of new

peaks in the carbonyl region of the infrared spectrum. These peaks are at 1887 cm^{-1} for unsubstituted chromocene, and at 1876 cm^{-1} for decamethylchromocene, and appear to result from decomposition of the starting material to form unidentified CO-containing products. Exposure of the solution to vacuum and backfilling with nitrogen does not affect the intensity of these absorptions, indicating that the decomposition reaction is not reversible. The dimer $(C_5H_5)_2Cr(CO)_4$ is reported as having ν_{CO} in isooctane solution of 1900 and 1880 cm^{-1}, while the pentamethyl-substituted analogue has ν_{CO} in benzene of 1876 and 1857 cm^{-1}.[5,6] The hexacarbonyl dimers are also known, and have ν_{CO} of 2008, 1945, 1922 and 1912 cm^{-1} for $(C_5H_5)_2Cr(CO)_6$ and 1985 and 1900 cm^{-1} for $(Me_5C_5)_2Cr(CO)_6$.[6] These dimers are possible decomposition products under these conditions. A blue precipitate is also observed after long reaction times, which may indicate the presence of the cubanes $[(C_5H_5)Cr(\mu\text{-}O)]_4$ and $[(Me_5C_5)Cr(\mu\text{-}O)]_4$. The mechanism of ring loss is not apparent but may be due to impurities in the gas causing a small amount of hydrolysis.

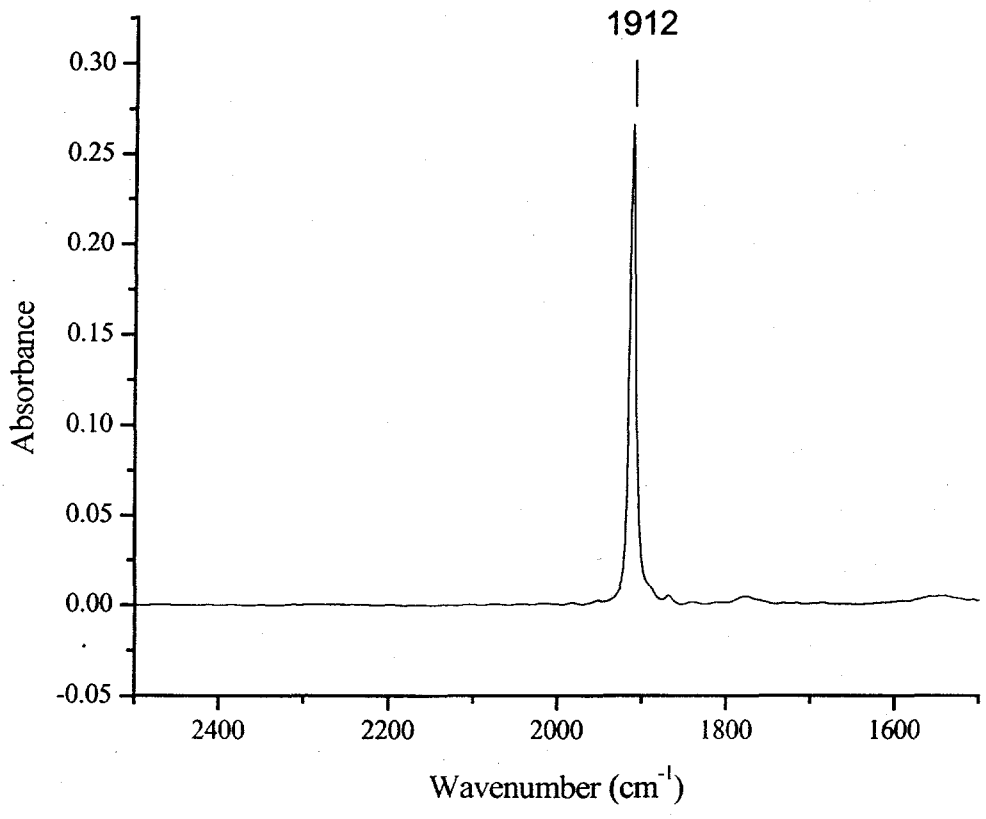

Figure 4.2. Infrared spectrum of $(C_5H_5)_2Cr(CO)$ in methylcyclohexane. This spectrum is background corrected for solvent and CO.

No immediate change in the infrared spectrum of a methylcyclohexane solution of the substituted chromocene $[1,3\text{-}(Me_3C)_2C_5H_3]_2Cr$ was observed upon addition of CO. The crystal structure of the chromocene was determined, and it has a bent sandwich structure in the solid state (Figure 4.3).[7] The centroid - metal - centroid angle in each of the two unique molecules of the asymmetric unit is 174°. This is the only example of a structurally characterized bent chromocene, and provides evidence that the two Me_3C groups on each ring are too large for the metal to readily accommodate. Thus, it is

unsurprising that they hinder the approach of a carbon monoxide ligand. This molecule, along with the other chromocenes, has a total of only 16 valence electrons, but it is unable to bind CO to fill its valence shell due to the steric encumbrance of the cyclopentadienide rings. Prolonged exposure of the compound to CO leads to the appearance of two absorbances at 1870 and 1958 cm^{-1}, presumably due to dimerization to a molecule of composition $[1,3\text{-}(Me_3C)_2C_5H_3]_2Cr_2(CO)_4$. The two stretching frequencies are similar to those observed for the chromium carbonyl dimers described above.

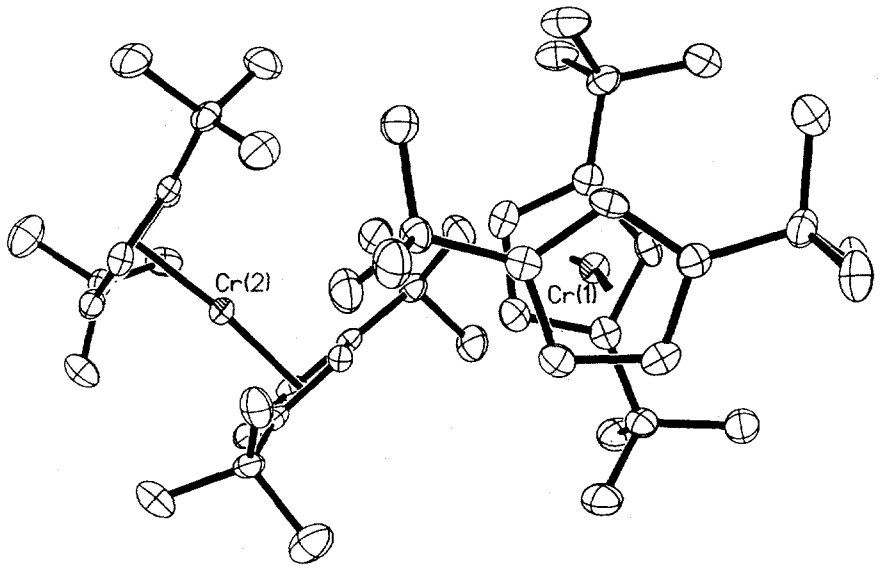

Figure 4.3. ORTEP diagram of $[1,3\text{-}(Me_3C)_2C_5H_3]_2Cr$ (50% probability ellipsoids) (2 unique molecules).

Changing the substituents on the cyclopentadienide ring to Me_3Si alters the steric effect of the rings, as the carbon - silicon bond is longer and more easily bent out of the cyclopentadienide plane. Thus, the molecule $[1,3\text{-}(Me_3Si)_2C_5H_3]_2Cr$ binds CO at one

atmosphere, giving a CO stretch at 1900 cm^{-1} in the infrared spectrum. This is close to the values observed for the chromocene carbonyl complexes described above. The relative values of the CO stretching frequencies of the three chromocene carbonyls are consistent with the degree of electron-richness of the cyclopentadienide rings, C_5H_5 < 1,3-$(Me_3Si)_2C_5H_3$ < Me_5C_5. This is expected, as a more electron-rich metal center is able to back-donate more electron density to a π-acceptor ligand.

Vanadocene and the substituted vanadocene [1,3-$(Me_3Si)_2C_5H_3]_2V$ each bind a single carbon monoxide ligand to give carbonyl complexes with ν_{CO} of 1895 and 1883 cm^{-1}, respectively. The lower value for the disubstituted complex is consistent with the greater electron richness of the cyclopentadienide ligands in that case. Vanadocene is known to react with carbon monoxide under reducing conditions to give $(C_5H_5)V(CO)_4$,[8] but that reaction is not observed under these conditions.

[1,3-$(Me_3C)_2C_5H_3]_2Mn$ does not bind CO under these conditions, which is not surprising given that it is a 17-electron complex, so addition of a 2-electron donor such as CO would lead to a 19-electron configuration. That is, the molecular orbital that could accept the ligand is half-filled already. In addition, the structure of this complex has been determined,[9] and it exists as a bent sandwich, forming the only example of a crystallographically characterized manganocene that is bent in the solid state. As was observed for the analogous chromocene, this is an indication of the extreme steric demands of the bulky 1,3-$(Me_3C)_2C_5H_3$ ligand on a first-row transition metal, and indicates that there is no room for an incoming ligand.

No absorption was observed for a carbonyl complex of the three ring uranium compound $[1,3\text{-}(Me_3Si)_2C_5H_3]_3U$ under these conditions. The less-substituted analogue $[(Me_3Si)C_5H_4]_3U$ is known to bind CO and forms one of two reported uranium carbonyl complexes.[10] The cerium complex $[1,3\text{-}(Me_3C)_2C_5H_3]_3Ce$ also did not bind CO, unsurprisingly as cerium is unlikely to be capable of back-donation to stabilize a carbonyl complex.

The base-free ytterbium silyl amide $Yb(N(SiMe_3)_2)_2$ does not appear to react with CO at one atmosphere, as no absorption is observed in the infrared spectrum. This molecule is known to be a dimer in the solid state[11] and is likely to exist as a dimer in solution also, which would prevent the approach of the CO ligand to the metal.

References

1) ASI *ReactIR 1000 User's Guide*; 3rd ed.; ASI Applied Systems, Inc: Millersville, MD, 1997.

2) Selg, P.; Brintzinger, H. H.; Andersen, R. A.; Horvath, I. T. *Angew. Chem., Int. Ed. Engl.* **1995**, *34*, 791.

3) van Raaij, E. U.; Brintzinger, H.-H. *J. Organomet. Chem.* **1988**, *356*, 315.

4) van Raaij, E. U.; Brintzinger, H.-H.; Zsolnai, L.; Huttner, G. *Z. Anorg. Allg. Chem.* **1989**, *577*, 217.

5) Ginley, D. S.; Wrighton, M. S. *J. Am. Chem. Soc.* **1975**, *97*, 3533.

6) Ginley, D. S.; Bock, C. R.; Wrighton, M. S. *Inorg. Chim. Acta* **1977**, *23*, 85.

7) Gavenonis, J.; Picraux, L. B.; Yeh, R. M.; Schultz, M. *Acta Crystallographica, Section C* submitted for publication.

8) Fischer, E. O.; Hafner, W. *Z. Naturforsch* **1954**, *9b*, 503.

9) Sofield, C. D. *PhD Thesis*; University of California: Berkeley, 2000.

10) Brennan, J. G.; Andersen, R. A.; Robbins, J. L. *J. Am. Chem. Soc.* **1986**, *108*, 335.

11) Boncella, J. M. *PhD Thesis*; University of California: Berkeley, 1984.

Experimental Section

General

All reactions and product manipulations were carried out under dry nitrogen using standard Schlenk and drybox techniques. Dry, oxygen-free solvents were employed throughout. The elemental analyses and mass spectra were performed at the analytical facility at the University of California at Berkeley. Elemental analyses of compounds containing silicon are observed to have lower than predicted percentages of carbon, presumably due to the formation of non-combustible silicon carbide. Melting points were measured in sealed capillaries on a Thomas-Hoover melting point apparatus and are uncorrected. Magnetic susceptibility measurements were made using a Quantum Designs MPMS superconducting magnetometer (SQUID). In a typical experiment, 100 mg of the compound to be studied was ground and weighed into a KEL-F container in a drybox, and small amount of grease was used to seal the two tightly-fitting halves of the container. The sample was suspended in the chamber and measurements were made at fields of 5 and 40 kG, at temperatures from 5 - 300 K. Sample data was corrected for the container (including the grease) and the diamagnetism of the sample. The effective magnetic moments were calculated as $\mu = 2.828\sqrt{(\chi T)}$. Optical spectra were collected on a Cary single beam spectrometer. ^{1}H NMR spectra were measured at 300 or 500 MHz at 23°C in C_6D_6 (unless otherwise noted).

The following compounds were prepared as previously described: $NaNH_2$,[1] YbI_2,[2] Me_5C_5Na,[3] $(Me_5C_5)_2Yb(OEt_2)$,[2] $(Me_5C_5)_2Yb$,[4] $[1,3\text{-}(Me_3Si)_2C_5H_3]_2Yb(OEt_2)$,[5] $[1,3\text{-}(Me_3Si)_2C_5H_3]_2Yb$,[5] $1,3\text{-}(Me_3C)_2C_5H_4$,[6] $Me_4C_5H_2$,[7] Me_2SiBr_2,[8] *ansa*-$[1,3\text{-}(Me_3C)_2C_5H_3]_2SiMe_2$,[9] *ansa*-$[1,3\text{-}(Me_3Si)_2C_5H_3]_2SiMe_2$,[9] *ansa*-$[1,3\text{-}(Me_3C)_2C_5H_2]_2SiMe_2Mg$,[9] *ansa*-$[1,3\text{-}(Me_3Si)_2C_5H_2]_2SiMe_2Mg$,[9] $Yb(N(SiMe_3)_2)_2(OEt_2)_2$,[10] $Yb(N(SiMe_3)_2)_2$,[10] and $Yb(OTf)_3$.[11] Me_4C_5HNa and $[1,3\text{-}(Me_3C)_2C_5H_3]Na$ were prepared by analogous procedures to that used to synthesize Me_5C_5Na.[3] The isocyanide ligands were purified by sublimation ($2,6\text{-}Me_2C_6H_3NC$) or distillation (Me_3CNC, $C_6H_{11}NC$). 2,2'-Bipyridyl, 4,4'-dimethyl-2,2'-bipyridyl, 1,10-phenanthroline and 4,7-dimethyl-1,10-phenanthroline were purified by sublimation; pyridine was distilled over sodium before use.

Infrared spectroscopy. The infrared spectra for solid samples were recorded as Nujol mulls on a Mattson Nicolet FTIR instrument. Solution infrared spectra were recorded using an ASI ReactIR instrument with a Cajon adapter to a modified Schlenk flask. A background spectrum was collected on the contents of the flask under a nitrogen atmosphere. Spectra of the solvent and solvent with solute were then collected. The latter two spectra were subtracted using an interactive procedure to achieve as flat a baseline as possible to give the spectrum of the compound. For carbonyl complexes, the flask was then exposed briefly to vacuum and backfilled with carbon monoxide (99.99% purity), and a third spectrum was recorded. The spectrum of the carbonyl complex was obtained by subtracting the spectrum of the solute from the spectrum of the solute in the presence of the gas.

{[1,3-$(Me_3C)_2C_5H_3$]YbI(OEt_2)}$_2$. The magnesocene [1,3-$(Me_3C)_2C_5H_3]_2Mg$ (0.5 g, 1.3 mmol) was weighed into a round-bottomed flask equipped with a magnetic stirrer bar. Ytterbous iodide (0.56 g, 1.3 mmol) was added under a flow of N_2. Diethyl ether was added and the slurry was stirred at room temperature. After 1 hr, the solution was green in color. After 3 hr, the solution was filtered from the gray solid which appeared to contain unreacted magnesocene by ^{1}H NMR spectroscopy. The volume of the green solution was reduced under reduced pressure; the solid that was deposited on the sides of the flask during this procedure was orange. Cooling to -40°C resulted in the formation of clear orange crystals which were insoluble in OEt_2, hot toluene or C_6D_6. The crystals turn brown at 130°C, and black at 230°C, but do not melt to 330°C. Anal. Calcd for $C_{17}H_{31}IOYb$: C, 37.0; H, 5.67. Found: C, 38.2; H, 5.96. The insolubility of the compound prevented recrystallization or the obtention of an NMR spectrum. Sublimation did not lead to the formation of the ytterbocene. Colorless crystals of unreacted magnesocene could be recovered from the mother liquor after several recrystallization steps. $MgI_2(OEt_2)_2$ was also crystallized from the mother liquor and identified by elemental analysis. Anal. Calcd for $C_8H_{20}O_2I_2Mg$: C, 22.5; H, 4.69. Found: C, 22.6; H, 4.56. ^{1}H NMR (C_6D_6): δ 3.64 (q, J = 7 Hz, 8H), 0.97 (t, J = 7 Hz, 12H) ppm. This reaction was also attempted in dibutyl ether but no pure product was obtained.

{[1,3-$(Me_3Si)_2C_5H_3$]YbI(OEt_2)}$_2$. The magnesocene [1,3-$(Me_3Si)_2C_5H_3]_2Mg$ (2.64 g, 6 mmol) was weighed into a Schlenk flask. Ytterbous iodide (2.55 g, 6 mmol) was added

followed by diethyl ether (60 mL). The slurry was stirred overnight at room temperature. The dark green-brown product was filtered into a clean flask and the volume of solvent was reduced. Cooling to -40°C led to the formation of the bright orange product in 68% yield. Anal. Calcd for $C_{15}H_{31}IOSi_2Yb$: C, 30.9; H, 5.35. Found: C, 32.3; H, 6.12. The similar color and solubility of this compound to those of the Me_3C analogue led to its formulation as a dimer, although it was not characterized crystallographically.

Reaction of $\{[1,3\text{-}(Me_3C)_2C_5H_3]YbI(OEt_2)\}_2$ with $(Me_5C_5)Na$. The crystalline orange dimer (0.70 g, 1.27 mmol) was transferred to a Schlenk flask equipped with a magnetic stirrer bar. Pentamethylcyclopentadienyl sodium (0.20 g, 1.27 mmol) was added followed by diethyl ether (20 mL). The slurry was stirred at room temperature and became bright green. After stirring overnight at room temperature the dark green slurry was filtered into a clean flask. The volume of the filtrate was reduced under dynamic vacuum and the solution was cooled to -40°C. A few small orange crystals formed along with a dark brown precipitate, but no pure product was obtained.

Reaction of $\{[1,3\text{-}(Me_3C)_2C_5H_3]YbI(OEt_2)\}_2$ with methyl lithium. $\{[1,3\text{-}(Me_3C)_2C_5H_3]YbI(OEt_2)\}_2$ (0.5 g, 0.9 mmol) was weighed into a Schlenk tube. OEt_2 was added (20 mL). Methyl lithium (4mL, 0.23 M, 0.9 mmol) was added via syringe. The solution became green, then orange and finally deep red, and the insoluble $\{[1,3\text{-}(Me_3C)_2C_5H_3]YbI(OEt_2)\}_2$ went into solution as the reaction progressed. After 3 hr, the solvent was removed under vacuum and the orange powder was washed in pentane. The

product was then extracted into OEt_2 and filtered. No pure product could be isolated, but the product mixture contained $[1,3\text{-}(Me_3C)_2C_5H_3]_2Yb$ by ^1H NMR spectroscopy.

$[1,3\text{-}(Me_3C)_2C_5H_3]_2Yb(OEt_2)$. A procedure similar to that used to prepare $(Me_5C_5)_2Yb(OEt_2)$ was employed.[2] with the difference that the slurry did not become green immediately upon addition of solvent. The $[1,3\text{-}(Me_3C)_2C_5H_3]Na$ (0.94 g, 4.7 mmol) and YbI_2 (0.95 g, 2.3 mmol) were weighed into a Schlenk flask equipped with a magnetic stirrer under a flow of N_2. Stirring at 25°C for 15 min resulted in a green slurry which was then stirred overnight. The isolated yield of green crystals was 78%. Under dynamic vacuum, the complex loses the coordinated diethyl ether at 65°C. Anal. Calcd. for $C_{30}H_{52}OYb$: C 59.9, H 8.71. Found: C 59.9, H 8.94. ^1H NMR (C_6D_6): δ 6.06 (d, 4H, J = 2.6 Hz), 5.66 (t, 2H, J = 2.5 Hz), 3.29 (q, 4H, J = 6 Hz), 1.32 (s, 36H), 1.01 (t, 6H, J = 6 Hz) ppm.[12] The optical data are in Table 1.6.

$[1,3\text{-}(Me_3C)_2C_5H_3]_2Yb(THF)$. The magnesocene $[1,3\text{-}(Me_3C)_2C_5H_3]_2Mg$ (2.0 g, 5.5 mmol) was weighed into a round-bottomed Schlenk flask equipped with a magnetic stirrer bar. Ytterbous iodide (2.42 g, 5.6 mmol) was added followed by THF (100 mL). The dark green slurry was stirred overnight at room temperature, then filtered into a clean Schlenk flask. The solvent was then removed under reduced pressure and the green solid was extracted into diethyl ether, from which green crystals were obtained after cooling to -80°C. Yield: 2.47 g (75 %). mp 130-132°C. Anal. Calcd for $C_{30}H_{50}OYb$: C, 60.1; H, 8.40. Found: C, 58.2; H, 8.44. ^1H NMR (C_6D_6): δ 6.19 (d, 4H, C_5H_3), 5.71 (t, 2H, C_5H_3),

3.47 (br, 4H, THF), 1.35 (s, 36H, Me_3C), 1.22 (br, 4H, THF). The optical data are in Table 1.6.

[1,3-$(Me_3C)_2C_5H_3]_2Yb$. A procedure identical to that used to prepare $(Me_5C_5)_2Yb$ was followed. The ether complex, [1,3-$(Me_3C)_2C_5H_3]_2Yb(OEt_2)$ (3.0 g, 5.8 mmol), was dissolved in a minimum amount of toluene (160 mL) and the green solution was transferred to a long-necked 250 mL round-bottomed flask equipped with a greaseless J.Young tap containing a magnetic stir bar. The flask was opened to dynamic vacuum briefly, closed and then heated to 100°C. The solvent was removed under dynamic vacuum over a period of 2 h, the black residue was redissolved in toluene (160 mL) and the procedure was repeated. The residue was then extracted into pentane (200 mL) and filtered into a large Schlenk tube. The volume of solvent was then reduced to 120 mL under dynamic vacuum and upon cooling the solution to -40°C green crystals were formed The isolated yield was 60%, mp 85-86°C. Anal. Calcd. for $C_{26}H_{42}Yb$: C 59.2, H 8.02. Found: C 58.5, H 8.24. ^1H NMR (C_6D_6, 20°C) δ 5.95 (d, 4H, J = 2.8 Hz), 5.62 (t, 2H, J = 2.7 Hz), 1.29 (s, 36H) ppm. IR (nujol): 1450 (s), 1380 (m), 1240 (m), 1175 (w), 1149 (w), 890 (w), 780 (s), 680 (m), 650 (w). The optical data are in Table 1.5 and Figure 1.10.

$(Me_4C_5H)_2Yb(OEt_2)$. A procedure identical to that used to prepare $(Me_5C_5)_2Yb(OEt_2)$ was employed.[2] The sodium salt $Na(Me_4C_5H)$ (2.3 g, 16 mmol) was weighed into a Schlenk flask equipped with a magnetic stirrer. Ytterbous iodide (3.7 g, 8.8 mmol) was added, followed by diethyl ether (180 mL). The green slurry was stirred overnight at

room temperature and then filtered. The volume of solvent was reduced and the solution was cooled to yield green crystals of the product in 53% yield (2.3 g). Under dynamic vacuum, the complex loses the coordinated diethyl ether at 80°C. Anal. Calcd for $C_{22}H_{36}OYb$: C, 54.0; H, 7.41. Found: C, 53.7; H, 7.18. ^1H NMR (C_6D_6): δ 5.65 (s, 2H, C_5H), 2.98 (q, J = 7 Hz, 4H, OEt_2), 2.21 (s, 12H, Me_4C_5), 2.03 (s, 12H, Me_4C_5), 0.93 (t, J = 7 Hz, 6H, OEt_2) ppm. The optical data are in Table 1.6.

$(Me_4C_5H)_2Yb(THF)_2$. The green ether complex $(Me_4C_5H)_2Yb(OEt_2)$ was dissolved in THF which resulted in an immediate color change to bright purple. The solvent was removed under dynamic vaccum and the purple solid was extracted into diethyl ether. Red crystals formed upon cooling to -80°C. mp 125-128°C. Anal. Calcd for $C_{26}H_{42}O_2Yb$: C, 55.8; H, 7.56. Found: C, 55.5; H, 7.47. ^1H NMR (C_6D_6): δ 5.59 (s, 2H, C_5H), 3.40 (br, 8H, THF), 2.24 (s, 12H, Me_4C_5), 2.11 (s, 12H, Me_4C_5), 1.34 (br, 8H, THF) ppm. This compound has been reported, although the solubility was found in this work to be higher than reported.[13] Use of a sample of the sodium salt $Na(Me_4C_5H)$ that contained residual THF in the synthesis of the diethyl ether complex also led to the isolation of red crystals of this adduct as a mixture with the diethyl ether adduct. Extraction into toluene and crystallization led to isolation of the mono-THF adduct, $(Me_4C_5H)_2Yb(THF)$. mp 135-139°C. Anal. Calcd for $C_{22}H_{34}OYb$: C, 54.2; H, 7.03. Found: C, 53.9; H, 7.21. ^1H NMR (C_6D_6): δ 5.55 (s, 2H, C_5H), 3.26 (br, 4H, THF), 2.18 (s, 12H, Me_4C_5), 2.07 (s, 12H, Me_4C_5), 1.27 (br, 8H, THF) ppm. The optical data are in Table 1.6.

$(Me_4C_5H)_2Yb$. The etherate, $(Me_4C_5H)_2Yb(OEt_2)$ (0.9 g, 1.8 mmol), was dissolved in toluene (80 mL). The volume of solvent was reduced to 50 mL and the green solution was cooled to -40°C. Pale green crystals of the base-free metallocene were isolated in 65% yield (0.5 g), mp 324-326°C. Anal. Calcd. for $C_{18}H_{26}Yb$: C 52.0, H 6.31. Found: C 51.3, H 5.58. The compound does not color toluene at reflux; its insolubility in non-coordinating solvents prevented recrystallization or solution characterization. IR (nujol): 1478 (s), 1380 (s), 1290 (w), 1230 (w), 1150 (m), 830 (m), 823 (m).

Reaction of $NaNH_2$ with 1,3-$(Me_3Si)_2C_5H_4$. Using a procedure analogous to that used to prepare [1,3-$(Me_3C)_2C_5H_3$]Na, sodium amide (2.08 g, 54 mmol) was allowed to react with 1,3-$(Me_3Si)_2C_5H_4$. The product was a sticky yellowish solid, and reaction with YbI_2 led to the formation of the known product $(Me_3SiC_5H_4)_2Yb(THF)_2$.[14] The C - Si bond was apparently cleaved by the $NaNH_2$ in the inital reaction.

***ansa*-[1,3-$(Me_3C)_2C_5H_2]_2SiMe_2Na_2$.** Sodium amide (0.72 g, 18.5 mmol) was transferred to a large Schlenk tube equipped with a magnetic stirrer and suspended in THF (60 mL). *Ansa*-[1,3-$(Me_3C)_2C_5H_3]_2SiMe_2$ (3.45 g, 8.4 mmol) was weighed into a Schlenk flask and dissolved in THF (50 mL). The solution of *ansa*-[1,3-$(Me_3C)_2C_5H_3]_2SiMe_2$ was added to the suspension with stirring and the yellowish suspension was stirred at room temperature overnight. A centrifuge was used to settle the solid, and the solution was decanted into a clean flask. The solvent was removed under reduced pressure and the product was washed in pentane. A sample in C_6D_6 was hydrolyzed and the ^1H NMR spectrum

indicated the presence of THF and OEt_2 in the sample, with approximately half an equivalent of each solvent molecule per ligand.

***ansa*-[1,3-$(Me_3C)_2C_5H_2]_2SiMe_2Yb(OEt_2)$.** The sodium salt *ansa*-[1,3-$(Me_3C)_2C_5H_2]_2$ $SiMe_2Na_2$ (1.0 g, 1.9 mmol) was stirred with YbI_2 (0.96 g, 2.2 mmol) in diethyl ether overnight. Pale green crystals were isolated. mp 275-282°C. Anal. Calcd for $C_{32}H_{56}OSiYb$: C, 58.4; H, 8.58. Found: C, 58.4; H, 8.67. ^{1}H NMR (C_6D_6): δ 6.26 (d, J = 2.6 Hz, 2H, C_5H_2), 5.99 (d, J = 2.6 Hz, 2H, C_5H_2), 3.02 (br q, 4H, OEt_2), 1.51 (s, 18H, Me_3C), 1.23 (s, 6H, $SiMe_2$), 1.22 (s, 18H, Me_3C), 0.96 (t, J = 7 Hz, 6H, OEt_2) ppm. IR (nujol): 1459 (vs), 1378 (s), 1355 (m), 1245 (m), 1199 (m), 1170 (w), 1137 (w), 1094 (m), 1058 (m), 1019 (w), 1002 (w), 833 (m), 805 (s), 770 (m), 678 (s). The optical data are in Table 1.6.

***ansa*-[1,3-$(Me_3C)_2C_5H_2]_2SiMe_2Yb(THF)_2$.** The green etherate *ansa*-[1,3-$(Me_3C)_2C_5H_2]_2$ $SiMe_2Yb(OEt_2)$ was dissolved in THF resulting in an immediate color-change to deep purple. The solvent was removed under reduced pressure and the resulting pink residue was extracted into diethyl ether and cooled. Red crystals were obtained in 50% yield. The low yield reflects the high solubility of the product rather than any side reactions. mp 248-255°C. Anal. Calcd for $C_{36}H_{62}O_2SiYb$: C, 59.4; H, 8.58. Found: C, 59.5; H, 8.48. ^{1}H NMR (C_6D_6): δ 6.26 (d, J = 2.4 Hz, 2H, C_5H_2), 5.97 (d, J = 2.4 Hz, 2H, C_5H_2), 3.42 (br m, 8H, THF), 1.54 (s, 18H, Me_3C), 1.28 (m, 8H, THF), 1.22 (s, 6H, Me_2Si), 1.20 (s, 18H, Me_3C) ppm. The second crop of crystals from the reaction of a sample of the sodium salt *ansa*-[1,3-$(Me_3C)_2C_5H_2]_2SiMe_2Na_2$ that was contaminated with residual THF

with YbI_2 in diethyl ether contained 40 % red crystals of this molecule which could be separated manually. The optical data are in Table 1.6.

Attempted synthesis of base-free *ansa*-[1,3-$(Me_3C)_2C_5H_2]_2SiMe_2Yb$. Several techniques were attempted in order to prepare the base-free *ansa*-metallocene.

1. Toluene reflux method: slow removal of refluxing toluene from a green solution of *ansa*-[1,3-$(Me_3C)_2C_5H_2]_2SiMe_2Yb(OEt_2)$ leads to a brown sticky solid, which is insoluble in non-coordinating solvents and does not sublime.

2. Sublimation: heating a green powder of *ansa*-[1,3-$(Me_3C)_2C_5H_2]_2SiMe_2Yb(OEt_2)$ uner dynamic vacuum leads to the precipitation of a yellow powder on the cold finger, and a brown residue. Neither of these fractions is soluble in non-coordinating solvent.

3. Reaction of tetraene with $[(Me_3Si)_2N]_2Yb$: The white crystalline *ansa*-[1,3-$(Me_3C)_2C_5H_3]_2SiMe_2$ was stirred in toluene with $[(Me_3Si)_2N]_2Yb$ for 2 days at room temperature. The reaction mixture was then filtered and cooled to -80°C, which resulted in the crystallization of unreacted *ansa*-[1,3-$(Me_3C)_2C_5H_3]_2SiMe_2$.

***ansa*-[1,3-$(Me_3Si)_2C_5H_2]_2SiMe_2Na_2$.** Attempts to prepare this reagent were unsuccessful. The Si - C bond appears to be weak, and the cyclopentadienide rings are readily cleaved from the $SiMe_2$ bridge under the reaction conditions.

High pressure NMR experiments of $(Me_5C_5)_2Yb$ under CO. A sample of $(Me_5C_5)_2Yb$ was dissolved in methylcyclohexane-d_{14} and transferred to a high pressure NMR tube fitted with a threaded cap. The $^{13}C\{^1H\}$ NMR spectrum of the sample was recorded and the sample was then pressurized with CO to approximately 40 psi, which resulted in a color-change from orange-brown to dark brown. The $^{13}C\{^1H\}$ NMR spectrum was recorded again and the pressure was increased in the sample by increments of approximately 40 psi. The maximum pressure used was 220 psi, after which the sample was gradually vented and the spectrum was recorded at decreasing pressures. A plot of δ vs T for the ring and methyl carbon atoms of the ytterbocene for three runs of this experiment is shown below. The scatter in the data are most likely due to random error in the pressure reading. The resonance of the carbonyl carbon atom is not observed under these conditions.

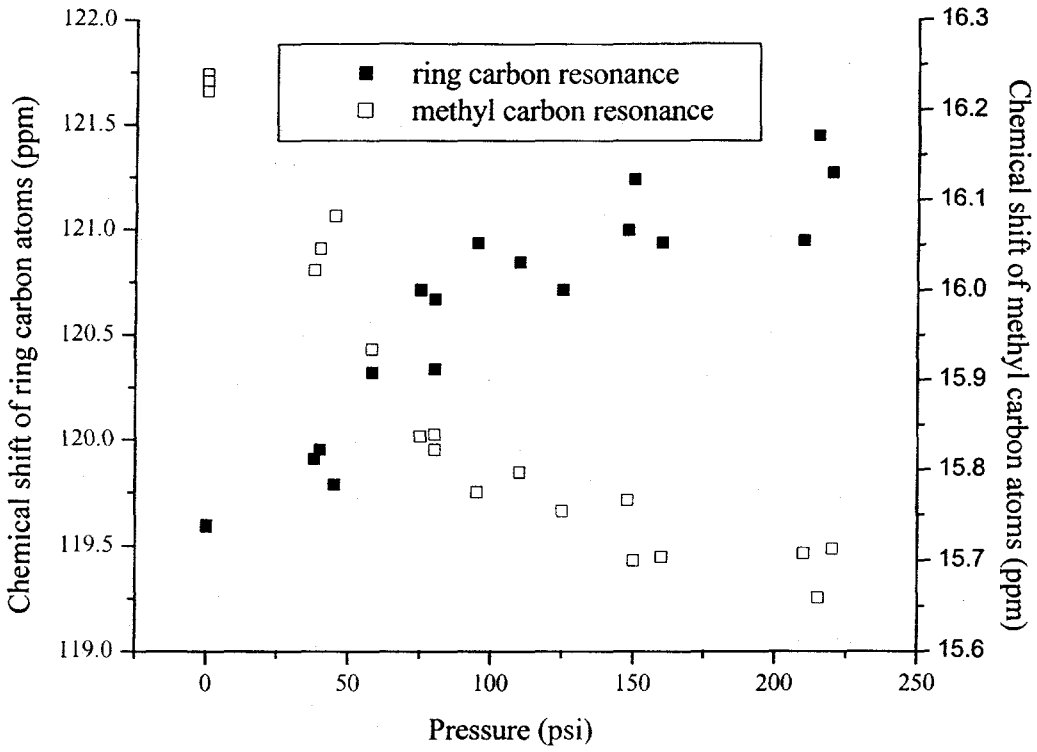

$(Me_5C_5)_2Yb(Me_3CNC)_2$. A solution of $(Me_5C_5)_2Yb(OEt_2)$ (0.5 g, 0.97 mmol) in toluene (30 mL) was combined with two equivalents of Me_3CNC (0.16 g, 1.93 mmol, 0.22 mL). The solution immediately became red-brown and the volume of solvent was reduced slightly. The solution was cooled to -40°C, yielding bright red crystals in 80% yield which contain one molecule of toluene of crystallization per metal atom by microanalysis and ^1H NMR spectroscopy. mp 105-109°C. Anal. Calcd for $C_{37}H_{56}N_2Yb$: C, 63.3; H 8.04; N, 3.99. Found: C, 64.1; H, 8.16; N, 3.96. ^1H NMR (C_6D_6): δ 7.05 (m, 5H, tol), 2.33 (s, 30H, Me_5), 2.11 (s, 3H, tol), 1.01 (br s, 18 H, Me_3) ppm. IR (nujol): 2160 (m), 1462 (s), 1377 (m), 1201 (w), 1022 (w), 727 (m), 696 (w). The optical data are in Table 2.5.

$(Me_5C_5)_2Yb(C_6H_{11}NC)_2$. A similar procedure to that used to prepare $(Me_5C_5)_2Yb(Me_3CNC)_2$ was followed, yielding bright red crystals. Yield: 70 %. mp 175-178°C. Anal. Calcd for $C_{34}H_{52}N_2Yb$: C, 61.7; H 7.92; N, 4.23. Found: C, 62.1; H, 7.97; N, 4.25. ^{1}H NMR (C_6D_6): δ 2.55 (br s, 2H, C_6H_{11}), 2.39 (s, 30H, Me_5), 1.35 (br s, 12H, C_6H_{11}), 0.81 (br s, 8H, C_6H_{11}) ppm. IR (nujol): 2164 (s), 1450 (s), 1370 (m), 1000 (w), 920 (w). The optical data are in Table 2.5.

$[1,3\text{-}(Me_3C)_2C_5H_3]_2Yb(2,6\text{-}Me_2C_6H_3NC)_2$. In a nitrogen-containing glove-box, $[1,3\text{-}(Me_3C)_2C_5H_3]_2Yb(OEt_2)$ (0.58 g, 0.97 mmol) and $2,6\text{-}Me_2C_6H_3NC$ (0.25 g, 1.94 mmol) were placed in a Schlenk flask. Toluene (30 mL) was added, the dark solution was briefly stirred, and the volume of solvent was reduced to 10 mL. Cooling to -40°C resulted in the formation of deep blue crystals. Yield: 0.6 g (85 %). mp 163-166°C. Anal. Calcd for $C_{44}H_{60}N_2Yb$: C, 66.9; H 7.66; N, 3.55. Found: C, 66.7; H, 7.76; N, 3.40. ^{1}H NMR (toluene-d_8): δ 6.77 (t, J = 7.7 Hz, 2H, C_6H_3), 6.56 (d, J = 7.6 Hz, 4H, C_6H_3), 6.14 (d, J = 2.5 Hz, 4H, C_5H_3), 6.10 (t, J = 2.4 Hz, 2H, C_5H_3), 2.12 (s, 12H, Me_2), 1.42 (s, 36H, Me_3C) ppm. IR (nujol): 2129 (s), 1470 (s), 1380 (s), 1230 (w), 1105 (w), 830 (s), 800 (m). The optical data are in Table 2.5.

$[1,3\text{-}(Me_3C)_2C_5H_3]_2Yb(Me_3CNC)_2$. Under a flow of nitrogen, $[1,3\text{-}(Me_3C)_2C_5H_3]_2Yb(OEt_2)$ (0.73 g, 1.2 mmol) was weighed into a Schlenk flask. Toluene (30 mL) was added followed by Me_3CNC (0.20 g, 0.275 mL, 2.4 mmol) and the solution was stirred briefly. The volume of the blood-red solution was reduced to 25 mL, and then it was cooled to -40°C to give deep red crystals. Yield: 0.7 g (85 %). mp 165-

169°C. Anal. Calcd for $C_{36}H_{60}N_2Yb$: C, 62.3; H 8.72; N, 4.04. Found: C, 63.4; H, 9.2; N, 4.08. ^{1}H NMR (toluene-d_8): δ 6.03 (br, 4H, C_5H_3), 5.98 (br, 2H, C_5H_3), 1.46 (s, 36H, ring Me_3C), 0.98 (s, 18H, isocyanide Me_3C) ppm. IR (nujol): 2164 (s), 1455 (s), 1377 (s), 1230 (m), 1210 (m), 1040 (w), 830 (s), 790 (m). The optical data are in Table 2.5.

[1,3-$(Me_3C)_2C_5H_3]_2Yb(C_6H_{11}NC)_2$. A procedure similar to that used to prepare [1,3-$(Me_3C)_2C_5H_3]_2Yb(Me_3CNC)_2$ was followed, yielding brick-red crystals. Yield: 89 %. mp 148-150°C. Anal. Calcd for $C_{40}H_{62}N_2Yb$: C, 64.4; H 8.65; N, 3.76. Found: C, 63.0; H, 8.64; N, 3.56. ^{1}H NMR (toluene-d_8): δ 6.18 (br, 4H, C_5H_3), 6.14 (br, 2H, C_5H_3), 2.79 (br, 2H, C_6H_{11}), 1.56 (s, 36 H, Me_3C), 1.36 (br, 12H, C_6H_{11}), 1.00 (br m, 8H, C_6H_{11}) ppm. IR (nujol): 2166 (s), 1460 (s), 1375 (m), 1240 (m), 1190 (w), 831 (m), 795 (m). The optical data are in Table 2.5 and Figure 2.3.

[1,3-$(Me_3Si)_2C_5H_3]_2Yb(2,6\text{-}Me_2C_6H_3NC)_2$. A procedure similar to that used to prepare [1,3-$(Me_3C)_2C_5H_3]_2Yb(2,6\text{-}Me_2C_6H_3NC)_2$ gave dark blue crystals. Yield: 90 %. mp 155-158°C. Anal. Calcd for $C_{40}H_{60}Si_4N_2Yb$: C, 56.2; H 7.08; N, 3.28. Found: C, 54.6; H, 6.64; N, 2.74. ^{1}H NMR (C_6D_6): δ 6.80 (br m, 12H, C_5H_3 and C_6H_3), 2.45 (br s, 12H, Me_2), 0.47 (s, 36H, Me_3Si) ppm. IR (nujol): 2142 (s), 1460 (s), 1375 (m), 1240 (m), 1090 (s), 830 (vs), 740 (m), 625 (w). The optical data are in Table 2.5.

[1,3-$(Me_3Si)_2C_5H_3]_2Yb(C_6H_{11}NC)_2$. A procedure similar to that used to prepare [1,3-$(Me_3C)_2C_5H_3]_2Yb(Me_3CNC)_2$ was followed, yielding brick-red crystals. Yield: 85 %. mp 142-144°C. Anal. Calcd for $C_{36}H_{64}Si_4N_2Yb$: C, 53.4; H 7.96; N, 3.46. Found: C,

53.0; H, 8.13; N, 3.40. ^{1}H NMR (C_6D_6): δ 6.72 (br, 4H, C_5H_3), 6.69 (br, 2H, C_5H_3), 2.90 (br s, 2H, C_6H_{11}), 1.48 (br s, 4H, C_6H_{11}), 1.37 (br s, 8H, C_6H_{11}), 0.93 (br m, 8H, C_6H_{11}), 0.50 (s, 36H, Me_3Si) ppm. IR (nujol): 2168 (s), 1455 (s), 1377 (m), 1314 (w), 1246 (s), 1078 (s), 925 (m), 833 (vs), 751 (s), 685 (w), 629 (w). The optical data are in Table 2.5.

$(Me_4C_5H)_2Yb(2,6\text{-}Me_2C_6H_3NC)_2$. A procedure similar to that used to prepare [1,3-$(Me_3C)_2C_5H_3]_2Yb(2,6\text{-}Me_2C_6H_3NC)_2$ was followed and dark blue-green crystals were isolated in 70 % yield. mp 180-182°C. Anal. Calcd for $C_{36}H_{44}N_2Yb$: C, 63.8; H, 6.54; N, 4.13. Found: C, 63.5; H, 6.34; N, 3.88. ^{1}H NMR (C_6D_6): δ 6.93 (t, J = 7 Hz, 2H, C_6H_3), 6.52 (d, J = 7 Hz, 4H, C_6H_3), 5.88 (s, 2H, C_5H), 2.44 (s, 12H, Me_4C_5), 2.39 (s, 12H, Me_4C_5), 2.03 (s, 12H, Me_2) ppm. IR (nujol): 2132 (m), 1462 (s), 1377 (s), 1170 (w), 735 (m). The optical data are in Table 2.5.

$(Me_4C_5H)_2Yb(Me_3CNC)_2$. A procedure similar to that used to prepare [1,3-$(Me_3C)_2C_5H_3]_2Yb(Me_3CNC)_2$ was followed and the product was isolated as red crystals, 80 % yield. mp 105-108°C. Anal. Calcd for $C_{28}H_{44}N_2Yb$: C, 57.8; H, 7.62; N, 4.82. Found: C, 58.7; H, 7.40; N, 4.29. ^{1}H NMR (C_6D_6): δ 5.9 (s, 2H, C_5H), 1.79 (s, 12H, Me_4C_5), 1.75 (s, 12H, Me_4C_5) ppm (Me_3CNC resonances were not observed). IR (nujol): 2162 (s), 1460 (s), 1377 (s), 1250 (m), 980 (w), 770 (m).

$(Me_4C_5H)_2Yb(C_6H_{11}NC)_2$. A procedure similar to that used to prepare [1,3-$(Me_3C)_2C_5H_3]_2Yb(Me_3CNC)_2$ was followed and the product was isolated as red crystals, 90 % yield. mp 136-139°C. Anal. Calcd for $C_{32}H_{48}N_2Yb$: C, 60.6; H, 7.63; N, 4.42.

Found: C, 60.6; H, 7.43; N, 4.16. ^{1}H NMR (C_6D_6): δ 5.89 (s, 2H, C_5H), 2.63 (s, 2H, C_6H_{11}), 2.47 (s, 12H, Me_4C_5), 2.40 (s, 12H, Me_4C_5), 1.3 (br m, 12 H, C_6H_{11}), 0.8 (br m, 8 H, C_6H_{11}) ppm. IR (nujol): 2173 (s), 2136 (m), 1452 (s), 1366 (m), 1261 (w), 1145 (w), 1021 (m), 924 (w), 893 (w), 785 (m), 753 (m). The optical data are in Table 2.5.

***ansa*-[1,3-$(Me_3C)_2C_5H_2]_2SiMe_2Yb(2,6\text{-}Me_2C_6H_3NC)_2$.** The isocyanide 2,6-$Me_2C_6H_3NC$ (0.18 g, 14.4 mmol) was added under a flow of nitrogen to a Schlenk flask containing *ansa*-[1,3-$(Me_3C)_2C_5H_2]_2SiMe_2Yb(OEt_2)$ (0.5 g, 7.7 mmol). Toluene (25 mL) was added and the dark red solution was stirred briefly. The volume of solvent was reduced slightly and the solution was cooled to -40°C, resulting in the formation of dark red crystals in good (80%) yield. mp 245-247°C. Anal. Calcd for $C_{46}H_{64}N_2SiYb$: C, 65.3; H, 7.62; N, 3.31. Found C, 64.3; H, 8.03; N, 3.17. ^{1}H NMR (C_6D_6): δ 6.80 (t, J = 7.5 Hz, 2H, C_6H_3), 6.51 (d, J = 2.5 Hz, 2H, C_5H_2), 6.49 (d, J = 7.5 Hz, 4H, C_6H_3), 6.36 (d, J = 2.5 Hz, 2H, C_5H_2), 2.09 (s, 12H, $\underline{Me}_2C_6H_3$), 1.67 (s, 18H, Me_3C), 1.56 (s, 18H, Me_3C), 1.31 (s, 6H, Me_2Si) ppm. IR (nujol): 2127 (m), 1462 (s), 1377 (s), 1260 (w), 1093 (w), 1022 (w), 804 (w), 770 (w), 722 (w), 676 (w). The optical data are in Table 2.5.

$\{(Me_5C_5)_2Yb(Me_3CNC)\}_2$-μ-CN. An impure sample of Me_3CNC was added to a solution of $(Me_5C_5)_2Yb(OEt_2)$ in toluene. The solution became deep red and red crystals immediately precipitated. It has one molecule of toluene of crystallization as determined by crystallography and microanalysis. The compound becomes gray at 250°C but does not melt to 330°C. Anal. Calcd for $C_{58}H_{86}Yb_2N_3$: C, 59.5; H, 7.40; N, 3.59. Found: C, 59.3; H, 7.33; N, 3.38. The compound is completely insoluble in non-coordinating

solvents, preventing solution characterization. The magnetic measurements indicate that it is paramagnetic with isolated Yb(III) and Yb(II) centers (Figure 2.9). IR (nujol): 2197 (m), 2159 (m), 2094 (m), 1463 (s), 1377 (s), 1237 (w), 1189 (w), 1025 (w), 732 (m), 697 (w).

Chapter Three

[1,3-$(Me_3C)_2C_5H_3]_2Yb(bipy)$. The ether adduct, [1,3-$(Me_3C)_2C_5H_3]_2Yb(OEt_2)$ (0.9 g , 1.5 mmol) was dissolved in toluene (20 mL). A toluene (10 mL) solution of 2,2'-bipyridyl (0.23 g, 1.5 mmol) was added and the green solution immediately became darker green. The solvent was removed under dynamic vacuum after stirring for 1 hr at room temperature and the blue-green residue was washed in pentane, then extracted into toluene (50 mL) and filtered. Cooling to -80°C gave a green-blue crystalline product in 90% yield that cocrystallizes with one molecule of toluene per ytterbocene unit as determined by crystallography and microanalysis. mp 278-280°C. Anal. Calcd for $C_{43}H_{58}N_2Yb$: C, 66.6; H, 7.53; N, 3.61. Found: C, 64.0; H, 7.34; N, 3.74. ^1H NMR (C_7D_8, 23°C): δ 49.53 (2H, $\nu_{1/2}$ = 30 Hz, bipy), 18.49 (2H, $\nu_{1/2}$ = 25 Hz, bipy), 10.58 (2H, $\nu_{1/2}$ = 22 Hz, bipy), 1.96 (36H, $\nu_{1/2}$ = 18 Hz, Me_3C), 1.00 (2H, $\nu_{1/2}$ = 10 Hz, bipy), 0.84 (4H, $\nu_{1/2}$ = 75 Hz, C_5H_3), -1.00 (2H, $\nu_{1/2}$ = 11 Hz, C_5H_3) ppm (toluene resonances were not observed as the spectrum was measured in toluene). IR (nujol): 1593 (m), 1461 (s), 1378 (m), 1248 (m), 1197 (w), 1161 (w), 1049 (w), 935 (w), 789 (m), 764 (m), 719 (m). The optical data are in Table 3.4.

[1,3-$(Me_3Si)_2C_5H_3]_2Yb(bipy)$. A similar procedure to that used to prepare [1,3-$(Me_3C)_2C_5H_3]_2Yb(bipy)$ was followed, yielding a blue-green crystalline product in 90% yield. mp 222-224°C Anal. Calcd for $C_{32}H_{50}N_2Si_4Yb$: C, 51.4; H, 6.74, N, 3.74. Found: C, 50.5; H, 6.72; N, 3.58. ^1H NMR (C_6D_6, 23°C): δ 13.20 (d, J = 4.5 Hz, 2H, bipy), 9.63 (t, J = 7.5 Hz, 2H, bipy), 7.72 (t, J = 5.4 Hz, 2H, bipy), 6.34 (t, J = 8.1 Hz, 2H, bipy), 6.31 (d, J = 1.6 Hz, 4H, C_5H_3), 5.07 (t, J = 2 Hz, 2H, C_5H_3), 0.26 (s, 36H, Me_3Si). IR (nujol): 1594 (w), 1462 (s), 1377 (m), 1249 (m), 1155 (w), 1076 (m), 924 (w), 831 (s), 751 (m), 686 (w), 629 (w). The optical data are in Table 3.4.

[1,3-$(Me_3Si)_2C_5H_3]_2Yb(dmb)$. A similar procedure to that used to prepare [1,3-$(Me_3C)_2C_5H_3]_2Yb(bipy)$ was followed, yielding a blue-green crystalline product in 90% yield that cocrystallizes with one molecule of toluene. mp 190-192°C Anal. Calcd for $C_{41}H_{62}N_2Si_4Yb$: C, 56.7; H, 7.20; N, 3.23. Found: C, 56.4; H, 6.90, N, 3.15. ^1H NMR (C_6D_6, 23°C): δ 9.68 (d, J = 5.2 Hz, 2H, bipy), 7.10 (m, 5H, tol), 6.99 (s, 2H, bipy), 6.83 (d, J = 5.0 Hz, 2H, bipy), 6.68 (d, J = 1.8 Hz, 4H, C_5H_3), 5.78 (t, J = 1.6 Hz, 2H, C_5H_3), 2.10 (s, 3H, tol), 0.99 (s, 6H, Me_2), 0.24 (s, 36H, Me_3Si).

[1,3-$(Me_3Si)_2C_5H_3]_2Yb(py)_2$. Pyridine (0.15 mL, 1.8 mmol) was added with stirring to a green toluene solution of [1,3-$(Me_3Si)_2C_5H_3]_2Yb(OEt_2)$ (0.61 g, 0.9 mmol). The solution immediately became deep blue. After filtration, the solution was concentrated and cooled to -30°C to give a deep blue microcrystalline powder in 90% yield. mp 145-150°C. Anal. Calcd for $C_{32}H_{52}N_2Si_4Yb$: C, 51.2; H, 6.99; N, 3.73. Found: C, 50.4; H, 7.01; N, 3.50. ^1H NMR (C_6D_6, 23°C): δ 8.51 (br, 4H, py), 6.96 (t, J = 6 Hz, 2H, py), 6.83 (d, J =

1.9 Hz, 4H, C_5H_3), 6.61 (t, J = 4 Hz , 4H, py), 6.28 (t, J = 1.9 Hz, 2H, C_5H_3), 0.24 (s, 36H, Me_3Si) ppm. IR (nujol): 1596 (m), 1461 (s), 1441 (s), 1377 (m), 1247 (s), 1079 (s), 925 (m), 832 (vs), 751 (m), 702 (w). The optical data are in Table 3.4.

$(Me_4C_5H)_2Yb(bipy)$. A similar procedure to that used to prepare $(Me_5C_5)_2Yb(dmb)$ was followed, yielding a red-brown crystalline product in quantitative yield. mp 285-288°C. Anal. Calcd for $C_{28}H_{34}N_2Yb$: C, 58.8; H, 6.00; N, 4.90. Found: C, 57.9; H, 5.86; N, 4.93. ^1H NMR (C_6D_6, 23°C): δ 173.7 (2H, $\nu_{1/2}$ = 60 Hz, bipy), 20.9 (12H, $\nu_{1/2}$ = 10 Hz, Me_4C_5), 20.5 (2H, $\nu_{1/2}$ = 25 Hz, bipy), -1.4 (2H, $\nu_{1/2}$ = 37 Hz, bipy), -3.2 (12H, $\nu_{1/2}$ = 9 Hz, Me_4C_5), -17.0 (2H, $\nu_{1/2}$ = 8 Hz, C_5H), -45.3 (2H, $\nu_{1/2}$ = 30 Hz, bipy). IR (nujol): 1549 (m), 1500 (m), 1456 (s), 1379 (s), 1318 (m), 1150 (m), 979 (m), 949 (m), 792 (w), 725 (m). The optical data are in Table 3.4 and the magnetic susceptibility is in Figure 3.4..

***ansa*-[1,3-$(Me_3C)_2C_5H_2]_2SiMe_2Yb(bipy)$.** 2,2'-Bipyridyl (0.07 g, 4 mmol) was added to the etherate *ansa*-[1,3-$(Me_3C)_2C_5H_2]_2SiMe_2Yb(OEt_2)$ (0.3 g, 4 mmol) and the mixture was dissolved in toluene (30 mL). The volume was reduced slightly and the flask was cooled to -80°C, resulting in the formation of dark blue crystals in 70% yield. mp 337-338°C. Anal. Calcd for $C_{38}H_{54}N_2SiYb$: C, 61.7; H, 7.36; N, 3.79. Found: C, 60.5; H, 6.91; N, 3.16. ^1H NMR (C_6D_6, 20°C): δ 32.9 (2H, $\nu_{1/2}$ = 20 Hz, bipy), 15.7 (2H, $\nu_{1/2}$ = 25 Hz, bipy), 10.8 (2H, $\nu_{1/2}$ = 12 Hz, bipy), 9.73 (2H, $\nu_{1/2}$ = 16 Hz, bipy), 5.71 (18H, $\nu_{1/2}$ = 2 Hz, Me_3C), 3.08 (d, J = 8 Hz, 2H, C_5H_2), 0.60 (18H, $\nu_{1/2}$ = 2 Hz, Me_3C), -0.44 (6H, $\nu_{1/2}$ = 3 Hz, Me_2Si), -3.88 (2H, $\nu_{1/2}$ = 8 Hz, C_5H_2) ppm. IR (nujol): 1594 (w), 1461 (s), 1377

(s), 1154 (w), 1095 (w), 803 (w), 765 (w), 723 (w), 670 (w). The optical data are in Table 3.4.

$(C_5H_5)_2Yb(bipy)$. $K(C_5H_5)$ (1.4 g, 13.5 mmol) and YbI_2 (3.3 g, 7.7 mmol) were weighed into a Schlenk flask equipped with a magnetic stirrer under a flow of nitrogen. THF (60 mL) was added and the bright purple slurry was stirred overnight at room temperature. 2,2'-Bipyridyl (1.2 g, 7.6 mmol) was weighed into a clean Schlenk flask and the purple THF solution of $(C_5H_5)_2Yb(THF)_2$ was filtered into that flask. The solution immediately became dark green-blue upon contact with the bipyridyl. The volume of THF was reduced to 40 mL under dynamic vacuum and the solution was cooled to -40°C which resulted in the isolation of a small amount of a green solid. The mother liquor was transferred into a clean Schlenk flask and the volume was again reduced, and a microcrystalline green solid precipitated which has very low solubility in toluene, pentane or diethyl ether. Yield: 2.38 g, 77%. mp 218-220°C. Anal. Calcd for $C_{20}H_{18}N_2Yb$: C, 52.3; H, 3.92; N, 6.10. Found: C, 52.3; H, 3.54; N, 6.08. ^1H NMR (C_6D_6, 23°C): δ 53.1 (2H, $\nu_{1/2}$ = 50 Hz, bipy), 18.7 (2H, $\nu_{1/2}$ = 30 Hz, bipy), 10.8 (2H, $\nu_{1/2}$ = 30 Hz, bipy), 0.6 (2H, $\nu_{1/2}$ = 25 Hz, bipy), -1.69 (10H, $\nu_{1/2}$ = 9 Hz, C_5H_5) ppm. IR (nujol): 1587 (m), 1566 (w), 1463 (s), 1431 (s), 1378 (m), 1271 (s), 1152 (m), 1055 (w), 1007 (s), 897 (w), 867 (w), 750 (vs), 729 (vs), 637 (w).

$(Me_5C_5)_2Yb(phen)$. In the box, $(Me_5C_5)_2Yb(OEt_2)$ (0.47 g, 0.9 mmol) was combined with 1,10-phenanthroline (0.16 g, 0.9 mmol). Toluene was added and the blue solution was briefly stirred at room temperature. Cooling led to the formation of a relatively

insoluble dark blue micorcrystalline powder. Yield: 85%. mp 297-300°C. Anal. Calcd for $C_{32}H_{38}N_2Yb$: C, 61.6; H, 6.14; N, 4.49. Found: C, 61.6; H, 6.18; N, 4.42. ^1H NMR (C_7D_8, 23°C): δ 4.14 ($\nu_{1/2}$ = 12.5 Hz) (phen protons were not observed). IR (nujol): 1610 (m), 1590 (w), 1550 (w), 1498 (m), 1445 (s), 1359 (s), 1308 (s), 1290 (m), 1224 (w), 1172 (w), 1117 (m), 1054 (m), 1022 (w), 859 (w), 823 (m), 798 (m), 734 (m), 689 (m). The field dependence of the magnetic susceptibility is shown in Figure 3.16, and the optical spectrum is in Figure 3.18 and Table 3.7.

[1,3-$(Me_3C)_2C_5H_3]_2$Yb(phen). A similar procedure to that used to prepare $(Me_5C_5)_2$Yb(phen) was followed, yielding a dark blue microcrystalline product in quantitative yield. mp 224-228°C Anal. Calcd for $C_{38}H_{50}N_2Yb$: C, 64.5; H, 7.12; N, 3.96. Found: C, 66.0; H, 7.07; N, 3.99. ^1H NMR (C_6D_6, 23°C): δ 48.19 (2H, $\nu_{1/2}$ = 16 Hz, phen), 22.22 (2H, $\nu_{1/2}$ = 20 Hz, phen), 11.27 (2H, $\nu_{1/2}$ = 14 Hz, phen), 5.04 (2H, $\nu_{1/2}$ = 4 Hz, C_5H_3), 2.07 (36H, $\nu_{1/2}$ = 9 Hz, Me_3C), 1.14 (4H, $\nu_{1/2}$ = 8 Hz, C_5H_3), -0.77 (2H, $\nu_{1/2}$ = 10 Hz, phen) ppm. IR (nujol): 1615 (m), 1591 (w), 1461 (s), 1375 (s), 1311 (m), 1246 (m), 1120 (w), 1055 (m), 822 (m), 748 (w), 691 (w). The magnetic susceptibility is shown in Figure 3.14 and the optical data are in Table 3.7.

[1,3-$(Me_3Si)_2C_5H_3]_2$Yb(phen). A similar procedure to that used to prepare $(Me_5C_5)_2$Yb(phen) was followed, yielding a red crystalline product in quantitative yield. mp 216-218°C. Anal. Calcd for $C_{34}H_{50}N_2Si_4Yb$: C, 52.9; H, 6.53; N, 3.63. Found: C, 53.3; H, 6.50; N, 3.63. ^1H NMR (C_6D_6, 23°C): δ 15.01 (d, J = 4 Hz, 2H, phen), 12.03 (d, J = 7.5 Hz, 2H, phen), 8.04 (dd, J = 8 Hz, J = 4.5 Hz, 2H, phen), 6.82 (s, 2H, phen), 6.22

(d, J = 1 Hz, 4H, C_5H_3), 5.05 (t, J = 1.5 Hz, 2H, C_5H_3), 0.17 (s, 36H, Me_3Si). IR (nujol): 1577 (w), 1461 (s), 1377 (s), 1248 (m), 1079 (m), 926 (w), 830 (s), 747 (m), 730 (m), 628 (w). The optical spectrum is shown in Figure 3.18 and the optical data are in Table 3.7.

$(Me_4C_5H)_2Yb(phen)$. A similar procedure to that used to prepare $(Me_5C_5)_2Yb(phen)$ was followed, yielding a deep blue microcrystalline product in quantitative yield. mp 230-233°C Anal. Calcd for $C_{30}H_{34}N_2Yb$: C, 60.5; H, 5.75; N, 4.70. Found: C, 60.3; H, 5.87; N, 4.56. ^1H NMR (C_6D_6, 23°C): δ 20.32 (12H, $\nu_{1/2}$ = 25 Hz, Me_4C_5), -3.00 (12H, $\nu_{1/2}$ = 25 Hz, Me_4C_5), -40.2 (2H, $\nu_{1/2}$ = 50 Hz, C_5H) ppm (phen resonances were not observed). IR (nujol): 1612 (m), 1551 (w), 1499 (m), 1462 (s), 1363 (s), 1310 (m), 1118 (w), 1056 (m), 797 (w), 735 (w), 689 (w). The magnetic susceptibility is in Figure 3.15 and the optical data are in Table 3.7.

$[(Me_5C_5)_2Yb(phen)]^+[I]^-$. The trivalent iodide $(Me_5C_5)_2YbI$ (0.55 g, 0.96 mmol) was weighed into a Schlenk flask equipped with a magnetic stirrer. 1,10-Phenanthroline (0.17 g, 0.96 mmol) was added, followed by toluene (60 mL). The slurry was stirred overnight, during which time the color changed from green to red. The supernatant was discarded and the product was extracted into methylene chloride (50 mL). Cooling to -80°C led to the formation of red-brown crystals which are found by microanalysis and X-ray crystallography to contain between one and two molecules of methylene chloride of crystallization. mp 173-177°C Anal. Calcd for $C_{34}H_{42}YbIN_2Cl_3$: C, 46.1; H, 4.78; N, 3.17. Found: C, 46.7; H, 4.80; N, 3.32. ^1H NMR (CD_2Cl_2, 23°C): δ 52.37 (2H, $\nu_{1/2}$ = 25 Hz, phen), 9.42 (2H, $\nu_{1/2}$ = 16 Hz, phen), 5.32 (2H, $\nu_{1/2}$ = 5 Hz, phen), 3.80 (30H, $\nu_{1/2}$ =

50 Hz, Me_5C_5), -2.56 (2H, $\nu_{1/2}$ = 20 Hz, phen) ppm. IR (nujol): 1622 (w), 1518 (w), 1460 (s), 1415 (m), 1377 (s), 1273 (w), 855 (m), 728 (s). The optical spectrum is shown in Figure 3.18 and Table 3.7 and the magnetic susceptibility is in Figure 3.17.

Chapter Four

[1,3-$(Me_3C)_2C_5H_3]_2Cr$. The sodium salt Na[1,3-$(Me_3C)_2C_5H_3$] (2.71 g, 0.0135 mol) and $Cr_2(OAc)_4$ (1.15 g, 3.39 mmol) were weighed into a Schlenk flask equipped with a magnetic stirrer under a flow of dinitrogen. THF (180 mL) was added and the slurry was stirred at room temperature for one hour, then heated to reflux and stirred at reflux overnight. The solvent was then removed under reduced pressure and the residue was extracted to pentane (100 mL). The volume of solvent was reduced and the solution was cooled to -80°C. Large red crystals formed in 77% yield. mp 183-184°C. ^{1}H NMR (C_6D_6, 23°C): δ 0.2 ($\nu_{1/2}$ = 250 Hz, Me_3C) ppm (ring protons were not observed). The molecule sublimes under dynamic vacuum at 80°C.

Attempted synthesis of [1,3-$(Me_3C)_2C_5H_3]_2Cr(2,6\text{-}Me_2C_6H_3NC)$. This reaction was attempted with a stoichiometric amount and an excess of isocyanide. In the former case, crystals of the chromocene were isolated from the reaction mixture while in the latter case, crystals of isocyanide were isolated. The infrared spectrum of a toluene solution of the chromocene with excess isocyanide contained only a single absorption, corresponding to the free isocyanide, at 2119cm^{-1}.

X-ray Crystallography

General

All measurements were made on a Siemens SMART[15] diffractometer with graphite monochromated Mo-Kα radiation. Neutral atom scattering factors were taken from Cromer and Waber.[16] Anomalous dispersion effects were included in F_c;[17] the values for $\Delta f'$ and $\Delta f''$ were those of Creagh and McAuley.[18] Mass attenuation coefficients of Creagh and Hubbel were used.[19] All calculations were performed using the teXsan crystallographic software package of Molecular Structure Corporation.[20]

Chapter One

1. {[1,3-$(Me_3C)_2C_5H_3$]YbI(OEt_2)}$_2$. Crystals were collected from the mother liquor of the reaction of $[1,3\text{-}(Me_3C)_2C_5H_3]_2Mg$ with YbI_2 in diethyl ether. An orange plate-like crystal having approximate dimensions of 0.40 × 0.30 × 0.15 mm was mounted on a glass fiber with Exxon Paratone N oil. Cell constants and an orientation matrix, obtained from a least-squares refinement using the measured positions of 6017 reflections with $I > 10\sigma$, in the range $4.0 < 2\theta < 46.5°$, corresponded to a primitive monoclinic cell with dimensions:

a = 13.7190(3) Å

b = 11.1690(1) Å β = 112.800(1)

c = 14.4440(3) Å

$V = 2040.28(6)$ Å^3

For $Z = 4$ and F.W. = 551.38, the calculated density is 1.79 g/cm^3. The systematic absences of:

h0l: $h + l \neq 2n$

0k0: $k \neq 2n$

uniquely determine the space group to be $P2_1/n$ (#14).

Frames corresponding to an arbitrary hemisphere of data were collected at -112°C using ω scans of 0.3° counted for 10 seconds per frame. Data were integrated using SAINT[21] to a maximum 2θ value of 46.5°. Of the total of 8633 reflections integrated, 3106 were unique ($R_{int} = 0.033$) and equivalent reflections were merged.

The linear absorption coefficient, μ, for Mo-Kα radiation is 60.9 cm^{-1}. Data were examined for agreement and possible absorption using XPREP and an empirical absorption correction was applied using $\mu R = 0.17$.[22] The transmission range was 0.470 - 0.981. The data were corrected for Lorentz and polarization effects. No correction was required for decay or secondary extinction.

The structure was solved by direct methods[23] and expanded using Fourier techniques.[24] All non-hydrogen atoms were refined anisotropically. Hydrogen atoms were included in calculated positions but not refined. The final cycle of full-matrix least-squares refinement was based on 2413 observed reflections ($I > 3\sigma(I)$) and 181 variables and

converged. The largest parameter shift was 0.02 times its esd. The weighted and unweighted agreement factors were:

$$R = \Sigma \left| \left| F_o \right| - \left| F_c \right| \right| / \Sigma \left| F_o \right| = 0.023$$

$$R_w = \sqrt{(\Sigma w(\left| F_o \right| - \left| F_c \right|)^2 / \Sigma w F_o^2)} = 0.031$$

The standard deviation of an observation of unit weight was 1.17. The weighting scheme was based on counting statistics and included a factor (p = 0.03) to downweight intense reflections. Plots of $\Sigma w(\left| F_o \right| - \left| F_c \right|)^2$ versus $\left| F_o \right|$, reflection order in data collection, sin θ/λ and various classes of indices showed no unusual trends. The maximum and minimum peaks on the final difference Fourier map corresponded to 1.03 and -1.09 $e^-/Å^3$, respectively.

formula	$YbC_{17}H_{31}OI$	diffractometer	SMART
FW	551.38	scan type, range	ω, 4 - 46.5°
space group	$P2_1/n$ (#14)	reflections integrated	8633
a (Å)	13.7190(3)	unique reflections	3106
b (Å)	11.1690(1)	reflections, $F_o^2 > 3\sigma(F_o^2)$	2413
c (Å)	14.4440(3)	variables	181
β (°)	112.800(1)	absorption correction	empirical
V ($Å^3$)	2040.28(6)	transmission range	0.981 - 0.470
Z	4	R	0.023
d_{calc} (g/cm^3)	1.795	R_w	0.031

μ(Mo-Kα)$_{calc}$ (cm^{-1})	60.93	R_{all}	0.033
size (mm)	0.40 × 0.30 × 0.15	GOF	1.17
temperature (K)	161		

2. [1,3-(Me$_3$C)$_2$C$_5$H$_3$]$_2$Yb(OEt$_2$). Crystals were grown by cooling a diethyl ether solution of the complex. A green block-like crystal having approximate dimensions of 0.26 × 0.25 × 0.15 mm was mounted on a glass fiber with Exxon Paratone N oil. Cell constants and an orientation matrix, obtained from a least-squares refinement using the measured positions of 8192 reflections with $I > 10\ \sigma$, in the range $4.0 < 2\theta < 52.2°$, corresponded to a primitive monoclinic cell with dimensions:

a = 11.1771(2) Å

b = 19.1123(1) Å β = 90.160(1)

c = 14.0739(2) Å

V = 3006.47(8) Å^3

For Z = 4 and F.W. = 601.78, the calculated density is 1.33 g/cm^3. The systematic absences of:

h0l: h + l ≠ 2n

0k0: k ≠ 2n

uniquely determine the space group to be P2$_1$/n (#14).

Frames corresponding to a hemisphere of data were collected at -142°C by taking 10 second exposures of 0.3° ω scans. Data were integrated using SAINT[21] to a maximum

2θ value of 52.2°. Of the total of 14404 reflections integrated, 5451 were unique (R_{int} = 0.045) and equivalent reflections were merged.

The linear absorption coefficient, μ, for Mo-Kα radiation is 31.3 cm^{-1}. Data were examined for agreement and possible absorption using XPREP[22] and an empirical absorption correction was applied. Using μR = 0.04 gave a transmission range of 0.796 - 0.989. The data were corrected for Lorentz and polarization effects. No correction was applied for decay or secondary extinction.

The structure was solved by direct methods[23] and expanded using Fourier techniques.[24] All non-hydrogen atoms were refined anisotropically. Hydrogen atoms were placed in calculated positions after peaks were observed in the difference map at their expected positions. The final cycle of full-matrix least-squares refinement was based on 3667 observed reflections ($I > 3\sigma(I)$) and 289 variables and converged. The largest parameter shift was 0.00 times its esd. The weighted and unweighted agreement factors were:

$$R = \Sigma \left| |F_o| - |F_c| \right| / \Sigma |F_o| = 0.033$$

$$R_w = \sqrt{(\Sigma w(|F_o| - |F_c|)^2 / \Sigma w F_o^2)} = 0.039$$

The standard deviation of an observation of unit weight was 1.29. The weighting scheme was based on counting statistics and included a factor (p = 0.03) to downweight intense reflections. Plots of $\Sigma w(|F_o| - |F_c|)^2$ versus $|F_o|$, reflection order in data collection, sin θ/λ and various classes of indices showed no unusual trends. The maximum and

minimum peaks on the final difference Fourier map corresponded to 1.52 and -0.71 $e^-/Å^3$, respectively.

formula	$YbC_{30}H_{52}O$	diffractometer	SMART
FW	601.78	scan type, range	ω, 4 - 52.2°
space group	$P2_1/n$ (#14)	reflections integrated	14404
a (Å)	11.1771(2)	unique reflections	5451
b (Å)	19.1123(1)	reflections, $F_o^2 > 3\sigma(F_o^2)$	3667
c (Å)	14.0739(2)	variables	289
β (°)	90.160(1)	absorption correction	empirical
V ($Å^3$)	3006.47(8)	transmission range	0.989 - 0.796
Z	4	R	0.033
d_{calc} (g/cm^3)	1.329	R_w	0.039
μ(Mo-Kα)$_{calc}$ (cm^{-1})	31.28	R_{all}	0.045
size (mm)	0.26 × 0.25 × 0.15	GOF	1.29
temperature (K)	131		

3. $(Me_4C_5H)_2Yb(OEt_2)$. Crystals were grown by cooling a diethyl ether solution of the complex. A green block-like crystal having approximate dimensions of 0.24 × 0.17 × 0.16 mm was mounted on a glass fiber with Exxon Paratone N oil. Cell constants and an orientation matrix, obtained from a least-squares refinement using the measured positions of 3694 reflections with $I > 10\sigma$, in the range $4.0 < 2\theta < 40°$, corresponded to a primitive orthorhombic cell with dimensions:

a = 16.4241(8) Å

b = 17.1874(7) Å

c = 30.573(1) Å

V = 8630.3(6) $Å^3$

For Z = 16 and F.W. = 489.57, the calculated density is 1.51 g/cm^3. The systematic absences of:

0kl: $k \neq 2n$

h0l: $l \neq 2n$

hk0: $h \neq 2n$

uniquely determine the space group to be P*bca* (#61).

Frames corresponding to an arbitrary hemisphere of data were collected at -155°C using ω scans of 0.3° counted for 20 seconds per frame. Data were integrated using SAINT[21] to a maximum 2θ value of 48.7°, although only data up to 2θ = 40.0° were used in the solution. Of the total of 36575 reflections integrated, 6845 were unique (R_{int} = 0.205) and equivalent reflections were merged.

The linear absorption coefficient, μ, for Mo-Kα radiation is 43.4 cm^{-1}. Data were examined for agreement and possible absorption using XPREP.[22] An empirical absorption correction based on comparison of redundant and equivalent reflections was applied using SADABS.[25] The transmission range was 0.649 - 0.914. The data were

corrected for Lorentz and polarization effects. No correction was applied for decay or secondary extinction.

The structure was solved by direct methods[23] and expanded using Fourier techniques.[24] Due to the lack of high-angle data, refinement was limited to data in the range 4 - 40°. The two unique ytterbium atoms were refined anisotropically while the remainder of the non-hydrogen atoms were refined isotropically. Hydrogen atoms were placed in calculated positions but not refined. The final cycle of full-matrix least-squares refinement was based on 1505 observed reflections ($I > 3\sigma(I)$) and 203 variables and converged. The largest parameter shift was 0.00 times its esd. The weighted and unweighted agreement factors were:

$$R = \Sigma \left| |F_o| - |F_c| \right| / \Sigma |F_o| = 0.029$$

$$R_w = \sqrt{(\Sigma w(|F_o| - |F_c|)^2 / \Sigma w F_o^2)} = 0.029$$

The standard deviation of an observation of unit weight was 0.71. The weighting scheme was based on counting statistics and included a factor ($p = 0.03$) to downweight intense reflections. Plots of $\Sigma w(|F_o| - |F_c|)^2$ versus $|F_o|$, reflection order in data collection, sin θ/λ and various classes of indices showed no unusual trends. The maximum and minimum peaks on the final difference Fourier map corresponded to 0.59 and -0.60 $e^-/Å^3$, respectively.

formula	$YbC_{22}H_{36}O$	diffractometer	SMART
FW	489.57	scan type, range	ω, 4 - 40.0°

space group	P*bca* (#61)	reflections integrated	36575
a (Å)	16.4241(8)	unique reflections	6845
b (Å)	17.1874(7)	reflections, $F_o^2 > 3\sigma(F_o^2)$	1505
c (Å)	30.573(1)	variables	203
V (Å^3)	8630.3(6)	absorption correction	empirical
Z	16	transmission range	0.914 - 0.649
d_{calc} (g/cm^3)	1.507	R	0.029
μ(Mo-Kα)$_{calc}$ (cm^{-1})	43.40	R_w	0.029
size (mm)	0.24 × 0.17 × 0.16	R_{all}	0.111
temperature (K)	118	GOF	0.71

4. *ansa*-[1,3-(Me$_3$C)$_2$C$_5$H$_2$]$_2$SiMe$_2$Yb(OEt$_2$). Crystals were grown by cooling a diethyl ether solution of the complex. A green needle-like crystal having approximate dimensions of 0.60 × 0.10 × 0.08 mm was mounted on a glass fiber with Exxon Paratone N oil. Cell constants and an orientation matrix, obtained from a least-squares refinement using the measured positions of 7889 reflections with I > 10σ, in the range 4.0 < 2θ < 46.6°, corresponded to a primitive orthorhombic cell with dimensions:

a = 29.0586(5) Å

b = 15.9398(2) Å

c = 24.5206(4) Å

V = 11357.7(3) Å^3

For Z = 12 and F.W. = 657.92, the calculated density is 1.15 g/cm^3. The systematic absences of:

h00: h ≠ 2n

0k0: k ≠ 2n

00l: l ≠ 2n

uniquely determine the space group to be $P2_12_12_1$ (#19).

Frames corresponding to an arbitrary hemisphere of data were collected at -117°C using ω scans of 0.3° counted for 30 seconds per frame. Data were integrated using SAINT[21] to a maximum 2θ value of 46.6°. Of the total of 47621 reflections integrated, 16331 were unique (R_{int} = 0.070). Only Friedel-equivalent (P222) data were merged.

The linear absorption coefficient, μ, for Mo-Kα radiation is 25.2 cm^{-1}. Data were examined for agreement and possible absorption using XPREP.[22] An empirical absorption correction based on comparison of redundant and equivalent reflections was applied using SADABS.[25] The transmission range was 0.787 - 928. The data were corrected for Lorentz and polarization effects. No correction was applied for decay or secondary extinction.

The structure was solved by direct methods[23] and expanded using Fourier techniques.[24] Five of the carbon atoms were refined isotropically while the remainder of the non-hydrogen atoms were refined anisotropically. Hydrogen atoms were placed in calculated positions but not refined. The absolute configuration analysis performed by teXsan

indicated that the enantiomorph was correct, and it has a lower R factor than the inverted structure.

A diffuse region of electron density in the structure which is possibly disordered solvent has been modelled as 24 partial occupancy carbon atoms. The initial positions of these atoms was based on the largest peaks in the difference Fourier map, and subsequent refinement and examination of the Fourier and difference Fourier maps indicated that the electron density is centered around those positions. The thermal parameters of these carbon atoms was fixed at 8.0 and their individual occupancy parameters were refined. Refinement led to occupancies of between 0.195 and 0.710. The sum of the occupancies is 9.855 which is approximately equal to one and a third ether molecules per asymmetric unit.

The final cycle of full-matrix least-squares refinement was based on 9671 observed reflections ($I > 3\sigma(I)$) and 1017 variables and converged. The largest parameter shift was 0.04 times its esd. The weighted and unweighted agreement factors were:

$$R = \Sigma \left| |F_o| - |F_c| \right| / \Sigma |F_o| = 0.046$$

$$R_w = \sqrt{(\Sigma w(|F_o| - |F_c|)^2 / \Sigma w F_o^2)} = 0.047$$

The standard deviation of an observation of unit weight was 1.24. The weighting scheme was based on counting statistics and included a factor ($p = 0.03$) to downweight intense reflections. The maximum and minimum peaks on the final difference Fourier map corresponded to 2.12 and -1.23 $e^-/Å^3$, respectively.

formula	$YbSiC_{32}H_{56}O$	diffractometer	SMART
FW	657.92	scan type, range	ω, 4 - 46.6°
space group	$P2_12_12_1$ (#19)	reflections integrated	47621
a (Å)	29.0586(5)	unique reflections	16331
b (Å)	15.9398(2)	reflections, $F_o^2 > 3\sigma(F_o^2)$	9671
c (Å)	24.5206(4)	variables	1017
V (Å^3)	11357.7(3)	absorption correction	empirical
Z	12	transmission range	0.928 - 0.787
d_{calc} (g/cm^3)	1.154	R	0.046
μ(Mo-Kα)$_{calc}$ (cm^{-1})	25.19	R_w	0.047
size (mm)	0.60 × 0.10 × 0.08	R_{all}	0.088
temperature (K)	156	GOF	1.24

5. [1,3-(Me$_3$C)$_2$C$_5$H$_3$]$_2$Yb. Brown-green crystals of the compound were grown by cooling a pentane solution to -80°C. A fragment of a crystal having approximate dimensions 0.14 mm × 0.09 mm × 0.05 mm was mounted on a glass fiber with Exxon Paratone N oil. Cell constants and an orientation matrix, obtained from a least-squares refinement using the measured positions of 6127 reflections with I > 10σ, in the range 4 < 2θ < 52°, corresponded to a primitive orthorhombic cell with dimensions:

a = 11.9795(6) Å

b = 13.3629(7) Å

c = 15.5938(8) Å

$V = 2496.3(2)\ Å^3$

For Z = 4 and F.W. = 527.66, the calculated density is 1.40 g/cm^3. The systematic absences of:

h00: $h \neq 2n$

0k0: $k \neq 2n$

00l: $l \neq 2n$

uniquely determine the space group to be $P2_12_12_1$ (#19).

Frames corresponding to an arbitrary hemisphere of data were collected at -128°C using ω scans of 0.3° counted for a total of 30.0 seconds per frame. Data were integrated using SAINT[21] to a maximum 2θ value of 45.0°. Of the 11966 reflections that were integrated, 4448 were unique (R_{int} = 0.054); equivalent reflections were merged

The linear absorption coefficient, μ, for Mo-Kα radiation is 37.54 cm^{-1}. Data were examined for agreement and possible absorption using XPREP.[22] An empirical absorption correction based on comparison of redundant and equivalent reflections was applied using SADABS.[25] The transmission range was 0.714 - 0.928. The data were corrected for Lorentz and polarization effects. No correction was applied for decay or secondary extinction.

The structure was solved by direct methods[23] and expanded using Fourier techniques.[24] Two carbon atoms (C(1) and C(17)) were refined isotropically as anisotropic refinement

led to non-positive definite thermal parameters. Hydrogen atoms were included in calculated positions and not refined. The Flack parameter was refined using SHELXTL[26] to determine whether the crystal was a racemic twin, and it refined to a low value with a high esd so it appears that the crystal is chiral. The absolute configuration was checked using the absolute configuration analysis in teXsan and found to be correct.

The final cycle of full-matrix least-squares refinement was based on 2323 observed reflections ($I > 3\sigma(I)$) and 234 variables and converged. The largest parameter shift was 0.02 times its esd. The weighted and unweighted agreement factors were:

$$R = \Sigma \left| |F_o| - |F_c| \right| / \Sigma |F_o| = 0.039$$

$$R_w = \sqrt{(\Sigma w(|F_o| - |F_c|)^2 / \Sigma w F_o^2)} = 0.044$$

The standard deviation of an observation of unit weight was 1.29. The weighting scheme was based on counting statistics and included a factor ($p = 0.03$) to downweight intense reflections. Plots of $\Sigma w(|F_o| - |F_c|)^2$ versus $|F_o|$, reflection order in data collection, $\sin\theta/\lambda$ and various classes of indices showed no unusual trends. The maximum and minimum peaks on the final difference Fourier map corresponded to 2.55 and -1.11 e/Å^3, respectively.

formula	$C_{26}H_{42}Yb$	diffractometer	SMART
FW	527.66	scan type, range	ω, $4° \leq 2\theta \leq 52°$
space group	$P2_12_12_1$	reflections integrated	11966
a (Å)	11.9795(6)	unique reflections	4448

b (Å)	13.3629(7)	reflections, $F_o^2 > 3\sigma(F_o^2)$	2323
c (Å)	15.5938(8)	variables	234
V (Å^3)	2496.3(2)	absorption correction	empirical
Z	4	transmission range	0.714 - 0.928
d_{calc} (g/cm^3)	1.40	R	0.039
μ (Mo-Kα)$_{calc}$ (cm^{-1})	37.54	R_w	0.044
size (mm)	0.14 × 0.09 × 0.05	R_{all}	0.05
temperature (K)	145	GOF	1.29

6. $(Me_4C_5H)_2Yb$. Crystals of the compound were grown by dissolving the etherate $(Me_4C_5H)_2Yb(OEt_2)$ in toluene followed by slow cooling to -40°C. A green needle-like crystal having approximate dimensions of 0.15 mm × 0.08 mm × 0.04 mm was mounted on a glass fiber with Exxon Paratone N oil. Cell constants and an orientation matrix obtained from a least-squares refinement using the measured positions of 2893 reflections with I > 10σ, in the range 4 < 2θ < 52°, corresponded to a primitive orthorhombic cell with dimensions:

a = 9.9528(3) Å

b = 10.1141(4) Å

c = 16.0538(3) Å

V = 1616.03(7) Å^3

For Z = 4 and F.W. = 415.44, the calculated density is 1.71 g/cm^3. The systematic absences of:

h00: $h \neq 2n$

0k0: $k \neq 2n$

00l: $l \neq 2n$

uniquely determine the space group to be $P2_12_12_1$ (#19).

Frames corresponding to an arbitrary hemisphere of data were collected at -108°C using ω scans of 0.3° counted for a total of 10.0 seconds per frame. Data were integrated using SAINT[21] to a maximum 2θ value of 52.2°. Of the 7842 reflections that were integrated, 1727 were unique (R_{int} = 0.065); equivalent reflections were merged. Although the space group is chiral, examination of the data and an absolute configuration analysis indicated that the crystal was a racemic twin, so Friedel pairs were treated as equivalent.

The linear absorption coefficient, μ, for Mo-Kα radiation is 57.73 cm^{-1}. Data were examined for agreement and possible absorption using XPREP.[22] An empirical absorption correction based on comparison of redundant and equivalent reflections was applied using SADABS.[25] The transmission range was 0.825 - 0.956. The data were corrected for Lorentz and polarization effects. No correction was applied for decay or secondary extinction.

The structure was solved by direct methods[23] and expanded using Fourier techniques.[24] All non-hydrogen atoms were refined anisotropically. The hydrogen atom bound to C(1) was found as the largest peak in the difference map and placed in that position; other hydrogen atoms were placed in calculated positions but not refined.

The final cycle of full-matrix least-squares refinement was based on 1136observed reflections ($I > 3\sigma(I)$) and 172 variables and converged. The largest parameter shift was 0.00 times its esd. The weighted and unweighted agreement factors were:

$$R = \Sigma \left| |F_o| - |F_c| \right| / \Sigma |F_o| = 0.026$$

$$R_w = \sqrt{(\Sigma w(|F_o| - |F_c|)^2 / \Sigma w F_o^2)} = 0.024$$

The standard deviation of an observation of unit weight was 0.74. The weighting scheme was based on counting statistics and included a factor (p = 0.03) to downweight intense reflections. Plots of $\Sigma w(|F_o| - |F_c|)^2$ versus $|F_o|$, reflection order in data collection, $\sin\theta/\lambda$ and various classes of indices showed no unusual trends. The maximum and minimum peaks in the final difference Fourier map corresponded to 0.67 and –0.79 e/Å^3, respectively.

formula	$C_{18}H_{26}Yb$	diffractometer	SMART
FW	415.44	scan type, range	ω, $4° \le 2\theta \le 52°$
space group	$P2_12_12_1$	reflections integrated	7842
a (Å)	9.9528(3)	unique reflections	1727
b (Å)	10.1141(4)	reflections, $F_o^2 > 3\sigma(F_o^2)$	1136
c (Å)	16.0538(3)	variables	172
V (Å^3)	1616.03(7)	absorption correction	empirical
Z	4	transmission range	0.825 - 0.956
d_{calc} (g/cm^3)	1.71	R	0.026

μ(Mo-Kα)$_{calc}$ (cm^{-1})	57.73	R_w	0.024
size (mm)	0.15 × 0.08 × 0.04	R_{all}	0.031
temperature (K)	165	GOF	0.74

Chapter Two

7. $(Me_5C_5)_2Yb(2,6\text{-}Me_2C_6H_3NC)_2$. Green crystals of the compound were grown by layering pentane onto a concentrated toluene solution. A green prismatic crystal with approximate dimensions of 0.55 × 0.22 × 0.24 mm was mounted on a glass fiber with Paratone N oil. Cell constants and an orientation matrix obtained from a least-squares refinement using the measured positions of 8192 reflections with I > 10σ, in the range 4 < 2θ < 51.6°, corresponded to a primitive orthorhombic cell with dimensions:

a = 14.7091(1) Å

b = 15.5227(2) Å

c = 14.6848(1) Å

V = 3352.91(4) Å^3

For Z = 4 and F.W. = 705.85, the calculated density is 1.40 g/cm^3. The systematic absences of:

0kl: k ≠ 2n

h0l: l ≠ 2n

hk0: h + k ≠ 2n

uniquely determine the space group to be P*bcn* (#60).

Frames corresponding to an arbitrary hemisphere of data were collected at -105°C using ω scans of 0.3° counted for a total of 10.0 seconds per frame. Data were integrated using SAINT[21] to a maximum 2θ value of 51.6°. Of the 15410 reflections that were integrated, 3394 were unique (R_{int} = 0.034); equivalent reflections were merged.

The linear absorption coefficient, μ, for Mo-Kα radiation is 28.2 cm^{-1}. Data were examined for agreement and possible absorption using XPREP and an empirical absorption correction was applied.[22] The transmission range was 0.565 - 0.944. The data were corrected for Lorentz and polarization effects. No correction was applied for decay. A secondary extinction coefficient was applied (1.4×10^{-7}).

The structure was solved by direct methods[23] and expanded using Fourier techniques.[24] All non-hydrogen atoms were refined anisotropically, while the quality of the data indicated that it was reasonable to locate and refine hydrogen atoms isotropically.

The final cycle of full-matrix least-squares refinement was based on 2053 observed reflections ($I > 3\sigma(I)$) and 283 variables and converged. The largest parameter shift was 0.11 times its esd. The weighted and unweighted agreement factors were:

$$R = \Sigma \left| \left| F_o \right| - \left| F_c \right| \right| / \Sigma \left| F_o \right| = 0.018$$

$$R_w = \sqrt{(\Sigma w(\left| F_o \right| - \left| F_c \right|)^2 / \Sigma w F_o^2)} = 0.026$$

The standard deviation of an observation of unit weight was 1.11. The weighting scheme was based on counting statistics and included a factor (p = 0.03) to downweight intense reflections. Plots of $\Sigma w(|F_o| - |F_c|)^2$ versus $|F_o|$, reflection order in data collection, sin θ/λ and various classes of indices showed no unusual trends. The maximum and minimum peaks in the final difference Fourier map corresponded to 0.44 and –0.47 $e^-/Å^3$, respectively.

formula	$YbC_{38}H_{48}N_2$	diffractometer	SMART
FW	705.85	scan type, range	ω, $4° \leq 2\theta \leq 52°$
space group	P*bcn* (#60)	reflections integrated	15410
a (Å)	14.7091(1)	unique reflections	3394
b (Å)	15.5227(2)	reflections, $F_o^2 > 3\sigma(F_o^2)$	2053
c (Å)	14.6848(1)	variables	283
V ($Å^3$)	3352.91(4)	absorption correction	empirical
Z	4	transmission range	0.565 - 0.944
d_{calc} (g/cm^3)	1.40	R	0.018
μ(Mo-Kα) (cm^{-1})	28.16	R_w	0.026
size (mm)	0.55 × 0.24 × 0.22	R_{all}	0.032
temperature (K)	168	GOF	1.11

8. [1,3-$(Me_3C)_2C_5H_3]_2$Yb(2,6-$Me_2C_6H_3NC)_2$. Crystals were grown by slow cooling of a toluene solution to -40°C. A red plate-like crystal having approximate dimensions of 0.35 × 0.18 × 0.05 mm was mounted on a glass fiber with Paratone N oil. Cell constants

and an orientation matrix obtained from a least-squares refinement using the measured positions of 7523 reflections with $I > 10\sigma$, in the range $4 < 2\theta < 52.3°$, corresponded to a primitive triclinic cell with dimensions:

a = 11.4729(6) Å	α = 76.607(1)°
b = 11.6642(6) Å	β = 86.592(1)°
c = 14.6848(1) Å	γ = 72.470(1)°
V = 1993.5(2) Å^3	

For Z = 2 and F.W. = 790.01 g, the calculated density is 1.32 g/cm^3. Based on a statistical analysis of intensity distribution, and the successful solution and refinement of the structure, the space group was determined to be P-1 (#2).

Frames corresponding to an arbitrary hemisphere of data were collected at -160°C using ω scans of 0.3° counted for a total of 10.0 seconds per frame. Data were integrated using SAINT[21] to a maximum 2θ value of 52.3°. Of the 9666 reflections that were integrated, 6713 were unique (R_{int} = 0.031); equivalent reflections were merged.

The linear absorption coefficient, μ, for Mo-Kα radiation is 23.8 cm^{-1}. Data were examined for agreement and possible absorption using XPREP and an empirical absorption correction was applied.[22] The transmission range was 0.844 - 0.998. The data were corrected for Lorentz and polarization effects. No correction was applied for decay. Analysis of the data indicated no need for a secondary extinction correction.

The structure was solved by direct methods[23] and expanded using Fourier techniques.[24] All non-hydrogen atoms were refined anisotropically, while hydrogen atoms were included in calculated positions but not refined.

The final cycle of full-matrix least-squares refinement was based on 5970 observed reflections ($I > 3\sigma(I)$) and 424 variables and converged. The largest parameter shift was 0.00 times its esd. The weighted and unweighted agreement factors were:

$$R = \Sigma \left| |F_o| - |F_c| \right| / \Sigma |F_o| = 0.029$$

$$R_w = \sqrt{(\Sigma w(|F_o| - |F_c|)^2 / \Sigma w F_o^2)} = 0.036$$

The standard deviation of an observation of unit weight was 1.36. The weighting scheme was based on counting statistics and included a factor (p = 0.03) to downweight intense reflections. Plots of $\Sigma w(|F_o| - |F_c|)^2$ versus $|F_o|$, reflection order in data collection, $\sin\theta/\lambda$ and various classes of indices showed no unusual trends. The maximum and minimum peaks in the final difference Fourier map corresponded to 1.00 and –1.09 $e^-/Å^3$, respectively.

formula	$YbC_{44}H_{60}N_2$	temperature (K)	113
FW	790.01	diffractometer	SMART
space group	P-1 (#2)	scan type, range	ω, $4° \leq 2\theta \leq 52°$
a (Å)	11.4729(6)	reflections integrated	9666
b (Å)	11.6642(6)	unique reflections	6713
c (Å)	16.0596(8)	reflections, $F_o^2 > 3\sigma(F_o^2)$	5970

α (°)	76.607(1)	variables	424
β (°)	86.592(1)	absorption correction	empirical
γ (°)	72.470(1)	transmission range	0.844 - 0.998
V (Å^3)	1993.5(2)	R	0.029
Z	2	R_w	0.036
d_{calc} (g/cm^3)	1.316	R_{all}	0.039
μ(Mo-Kα)$_{calc}$ (cm^{-1})	23.76	GOF	1.36
size (mm)	0.35 × 0.18 × 0.05		

9. [1,3-(Me$_3$Si)$_2$C$_5$H$_3$]$_2$Yb(2,6-Me$_2$C$_6$H$_3$NC)$_2$. Crystals were grown by slow cooling of a toluene solution to -40°C. A dark blue needle-like crystal having approximate dimensions of 0.40 × 0.18 × 0.15 mm was mounted on a glass fiber with Paratone N oil. Cell constants and an orientation matrix obtained from a least-squares refinement using the measured positions of 8099 reflections with I > 10σ, in the range 4 < 2θ < 52.3°, corresponded to a primitive orthorhombic cell with dimensions:

a = 19.9719(9) Å

b = 20.6253(9) Å

c = 22.099(1) Å

V = 9103(1) Å^3

For Z = 8 and F.W. = 854.31 g, the calculated density is 1.25 g/cm^3. The systematic absences of:

0kl: k ≠ 2n

h0l: $l \neq 2n$

hk0: $h \neq 2n$

uniquely determine the space group to be P*bca* (#61).

Frames corresponding to an arbitrary hemisphere of data were collected at -99°C using ω scans of 0.3° counted for a total of 10.0 seconds per frame. Data were integrated using SAINT[21] to a maximum 2θ value of 52.3°. Of the 42914 reflections that were integrated, 9085 were unique (R_{int} = 0.071); equivalent reflections were merged.

The linear absorption coefficient, μ, for Mo-Kα radiation is 21.9 cm^{-1}. Data were examined for agreement and possible absorption using XPREP.[22] An empirical absorption correction based on comparison of redundant and equivalent reflections was applied using SADABS.[25] The transmission range was 0.686 - 0.977. The data were corrected for Lorentz and polarization effects. No correction was applied for decay or secondary extinction.

The structure was solved by direct methods[23] and expanded using Fourier techniques.[24] All non-hydrogen atoms were refined anisotropically, while hydrogen atoms were included in calculated positions but not refined.

The final cycle of full-matrix least-squares refinement was based on 3830 observed reflections ($I > 3\sigma(I)$) and 424 variables and converged. The largest parameter shift was 0.00 times its esd. The weighted and unweighted agreement factors were:

$$R = \Sigma \| |F_o| - |F_c| \| / \Sigma |F_o| = 0.028$$

$$R_w = \sqrt{(\Sigma w(|F_o| - |F_c|)^2 / \Sigma w F_o^2)} = 0.029$$

The standard deviation of an observation of unit weight was 0.91. The weighting scheme was based on counting statistics and included a factor (p = 0.03) to downweight intense reflections. Plots of $\Sigma w(|F_o| - |F_c|)^2$ versus $|F_o|$, reflection order in data collection, $\sin \theta/\lambda$ and various classes of indices showed no unusual trends. The maximum and minimum peaks in the final difference Fourier map corresponded to 0.78 and -0.46 $e^-/Å^3$, respectively.

formula	$YbC_{40}Si_4H_{60}N_2$	diffractometer	SMART
FW	854.31	scan type, range	ω, $4° \leq 2\theta \leq 52°$
space group	P*bca* (#61)	reflections integrated	42914
a (Å)	19.9719(9)	unique reflections	9085
b (Å)	20.6253(9)	reflections, $F_o^2 > 3\sigma(F_o^2)$	3830
c (Å)	22.099(1)	variables	424
V ($Å^3$)	9103(1)	absorption correction	empirical
Z	8	transmission range	0.686 - 0.977
d_{calc} (g/cm^3)	1.247	R	0.028
μ(Mo-Kα)$_{calc}$ (cm^{-1})	21.86	R_w	0.029
size (mm)	0.40 × 0.18 × 0.15	R_{all}	0.095
temperature (K)	174	GOF	0.91

10. ***ansa*-[1,3-$(Me_3C)_2C_5H_2]_2SiMe_2Yb(2,6\text{-}Me_2C_6H_3NC)_2$.** Red crystals of the compound were grown by slow cooling of a toluene solution to -40°C. A red plate-like crystal having approximate dimensions of 0.36 mm × 0.11 mm × 0.08 mm was mounted on a glass fiber with Exxon Paratone N oil. Cell constants and an orientation matrix obtained from a least-squares refinement using the measured positions of 5103 reflections with $I > 10\sigma$, in the range $4 < 2\theta < 52.3°$, corresponded to a primitive monoclinic cell with dimensions:

$a = 11.8426(6)$ Å

$b = 16.4380(9)$ Å $\quad \beta = 99.068(1)$

$c = 22.338(1)$ Å

$V = 4294.1(3)$ Å^3

For $Z = 4$ and F.W. = 846.15, the calculated density is 1.31 g/cm^3. The systematic absences of:

$h0l: h + l \neq 2n$

$0k0: k \neq 2n$

uniquely determine the space group to be $P2_1/n$ (#14).

Frames corresponding to an arbitrary hemisphere of data were collected at -110°C using ω scans of 0.3° counted for a total of 10.0 seconds per frame. Data were integrated using SAINT[21] to a maximum 2θ value of 52.3°. Of the 17261 reflections that were integrated, 6369 were unique ($R_{int} = 0.083$); equivalent reflections were merged.

The linear absorption coefficient, μ, for Mo-Kα radiation is 22.4 cm^{-1}. Data were examined for agreement and possible absorption using XPREP.[22] An empirical absorption correction based on comparison of redundant and equivalent reflections was applied using SADABS.[25] The transmission range was 0.626 - 0.977. The data were corrected for Lorentz and polarization effects. No correction was applied for decay or secondary extinction.

The structure was solved by direct methods[23] and expanded using Fourier techniques.[24] One cyclopentadienide ring carbon atom was refined isotropically while the remainder of the non-hydrogen atoms were refined anisotropically with an exception as follows: One of the Me_3C groups on one of the cyclopentadienide rings was disordered. It was modelled with two sets of three methyl groups, each set having their occupancies constrained to be equal, and the sum of the occupancies of the two sets constrained to 1.0. Refinement led to occupancies of 0.49 and 0.51 for the sets of methyl carbon atoms. These atoms were refined isotropically. Hydrogen atoms were placed in calculated positions but not refined.

The final cycle of full-matrix least-squares refinement was based on 3243 observed reflections ($I > 3\sigma(I)$) and 444 variables and converged. The largest parameter shift was 0.01 times its esd. The weighted and unweighted agreement factors were:

$$R = \Sigma \left| |F_o| - |F_c| \right| / \Sigma |F_o| = 0.045$$

$$R_w = \sqrt{(\Sigma w(|F_o| - |F_c|)^2 / \Sigma w F_o^2)} = 0.051$$

The standard deviation of an observation of unit weight was 1.18. The weighting scheme was based on counting statistics and included a factor (p = 0.03) to downweight intense reflections. The maximum and minimum peaks in the final difference Fourier map corresponded to 1.20 and −1.42 $e^-/Å^3$, respectively.

formula	$YbSiN_2C_{46}H_{64}$	diffractometer	SMART
FW	846.15	scan type, range	ω, 4 - 52.3°
space group	$P2_1/n$ (#14)	reflections integrated	17261
a (Å)	11.8426(6)	unique reflections	6369
b (Å)	16.4380(9)	reflections, $F_o^2 > 3\sigma(F_o^2)$	3243
c (Å)	22.338(1)	variables	444
β (°)	99.068(1)	absorption correction	empirical
V ($Å^3$)	4294.1(3)	transmission range	0.977 - 0.626
Z	4	R	0.045
d_{calc} (g/cm^3)	1.309	R_w	0.051
μ(Mo-Kα)$_{calc}$ (cm^{-1})	22.37	R_{all}	0.102
size (mm)	0.36 × 0.11 × 0.08	GOF	1.18
temperature (K)	163		

11. **$\{(Me_5C_5)_2Yb(Me_3CNC)\}_2$-μ-CN.** Insoluble crystals were formed upon addition of impure Me_3CNC to a solution of $(Me_5C_5)_2Yb$ in toluene. A dark red fragment having approximate dimensions of 0.18 × 0.10 × 0.06 mm was mounted on a glass fiber using Paratone oil. Cell constants and an orientation matrix obtained from a least-squares

refinement using the measured positions of 1839 reflections with $I > 10\sigma$, in the range $4 < 2\theta < 52.0°$, corresponded to a primitive triclinic cell with dimensions:

$a = 10.382(1)$ Å $\quad \alpha = 98.483(2)°$

$b = 14.927(2)$ Å $\quad \beta = 91.805(2)°$

$c = 18.387(2)$ Å $\quad \gamma = 92.803(2)°$

$V = 2812.8(6)$ Å^3

For Z = 2 and F.W. = 1171.4 (including one molecule of toluene of crystallization per dimer), the calculated density is 1.31 g/cm^3. Based on a statistical analysis of intensity distribution, and the successful solution and refinement of the structure, the space group was determined to be P-1 (#2).

Frames corresponding to an arbitrary hemisphere of data were collected at -120°C using ω scans of 0.3° counted for a total of 10.0 seconds per frame. Data were integrated using SAINT[21] to a maximum 2θ value of 46.5°. Of the 12842 reflections that were integrated, 7952 were unique ($R_{int} = 0.056$); equivalent reflections were merged.

The linear absorption coefficient, μ, for Mo-Kα radiation is 33.4 cm^{-1}. Data were examined for agreement and possible absorption using XPREP.[22] An empirical absorption correction based on comparison of redundant and equivalent reflections was applied using SADABS.[25] The transmission range was 0.795 - 0.977. The data were corrected for Lorentz and polarization effects. No correction was applied for decay or secondary extinction.

The structure was solved by Patterson methods and expanded using Fourier techniques.[24] The ytterbium atoms were refined anisotropically, while the carbon and hydrogen atoms were refined isotropically as there was insufficient data for anisotropic refinement. After location and refinement of the dimeric core, peaks were observed in the difference map corresponding to one molecule of toluene of crystallization per dimeric unit. The two Me_5C_5 rings on Yb(2) are disordered and the disorder was modelled as follows. For the ring C 27 - C 32, the ring carbon atoms C27, C28 and C29 and their attached methyl carbon atoms C33, C34, C35 are full occupancy. The three other ring carbon positions C30, C31 and C32 were refined at 2/3 occupancy. The methyl carbon atoms for those positions were refined as four half-occupancy positions C36, C37, C38, C39.

For the ring C40 - C45, the ring carbon atoms C41 and C44 are full occupancy, along with their attached methyl carbon atoms, C48 and C52, respectively. The remaining ring carbon positions C40, C42, C43 and C45 had their occupancies refined to values in the range 0.51 - 0.94. Of the remaining methyl carbon positions, C 46 and C 47 are full occupancy, while C49, C50 and C51 had their occupancies refined to values between 0.43 and 0.80.

The data were of insufficient quality to justify placing hydrogen atoms. The final cycle of full-matrix least-squares refinement was based on 2676 observed reflections ($I > 3\sigma(I)$) and 294 variables and converged. The largest parameter shift was 0.01 times its esd. The weighted and unweighted agreement factors were:

$$R = \Sigma \left| |F_o| - |F_c| \right| / \Sigma |F_o| = 0.054$$

$$R_w = \sqrt{(\Sigma w(|F_o| - |F_c|)^2 / \Sigma w F_o^2)} = 0.059$$

The standard deviation of an observation of unit weight was 1.50. The weighting scheme was based on counting statistics and included a factor (p = 0.03) to downweight intense reflections. The maximum and minimum peaks in the final difference Fourier map corresponded to 0.97 and -0.81 $e^-/Å^3$, respectively.

formula	$Yb_2N_3C_{58}H_{86}$	temperature (K)	153
FW	1171.4	diffractometer	SMART
space group	P-1(#2)	scan type, range	ω, 4 -46.5°
a (Å)	10.382(1)	reflections integrated	12842
b (Å)	14.927(2)	unique reflections	7952
c (Å)	18.387(2)	reflections, $F_o^2 > 3\sigma(F_o^2)$	2676
α (°)	98.483(2)	variables	294
β (°)	91.805(2)	absorption correction	empirical
γ	92.803(2)	transmission range	0.977 - 0.795
V ($Å^3$)	2812.8(6)	R	0.054
Z	2	R_w	0.059
d_{calc} (g/cm^3)	1.383	R_{all}	0.072
μ(Mo-Kα)$_{calc}$ (cm^{-1})	33.40	GOF	1.50
size (mm)	0.18 × 0.10 × 0.06		

12. $[1,3\text{-}(Me_3C)_2C_5H_3]_2Yb(bipy)$. Blue-green crystals of the compound were grown by slow cooling of a concentrated toluene solution. A fragment of a crystal with approximate dimensions of 0.22 × 0.10 × 0.05 mm was mounted on a glass fiber with Paratone N oil. Cell constants and an orientation matrix obtained from a least-squares refinement using the measured positions of 4196 reflections with $I > 10\sigma$, in the range $4 < 2\theta < 49.5°$, corresponded to an F-centered orthorhombic cell with dimensions:

$a = 19.3445(4)$ Å

$b = 24.4600(5)$ Å

$c = 30.1051(4)$ Å

$V = 14244.7(4)$ Å^3

For Z =16 and F.W. = 776.0, the calculated density is 1.45 g/cm^3. The systematic absences of:

hkl: $h + k, k + l, h + l \neq 2n$

0kl: $k + l \neq 4n$

h0l: $h + l \neq 4n$

hk0: $h + k \neq 4n$

uniquely determine the space group to be F*ddd* (#70).

Frames corresponding to an arbitrary hemisphere of data were collected at -135°C using ω scans of 0.3° counted for a total of 20.0 seconds per frame. Data were integrated using

SAINT[21] to a maximum 2θ value of 49.3°. The integration was constrained to be face centered and orthorhombic. Of the 16914 reflections that were integrated, 3264 were unique (R_{int} = 0.073); equivalent reflections were merged.

The linear absorption coefficient, μ, for Mo-Kα radiation is 26.6 cm^{-1}. Data were examined for agreement and possible absorption using XPREP.[22] An empirical absorption correction based on comparison of redundant and equivalent reflections was applied using SADABS.[25] The transmission range was 0.732 - 0.962. The data were corrected for Lorentz and polarization effects. No correction was applied for decay or secondary extinction.

The location of the ytterbium atom was determined by Patterson methods.[27] The structure was then expanded using Fourier techniques.[24] The asymmetric unit consists of half the molecule as the ytterbium atom lies on a 2-fold axis. After the ytterbocene-bipyridyl molecule had been located and refined, peaks were observed in the difference map corresponding to one equivalent of toluene per ytterbocene molecule. The toluene molecule lies on a 222 special position, so only three atoms are seen in the asymmetric unit. The methyl group of the toluene molecule is disordered over four symmetry-equivalent positions, and has been modelled with that atom having 1/4 occupancy. This methyl carbon atom (C21) was refined isotropically, while all other non-hydrogen atoms were refined anisotropically. Hydrogen atoms were included in calculated positions for the ytterbocene molecule and not refined. No hydrogen atom positions were calculated for the disordered toluene molecule.

The final cycle of full-matrix least-squares refinement was based on 1726 observed reflections ($I > 3\sigma(I)$) and 195 variables and converged. The largest parameter shift was 0.00 times its esd. The weighted and unweighted agreement factors were:

$$R = \Sigma \left| |F_o| - |F_c| \right| / \Sigma |F_o| = 0.025$$

$$R_w = \sqrt{(\Sigma w(|F_o| - |F_c|)^2 / \Sigma w F_o^2)} = 0.025$$

The standard deviation of an observation of unit weight was 0.75. The weighting scheme was based on counting statistics and included a factor (p = 0.03) to downweight intense reflections. Plots of $\Sigma w(|F_o| - |F_c|)^2$ versus $|F_o|$, reflection order in data collection, $\sin \theta/\lambda$ and various classes of indices showed no unusual trends. The maximum and minimum peaks in the final difference Fourier map corresponded to 0.49 and –0.64 $e^-/Å^3$, respectively. These peaks were located near the ytterbium atom and close to the disordered toluene molecule, respectively.

formula	$YbN_2C_{43}H_{58}$	diffractometer	SMART
FW	776.0	scan type, range	ω, 3 - 49.3°
space group	F*ddd* (#70)	reflections integrated	16914
a (Å)	19.3445(4)	unique reflections	3264
b (Å)	24.4600(5)	reflections, $F_o^2 > 3\sigma(F_o^2)$	1726
c (Å)	30.1051(4)	variables	195
V ($Å^3$)	14244.7(4)	absorption correction	empirical
Z	16	transmission range	0.962 - 0.732

d_{calc} (g/cm^3)	1.451	R[b]	0.025
μ(Mo-Kα)$_{calc}$ (cm^{-1})	26.59	R_w	0.025
size (mm)	0.27 × 0.10 × 0.05	R_{all}	0.032
temperature (K)	138	GOF	0.75

13. [1,3-(Me$_3$Si)$_2$C$_5$H$_3$]$_2$Yb(phen). Crystals were grown by cooling a toluene solution of the complex. A red-brown fragment of a crystal having approximate dimensions of 0.29 × 0.08 × 0.05 mm was mounted on a glass fiber with Exxon Paratone N oil. Cell constants and an orientation matrix, obtained from a least-squares refinement using the measured positions of 4536 reflections with I > 10σ, in the range 4.0 < 2θ < 45°, corresponded to a primitive monoclinic cell with dimensions:

a = 11.2208(2) Å

b = 19.2665(1) Å β = 104.796(1)°

c = 17.9251(1)Å

V = 3746.65(6) Å^3

For Z = 4 and F.W. = 772.16, the calculated density is 1.37 g/cm^3. The systematic absences of:

h0l: h + l ≠ 2n

0k0: k ≠ 2n

uniquely determine the space group to be P2$_1$/n (#14).

Frames corresponding to an arbitrary hemisphere of data were collected at -112°C using ω scans of 0.3° counted for 20 seconds per frame. Data were integrated using SAINT[21] to a maximum 2θ value of 46.5°. Of the total of 15300 reflections integrated, 5550 were unique (R_{int} = 0.051) and equivalent reflections were merged.

The linear absorption coefficient, μ, for Mo-Kα radiation is 26.5 cm^{-1}. Data were examined for agreement and possible absorption using XPREP and an empirical absorption correction was applied.[22] The transmission range was 0.707 - 0.945. The data were corrected for Lorentz and polarization effects. No correction was applied for decay or secondary extinction.

The structure was solved by direct methods[23] and expanded using Fourier techniques.[24] The non-hydrogen atoms were refined anisotropically. Hydrogen atoms were placed in calculated positions for the methyl groups and phenanthroline rings, and in found positions for the cyclopentadienide rings, but not refined. The final cycle of full-matrix least-squares refinement was based on 3199 observed reflections ($I > 3\sigma$ (I)) and 370 variables and converged. The largest parameter shift was 0.00 times its esd. The weighted and unweighted agreement factors were:

$$R = \Sigma \left| |F_o| - |F_c| \right| / \Sigma |F_o| = 0.024$$

$$R_w = \sqrt{(\Sigma w(|F_o| - |F_c|)^2 / \Sigma w F_o^2)} = 0.024$$

The standard deviation of an observation of unit weight was 0.73. The weighting scheme was based on counting statistics and included a factor (p = 0.03) to downweight intense

reflections. Plots of $\Sigma w(|F_o| - |F_c|)^2$ versus $|F_o|$, reflection order in data collection, sin θ/λ and various classes of indices showed no unusual trends. The maximum and minimum peaks on the final difference Fourier map corresponded to 0.52 and -0.34 $e^-/Å^3$, respectively.

formula	$YbSi_4N_2C_{34}H_{50}$	diffractometer	SMART
FW	772.16	scan type, range	ω, 3 - 46.5°
space group	$P2_1/n$ (#14)	reflections integrated	15300
a (Å)	11.2208(2)	unique reflections	5550
b (Å)	19.2665(1)	reflections, $F_o^2 > 3\sigma(F_o^2)$	3199
c (Å)	17.9251(1)	variables	370
β (°)	104.796(1)	absorption correction	empirical
V ($Å^3$)	3746.65(6)	transmission range	0.945 - 0.707
Z	4	R^b	0.024
d_{calc} (g/cm^3)	1.369	R_w	0.024
μ(Mo-Kα)$_{calc}$ (cm^{-1})	26.48	R_{all}	0.059
size (mm)	0.29 × 0.08 × 0.05	GOF	0.73
temperature (K)	138		

14. $[(Me_5C_5)_2Yb(phen)]^+[I]^-$. Crystals were grown by cooling a methylene chloride solution of the complex. A red-brown fragment of a crystal having approximate dimensions of 0.25 × 0.12 × 0.09 mm was mounted on a glass fiber with Exxon Paratone N oil. Cell constants and an orientation matrix, obtained from a least-squares refinement

using the measured positions of 4838 reflections with $I > 25\sigma$, in the range $4.0 < 2\theta < 45°$, corresponded to a primitive monoclinic cell with dimensions:

$a = 14.3923(2)$ Å

$b = 14.6609(4)$ Å $\quad \beta = 100.925(1)°$

$c = 17.4018(3)$Å

$V = 3605.3(1)$ Å^3

For Z = 4 and F.W. = 920.5, the calculated density is 1.70 g/cm^3. The systematic absences of:

$h0l: h + l \neq 2n$

$0k0: k \neq 2n$

uniquely determine the space group to be $P2_1/n$ (#14).

Frames corresponding to an arbitrary hemisphere of data were collected at -122°C using ω scans of 0.3° counted for 30 seconds per frame. Data were integrated using SAINT[21] to a maximum 2θ value of 46.6°. Of the total of 16716 reflections integrated, 5383 were unique ($R_{int} = 0.053$) and equivalent reflections were merged.

The linear absorption coefficient, μ, for Mo-Kα radiation is 37.7 cm^{-1}. Data were examined for agreement and possible absorption using XPREP.[22] An empirical absorption correction based on comparison of redundant and equivalent reflections was applied using SADABS.[25] The transmission range was 0.744 - 0.962. The data were

corrected for Lorentz and polarization effects. No correction was applied for decay or secondary extinction.

The structure was solved by direct methods[23] and expanded using Fourier techniques.[24] The non-hydrogen atoms were refined anisotropically. After location and refinement of the ytterbocene molecule, peaks were observed in the difference map corresponding to two molecules of methylene chloride of crystallization per ytterbocene unit. Further refinement led to large thermal parameters for the atoms of one of these molecules, so the occupancy of that molecule was refined (refined value 0.62). Hydrogen atoms were placed in calculated positions but not refined. The final cycle of full-matrix least-squares refinement was based on 2985 observed reflections ($I > 3\sigma(I)$) and 380 variables and converged. The largest parameter shift was 0.00 times its esd. The weighted and unweighted agreement factors were:

$$R = \Sigma \left| |F_o| - |F_c| \right| / \Sigma |F_o| = 0.034$$

$$R_w = \sqrt{(\Sigma w(|F_o| - |F_c|)^2 / \Sigma w F_o^2)} = 0.035$$

The standard deviation of an observation of unit weight was 1.08. The weighting scheme was based on counting statistics and included a factor ($p = 0.03$) to downweight intense reflections. Plots of $\Sigma w(|F_o| - |F_c|)^2$ versus $|F_o|$, reflection order in data collection, $\sin\theta/\lambda$ and various classes of indices showed no unusual trends. The maximum and minimum peaks on the final difference Fourier map corresponded to 1.06 and -1.50 $e^-/Å^3$, respectively.

formula	$YbCl_4IN_2C_{34}H_{42}$	diffractometer	SMART
FW	920.5	scan type, range	ω, 3 - 46.6°
space group	$P2_1/n$ (#14)	reflections integrated	16716
a (Å)	14.3923(2)	unique reflections	5383
b (Å)	14.6609(4)	reflections, $F_o^2 > 3\sigma(F_o^2)$	2985
c (Å)	17.4018(3)	variables	380
β (°)	100.925(1)	absorption correction	empirical
V (Å^3)	3605.3(1)	transmission range	0.962 - 0.744
Z	4	R[b]	0.034
d_{calc} (g/cm^3)	1.70	R_w	0.035
μ(Mo-Kα)$_{calc}$ (cm^{-1})	37.72	R_{all}	0.041
size (mm)	0.25 × 0.12 × 0.09	GOF	1.08
temperature (K)	151		

References

1) Greenlee, K. W.; Henne, A. L. *Inorg. Synth.* **1946,** *2*, 128.

2) Tilley, T. D.; Boncella, J. M.; Berg, D. J.; Burns, C. J.; Andersen, R. A. *Inorg. Synth.* **1990**, *27*, 146.

3) Bercaw, J. E.; Marvich, R. H.; Bell, L. G.; Brintzinger, H. H. *J. Am. Chem. Soc.* **1972,** *94*, 1219.

4) Schultz, M.; Burns, C. J.; Schwartz, D. J.; Andersen, R. A. *Organometallics* **2000**, *19*, 781.

5) Hitchcock, P. B.; Howard, J. A. K.; Lappert, M. F.; Prashar, S. *J. Organomet. Chem.* **1992**, *437*, 177.

6) Venier, C. G.; Casserly, E. W. *J. Am. Chem. Soc.* **1990**, *112*, 2808.

7) Fendrick, C. M.; Schertz, L. D.; Day, V. W.; Marks, T. J. *Organometallics* **1988**, *7*, 1828.

8) Leffler, A. J. *Inorg. Chem.* **1968**, *7*, 2651.

9) Sofield, C. D. *PhD Thesis*; University of California: Berkeley, 2000.

10) Boncella, J. M. *PhD Thesis*; University of California: Berkeley, 1984.

11) Edelmann, F. T. *Lanthanides and Actinides*; Hermann, W. A., Ed.; Georg Thieme Verlag: Stuttgart, 1997; Vol. 6.

12) Khvostov, A. V.; Sizov, A. I.; Bulychev, B. M.; Knjazhanski, S. Y.; Belsky, V. K. *J. Organomet. Chem.* **1998**, *559*, 97.

13) Schumann, H.; Glanz, M.; Hemling, H.; Hahn, F. E. *Z. Anorg. Allg. Chem.* **1995**, *621*, 341.

14) Lappert, M. F.; Yarrow, P. I. W.; Atwood, J. L.; Shakir, R.; Holton, J. *J. Chem. Soc., Chem. Commun.* **1980**, 987.

15) *SMART Area-Detection Software Package*; Siemens Industrial Automation, Inc: Madison, WI, 1995.

16) Cromer, D. T.; Waber, J. T. *International Tables for X-ray Crystallography; Table 2.2A*; Ibers, J. A. and Hamilton, W. C., Ed.; The Kynoch Press: Birmingham, England, 1974; Vol. IV, pp 71-98.

17) Ibers, J. A.; Hamilton, W. C. *Acta Crystallogr.* **1964**, *17*, 781.

18) C reagh, D . C .; M cAuley, W . J . *I nternational Tables for Crystallography; Table 4.2.6.8*; Wilson, A. J. C., Ed.; Kluwer Academic Publishers: Boston, 1992; Vol. C, pp 219-222.

19) Creagh, D. C.; Hubbell, J. H. *International T ables fo r C rystallography; T able 4.2.4.3*; Wilson, A. J. C., Ed.; Kluwer Academic Publishers: Boston, 1992; Vol. C, pp 200-206.

20) *teXsan Crystal Structure Analysis Package*; Molecular Structure Corporation, Inc: The Woodlands, TX, 1992.

21) *SAINT*; 4.024 ed.; Siemens Industrial Automation, Inc: Madison, WI, 1995.

22) Sheldrick, G. M. *XPREP*; 5.03 ed.; Siemens Industrial Automation, Inc: Madison, WI, 1995.

23) Altomare, A.; Cascarano, M.; Giacovazzo, C.; Guagliardi, A. *J. Appl. Cryst.* **1993**, *26*, 343.

24) Beurskens, P. T.; Admiraal, G.; Beurskens, G.; Bosman, W. P.; de Gelder, R.; Israel, R.; Smits, J. M. M. *The DIRDIF-94 Program System*; University of Nijmegen: Nijmegen, The Netherlands, 1994.

25) Sheldrick, G. M. *SADABS*; Siemens Industrial Automation, Inc: Madison, WI, 1996.

26) Sheldrick, G. M. *SHELXTL Crystal Structure Determination Package*; Siemens Industrial Automation, Inc: Madison, WI, 1981.

27) *Patterson Methods, part of the SHELXTL Crystal Structure Determination Package*; Siemens Industrial Automation, Inc.: Madison, WI, 1995.